2013

Observing and understanding the Southeast Asian aerosol system by remote sensing: An initial review and analysis for the Seven Southeast Asian Studies (7SEAS) program

Jeffrey Reid
Marine Meteorology Division, Naval Research Laboratory, Monterey, CA, jeffrey.reid@nrlmry.navy.mil

Edward Hyer
Naval Research Laboratory, edward.hyer@nrlmry.navy.mil

Randall Johnson
University of North Dakota

B. N. Holben
NASA Doddard Space Flight Center

Robert Yokelson
University of Montana - Missoula

See next page for additional authors

Authors
Jeffrey Reid, Edward Hyer, Randall Johnson, B. N. Holben, Robert Yokelson, Jianglong Zhang, James Campbell, Sundar Christopher, Larry DiGirolamo, Louis Giglio, Robert Holz, Courtney Kearney, Jukka Miettinen, Elizabeth Reid, F. Joseph Turk, Jun Wang, Peng Xian, Guangyu Zhao, Rajasekhar Balasubramanian, Boon Ning Chew, Serm Janjai, Nofel Lagrosas, Puji Lestari, Neng-Huei Lin, Mastura Mahmud, Anh X. Nguyen, Bethany Norris, Nguyen T.K. Oanth, Min Oo, Santo V. Salinas, E. Judd Welton, and Soo Chin Liew

Atmospheric Research 122 (2013) 403–468

Contents lists available at SciVerse ScienceDirect

Atmospheric Research

journal homepage: www.elsevier.com/locate/atmos

Observing and understanding the Southeast Asian aerosol system by remote sensing: An initial review and analysis for the Seven Southeast Asian Studies (7SEAS) program

Jeffrey S. Reid [a,*], Edward J. Hyer [a], Randall S. Johnson [b], Brent N. Holben [c], Robert J. Yokelson [d], Jianglong Zhang [b], James R. Campbell [a], Sundar A. Christopher [e], Larry Di Girolamo [f], Louis Giglio [g], Robert E. Holz [h], Courtney Kearney [i], Jukka Miettinen [j], Elizabeth A. Reid [a], F. Joseph Turk [k], Jun Wang [l], Peng Xian [m], Guangyu Zhao [f], Rajasekhar Balasubramanian [n], Boon Ning Chew [j], Serm Janjai [o], Nofel Lagrosas [p], Puji Lestari [q], Neng-Huei Lin [r], Mastura Mahmud [s], Anh X. Nguyen [t], Bethany Norris [f], Nguyen T.K. Oanh [u], Min Oo [h], Santo V. Salinas [j], E. Judd Welton [c], Soo Chin Liew [j]

[a] Marine Meteorology Division, Naval Research Laboratory, Monterey, CA, United States
[b] Dept. of Atmospheric Science, University of North Dakota, Grand Forks, ND, United States
[c] NASA Goddard Space Flight Center, Greenbelt, MD, United States
[d] Dept. of Chemistry, University of Montana, Missoula, MT, United States
[e] Dept. of Atmospheric Science, University of Alabama, Huntsville, AL, United States
[f] Dept. of Atmospheric Science, University of Illinois, Urbana-Champlain, IL, United States
[g] Dept. of Geography, University of Maryland, College Park, MD, United States
[h] Space Sciences and Engineering Center, University of Wisconsin, Madison, WI, United States
[i] Ocean Sciences Division, Naval Research Laboratory, Stennis, MS, United States
[j] Center for Remote Imaging, Sensing and Processing, National University of Singapore, Singapore
[k] Jet Propulsion Laboratory, California Institute of Technology, Pasadena, CA, United States
[l] Dept. of Atmospheric Science, University of Nebraska, Lincoln, NE, United States
[m] ASEE Fellow, Naval Research Laboratory, Monterey, CA, United States
[n] Department of Civil and Environmental Engineering, National University of Singapore, Singapore
[o] Dept. of Physics, Silpakorn University, Nakhon Pathom, Thailand
[p] Manila Observatory, Ateneo de Manila University, Quezon City, Philippines
[q] Dept. of Environmental Engineering, Bandung Institute of Technology, Bandung, Indonesia
[r] Department of Atmospheric Sciences, National Central University, Chung-Li, Taiwan
[s] Earth Observation Center, Universiti Kebangsaan Malaysia, BaBangi Selangor, Malaysia
[t] Inst. of Geophysics, Vietnam, Academy of Science and Technology, Hanoi, Viet Nam
[u] Dept. Environmental Engineering and Management, Asian Institute of Technology, Thailand

ARTICLE INFO

Article history:
Received 15 August 2011
Received in revised form 5 June 2012
Accepted 6 June 2012

Keywords:
Southeast Asia
Maritime Continent
Meteorology
Aerosol

ABSTRACT

Southeast Asia (SEA) hosts one of the most complex aerosol systems in the world, with convoluted meteorological scales, sharp geographic and socioeconomic features, high biological productivity, mixtures of a wide range of atmospheric pollutants, and likely a significant susceptibility to global climate change. This physical complexity of SEA is coupled with one of the world's most challenging environments for both in situ and remote sensing observation. The 7-Southeast Asian Studies (7SEAS) program was formed to facilitate interdisciplinary research into the integrated SEA aerosol environment via grass roots style collaboration. In support of the early 7SEAS program and the affiliated Southeast Asia Composition, Cloud, Climate Coupling Regional Study (SEAC^{4}RS), this review was created to outline the network of connections linking aerosol particles in SEA with meteorology, climate and the total earth system. In this review, we

* Corresponding author at: Marine Meteorology Division, Naval Research Laboratory, 7 Grace Hopper Ave, Stop 2, Monterey, CA 93943-5502, United States. Tel.: +1 831 656 4725; fax: +1 831 656 4769.
E-mail address: jeffrey.reid@nrlmry.navy.mil (J.S. Reid).

0169-8095/$ – see front matter. Published by Elsevier B.V.
doi:10.1016/j.atmosres.2012.06.005

Remote Sensing
Biomass Burnig
Air Pollution

focus on and repeatedly link back to our primary data source: satellite aerosol remote sensing and associated observability issues. We begin with a brief rationale for the program, outlining key aerosol impacts and, comparing their magnitudes to the relative uncertainty of observations. We then discuss aspects of SEA's physical, socio-economic and biological geography relevant to meteorology and observability issues associated with clouds and precipitation. We show that not only does SEA pose significant observability challenges for aerosol particles, but for clouds and precipitation as well. With the fundamentals of the environment outlined, we explore SEA's most studied aerosol issue: biomass burning. We summarize research on bulk aerosol properties for SEA, including a short synopsis of recent AERONET observations. We describe long range transport patterns. Finally, considerable attention is paid to satellite aerosol observability issues, with a face value comparison of common aerosol products in the region including passive and active aerosol products as well as fluxes. We show that satellite data products diverge greatly due to a host of known artifacts. These artifacts have important implications for how research is conducted, and care must be taken when using satellite products to study aerosol problems. The paper ends with a discussion of how the community can approach this complex and important environment.

Published by Elsevier B.V.

Contents

1. Introduction

The *2007 IPCC Report on Impacts, Adaptation and Vulnerability* lists Southeast Asia as one of the most vulnerable regions of the world to climate change (IPCC, 2007a, Table 10.11). Biodiversity, coastal ecosystems, food and fiber, and land degradation are all listed as highly vulnerable, with settlements and water resources listed as moderately vulnerable. Similarly, in a recent report by Yusef and Francisco (2009), within a generally vulnerable Southeast Asia, significant hazards exist on Java, Sumatra, Vietnam and the Philippines. One prominent aspect of Southeast Asia's (henceforth SEA) Earth system is the role of aerosol particles. Any visitor to the large cities of SEA will notice air pollution's ubiquitous and sometimes oppressive nature. Over the last several decades, the region extending from the Maritime Continent (MC) of Brunei, Indonesia, Malaysia, Singapore and Timor through the Indochina (IC) areas of peninsular SEA (e.g., Cambodia, Laos, Myanmar, Thailand, Vietnam) and the islands surrounding the South China Sea/East Sea (SCS/ES, including the Philippines and Taiwan) has seen significant economic and population growth. Air pollution originating from such sources as biomass burning, industry, mobile sources, biofuel, and domestic cooking, in conjunction with the domestic and international demand for agricultural products such as palm oil, sugar, and rice leading to deforestation and biomass burning, has further reduced air quality.

The *2007 IPCC Report on the Physical Science Basis* (IPCC, 2007b) describes aerosol particles as an important part of the earth and climate systems. Climate impacts of aerosol particles can be loosely divided between interrelated perturbations to the atmosphere's radiative and thermodynamic properties. In the warm tropical environment of SEA, there are open questions about basic properties of the interactions between radiative and thermodynamic properties of aerosol particles, clouds and precipitation. Even under "clear sky" conditions, the aerosol particles' influence on the surface heat budget and the atmosphere's temperature profile may feed back into the clouds, which in turn feed back to other aerosol particle effects (Lohmann and Feicher, 2005). Despite the clear importance of aerosol particles in the SEA climate system, current understanding of key processes is riddled with knowledge gaps and large uncertainties.

The complex relationships between aerosol properties, forcing, and impacts have notable parallels in neighboring regions such as the Indian subcontinent (e.g., Lawrence and Lelieveld, 2010). There has been much scientific discussion in that region on the relative merits and issues about aerosol–meteorology coupling and their relationships to observations and models (e.g., see the exchange Lau and Kim, 2006a,b; Lau and Kim, 2011; versus Nigam and Bollasina, 2010, 2011). Indeed, even under ideal conditions, the community struggles to link cause and effect in the aerosol–earth system science–climate system. However, given SEA's geographic, meteorological, and hydrological complexity, establishing the quantitative linkages of aerosol particles to the regional environmental system is staggeringly difficult. Monsoonal flows coupled with a host of tropical wave phenomena, prominent topography and a very heterogeneous land surface make atmospheric observation, analysis and prediction a challenge. Ocean physical and biological systems are a composite network of currents, reefs, shallow waters and large river outflows. The land surface is under heterogeneous mosaic agricultural production and experiencing rapid change via deforestation. Interannual climate variability such as through the El Niño/Southern Oscillation (ENSO) creates another layer of relationships. Finally, research efforts and data collection across SEA have been hindered by lack of domestic funds and the SEA political climate.

Remote sensing provides a fundamental tool to understand the role of aerosol particles in earth system science and climate in general, and constitutes the only observations available for many parts of SEA. With useful sensors on geostationary, polar and high inclination platforms, remote sensing provides systematic data over large areas at high frequency. Satellites do not know political boundaries and are the cornerstone of models through initialization and assimilation. Satellites provide copious amounts of data on a number of facets of regional atmosphere, land, and ocean systems. For researchers attempting to understand aerosol lifecycle and impacts, there are terabytes of data generated each day with information on aerosol particle loadings, microphysics, and radiative properties. Data on related species, such as CO, NO_2, and SO_2 are now commonplace.

Despite remote sensing's significant contributions, there are several limiting issues when reviewing satellite data for SEA. 1) The geographic and environmental complexity of the system creates a host of sampling and retrieval biases; 2) Satellites may not know political boundaries, but political boundaries often co-vary with physical, cultural, and economic boundaries which can impact the atmosphere and land surface, and hence satellite data retrievals; 3) Satellite data records are temporally inconsistent, with sensors of varying efficacy entering and leaving the observing system; and 4) SEA has ubiquitous cloud cover which interferes with many relevant retrievals. Worse, cloud and aerosol properties co-vary with the meteorology, creating complex sampling biases, and potentially confounding attempts to separate causes from effects.

1.1. The 7SEAS program and its relation to this paper

To help understand the SEA aerosol–environment system, the 7-Southeast Asian Studies (7SEAS) project was created. The cornerstone of 7SEAS is remote sensing through product analysis as well as data assimilation in models (Zhang et al., 2008). Error characterization, including an understanding of sampling bias and representativeness, is a prominent component of satellite, in situ, and model studies alike. Through collaboration with Southeast Asia regional science partners (Indonesia, Malaysia, Philippines, Singapore, Taiwan, Thailand and Vietnam), the National Aeronautics and Space Administration (NASA), the Naval Research Laboratory (NRL), Office of Naval Research (ONR), and Office of Naval Research-Global (ONRG), 7SEAS has become a vibrant interdisciplinary, grass-roots style program which allows collaboration and information sharing throughout the region on science, field data, and observing systems. The '7' in 7SEAS refers not only to the number of regional participant countries, but to the core interdisciplinary research topic areas connected to the aerosol system: 1) aerosol lifecycle and air quality; 2) tropical meteorology; 3) radiation and heat balance; 4) clouds and precipitation; 5) land processes and fire; 6) physical and biological oceanography; and 7) environmental characterization through satellite analyses, model predictions, and verification.

While a review paper on SEA could take a number of different approaches, such as a focus on emissions, particle chemistry, carbon pools, climate impacts, etc., here we wish to set the stage for the largely ground and network based 7SEAS activities. We wish to summarize what is known about the SEA aerosol system, identify multiple links to the environment, and note large gaps in current scientific understanding. From this we can design targeted observational strategies. In particular, we examine the relationships between the environment and how remote sensing data is or can be applied. Much discussion is devoted to current challenges and uncertainties as a starting point for future studies. Indeed, the timing is critical as the year 2009 was the pinnacle of Earth observations from space: for the foreseeable future the world will see more declines than advances in observing capability. Field missions such as 7SEAS and the affiliated airborne Southeast Asia Composition, Clouds, Climate Coupling Regional Study (SEAC^{4}RS) need to carefully design experiments to make the most of currently available satellite data.

We begin this paper by discussing the context of aerosol research in SEA, with hypothesized aerosol impacts. This is followed by a brief presentation of standard climate grade aerosol and gas products. Next, SEA geography, meteorology, and biomass burning systems are reviewed, including brief demonstrations of key uncertainties or holes in the observing system. The second third of the paper is devoted to aerosol particles themselves, with an overview of their satellite relevant lifecycle properties such as microphysics and transport patterns. In the final third of the paper, we perform a face value comparison of common aerosol products as a basis for a discussion of their general merits and liabilities. In conclusion, we reflect on how review findings should influence future SEA aerosol studies, and how technological advances may help support a further understanding of the SEA aerosol system.

1.2. Data and information used in this paper

We should emphasize that this is a review paper with regional critical analysis. For the review, we largely draw our findings and conclusions from the peer reviewed literature, including findings included in this Atmospheric Research 7SEAS special issue. For the analyses, we sometimes take published studies further, and replot data in a way conducive to understanding the environment. To this end, we draw heavily from a number of data sets which we do not use in isolation, and try to discuss the limitations of each with respect to the analyses. But in general, we use "standard" datasets that are easily available to the authors and potential users. In all cases, citations are given to papers describing in detail the data processing involved.

1) Aerosol, cloud, and gas satellite data: There are very few comprehensive papers on aerosol, cloud, or gas remote sensing in SEA. The majority of work in the literature consists of case studies. There are global evaluations available, but generally these neglect our study region. To this end, we frequently utilize standard gridded 'level 3' products for a number of sensors such as can be found in the NASA Giovanni data access and plotting portal (Acker and Leptoukh, 2007).
2) Meteorology: For general characteristics of SEA, we draw from the Navy Global Atmospheric Prediction System (NOGAPS; Hogan and Rosmond, 1991; http://www.godae.org/), precipitation from the high resolution Climate Prediction Center (CPC) MORPHing technique (CMORPH, Joyce et al., 2004), and lightning from the High Resolution Monthly Climatology (HRMC) datasets produced and archived at the NASA's Global Hydrology Resource Center (Christian et al., 2003a).
3) Land and fire products: Here we find great diversity between global and local products. In the interest of this paper, we focus on easily available global products as these are most commonly used to the global climate community including the Fire Locating and Modeling of Burning Emissions—FLAMBE dataset described in Reid et al. (2009) and Global Fire Emissions Database—GFEDv3.1 described in van der Werf et al. (2010). However, we do point to localized studies to evaluate global product strengths and weaknesses.

For citations, emphasis and examples are drawn from the region whenever possible. SEA is not like other tropical environments and we do not generally cite other work in tropical regions (say South America or Africa) unless there is a specific relationship to SEA. Acronyms are frequently used in remote sensing science, and for brevity a list is provided in Appendix A. Acronyms for key systems used in the review are also defined in the text.

2. Rationale: uncertainty in the SE Asian aerosol system

Précis: Much of this manuscript on the study of aerosol lifecycles and impacts in SEA tries to bridge the gap between physical understanding and remote sensing. We note that nearly all of aerosol particles' impacts are interdisciplinary, both in science and in outcome. From

satellite observations, scientists can only infer desired quantities from retrieved products by relating them to quantities that are measurable, such as spectral radiance. Qualitatively, satellite products provide a valuable depiction of aerosol particles in the earth system. Quantitatively, large differences exist between products. Remote sensing approaches systematically undersample environmental variability and can underestimate or miss significant events, which often have the largest impact signals. This leads to a form of sampling bias which is inherent in satellite based methodologies.

2.1. Interdisciplinary nature of aerosol impacts in SEA

In considering the role of aerosol particles in the SEA earth system, we can broadly assign impact categories such as environmental quality, climate, meteorology, etc. For SEA, notable studies include:

Environmental quality and chemistry: SEA urban centers and rural receptors are known to suffer from poor regional air quality. Aerosol particles are important to biological and visual air quality with clear impacts on the local community (Kunii et al., 2002; Dawud, 1998; Emmanuel, 2005; Field et al., 2009; Pengchai et al., 2009; Betha et al., 2013-this issue). Acid deposition has been shown to influence river and ocean chemistry (Sundarambal et al., 2010; He and Balasubramanian, 2009a,b; He et al., 2011). Aerosol particle radiative effects impact photochemical rates (Tang et al., 2003b). Aerosol particles in SEA have even been identified contaminating food (Srinivas et al., 2009).

Direct radiative forcing: Through scattering and absorption of solar and terrestrial radiation, aerosol particles play a primary role in the clear sky (and, as we suggest later, in some cases in the cloudy sky) radiative budget (Davison et al., 2004; Rajeev et al., 2008; Feng and Christopher, 2013-this issue). Perturbations to photosynthetic active radiation at the surface by regional smoke can be significant (Kobayashi et al., 2004).

Meteorology, semi-direct, and indirect forcing: Through perturbation of the surface radiation budgets, aerosol particles impact sensible and latent heat fluxes (Bala Subrahamanyam et al., 2011). With respect to cloud development, there have been suggestions of both increased storm and lighting severity (Hamid et al., 2001; Yuan et al., 2011) and perhaps precipitation effects (Rosenfeld, 1999; Jiang et al., 2008; Tosca et al., 2010). It is hypothesized that absorption of solar radiation in the atmosphere coupled with the microphysical influence of aerosol particles on cloud droplets impact cloud formation and lifetime (Mcfarquahar and Wang, 2006; Dey et al., 2011) as well as precipitation (Barbel, 2007; Tosca et al., 2010).

Geochemical cycles: Aerosol particles are a significant component to a host of geochemical cycles, such as carbon (Page et al., 2011), and trace elements (Langmann and Graf, 2003; He and Balasubramanian, 2009a). The carbon pools of SEA, especially in relation to peatland, are tremendous (Hergoualch and Verchot, 2011).

Tracers: Used as imagery or tracer products, aerosol particles are indicators of air-mass types, magnitude and transport mechanisms (Gutman et al., 2000; Ji and Stocker, 2002; Duncan et al., 2003b; Lin et al., 2007; Xian et al., 2013-this issue).

Oceans: Radiation perturbations can impact ocean photochemistry and have even been seen in the coral record (Risk et al., 2003).

Interference: In many cases aerosol particles simply interfere with other earth observations. With heavy aerosol loadings, atmospheric correction is an important consideration for land products as well as ocean surface and bathometry products (Toratani et al., 2005). Misclassification of aerosol features as clouds can disrupt analyses of aerosol and cloud properties alike (Zhang et al., 2005a). Aerosol particles can be a consideration for many atmospheric products such as gas constituent retrievals.

Clearly, nearly all of aerosol particles' detrimental impacts are intertwined with other gas chemistry, meteorology, land, or oceanographic systems. Therefore in studying aerosol impacts, knowledge must span multiple topic areas; in particular when using satellite products from different fields. For example, scientists studying how biomass burning impacts precipitation in SEA, can use fire products used to interpret aerosol products, which are used in combination with cloud and precipitation products to link fire and precipitation. As this review will clearly show, the complexity of the SEA environment requires a reasonable understanding of remote sensing science in multiple disciplines.

2.2. Nature of remote sensing science

While in the Introduction we argued that atmospheric research, particularly in SEA, is heavily dependent on remote sensing, in most cases satellites do not directly provide what is needed to understand these relationships. The system being observed is four-dimensional (i.e., space and time) with sharp gradients in every dimension of particle concentration (mass and number), size, speciation, thermodynamic parameters, and radiative parameters related to spectral phase function scattering and absorption efficiencies. The systematic observations we have are centered on Aerosol Optical Depth (AOD) in clear sky regions with some co-emitted gas species. If multiple wavelengths are retrieved, some information on fine/coarse partition can be estimated over ocean. If multiple angles or polarization are used, more reliable information on modal contributions to AOD can be derived. If UV or polarization channels are applied, additional information on aerosol particle speciation, absorption or cloudy scene loadings can be derived. With the advent of space-based lidar, two-dimensional curtains of backscatter are available, but coverage is limited and interpretation can be difficult. A different but equally complex set of issues apply to satellite based fire products, which are an absolute necessity for understanding biomass burning emissions in SEA, despite their large uncertainties. Satellites can most directly observe thermal hotspots and burn scars, but not emissions. Higher resolution imagery improves these two measurements, at the expense of temporal coverage. But even, high resolution also does not overcome cloud issues. Estimates of fire emissions

remain highly under-constrained, even if fire observations were completely accurate.

Because of both fiscal and technological constraints, the information content of satellite products is typically anti-correlated to total area coverage. Further, the variables that satellites can observe (e.g., spectral radiance, polarization etc.), are often only indirectly related to the properties of the earth system needing constraint (e.g., flux, optical depth, particle/droplet size, etc.), which are then in turn used to infer impacts. That is, almost everything scientists need requires inference from under-determined retrievals. Achieving useful inferences demands a thorough understanding of the various components of the systems, and coupling with a series of models to quantify findings.

2.3. Perceived variability in remote sensing data

As we demonstrate, taken at face value, satellite products tend to have some qualitative agreement. But, the current observing system is challenged by the complexity of SEA. We face an extremely difficult error propagation environment for quantitative aerosol applications. Further, we can surmise that uncertainties in satellite products often co-vary with the phenomena to which they are linked. This is exemplified in Figs. 1 and 2, which make a useful preamble for this paper. Fig. 1(a–f) provides a 0.5°×0.5° point by point maximum, minimum and range (max–min) of Aerosol Optical Depth (AOD) drawn from a host of average NASA aerosol "level 3" retrievals. For illustrative purposes we divide SEA into its two state December-through-May (DJFMAM) winter and June-through-November (JJASON) summer monsoonal components (Fig. 1(a)/(c) and (b)/(d), respectively) on which we elaborate in later sections. For each AOD product, a seasonal average is calculated. Each point in Fig. 1(a–f) represents the minimum, maximum and range of this ensemble of climatological means. Included in the calculation were a total of 6 products, derived from (1) Moderate Resolution Imaging Spectroradiometer (MODIS) standard collection 5 from both Terra and Aqua (Remer et al., 2005; Levy et al., 2007); (2) Deep Blue version 5.2 from both Terra and Aqua, a classic dark target retrieval which relies on the sensors blue wavelengths (Hsu et al., 2004, 2006), (3) Deep Blue version 5.2 from SeaWiFS (Sayer et al., 2011), and (4) Multi-angle Imaging SpectroRadiometer MISR version 22 on Terra (Kahn et al., 2009, 2010). The period 2005–2007 was used to calculate a multi-product average seasonal AOD for this comparison (this period was selected as it included one El Niño Southern Oscillation cycle; see Section 5). Product Quality Assurance (QA) flags were used to identify and exclude "bad" retrievals from the analysis. For comparison, the Ozone Monitoring Instrument (OMI) aerosol index (Torres et al., 2002, Section 8) for the same time period is provided in Fig. 1(g) and (h). Similarly, to provide context, OMI column NO_2 (Bucsela et al., 2006) and Microwave Limb Sounder (MLS) 147, and 215 hPa CO (Livesey et al., 2008) are provided in Fig. 2.

Fig. 1 clearly demonstrates that there is a range of perceived aerosol loadings throughout SEA and its surrounding areas, from exceptionally clean to highly polluted. AODs <0.1 exist well east of the Philippines and into the middle of the Indian Ocean. These are levels which are considered typical in remote clean marine environments (Smirnov et al., 2003, 2011). Conversely seasonal maximums in isolated areas range from 0.4 to 1 over much of the populated land regions. Differences between the maximum and minimum tend to be structurally coherent with hotspots associated with urban centers and fire activity (Section 3), as well as other areas of fairly long correlation lengths demonstrating long range transport. The Bay of Bengal and Gulf of Thailand show good consistency among products. At the same time, the dynamic range in Fig. 1 suggests that diversity between climatological averages from commonly used products often varies by a factor of 2 or more. For example, in boreal summer monsoonal Borneo and Sumatra, over both land and water, all products see an AOD maximum associated with burning, but have a factor of 3 difference in magnitude. Over land in regions with dark surface albedos (such countries as Burma, Vietnam and the Philippines), products range from very clean AODs<0.1 to AOD>0.25. The Western Pacific and Gulf of Tonkin show significant divergence.

The aerosol AOD fields are often not used in isolation but in conjunction with other products. The OMI aerosol index, well known for its ability to identify absorbing aerosol particles, clearly highlights burning activity in Indochina in boreal spring and on Borneo for boreal summer and fall. From Fig. 2 we see that NO_2 is an excellent tracer for high temperature combustion products, with multiple hotspots in urban environments throughout SEA. Large amorphous NO_2 features also appear seasonally around the biomass burning regions, due to the oxidation of fuel nitrogen to NO_x (Burling et al., 2010). Even well-defined sea lanes passing around Singapore into the Indian Ocean and SCS/ES are clear (Franke et al., 2009). Finally, if we examine CO aloft (Fig. 2(c–f)), we find significant seasonal structure which may be related to convective pumping of pollutants to the top of the troposphere by the Indian Monsoon (depicted here by 147 hPa CO levels, which clearly demonstrate the Indian monsoonal anticyclone aloft), as well as convective pumping of SEA industrial and biomass burning emissions in the middle and upper troposphere (depicted by MLS 215 hPa CO levels). These are discussed in more detail in Section 4.

Climatology-grade products such as Figs. 1 and 2, even with potentially large artifacts, clearly convey the general nature of the SEA aerosol environment. However, it is a significant leap from a qualitative description of aerosol formation and transport mechanisms to quantitative values for such variables as emissions, sinks, and radiative impacts. Indeed, remote sensing in general is ill equipped to cope with significant events which may have the largest impact signals. This leads to a form of sampling bias which is inherent in satellite based methodologies. For example, consider Fig. 3, which shows NASA MODIS images from the NASA Visible Earth System (http://visibleearth.nasa.gov/) for two biomass burning events for (a) and (b) smoke from Thailand and Laos transporting over Vietnam into the Pacific Ocean on April 2, 2002, and (c) and (d) a significant burning event in Borneo and Sumatra for Sept. 18, 2002. Fire hotspots marked in red are from the MOD14 MODIS products (Justice et al., 2002; Giglio et al., 2003a). These two cases are used because, by regional standards, these periods are relatively cloud free. In Fig. 3(a), Thailand, Laos and Vietnam are covered with a thick

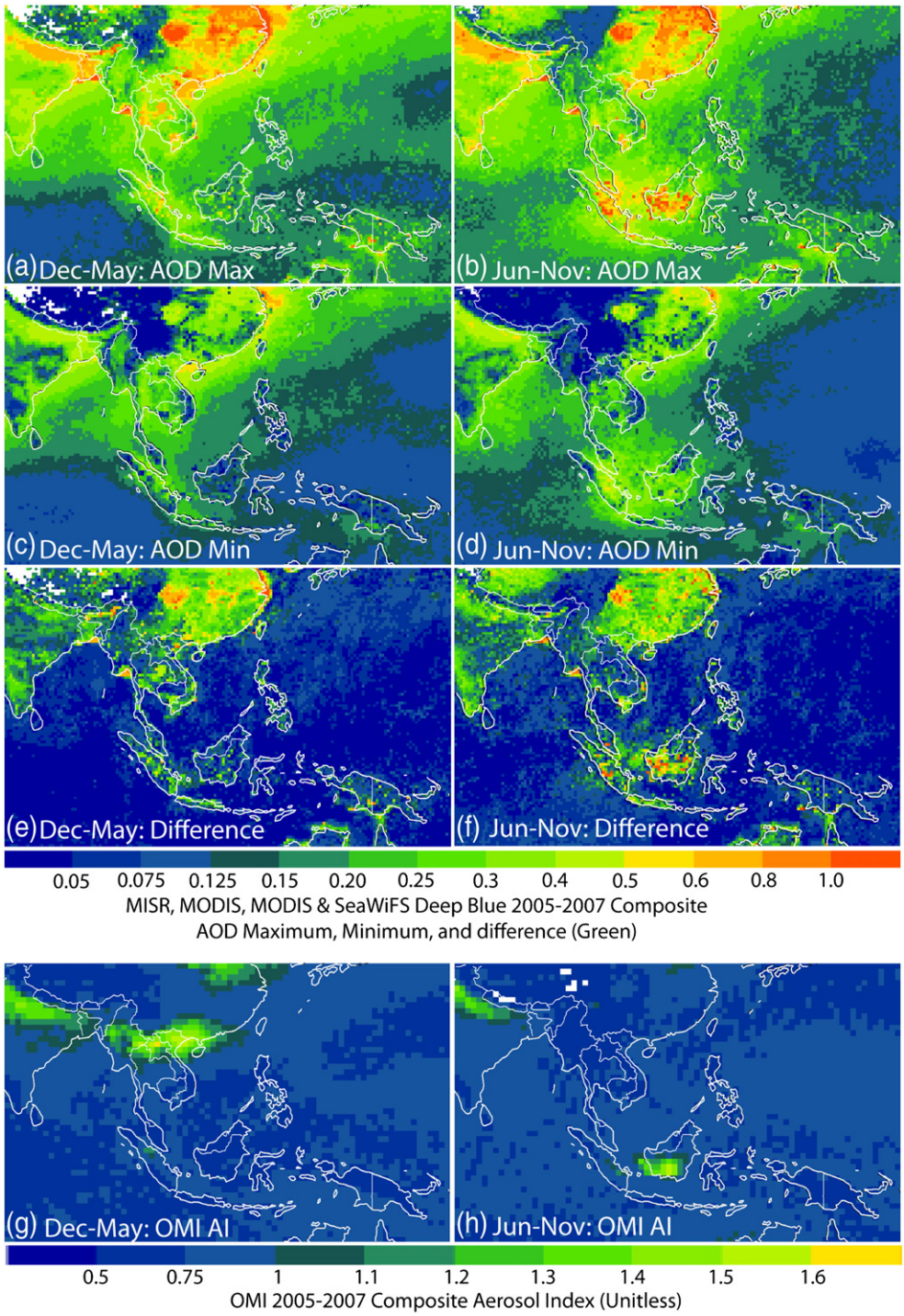

Fig. 1. (a)–(f) Seasonal maximum, minimum and max–min difference of aerosol optical depths (AOD) composites from MODIS Collection 5 (550 nm), MODIS and SeaWiFS Deep Blue (550 nm), and MISR (553 nm) for each 0.5×0.5 degree point. Also shown (g) and (h) is the OMI 1×1 degree average Aerosol Index (AI). (a), (c), (e), and (g) December to May. (b), (d), (f), and (h) June to November.

regional smoke plume, typical for the boreal spring when burning is at a maximum. However, the details of Fig. 3(b) are quite telling. The smoke contains many fine features and is often constrained in valleys in the mountainous region. Smoke is also transported over northern Vietnam above a stratus cloud deck. For the Indonesia case (Fig. 3(c)), we see many observed fires in Sumatra with convection beginning over the mountains that will later produce large thunderstorms. However, there is clearly much more smoke on Borneo, but fewer observed fires. Again, looking at higher

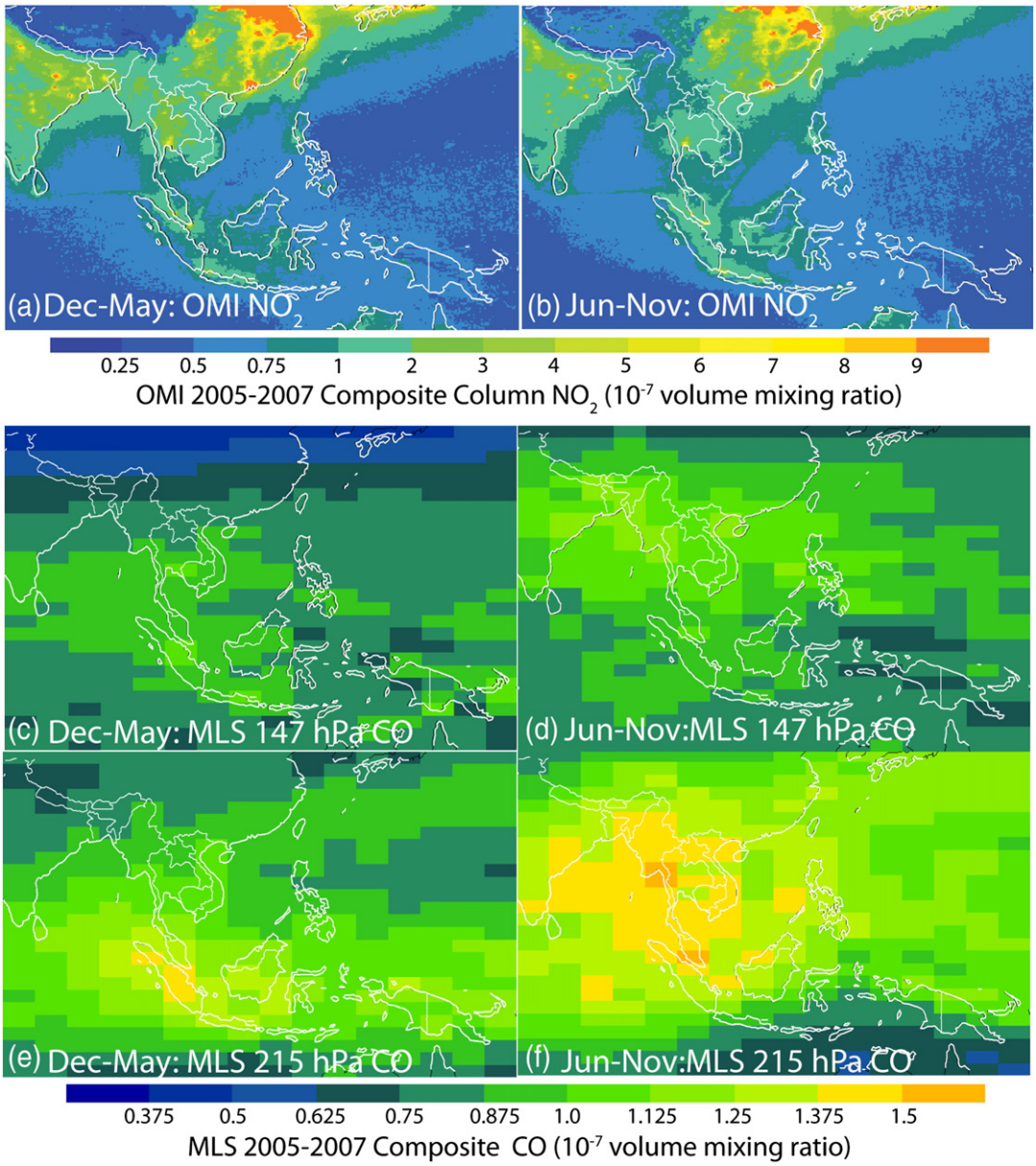

Fig. 2. Same as Fig. 1 for seasonal OMI total column NO_2 and MLS CO at 147 and 215 hPa (~14 and 11 km, respectively). MLS data courtesy of Ryan Fuller and Nathaniel Livesey, JPL.

resolution section (Fig. 3(d)) we find a thick mix of smoke, clouds and thin cirrus. In the case of Fig. 3(d) the image is enhanced for maximum contrast. Many individual smoke plumes are visible that are not detected by the fire hotspot algorithm. Low temperature peat fires may be large emitters but have a small thermal signature. Some of these fires are clearly obscured by capping cumulus clouds. In other cases, we speculate smoke may be so thick that it even disrupts infrared channels (see Section 5). In both cases, we can clearly see that smoke is so opaque that the ground is not visible in many locations.

High resolution can provide more detail on the situation on the ground in SEA. As an example, Système Pour l'Observation de la Terre-SPOT imagery (©Centre National d'Etudes Spatiales—CNES, 2005 and 2006) showing forest and agricultural burning on Sumatra is provided in Fig. 3(e) and (f) respectively. For forest burning in Fig. 3(e), red, green and blue correspond to near IR, red and green; hence vegetation is red, no vegetation/burn scar is green, smoke is white. In Fig. 3(f) red, green and blue correspond to the short wave IR, near IR, and red, hence fire is red, vegetation green, burn scar black, smoke bluish white. The case of agricultural burning likely represents the easiest of all scenarios to observe. The variability in flame fronts and isolated fire is clear. Smoke plumes are also visible, but notice that there is fine structure between relative thermal signatures and fine plume features.

Finally consider the view from the ground (Fig. 3(g), (h) and (i)) which shows variability in fuel sources that are

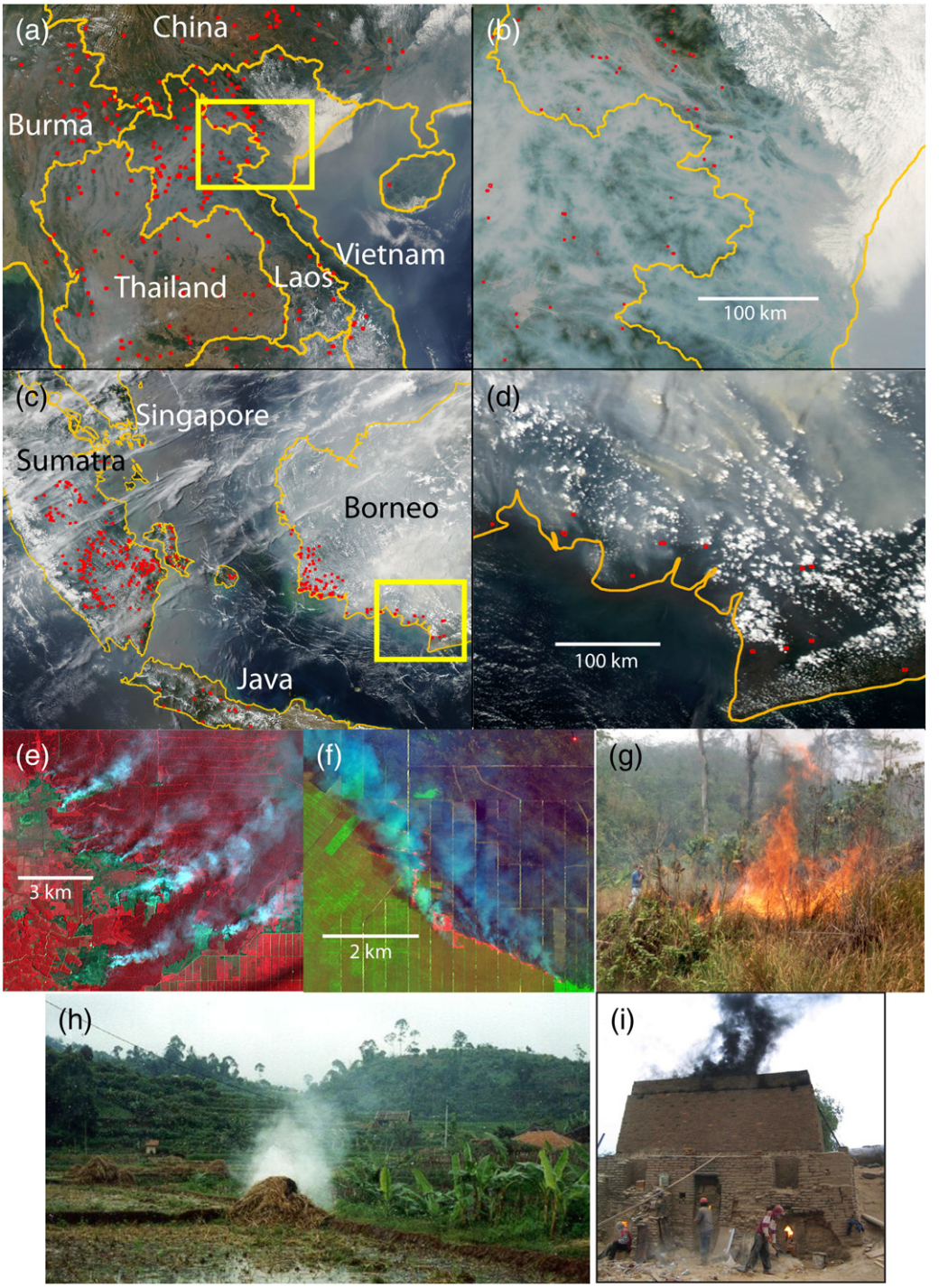

Fig. 3. MODIS true-color images, depicting the complexity of the Southeast Asian biomass burning system. (a) Terra MODIS for 7 April 2002, with regional smoke and fire (red) transporting over a stratus deck in Vietnam; (b) Zoom of (a); (c) Massive Indonesian fire event on Borneo and Sumatra captured by Aqua MODIS Sept. 18, 2002; (d) Zoom of (c) with contrast enhancement; (e) SPOT 2 image of forest burning in Riau, Sumatra August 8, 2005 (RGB = NIR, red, green; that is vegetation is red, no vegetation/burn scar is green, smoke is white); (f) SPOT 4 Image of agricultural burning in south Sumatra, September 28, 2006 (RGB = SWIR, Near IR, red; that is fire is red, vegetation green, burn scar black, smoke bluish white). (g), (h), (i) Photos of nontraditional burning: Invasive grass burn, stacked rice stubble burn and a brick kiln, respectively.

Credits: (a)–(d) Adapted from NASA Visible Earth; (e) and (f) © CNES (2005 and 2006), acquired by Center for Remote Imaging, Sensing and Processing, National University of Singapore. (g)–(i) Robert Yokelson, University of Montana.

abundant, but not classic "biomass burning" (photo credit Robert Yokelson, University of Montana). In Fig. 3(g) we see a small burn to clear alang-alang grass, a fire-maintained, and highly flammable invasive species that covers large areas of degraded land. This patch was starting to get covered by brush (known in Indonesia as "semak"). Fig. 3(e) shows an example of the ubiquitous stack and burn of rice straw, common throughout SEA. Such stacks can smolder for days. Finally, Fig. 3(i) shows a typical SEA brick kiln using wood and forest slash for fuel. While not thought of as biomass burning, they are common throughout the developing world and in SEA, often use wood fuels and may have similar chemical signatures. These sources are ubiquitous and their impact largely unconstrained.

Another example of the complexity of the SEA environment is depicted in Fig. 4, where a recent serendipitous photograph was taken above the Micropulse Lidar Network site at Singapore on March 28, 2012 at ~10Z (18:00 LST). In this case, a large isolated thunderstorm developed in the presence of a significant air pollution plume. The comparison of the photo (Fig. 4(a)), with the lidar normalized backscatter image Fig. 4(b) adds critical vertical context to the aerosol and radiative environment. Based on comparison of the 12Z sounding at Singapore along with backscatter data, we find the highest aerosol concentrations within a 500 m marine boundary layer (MBL). Above this, a convective boundary layer/entrainment zone pumps and processes smoke in moderate quantities to ~3 km (e.g., Cohn and Angevine, 2000). Thin aerosol layers, likely detrained from larger clouds, can be observed up to the melting level (~5 km; 0 °C), where at the end of the time series what is likely a melting level shelf cloud formed (e.g., Johnson et al., 1996; Yasunaga et al., 2006; Posselt et al., 2008). Very slight evidence also exists for aerosol layers up to the absolute freezing level (~9 km; −37 °C; Wang et al., 2004b). There a thin cloud with virga is present. At such temperatures, this cloud could be considered as ice cirrus by many standards. However, the rapid pulse attenuation occurring, indicated by dark signal shadowing above the apparent cloud top height, is more characteristic of liquid water, thus suggesting a likely mixed phase cloud with transmissive ice virga below (e.g., Sassen et al., 1985; Rosenfeld and Woodley, 2000; Wang et al., 2004a; Campbell and Shiobara, 2008). Its phase state is ultimately ambiguous. Further aloft, anvil outflow from the thunderstorm is visible (~12.5 km; −52 °C), followed by finally an optically thin tropopause transition layer cloud (~17 km; registered by the 0Z radiosonde at −88 °C; e.g., Jensen et al., 1996; Fueglistaler et al., 2009). Due to solar noise in the lidar signal, this cloud might only be resolvable after sunset (12Z), thus exhibiting cloud optical depths near and/or below 0.03 (Sassen and Cho, 1992). Such vertical complexity as demonstrated here is common place in SEA, representing a significant challenge for both in situ and remote sensing systems to characterize.

We use Figs. 1–4 as example of how one can have a good qualitative idea about aerosol processes, yet still have significant quantitative disagreement between aerosol related products (AOD, fire, land cover, etc.) and their interpretation in SEA. Fig. 3 in particular demonstrates the challenge of scale. What we can observe may be incomplete or even misleading vis-à-vis the actual physical situation. The details of processing remotely sensed data, whether for climatology or for assimilation of individual observations, requires considerable thought and planning of how data are collected and applied. This review will demonstrate that in all but the most qualitative applications, the use of "face value" products or averages can be misleading in SEA and result in erroneous conclusions. This review paper will not resolve the issue, but we hope that it will alert readers to those processes that interfere with observations, confuse the physical interpretation, and obstruct quantitative analysis of aerosol processes in SEA. That said, with advances in data processing and assimilation of multiple aerosol, gas, fire and meteorological products, the future of SEA aerosol research is quite exciting.

3. Fundamentals of Southeast Asia geography

The physical review begins with a brief section on the physical, socio-economic, and biological geography of SEA.

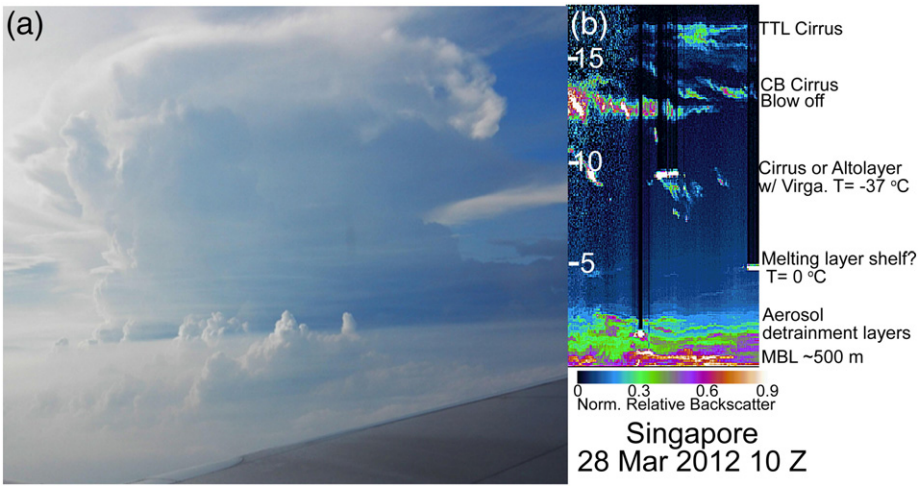

Fig. 4. Airborne photo with associated MPLnet normalized relative backscatter image of the cloud and aerosol environment at Singapore on 28 March 2012 at ~10Z. Lidar image is from 9 to 15Z, with a vertical coordinate from 0 to 18 km. Annotated are a number of aerosol and cloud features demonstrating the complex vertical characteristics of the Southeast Asian environment.

SEA has many sharp mountain ranges which dictate political and socioeconomic boundaries. Volcanism is important in the region, especially in the Maritime Continent. Population densities are high, with numerous mega cities in most SEA countries. The region around the Pearl River delta on the border of SEA cannot be ignored. The island of Java, Indonesia, stands out as a massive population center. In contrast with its teeming cities, SEA hosts a profound array of wet and dry tropical forests with numerous globally significant biodiversity hotspots in the region. The human encroachment on SEA forests, and in particular peatlands, is an area of high scientific interest. In particular, the last two decades have seen a marked change from swidden to plantation style agriculture which is changing land use and fire dynamics. Because encroachment is slow and the geography complex, scale effects will figure strongly in any comparison of satellite products. Systematic updating of satellite derived land surface databases a key issue for the community.

3.1. Regional definitions of Southeast Asian geography

For the purposes of this paper and the 7SEAS program, SEA can be divided into two distinct parts: 1) the Asian continental SEA, sometimes referred to as Peninsular SEA or Indochina (henceforth IC) and 2) the archipelagic or insular SEA, also often referred to meteorologically as the Maritime Continent (MC, Ramage (1968)). The domain of this review is presented in Fig. 5, including key physical, population, and biological features. The continental portion of SEA includes Burma (Myanmar), Thailand, Laos, Cambodia, and Vietnam. Due to some natural characteristics, West Malaysia (i.e. the Malaysian part of the Malay Peninsula) is usually considered part of the archipelagic SEA rather than the continental SEA. In addition to Malaysia, the MC includes Indonesia, Singapore, Brunei, and Timor-Leste. There are two ambiguous areas in regard to these definitions. First, the Philippines are commonly considered to be part of the MC, yet as we will show, climatologically are better grouped with IC. Second, Papua New Guinea has been left out of many analyses of the SEA environment, despite sharing an island with Indonesian Papua. But for climate purposes we include it in this review as part of the MC.

3.2. Physical geography

The topographic geography of SEA is complex including a series of high mountain ranges and large lowlands which influence our later interpretation of regional meteorology and aerosol lifecycle. An elevation map is provided in Fig. 5(b). The IC hosts a series of mountain ranges fanning out from the southeast corner of the Tibetan Plateau, separated by plateaus and river drainage basins. As was evident in Fig. 3(b), fine details likely play an important role in aerosol transport, but modeling studies to-date have largely been at coarse scales which do not adequately reflect the influence of topography. The mountain ranges of the IC are a result of orogeny, the gradual collision of the Indian subcontinent with the Eurasian continental plate; with the southeastern edge of the Eurasian continent being "bent around" and deformed by the Indian sub-continental block. This results in three largely parallel high mountain ranges separated by large blocks or plateaus of ancient continental terrain, and by several large river drainages and delta plains:

1) Running roughly N to SW in an S-shaped curve, the Arakan Mountains (Rakhine Yoma) are a fold belt mountain range that runs through Burma (Myanmar) and into the Indian Ocean forming the Andaman Islands. With several peaks above 5 km, the mountain range effectively isolates Myanmar from neighboring Bangladesh.
2) Running roughly N to S, the Tenassem Hills/Range is a combination of granite ridges and folded ancient marine sediments deeply eroded into steep valleys by rivers. The Tenassem Hills run from the SE corner of Tibet roughly along the Burmese and Thai border, and down the Malay Peninsula with peaks up to 1 km. Like the Arakan mountain range, the Tenassem proves a formidable isolating influence on Burma (Myanmar).
3) Running NW to SE, the Annamite Range (or Annamese Mountains or Annamese Cordillera) runs from Laos through Vietnam along the S. China Sea. In the Thailand and Laos border region between the Annamite Range and the Tenassem Hills, is the Korat Plateau. With 2–2.5 km peaks Annamite Range also provides a north south barrier between Vietnam and Laos.

Within the MC, the dominant geography is associated not with orogeny but with the volcanic activity of the "Ring of Fire" which passes through the Philippines, onto Borneo, the southern Malay Peninsula, Sumatra, Java, Timor, Maluku and Papua. Indeed, the MC is recognized as one of the most active regions of the Pacific Ring of Fire and includes some of the largest historical eruptions: Tambora in Indonesia 1815, Krakatau in Indonesia 1883, and Pinatubo in the Philippines 1991. This region has over 200 Holocene (active within the last 10,000 years) volcanoes, with the vast majority in Indonesia (145) and the Philippines (47) (Smithsonian Institute, Global Volcanism Network). The Holocene volcanoes range in morphology from calderas up to 7 km in width (Krakatau) to stratovolcanoes nearly 4 km asl (Mount Kerinci, Sumatra, Indonesia). These result in very high mountain ranges and volcanic peaks that range from 1 to 2.5 km in the Philippines, 2–4 km on Sumatra (e.g., Barisan Range), 1–2 km on Borneo (e.g., Crocker Range), 2–2.5 on Java, 1.5–2.5 km on Sulawesi, and 3.5–4.8 km on New Guinea (Central range). As discussed in Section 6.5, not only is MC volcanic activity important for transport but it is also an important primary and precursor aerosol source, particularly for SO_2. Currently, the most highly active volcanoes are in the Philippines, Sumatra, and Java. Some residual volcanic activity occurs in northern Borneo and Sulawesi.

3.3. Social geography

The social geography of SEA is clearly demonstrated in Fig. 5(c), which logarithmically plots population density derived from the Gridded Population of the World, version 3 open dataset (http://sedac.ciesin.columbia.edu/gpw/). For example, low population density is found in Cambodia and Laos between Thailand and Vietnam. Similarly, a clear boundary exists between Burma (Myanmar) and its S. Asian neighbors Bangladesh and India. The mountain ranges described in

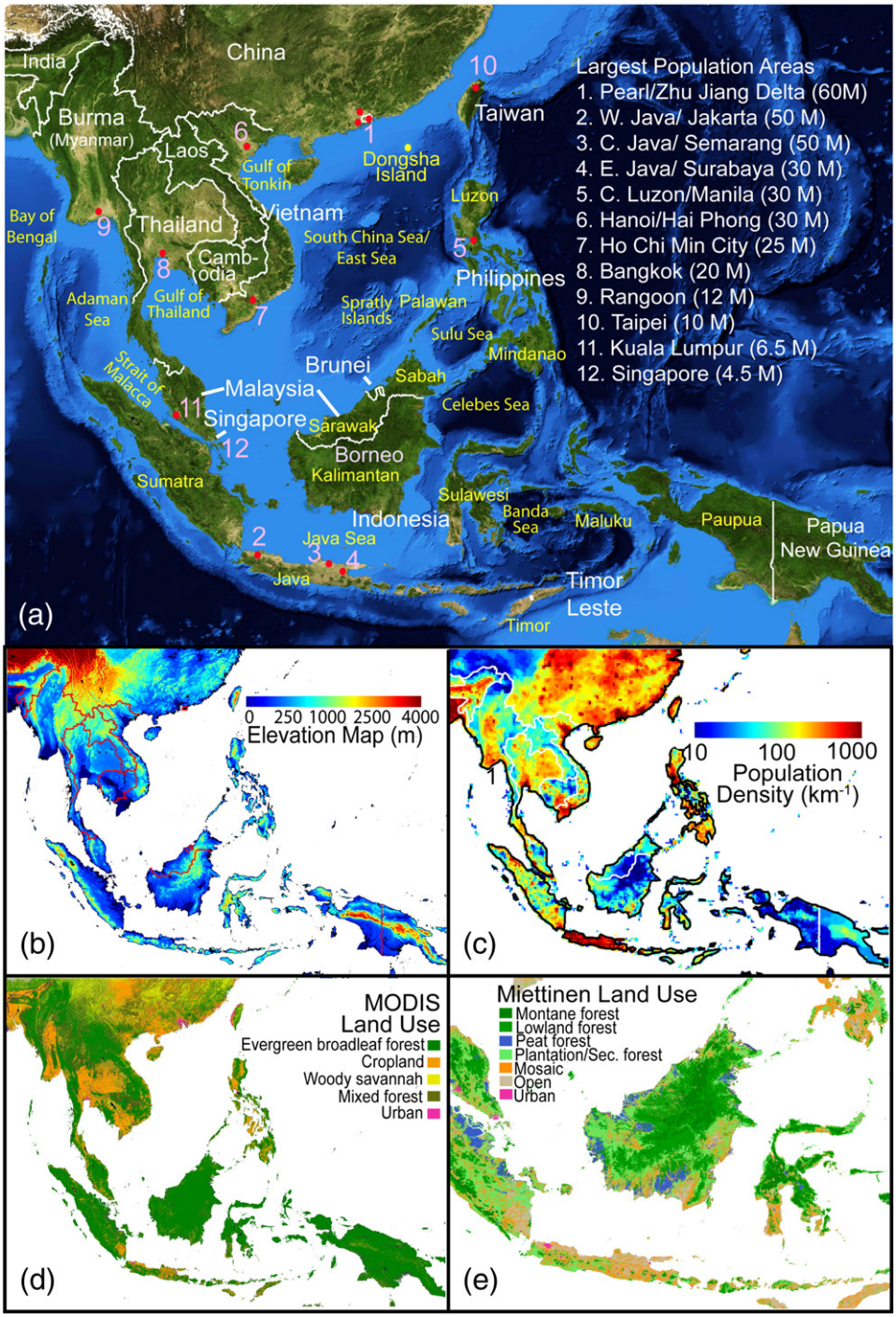

Fig. 5. Maps of key geographic features of Southeast Asia. (a) NASA MODIS Blue Marble RBG product labeled with key countries, regions, and major urban centers with total urban area populations. (b) NASA Blue Marble Elevation map; (c) 2010 population Density (CIESIN, 2004); (d) MODIS 2001 Global Land Use (Friedl et al., 2002); (e) Regional subset of *Miettinen* MODIS composite. Note, middle/high montane forest and mosaic classes grouped here into single categories for simplicity.

Section 3.2 dictate political boundaries. In IC in particular, the north–south mountain ranges clearly delineate population, cultural, and economic boundaries, which in turn influence the spatial distribution of emissions.

SEA has numerous densely populated regions, with the largest 12 population centers identified in Fig. 5(a). With a ~60 M population, the Pearl River/Zhu Jiang Delta region hosts Guangzhou, Hong Kong, and Macau. While this region is

outside SEA, as defined in this study, it is discussed later as pollution from this region frequently intrudes into the northern South China Sea/East Sea (SCS/ES) and Vietnam. Indeed, Fig. 2(a) and (b) shows the Pearl River Delta region as the most significant NO_2 hotspot. Java has the highest SEA population density, hosting 130 M of Indonesia's 225 M inhabitants. In Fig. 5(a) Java is divided into three areas for simplicity. To provide context, Indonesia has 85% of the population of the contiguous USA in 25% of the land area. Further, Java has nearly 60% of Indonesia's population in 6.7% of the Indonesian land area (so, approximately 51% of the USA population in 1.7% of the land area). Central Luzon/Manila in the Philippines, and the Hanoi–Haiphong corridor and Ho Chi Minh City in Vietnam also have ultra-high population densities, and total urban populations in the 30–35 M range.

From an environmental point of view, population is only a part of the equation; economics, politics and culture have a significant role. The socio-economic disparity among the countries of SEA, as well as between urban and rural populations within each country, is extreme. Economic development ranges from prosperous Singapore on one end of the scale, to Timor-Leste and Burma (Myanmar) on the other (e.g., Rigg, 2003, http://data.worldbank.org/data-catalog/world-development-indicators). Simultaneously, the economies and agriculture in SEA are evolving rapidly (Rigg, 2003; Alauddin, 2004; Fox et al., 2009). This makes rigorous scientific characterization for earth system science, climate change and climate adaptation difficult (Adger, 2003). Result accuracy may be short lived. But qualitatively, comparison of the population map of Fig. 5(c) with the NO_2 map of Fig. 2(a) and (b), shows that NO_2, a short lived species that is most often a product of higher temperature combustion (e.g., industrial or vehicle emissions), does not always track with population. For example, Yangon in Burma (Myanmar) has a high population, but little NO_2, while the ship lanes around Singapore and the Strait of Malacca, perhaps the world's most important shipping lane (>70,000 large ships per year-NBAS, 2010), are clearly visible in the OMI NO_2 product of Fig. 2.

Even within countries, there is a large disparity between urban and rural population (Rigg, 2003). Cultural issues that may vary between islands or regions dictate aspects of daily life and, by extension, emissions. For example, do families cook their own meals, or do they use communal food vendors? In the valleys of SEA, the warm climate rarely requires domestic heating, but, SEA has large mountains and even snow. Fuel for domestic cooking and heating use varies from electric, to propane, to various forms of biofuel (including wood, charcoal, dung, and rice stubble). In addition, numerous small-scale enterprises such as brick kilns burn a variety of fuels including garbage, crop waste, tires, used motor oil, scrap wood, sawdust, and charcoal (Le and Oanh, 2010). Although an inventory of these fuel-intensive enterprises has not been performed in SEA, such informal operations account for up to 50% of non-agricultural employment in some similar economic areas over the globe (Christian et al., 2010).

3.4. Biological geography

The combination of physical and socio-economic geography of SEA also strongly relates to SEA's biological geography. Land cover and land use are dynamic, with land cover conversion from forest to mosaic to agriculture and urban land uses. Land use issues are critically important to climate change as a whole, and in regard to this review, to fire emissions.

The monsoonal climate of SEA has a profound effect on the vegetation and is well described by Corlett (2009). We largely draw from this work. The original lowland vegetation types in IC included tropical seasonal forests and tropical deciduous forests. The tropical seasonal forest areas have been especially favored for agriculture, leading to great reduction in the area of this forest type over the last several hundred years. Simultaneously, in drier areas, anthropogenic fire activity in recent history has led to replacement by more fire tolerant deciduous forest types. In the driest areas of the region, fire activity has caused degradation of the deciduous tropical forests into savanna and grasslands. Due to long term human impact, large fractions of natural forest and wetland areas have been converted to managed land cover types or reduced to savannas, grassland, and "unnatural" grasslands (e.g. Seavoy, 1975). In addition to IC and parts of the Philippines, similar seasonal/deciduous forest/shrub transformations could be expected to be dominant in some parts of the MC.

As is discussed in Section 4, the northern 2/3 of the MC typically sees some rain year-around, permitting the humid tropical forests which dominate the lowland vegetation in natural conditions. The drier areas of east Java, Bali and Timor contain natural dry tropical forest, with a more seasonal climate (Whitmore, 1984). The humid tropical part of SEA is considered to contain the highest biodiversity of all regions in the world (Whitmore, 1984; Corlett, 2009). Perhaps the most distinctive feature of the MC is the vast extent of tropical peatlands up to 20 m thick. These peatlands and peat forests have formed over thousands of years through accumulation of organic material in waterlogged conditions (Rieley and Page, 2005; Page et al., 2006). Extensive peatlands are mainly located in the lowlands of Borneo, Sumatra, and New Guinea. Page et al. (2011) estimated that SEA peatlands cover around 250,000 km^2 (~56% of total tropical peatland) and contain up to 70 Gt of carbon (~77% of tropical peat carbon). This is 11% of total carbon peat pool of the earth. In addition to being globally significant carbon deposits, the peatlands support peat swamp forest ecosystems containing unique flora and fauna, and have numerous hydrological and societal functions in the region (Rieley and Page, 2005; Corlett, 2009).

Currently much of the natural vegetation types in SEA have been degraded by logging of varying intensity, reduced to savannas and grasslands, or converted into managed land cover types. Indeed, rapid environmental degradation and land cover changes continue to take place in this region (Kauppi et al., 2006; Hansen et al., 2009; Miettinen et al., 2011a,b). This conversion not only jeopardizes the region's high biodiversity, but also makes the region increasingly susceptible to fire (Cochrane, 2003), thus intensifying the numerous negative effects that biomass burning has in SEA (e.g. haze, carbon emissions, ecosystem destruction, etc.).

From an aerosol system point of view, the complexity of the SEA land use system described above poses one of the field's great challenges. Most importantly, there is little consistent information on regional land use, crops, above ground biomass, and the application of fire as a land management tool. Governments do keep some statistics which appear in

hard-to-acquire reports. But, given the prevalence of both small holders and large-scale illegal activity, these data are likely to be unrepresentative and uncertain (Gadde et al., 2009; http://e360.yale.edu/feature/chinas_appetite_for_wood_takes_a_heavy_toll_on_forests/2465/). Indeed, small holder illegal deforestation that often occurs at night in small operations (called "kayu bulan" — literally "wood moon" in the Indonesian language). The land use community, in particular those addressing aerosol problems, largely utilizes remote sensing data due to its availability and consistency. Such data are commonly used to identify emissions from deforestation and, when possible, separate those emissions from those related to agricultural maintenance (e.g., Stolle and Lambin, 2003; Stolle et al., 2003). Fuel loads and burned area have been estimated in numerous studies, but largely by extrapolation. High resolution products are available and applied from such products as Landsat (Giri and Shrestha, 2000; Miettinen et al., 2007; Segah et al., 2010), but studies are not comprehensive, footprints are small and there is a lack of uniformity in processing between researchers.

The scale problem between global analyses and detailed plot studies is well demonstrated in Fig. 5(d) and (e). Here we present two MODIS products sets, the global 1 km MODIS land use product of Friedl et al. (2002) based on 2001 (Fig. 5(d)), and in comparison, a small portion of the MC specific 500 m MODIS based product by Miettinen et al. (2008) for the first half of 2008 (Fig. 5(e)). Both of these products are based on MODIS data, but use different processing and ancillary data. For MODIS land use, we identify the five most significant categories, of which 'Evergreen broadleaf forest' and 'cropland' account for over 90% of land surface area in SEA. In contrast, the Miettinen land use product shows considerable stratification, and our figure aggregates several montane forest and mosaic categories (middle and high) into single categories. The difference between the Friedl and Miettinen databases is most apparent on Java. We know, based on the true color image images in Figs. 3(a) and 5(a) as well as its large population, that Java is almost completely deforested of primary forests. Classification of heterogeneous landscapes with moderate-resolution data is an exercise in approximation, and small differences in tuning of classifiers can lead to dramatic differences in estimates of forest cover.

More important than simple classification is the rapid evolution of land use in parts of SEA. Over the last decade, peatlands are diminishing at a significant rate in favor of plantation style agriculture-notably in favor of oil palm (e.g., Kauppi et al., 2006; Koh, 2007; Hansen et al., 2009; Langner et al., 2007; Langner and Siegert, 2009; Miettinen and Liew, 2010; Miettinen et al., 2011a). This makes the systematic updating of satellite derived land surface databases a key issue for the community.

4. Southeast Asia meteorology and related satellite products

Straddling the equator, Southeast Asia has a monsoonal climate largely dictated by the annual migration of the Inter-tropical Convergence Zone (ITCZ), with a dry and wet IC in boreal winter and summer respectively. Conversely, the MC has what could be construed as a "wet" and "wetter" boreal summer and winter monsoonal cycle. A boreal summertime dry area exists south of 5° S latitude. For illustration purposes, nearly all figures in this review have reduced the complex seasonality of SEA meteorology to a "two state" December–May and June–November system, with transitional periods being at the end of these classifications. This treatment is informative but ultimately reductive, glossing over the multitude of multi-scale meteorological features, ranging from interannual El Niño Southern Oscillation (ENSO), the Madden Julian Oscillation (MJO), tropical Kelvin, easterly and Rossby waves, tropical cyclones, the sea breeze, and isolated convection, to name a few. Cloud cover in SEA is nearly ubiquitous, with thin cirrus covering 80% of the sky. In a brief review of meteorological remote sensing in SEA, we show how SEA is not only one of the most challenging regions of the world for remote sensing, but displays large diversity in cloud and precipitation products as well. SEA weather phenomena impact aerosol lifecycle and, as discussed in the next section, the *observability* of the aerosol system. The human element (Vayda, 2006), including how anthropogenic activities such as biomass burning co-vary with meteorology, must also be considered.

4.1. Key monsoonal features

There is no single review paper that covers all of the important aerosol relevant meteorology for all of SEA. However, the very recent publication of Chang et al. (2011) provides many useful chapters on SEA's summer and winter monsoonal period. For monsoonal flows, we also recommend Chang et al., 2005a; Moron et al., 2009; Wang et al., 2009 as important reading. In addition to the references above, we would like to draw attention to specific broad-scoped papers on meteorology–aerosol relationships such as the review paper on South Asia by Lawrence and Lelieveld (2010) and meteorological context of biomass burning in the MC by Reid et al. (2012). Within this special issue, we point to papers on MC transport patterns by Xian et al. 2013-this issue, precipitation by Turk and Xian (2013–this issue), and examples of mesoscale phenomenon for the 2006 fire outbreak by Wang et al. (2012b). This synopsis draws largely from this bibliography.

It is illustrative to begin with simple plots demonstrating the monsoonal cycle. In Fig. 6, we provide average meteorological parameters over 2003–2009 associated with the winter (DJFMAM) and summer (JJASON) monsoonal periods: (a) and (b) NOGAPS 30 m winds (Hogan and Rosmond, 1991) and CMORPH precipitation (Joyce et al., 2004), (c) and (d) NOGAPS 700 hPa winds and 500 hPa vertical velocity (2003–2009), and (e) and (f) 200 hPa winds and lightning frequency (Christian et al., 2003a). Fig. 6(a) and (b) intend to demonstrate the overall nature of the SEA monsoon. The tendency is for precipitation to follow maximum solar insolation, which fuels convection. Hence, tropical precipitation tends to follow the hemispheres summer season (a maximum precipitation in the northern hemisphere 10–15° N in July–October and a maximum in the southern hemisphere at −6° S in January–April). Starting east and working westward, we have the primary ITCZ and a secondary convergence zone resulting in two zonal rain bands embedded in trade winds in the central Pacific (i.e., so called "Double ITCZ" Masunaga and L'Ecuyer, 2010). Just east of New Guinea, the monsoonal trough pivots from a zonal feature in the winter monsoon across the MC to a summertime

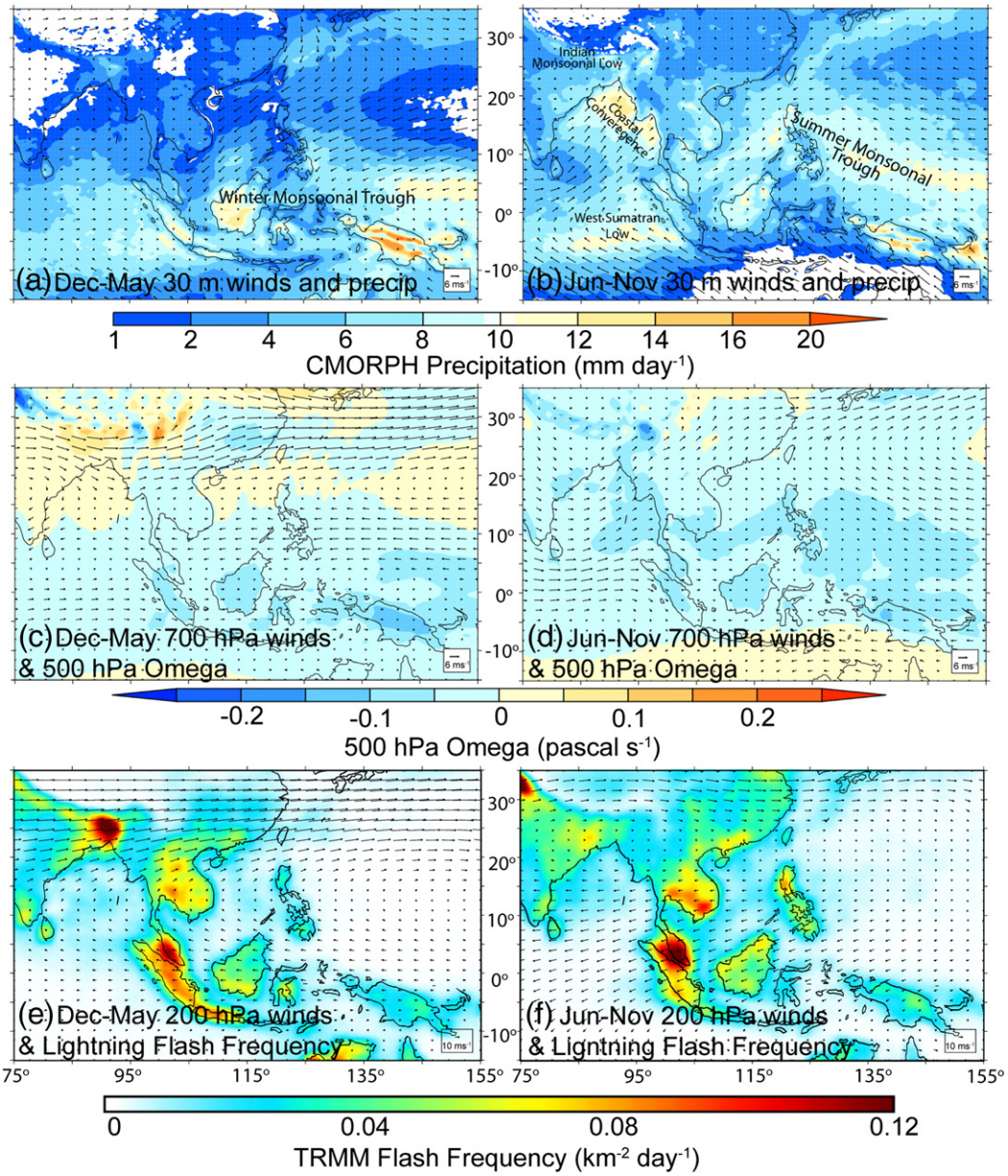

Fig. 6. Key 2003–2009 meteorology variables divided by December to May winter and June to November summer monsoonal periods. (a) and (b) NOGAPS 30 m winds and CMORPH precipitation rate (white <1 mm day^{-1}). (c) and (d) NOGAPS 700 hPa winds and 500 hPa vertical velocity (omega). (e) and (f) NOGAPS 200 hPa winds and Tlightning flash frequency from LIS sensor on TRMM (updated form Christian et al., 2003a).

diagonal feature that extends into the northern SCS/ES where it is anchored over land in IC and into the Indian monsoonal low. This monsoonal change comes with a significant change in the wind field, most notably a surface flow reversal from northeasterly to southwesterly winds in the SCS/ES from boreal winter to summer, and from very light easterly to intense westerlies on the northern Indian Ocean and the Bay of Bengal. As one would expect, aerosol loadings in Fig. 1 largely anti-correlate to the position of the monsoonal trough.

While the monsoon is often thought of as simply tracking seasonal solar heating, there are numerous complexities which are important for understanding the aerosol environment. Within IC, the CMORPH precipitation fields clearly illustrate the relative "Dry" and "Wet" seasons which correspond to burning and non-burning periods. What precipitation is visible in IC in Fig. 1(a) is largely from the transitional month of May, although on very rare occasions cold fronts from the north enter IC. Within the MC, the difference between precipitation in the summer and winter monsoonal periods is about 50%, and could be better characterized as "Wet" and "Wetter." This "asymmetry" is described by Chang et al. (2005a, 2005b) and is further demonstrated in Fig. 6(c) and (d) which show NOGAPS 500 hPa vertical velocity, and generally rising air over Borneo and Sumatra due to convection even during the supposed MC dry season. A corresponding "Total dry line" is roughly at ~3–5 S latitude and encompasses Java, Bali, southern Sulawesi and

Timor. North of this line, scattered convective precipitation is normal throughout the "dry season". Finally, a persistent rainfall maximum occurs over the Indian Ocean west of Sumatra, with winter monsoon periods being dominated by the ITCZ. In the summer, the precipitation feature is associated with what local forecasters term the "West Sumatran Low", a vorticity maximum formed by counter flowing monsoonal winds, with easterlies to the south, westerlies to the north in the vicinity of the Barisan Range of Sumatra (Reid et al., 2012). Some have suggested this forms from convection spawned over the mountains of Sumatra (Wu et al., 2009a). As described by Reid et al. (2012) and Xian et al. 2013-this issue, this is an important sink region for MC biomass burning emissions as well as pollution from Java.

For IC, the most interesting feature is not associated with precipitation but rather wind fields. During the summer monsoon, boundary layer winds generally track those of the lower free troposphere. This makes interpretation of transport patterns associated with AOD fairly straightforward. During the winter monsoon, however, there is significant vertical wind shear in the northern SCS/ES (Fig. 5(a) and (c)) with boundary layer and lower free tropospheric winds almost entirely in opposite directions. This may lead to decoupling of the boundary layer from the lower free troposphere. The free troposphere feeds smoke from IC via westerly winds aloft (as demonstrated in the OMI AI in Fig. 1(e) and described by Lin et al., 2009 and Fu et al., 2012); while the boundary layer is often being fed from air originating from China and the Pearl River Delta by the surface northeasterly winds (Cohen et al., 2010a,b).

Also in IC and the upper MC, the important summertime upper tropospheric anticyclone, depicted as a large counterclockwise flow in Fig. 6(f), is a result of convection associated with the Indian monsoon (Figs. 2(d) and 6(b)). This demonstrates a mechanism of convective pumping of lower atmosphere constituents from India into the upper troposphere and perhaps lower stratosphere (Gettelman et al., 2004; Jiang et al., 2007; Lau and Ploshay, 2009; Randel et al., 2010; Vernier et al., 2011).

The monsoonal meteorology, coupled with SEA's complex orography, leads to a high frequency of severe thunderstorms and lightning. Lightning frequency is often used as an indicator of severe storms as well as a metric for storm intensification due to the impact of aerosol particles (Hamid et al., 2001; Yuan et al., 2011). A climatology of SEA combining nighttime cloud-to-cloud and cloud-to-ground lightning is presented in Fig. 6(e) and (f) based upon the LIS/OTD 0.5 Degree High Resolution Monthly Climatology (HRMC) datasets produced and archived at the NASA's Global Hydrology Resource Center (Christian et al., 2003a). Best-available detection efficiency corrections and instrument cross validations (Boccippio et al., 2000; Boccippio et al., 2002; Christian et al., 2003a), as of the product generation date (09/01/06), have been applied. A 2.5°×2.5° spatial smoothing is applied to each 0.5°×0.5°grid box. As one would expect, lightning over SEA is concentrated over land, with very specific hotspots, particularly around Sumatra and the Malay Peninsula in the MC (Sow et al., 2011), and southern Vietnam/Cambodia and Thailand in the IC. Interestingly, lightning hotspots are over major population areas, including one which covers Kuala Lumpur and Singapore, and a second significant maximum over Ho Chi Min City, with smaller peaks in the vicinity of Bangkok and Manila. SEA is well known for frequent electrified storms (e.g., Zipser et al., 2006), although not as intense as other tropical locations such as central Africa. An example of a thunderstorm with significant lightning activity on the Malay Peninsula can be found in Sow et al. (2011). Convection over land follows the typical diurnal cycle of surface heating; clear mornings, cumulus and cumulus congestus in the early afternoon and thunderstorms by 5–6 LST. Over ocean, convection and precipitation reaches a maximum at ~6 AM, hypothesized as due to cloud top cooling (Yang and Smith, 2006; Yang et al., 2008). A line of lighting activity is also visible along the southern and northwest coasts of Borneo in the winter and summer monsoon, respectively. This is likely a result of convection spawned by island coastal sea breezes.

4.2. Meteorological scales

The two phase view of SEA meteorology in this section is enlightening, but one must consider that the monsoon is an evolving entity. Even in the middle of a season, the monsoon has active and weaker periods. Clouds and convection wax and wane on multiple time scales. For biomass burning in particular, we will later show that monsoonal transitional periods are critical. Often the classic seasonal meteorology (e.g., DJF, MAM, JJA, SON) is insufficient to describe the aerosol environment. If one wishes to move from the qualitative to even the semi-quantitative, one must consider SEA's many highly interrelated climate and meteorological features. Nominally there are five atmospheric scales of concern over greater SEA, from largest to smallest: 1) Interannual features such as El Niño Southern Oscillation (ENSO Rasmusson and Wallace, 1983; Mcbride et al., 2003), ENSO Modoki (Ashok et al., 2007) and the Indian Ocean Dipole (IOD, Saji et al., 1999; Saji and Yamagata, 2003; Schott et al., 2009); 2) Seasonal migration of the Intertropical Convergence Zone (ITCZ) and its associated summer and winter monsoonal period and transitions (Chang et al., 2005a; Moron et al., 2009; Wang et al., 2009); 3) Intraseasonal synoptic phenomenon such as the 30–90 day oscillation or the Madden Julian Oscillation (MJO) (Madden and Julian, 1971; Zhang, 2005; Wu and Hsu, 2009; Wu et al., 2009), the quasi-monthly oscillation (Wang et al., 2006), Borneo Vortex (Chang et al., 2005b), the west Sumatran low (Wu et al., 2009a), or at the most northern extent of our domain, the Meiyu front (Ding, 2002; Ding and Chan, 2005); 4) Wave and mesoscale features such as fronts and tropical cyclones (Goh and Chan, 2010) in northern SEA, and equatorial waves, such as the Kelvin, Rossby, and Easterly waves in the MC (Wheeler and Kiladis, 1999; Kiladis et al., 2009), tropical cyclones, or mid-level dry tongue (Ridout, 2002; Yasunaga et al., 2003; Zhang et al., 2003); and 5) Regional convection from localized weather phenomena, such as fair weather cumulus, orographically modified flows, thunderstorms, isolated small or trade convection, convective cold pools, sea breeze circulation, etc. (Schafer et al., 2001; Yang and Smith, 2006; Mahmud, 2009a,b; Mahmud, in press; Li et al., 2010; Sow et al., 2011; Zuidema et al., 2012). It must be recognized that the meteorology of SEA has interconnecting influences among all of the above meteorological scales.

In the context of this review paper, we cannot even briefly discuss all of these scales other than provide the example

references above. However, all of these phenomena are important and need to be recognized when aerosol–cloud interaction studies are undertaken. Of particular note is the importance of ENSO. Boreal summer precipitation over the MC is strongly negatively correlated with ENSO indices, and these dry periods can carry over all through the following spring (McBride et al., 2003), a fact punctuated by the massive accompanying fire event of 1997. Nominally, El Niño conditions result in an eastward shift or extension in the summer monsoonal trough and the Walker circulation, along with cooler sea surface temperatures surrounding the MC. Significant precipitation deficits begin immediately at El Niño formation in the Boreal spring to early summer, and follow into the following spring. Each island and sub-region has a different precipitation and fire sensitivity to ENSO (Reid et al., 2012). While overall precipitation is reduced, a significant increase in lightning activity over SEA with ENSO has been detected (Hamid et al., 2001; Satori et al., 2009).

A second area worth expanding on is the Madden Julian oscillation, reviewed by Zhang (2005). The MJO is a large scale, coupled pattern of a meso-synoptic scale circulation and deep convection which forms in the Indian Ocean and propagates eastward at ~5 $m\,s^{-1}$ through and around the MC and into the Pacific Ocean. Once this convective region passes into the central/eastern Pacific and decays, a new event may start in the Indian Ocean, thus repeating the cycle. Subsidence, and consequently negative precipitation anomalies, leads and lags this convective region, with the more dominant subsidence being observed on the eastern side when the convective region is in the Indian Ocean, and on the western side when the convective region is in the Pacific. Thus, from an aerosol point of view, the wet and dry phases of the MJO largely dictate the timing of significant smoke events in the MC (Reid et al., 2012), and the MJO was hypothesized to influence overall AOD (Tian et al., 2008). The amplitude of the MJO is the strongest in boreal winter and early boreal spring with a secondary maximum in boreal summer (Zhang and Dong, 2004). In the boreal summer the convection associated with MJO propagates eastward and northward, contributing to the Asian monsoon active and break cycles. With its 30–90 day cycle, we can expect 1–2 MJO cycles to occur during any fire season. In regard to El Niño, there is no simultaneous correlation between the MJO and ENSO SST, but the MJO is usually stronger prior to the El Niño peak (Zhang and Gottschalck, 2002).

4.3. Clouds in SEA

The meteorology associated with the wet and dry monsoon can also be examined in the context of cloud properties. Indeed, aerosol indirect effects are a dominant topic area of research in the atmospheric science community. Further, as is shown throughout this review, the high frequency of clouds in SEA, and in particular the ubiquity of high thin cirrus (e.g., Fig. 4), likely leads to artifacts in aerosol products generated from a variety of remote sensing instruments. Clouds also dominate SEA's Top-of-Atmosphere (ToA) radiation budget (Feng and Christopher, 2013-this issue; Section 8). A clear understanding of each instrument's strengths and limitations allows one to better interpret the discrepancies between instruments and products and turn differences into knowledge.

To allow a clearer view of the multiple cloud layers, we turn to MISR for a baseline cloud climatology to start our discussion. MISR's stereoscopic technique measures the altitude in which maximum spatial contrast occurs (Moroney et al., 2002). This typically originates from the clouds that contribute the most to the top-of-atmosphere shortwave fluxes. The presence of thin cirrus above these clouds does not degrade the precision in the stereo-retrieved altitude, which has been validated to ~560 m. As with all polar orbiting satellites, one must be mindful of the relationship between orbit and the strong diurnal cycle of convection. For clear sky aerosol purposes, the AM (sun-synchronous) orbit of MISR is an advantage. While major over land convection is not seen, boundary layer clouds are visible.

Fig. 7 presents ten-year statistics from MISR's Cloud Fraction By Altitude (CFBA) product (Di Girolamo et al., 2010a). Fig. 7(a) and (b) show that total cloud during the dry and wet periods generally follows the precipitation fields presented in Fig. 6(a) and (b). The IC has distinct clear and cloudy regions anti-correlated with the monsoonal trough. The MC however shows generally high cloud cover regardless of season, with only slight clearing in the boreal summer monsoon for the island chain from Java through Timor. Cloud fractions appear to be distinctly lower over land than over water, but part of this is artifact related to the difficulty of detecting thin cirrus with MISR over land compared to water (Section 4.2).

The cross sections provided in Fig. 7(c)–(h) help to provide a 3-dimensional view of cloud cover over SEA. Again, one must keep in mind MISR's retrieved cloud-top altitudes are from the clouds that produce the maximum spatial contrast, which tend not to be the thin cirrus such as that form in the TTL. We note a tri-modal distribution in cloud top heights, with a boundary layer mode (~0.5–1 km), a midlevel mode of perhaps cumulus congestus or altocumulus (~6 km) and an upper level mode of deep convection or thick cirrus (~15 km). This is consistent with the report by Johnson et al. (1999) and papers thereafter. A signal from thin TTL cirrus is absent. As expected, these modes spread northward during the boreal summer monsoon period. We also note the high boundary layer cloud fraction over the region, typically with cloud top coverage peaking in the 500–1000 m altitude bin over water, and 1 km to 2 km above ground altitude over land, corresponding well to the expected ~500 m marine boundary layer (MBL) and ~2000 m planetary boundary layer (PBL) heights. In context, the RGB images provided in Fig. 3 are considered to be some of the best days available over the 10 year MODIS data record for surface and aerosol imagery. Even here cloud fraction is high.

Interestingly, the MISR CFBA demonstrates an important yet largely unstudied regional boundary layer cloud feature that exists in Northern Vietnam. Each November through April, a thick stratocumulus feature, known locally as the "Crachin," frequently forms in the Gulf of Tonkin. This synoptically induced drizzly cloud feature is almost entirely unstudied in the peer-reviewed literature, but is well forecast by local meteorologists (as well as noted in Vietnam tourism guides). The deeper nature of these clouds, making them capable of forming drizzle, is nicely picked up by MISR in Fig. 7(e). Given its location as a receptor for many major sources (Section 5), these could be among the most

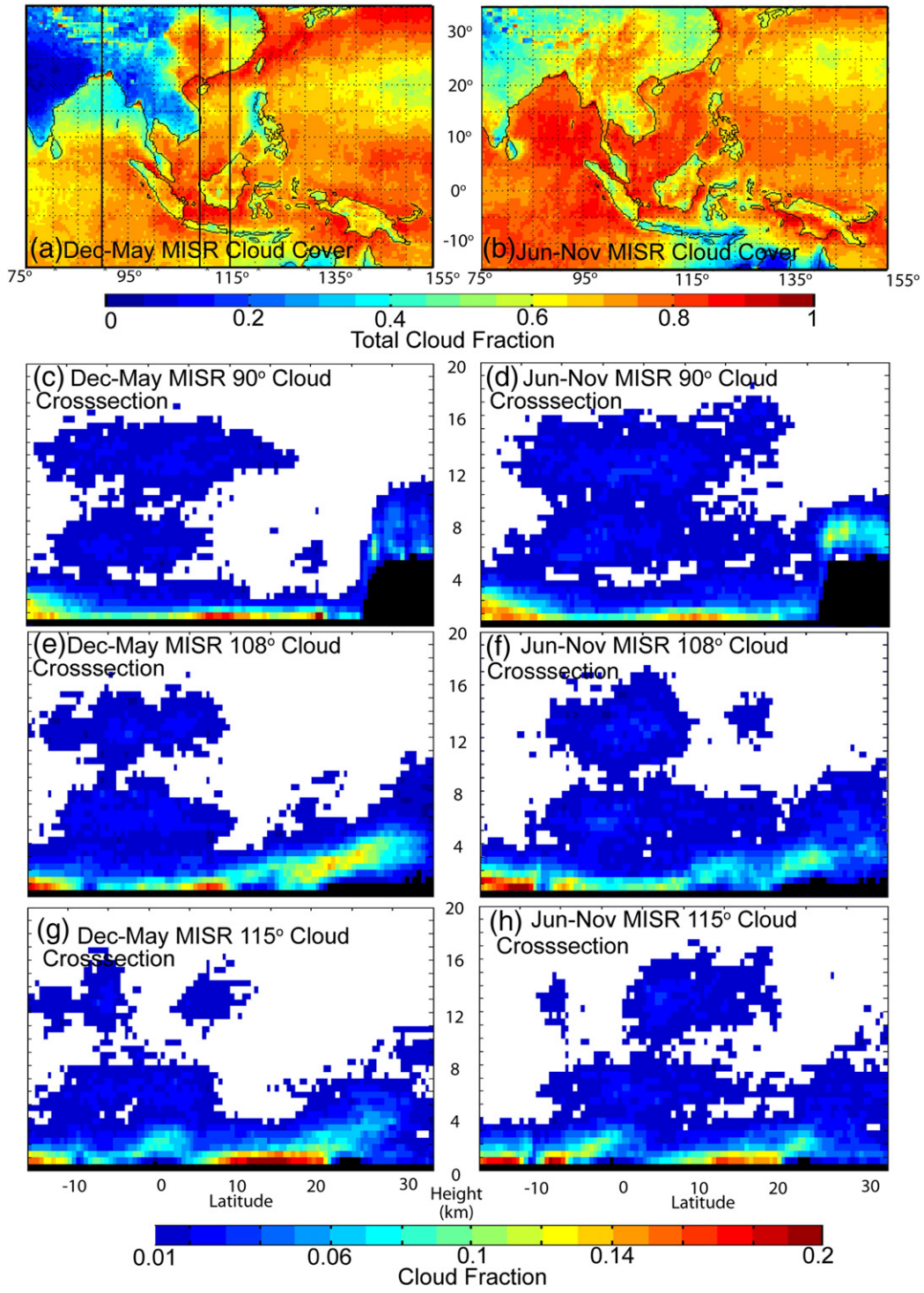

Fig. 7. MISR Level 3 2001–2010 cloud fractions statistics (Di Dirolamo et al., 2010) for Southeast Asia divided by December to May winter and June to November summer monsoonal periods. (a) and (b) Total integrated cloud fraction.; (c) and (d) respective latitude-height crosssections for 90o East; (e) and (f) respective latitude-height crosssections for 108o East; (g) and (h) respective latitude-height crosssections for 115o East.

polluted stratus on the planet. The combination of this stratus deck with smoke transport aloft makes an interesting study area for absorbing aerosol particles over clouds (Hsu et al., 2003).

Returning to cirrus aloft, we do see a broad spread of clouds between 11 and 16 km, but clouds in this vertical band are known to be significantly underestimated by current satellite products. For MISR, we expect a minimum required cloud

optical depth of 0.3 for detection. Recent progress has been made in improving the sensitivity of MISR thin-cloud detection, which is not reflected in the data shown here (Pierce et al., 2010). For cloud overlap situations, MISR will key on the cloud with the highest contrast, likely those that are opaque. Optically sub-visual and thin cirrus are known to be ubiquitous in the tropics, and the MC in particular owing to the western Pacific Warm Pool. For example, Wang et al. (1996) using SAGE II found over 60% sub-visual cirrus fractions over the MC in the 12–17 km height range, compared to <10% of totally opaque cirrus. Most recently with Cloud–Aerosol Lidar and Infrared Pathfinder Satellite Observations—CALIPSO data, Virts and Wallace (2010) found ~20% thin cloud fraction for cirrus over 15 km in height.

As part of the study of cirrus cloud properties and their impact on AOD retrievals, Robert Holz (Personal communication 2012) gridded the CALIPSO 5 km product and derived statistics of cirrus cloud coverage, height and optical depth. An example of these for the 2007 August–October biomass burning season is presented in Fig. 8. Fig. 8(a) shows total cloud probability. Over most of SEA, cloud fractions are above 80%, only decreasing below this number south of Borneo. This corresponds with the dry line latitude in Fig. 6(b). Cirrus top heights are on the order of 6–15 km and largely match the cloud tops from MISR (Fig. 7). These are likely a combination of convective and TTL cirrus (Fueglistaler et al., 2009; Virts and Wallace, 2010). Holz et al. (2012, in preparation) examined in particular properties of cirrus clouds which allowed the CALIPSO beam to penetrate (i.e., un-attenuated cirrus cases). In such cases we find mean cirrus cloud optical depths on the order of 1–1.5 over the MC, and over 2 for the IC (Fig. 8(c)). However, this is predicated on the beam penetrating the cloud. For aerosol studies, we are perhaps most interested in thin cirrus such as forms in the TTL. Given that on average over the region for this period, aerosol AODs are estimated to be between 0.2 and 0.4 (e.g., Fig. 1), a reasonable thin cirrus cutoff optical depth of 0.3 is appropriate for comparison (Fig. 8(d)). Over the MC, we typically find that 25–50% of the time cirrus clouds are optically thin. If cloud screening and other quality control procedures in retrieving AOD are not strict in removing thin cirrus, the potential for cirrus contamination in the AOD retrievals is high. This suggests that from an aerosol radiation point of view, the atmosphere should be treated as a two layer system — thin cirrus aloft and aerosol particles below.

4.4. Variability in satellite cloud properties in SEA

Already from Section 4.3, it is clear that satellite cloud data products are weighted to different parts of the cloud system, depending on the satellite instrument utilized. Numerous global satellite cloud products are publically available and commonly used by investigators. Depending on the scientific investigation, the choice of satellite product will

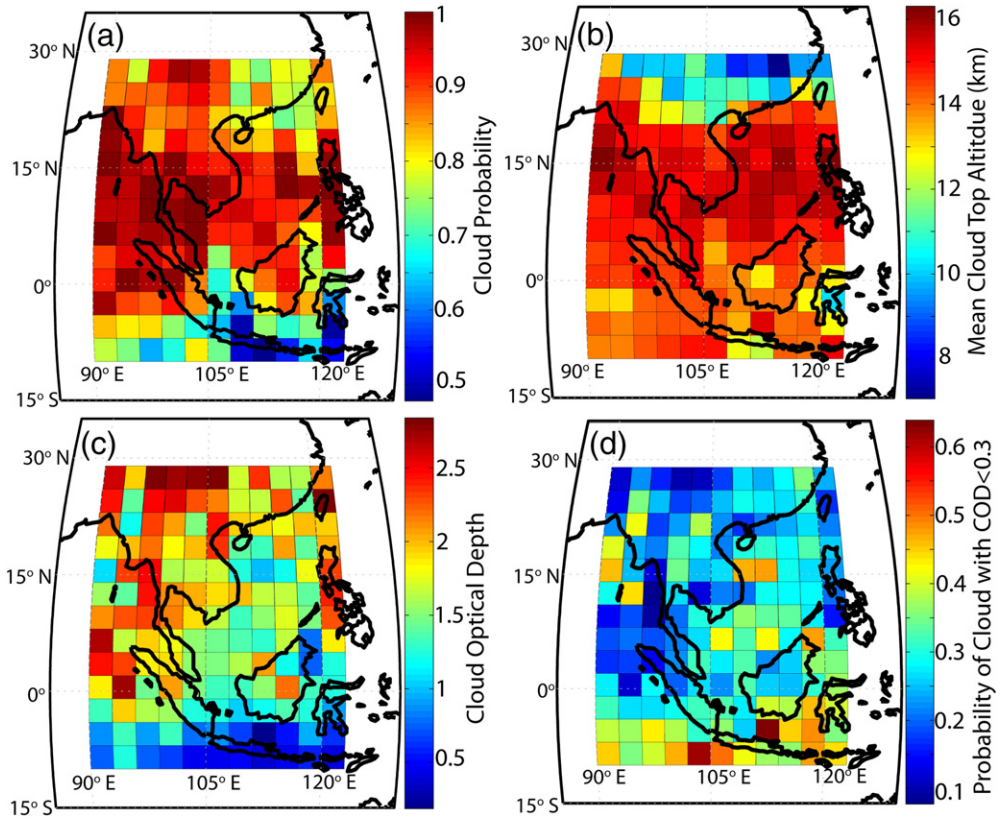

Fig. 8. CALIPSO cirrus cloud statistics for 3×3 degree grids from August to October 2007, derived from the CALIPSO Level 2 5-km Cloud Profile product. (a) Total cloud probability. (b) Mean cloud top altitude for cloudy fields of view. (c) Mean cloud optical depth (COD) for non-attenuated retrievals. (d) Probability of the total cloud column exhibiting COD <0.3.

often have important ramifications. In isolated case studies, experienced investigators can control for differences and hence sequester potential bias. Difficulty emerges is in the transition from case study to climatology, anytime a large number of samples is required, and in the subsequent interpretation of such climatologies by a broader scientific community who may be less familiar with the details of its generation.

An assessment of cloud product variability in SEA is far outside the scope of this review. But it is worthwhile to elucidate recent findings of the GEWEX Radiation Panel, under a Cloud Assessment Working Group, who are currently examining a variety of products which see widespread use. Datasets being evaluated include International Satellite Cloud Climatology Project (ISSCP), Pathfinder Atmospheric Science dataset (PATMOS-X), High Resolution Infrared Sounder (HIRS), TIROS Operational Vertical Sounder (TOVS) Path-B, Atmospheric Infrared Sounder (AIRS), MODIS-Science-Team, MODIS-CERES-Science-Team, MISR, POLarization and Directionality of the Earth's Reflectances—POLDER, CALIPSO and Global Retrieval of ATSR Cloud Parameters and Evaluation—GRAPE. The report continues to evolve (Stubenrauch et al., 2011), and challenges in interpreting differences in cloud properties amongst the datasets continue to be tackled. It is of paramount importance to note that SEA is a region where the greatest differences amongst satellite cloud datasets exist. For example, Fig. 9 shows the 2000–2007 total, high, middle, and low (as defined by ISCCP) cloud-top fraction from a diverse set of instruments for retrieving cloud top: MISR (multi-angle stereo), MODIS (CO_2-slicing and temperature), ISSCP (temperature), and CALIPSO (lidar). This face value comparison is provided for the (a) December–May and (b) June–November monsoonal periods.

In Fig. 9 the CALIPSO lidar, arguably the most sensitive instrument for thin cirrus detection, shows greater than 90% cloud cover over half of the SEA domain, much of which comes from high clouds. The noisiness of the CALIPSO climatology is caused by the low number of samples provided by CALIPSO (Astin et al., 2001). MODIS has the second largest high cloud amount, owing to the sensitivity of the CO_2-slicing technique for thin cirrus detection, but also due to strong view-angle dependence in cloud cover across the MODIS swath (Maddux et al., 2010). ISCCP carries less sensitivity to thin cirrus detection. It shows the greatest fraction of mid-level clouds, but this is an artifact of the blackbody temperature technique placing low-emissivity high cirrus at lower altitudes. MISR, as discussed in Section 4.1, has less sensitivity in detecting thin cloud when greater spatial contrast surfaces (either from land or lower clouds) lie below. The result is a greater frequency in detecting low clouds, as evident in Fig. 9. The dip in total cloud cover over land is partly due the dominance of thin cirrus, and the lower contrast between surface and cloud over land relative to water for the MISR spectral channels. Over low contrast surfaces, such as water, thin cirrus is more readily detectable by MISR stereo if they do not overlap over lower clouds. Note that while these plots show large differences amongst the datasets, these differences can be interpreted into meaningful information about cloud properties when one is familiar with the remote sensing techniques used to generate these datasets, a point that is nicely explored further in Marchand et al. (2010).

It is important to note that differences in these cloud datasets do not necessarily represent the level of cloud contamination that would be present in global datasets of aerosol properties. Aerosol retrievals, for example as performed by MISR and MODIS, use a different set of cloud masks and quality control procedures that lead to a much more clear-conservative mask (that is, a highly aggressive cloud mask). However, the dominance of thin cirrus in the SEA region brings into question the potential for greater cirrus contamination in global aerosol products in the SEA region compared to any other snow- and ice-free region of the world.

Cloud optical properties are also quite varied amongst satellite datasets and differences are relevant to studies of aerosol impacts on clouds. This issue continues to be examined by the GEWEX Cloud Assessment Working Group, and given the dominance of thin cirrus in the SEA environment, it remains a continuing problem for the community. Indeed, assumptions in the retrievals lead to sampling differences, changing what is included in the climatologies. Difficulties also arise in assigning a proper crystal habit during the retrieval. But even for water clouds, the structural characteristics of these clouds in our SEA domain strain the common plane-parallel assumption within the cloud retrieval algorithms, even under high-sun conditions. This point is explored in detail in Di Girolamo et al. (2010b).

4.5. Satellite precipitation products in SEA

Like clouds, precipitation monitoring in the MC is challenging. Given the strong coupling between precipitation, fire, emissions, and perhaps feedbacks between them, an understanding of the precipitation fields in SEA is critical. Of the four primary sources (rain gauge networks, ground-based radar, satellite methods-including radar/passive microwave, and NWP model analyses) only the last two are viable sources over ocean. Over land, rain gauges have spatial sampling biases and radar data, while collected, have uncertain calibration and are largely unavailable to the public. Over both land and water, NWP tropical precipitation estimates have been shown to have qualitative skill and adequate performance at capturing tropical rainfall amounts at monthly and seasonal scales. However, models have difficulty resolving the timing and magnitude of daily or even weekly convection (Adler et al., 2001; Mahmud and Ross, 2005; Dai, 2006; Sun et al., 2007; Xian et al., 2009).

Fortunately, there is an ample supply of satellite-based precipitation data over the MC. Most importantly, the joint NASA and Japanese Space Agency—JAXA Tropical Rainfall Measuring Mission (TRMM) continues (as of early-2012) to collect joint passive microwave (PMW) and Ku-band (14 GHz) precipitation radar (PR) observations since late 1997. One common characteristic of all passive microwave (PMW)-based precipitation estimates such as the TRMM Microwave Imager (TMI) and the Advanced Microwave Scanning Radiometer (AMSR-E, onboard Aqua) is that they are far less sensitive to light rainfall over ocean, and it is likely that they underestimate light events or miss them completely. Over land, the PMW algorithms are based on hydrometeor scattering and often retrievals have difficulty detecting non-convective precipitation. Therefore these PMW-based precipitation datasets carry information on convective and some stratiform precipitation

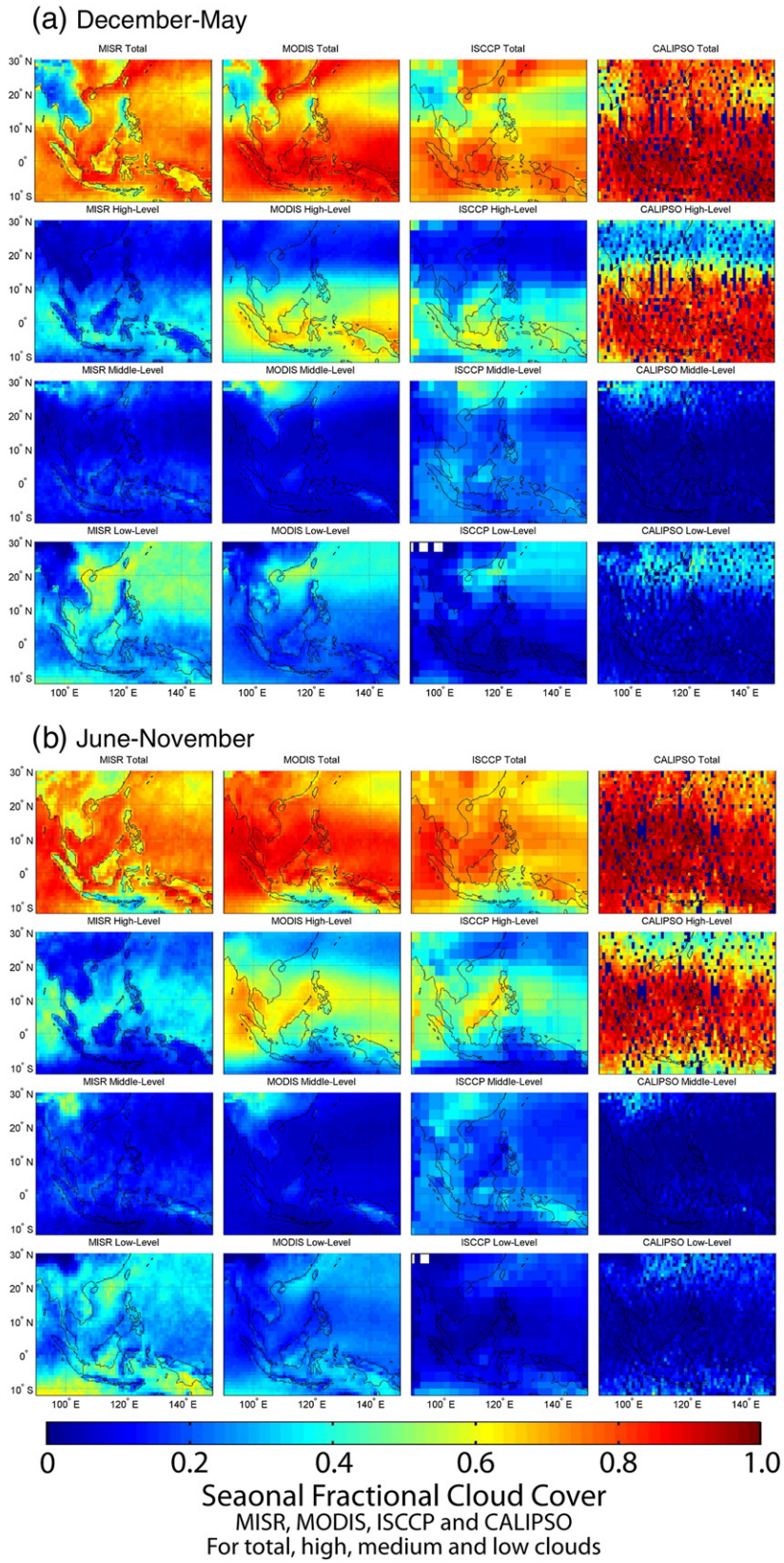

Fig. 9. Total, high, middle and low cloud fraction (as defined by ISCCP) for the (a) December–May and (b) June–November periods. Periods used in average are 2001–2009 for MISR and MODIS, 2000–2007 for ISCCP, and 2007–2008 for CALIPSO. This figure was drawn from the ongoing GEWEX cloud Assessment dataset.

over ocean, and mainly evolution of convective precipitation over land. As an active sensor, the PR can directly observe precipitation near the surface, with a lower detection limit near 1–2 mm h^{-1}. Owing to different responses to subtle variations in rainfall microphysics, the TRMM radar and radiometer do not always agree. Berg et al. (2006) concluded that differences between precipitation retrieved from TMI and PR were correlated with column water vapor, and that enhanced aerosol concentration also may contribute to abnormally high liquid water contents within non-precipitating clouds. Hence, aerosol impacts may covary with cloud observability, even when we may expect to see cause and effect the most (e.g., during high biomass burning emission events).

Currently, TRMM is well beyond its expected life but will continue to collect observations until it exhausts its station-keeping fuel supply (largely determined by the solar cycle), after which it will begin its gradual deorbit. There is a possibility that TRMM will overlap with the upcoming (2013) NASA/JAXA Global Precipitation Measurement (GPM) mission (Hou et al., 2008). The core GPM spacecraft will deploy an advanced dual-frequency (Ku/Ka-band) radar, and like TRMM will orbit sun-asynchronously but in a 65 degree orbit inclination. Throughout the next several years, the joint French CNES and Indian Space Research Organization-ISRO Megha-Tropiques satellite (also orbiting asynchronously in a 20-degree inclination), JAXA's Global Change Observing Mission (GCOM-W), and the Chinese Meteorological Agency (CMA) FY-3 series are scheduled to be launched, all with payloads including a PMW imaging radiometer.

In SEA, the cellular nature of quickly evolving convective precipitation is not well captured by an intermittently spaced sequence of low Earth-orbiting (LEO) satellite overpasses from TRMM or Aqua. Moreover, since precipitation algorithms based on satellite instruments do not directly observe the underlying flow and topography, they tend to have systematic biases over complicated scenes such as are present in SEA and the MC in particular. For sub-daily time scale High Resolution Precipitation Products (HRPP), nearly all satellite-based techniques utilize the fast-refresh observational capabilities from imagers onboard one or more geostationary earth orbiting platforms. In recent years, a series of satellite-based and model-based precipitation validation experiments performed under the direction of the International Precipitation Working Group (IPWG) has shown that NWP models tended to underperform these multi-satellite based precipitation techniques (on a daily, 1/4-degree scale) in the tropics, with the opposite behavior for the mid-latitudes and cold seasons [Ebert et al., 2007]. Since the HRPPs rely upon the PMW-based precipitation estimates to either advect or adjust IR radiances into precipitation rates, these same characteristics are eventually carried over to each HRPP. The closely packed land-sea boundaries which are characteristic of the MC can bring further uncertainty, since there are different algorithms for over-water and over-land backgrounds, relative to the fairly coarse scale of the PMW observations (~25 km). Nonetheless these datasets have attained a high degree of utilization owing to their extended record, for example the Global Precipitation Climatology Program (GPCP), available back to 1979 [Huffman et al., 2007].

Unlike HRPP techniques that use geostationary data to quantitatively assign precipitation rates, for example the GPCP product, transport-style HRPP techniques use geostationary data in a qualitative fashion, to transport precipitation between adjacent LEO (i.e., PMW-based precipitation) satellite revisits. Examples of these products include the Climate Prediction Center (CPC) MORPHing technique (CMORPH) (Joyce et al., 2004) and the Global Satellite Mapping of Precipitation (GSMaP) (Ushio et al., 2009). Analyses are based mostly on the CMORPH data gridded at a three-hour and one-quarter degree (latitude and longitude) resolution as these data are available in a consistent form since early 2002.

Ultimately, all satellite products need a firm footing for verification within SEA. Despite the sparseness of rain gauges in SEA land areas, the half-degree global Unified Gauge Analysis (Chen et al., 2008), produced by the National Oceanic and Atmospheric Administration (NOAA) Climate Prediction Center (CPC), is commonly employed for verification globally and the MC. The Asian Precipitation-Highly-Resolved Observational Data Integration Towards the Evaluation of Water Resources (APHRODITE) analysis of Yatagai et al. (2009) is now seeing usage (Jamandre and Narisma, 2013-this issue). While no fully comprehensive satellite validation study has been conducted in SEA, CMORPH in general appears to have the best representation of temporal and spatial patterns of tropical precipitation and complex terrain (Janowiak et al., 2005; Dinku et al., 2008; Sapiano and Arkin, 2009; Shen et al., 2010). Even so, systematic biases exist in the individual satellite products used in the morphing algorithm (Sapiano and Arkin, 2009; Wolff and Fisher, 2009). In a limited comparison, CMORPH consistently underestimated precipitation by ~30% compared to the CPC gauge estimate on the monthly timescale over land in the MC (Reid et al., 2012), opposite in sign to the global bias reported by Sapiano and Arkin (2009). Jamandre and Narisma (2013-this issue) found both TRMM and CMORPH to underestimate precipitation in the Philippines, and yet had correlations on the order of ~70%. Given the inadequacies of gauge estimates as well, such diversity cannot currently be reconciled. But, such diversity does demonstrate the relative amount of baseline uncertainty in these products.

Like all satellite products, the relative utility of the satellite precipitation products in SEA depends on application, and studies must account for their uncertainties in the experiment plan. As is typical, they clearly qualitatively capture precipitation features. Interannual variability is also well captured giving confidence for their semi-quantitative use. However, the utility of these products for quantitative uses is an outstanding issue for SEA meteorology in general. Linkages between precipitation and other products, such as aerosol retrievals, require significant scrutiny in SEA.

5. Biomass burning

Based on our knowledge of regional geography and meteorology, in this section we examine the nature of fire and smoke particle emissions in SEA. Fire is a deeply rooted agricultural instrument in SEA, and the region's rapid economic development suggests that fire use may currently be in a transitional period. The scientific community has been

captivated by the large biomass burning events in Indonesia associated with El Niño. Extreme episodes of fire activity in the Maritime Continent have been largely linked to peat burning. While the largest events are indeed associated with these El Niño peat burning regimes, fire activity and smoke emissions in the Maritime Continent are important in all years. Indochina, which actually has higher observed fire prevalence compared to the MC, has received much less attention; this is despite significant deforestation there as well. We briefly compare two biomass burning emission products based on active fire hot spot and burn scars (FLAMBE and GFED3.1), and show that while there are broad similarities, there are regional differences between them as large as an order of magnitude in some areas. This comparison, which demonstrates diversity between products, does little to aid in actual verification. Comparisons of products derived from meteorological satellites to high-resolution imagery or in situ observations unanimously show that such products significantly undersample true fire activity and emissions. These products can capture broad spatial and temporal patterns of fire activity, but their quantitative use requires significant statistical adjustment.

5.1. The nature of biomass burning emissions in SEA

Because of the publicity associated with Indonesian fire events, the public and scientists alike often associate SEA aerosol pollution with biomass burning; hence SEA aerosol research tends focuses on this aerosol source. The very strong 1997 El Niño (Wolter and Timlin, 1998) and its associated fires largely in Indonesia drew worldwide attention to burning and peat forest deforestation in the MC. Burning associated with agriculture, including rice, sugar cane, and pasture as well as deforestation burning, are common seasonal features throughout SEA. However, with frequent long range transport events into the Pacific basin (Giglio et al., 2006; Gadde et al., 2009; Lin et al., 2009; Reid et al., 2009), emissions from SEA fires, especially peatland fire, make a significant contribution to atmospheric composition and climate change (Page et al., 2002; van der Werf et al., 2004; 2010; Ballhorn et al., 2009). Vegetation fires cause serious smoke pollution and trans-boundary haze episodes throughout SEA (e.g., Qadri, 2001). Overall, biomass burning in SEA is associated with poor air quality and widespread environmental decline (e.g., Kunii et al., 2002; Dawud, 1998; Balasubramanian et al., 1999; Aditama, 2000; Kunii et al., 2002; Zhan et al., 2002; Zhang and Oanh, 2002; Tipayarom and Oanh, 2007; Wiwanitkit, 2008; Pengchai et al., 2009; Hyer and Chew, 2010; Silva et al., 2010; Sundarambal et al., 2010; Oanh et al., 2011).

Biomass burning is also often a proxy, or at times confounder, for other land use processes. While rapid regrowth of secondary forest at times prevents a clear "arc of deforestation" seen in other tropical regions, fire activity can nonetheless help indicate land change practices at work (e.g., Stolle and Lambin, 2003; Miettinen et al., 2010). Peat fires themselves are often thought of as being directly responsible for large carbon emissions. However, carbon emissions directly from burning may be small fraction of the total carbon released due to land use conversion. Decadal scale microbial emissions that occur after peatland is drained and more susceptible to aerobic decomposition may in fact be a more dominant CO_2 source (Leifled et al., 2011; Hooijer et al., 2011).

5.2. Socio-economics of biomass burning in Southeast Asia

Throughout SEA nearly all fires can be considered to be of anthropogenic origin, and fire is strongly connected to land use practices in the region. Open burning is used for disposal of crop waste/residue, preparation of agricultural fields, maintenance of open understory, stimulation of grass growth, forest clearing and conversion to cultivated lands. This is done by large-scale commercial plantation developers, small-scale shifting cultivators, and small-holder farmers (Goldammer, 2006; Corlett, 2009). In addition, fires originally meant to be used for one of the abovementioned purposes may escape and develop into uncontrollable wildfires (Miettinen and Liew, 2009), a common occurrence in dry El Niño years (Section 5.2).

For studies focusing on fire and aerosol emissions, it is imperative to recognize the complexities associated with the anthropogenic origin of fire coupled with SEA's meteorology. Historically, deforestation, agriculture and fire are often viewed as part of a shifting agricultural system such as swidden (i.e., slash and burn). Forest clearing and harvest is followed by agriculture conversion. If the soil becomes depleted it may be then converted to livestock pasture, or allowed to lay fallow and reforest (Fukushima et al., 2008). The process can start again several years later. Swidden practices have a characteristic profile of emissions, with a strong pulse during the initial slash and burn, followed by agriculture or field maintenance fires (Corlett, 2009). Forest regrowth in the MC can be rapid, with secondary forests looking very similar, to the untrained eye, to the primary forest they replace in as little as 20–30 years. This is a property of many tropical regions that stands in contrast to other regions owing to year around wet conditions, and in the MC, volcanic soil fertility. Because of loss of sensitivity in passive visible/NIR observations at high leaf area index, secondary forests are sometimes indistinguishable from primary forest in satellite data, even though they may have substantially different carbon content (Pu et al., 2005).

Swidden agriculture is deeply ingrained in SEA socio-economics, and its associated fire activity has been practiced in SEA for over 9000 years (Maxwell, 2004). In fact, Maxwell (2004) suggests that IC fire activity may even have been greater in the past, in association with different climate conditions. While swidden slash and burn practices may have a poor reputation in the popular press, it is in reality one of the most sustainable agricultural methods on the planet provided cleared/burned areas are given ~15 years to regenerate carbon stocks (Montagnini and Jordan, 2005). Thus, swidden practices are ostensibly unsustainable in some regions in some areas with high population density.

Currently, swidden small holders are an important part of the SEA agricultural economy but they are underestimated in the population census and often not included in land use maps (Mertz et al., 2009; Schmidt-Vogt et al., 2009). This is changing as much of the land occupied by small holding swidden has been converted to persistent farming and agribusiness plantation agriculture (Padoch et al., 2007; Schmidt-Vogt et al., 2009). Even so, in some areas swidden practices remain persistent (Hansen and Mertz, 2006) and some organizations have formed to

advocate for small-holder (chiefly "orang asli" the "original people") interests (e.g. http://www.temiar.com/burning.html). Regardless, emissions dynamics in SEA may change as more land is permanently converted to agriculture and less forest regrowth is observed. A notable example of this is the very rapid destruction of peatlands in favor of oil palm plantations in Malaysia and oil palm and rice in Indonesia (e.g., Yule, 2010; Verhoeven and Setter, 2010). Because land cover conversion in Indonesia is often associated with fire activity and subsequently haze in the popular press and Indonesia is the largest country in the region, Indonesia is often highlighted in regard to peatland destruction in Sumatra and the Kalimantan provinces of Borneo. However, Sarawak, Malaysia on Borneo, also has high rates of peatland destruction and conversion (Miettinen et al., 2011a,b). Both Indonesia and Malaysia have banned agricultural burning since ~1998 in response to the haze problem, which peaked in 1997 (Suyanto et al., 2004; Mohd Noor, 2003). Implementation of zero burn techniques has been extremely problematic in both countries. The use of fire increases the availability of inorganic nutrients and eliminates pests and diseases. In the absence of fire more chemical fertilizers are needed and crop losses of 40–90% can occur from pests such as the rhinoceros beetle (Suyanto et al., 2004; Ooi and Heriansyah, 2005). Zero-burn techniques require large capital investments in machinery that are not remotely possible for small holders (Suyanto et al., 2004; http://www.temiar.com/burning.html). Zero-burn techniques are considerably more expensive than traditional methods even for large corporations (Suyanto et al., 2004). From a climate perspective, zero-burning techniques are more problematic as they tend to convert a larger percent of the cleared biomass to CO_2 (albeit via decomposition) and these techniques generate additional CO_2 and some aerosol thru operation of the large diesel equipment required to shred the large quantities of biomass. Thus, it is not clear if adoption of zero-burn techniques is desirable or prevalent. On one hand, once a day MODIS active fire detection in northern Borneo suggests reduced fire activity during prolonged drought compared to the peatlands of Kalimantan (Reid et al., 2012), but Hyer et al. (2013-this issue) found substantial burning in Malaysia outside of the MODIS overpass time using geostationary data.

In regard to other agriculture, the tropical environment provides good agricultural production. In both the IC and MC rice production is significant, as is sugar cane in Thailand. In these cases, the use of fire appears to be mixed. For rice cultivation (the dominant crop), depending on such factors as pest infestation or the current market for rice straw, rice straw may be collected for feed or biofuel, burned off, or plowed under (Yevich and Logan, 2003; Gadde et al., 2009). There has been an effort by the Thai government to convince farmers to plow under unused rice stubble rather than burn it. In practice, however, the fate of rice stubble is likely sensitive to a host of economic, political, social, legal, and meteorological factors. Rice and sugar cane demonstrate that even if crop characteristics are known, there are dynamic economic and cultural considerations when developing an emissions model (Yokelson et al., 2008).

Finally, a shift to oil palm plantation farming comes with its own emissions characteristics. Plantations need to be cleared and replanted every 10–20 years (Palm, 1999). Fire is clearly seen as a tool for such regeneration. For example, regeneration of oil palm plantations older than 15–25 years are associated with fire; younger ones are not (Stolle and Lambin, 2003). Given the rapid expansion of oil palms in the MC, if land management practices do not change, we surmise that a pulse of agricultural burning may occur in 10–20 years.

5.3. Observed fire patterns

A consistent regional picture of biomass burning in SEA requires the use of satellite remote sensing (although as we note in the next section we have reason to believe such information is only semi-quantitative). For demonstration purposes, Fig. 10 shows bi-monthly maps of average fire hot spot counts from the sum of the MOD/MYD14 product between 2003 and 2009 of MODIS Terra (~10:30 LST)/Aqua (~13:30 LST), respectively where a complete record exists (Justice et al., 2002; Giglio et al., 2003a). The seasonal cycle of observed fires follows a very clear pattern that is loosely opposite of the winter and summer monsoonal trough (Giglio et al., 2006; Reid et al., 2012). At the sub-continental scale, fire activity generally intensifies over the course of the dryer season, ending more abruptly with the onset of the rainy season. Even so, timing of fires during dry periods is heavily influenced by human decisions.

The winter monsoon is at its southernmost extent in January–February when, generally, IC burning begins to develop in Cambodia. Fire activity progresses through Thailand, Laos, and Myanmar, peaking in March, April and May, respectively and ending with the monsoonal transition from winter to summer in early May. In IC, significant open burning effectively ceases with the monsoon onset until the following late December/early January. May and June is a period of relative quiescence over all of SEA. Rains have stopped burning in IC, while in the MC farmers are harvesting and cutting forests and stacking fuel to allow drying. Significant burning associated with agriculture begins in central Sumatra in July, peaking in August. Peak fire activity then progresses eastward across the MC in time, with a maximum in Papua in November. The end date of burning in the MC also progresses eastward in time, as related to the eastward progression of winter monsoon onset in the MC (e.g., ending in Sumatra in late September, Borneo in October, Papua in mid-November, Moron et al., 2009; Reid et al., 2012). After another brief period of relative quiescence, the cycle then repeats itself beginning in late December and early January. The IC has almost no observed fire during the wet season, but there is some observed burning in the MC wet seasons. Central Sumatra appears to be capable of significant fire activity at any time of the year with a prolonged dry spell, as underscored by a significant event in early 2005 (Reid et al., 2012). Isolated portions of Borneo also exhibit occasional burning all year around.

By combining the reviewed fundamentals of geography, meteorology, and socio-economics, we can now attempt to explain at least some of the observed fire patterns in SEA, in particular in regards to interannual variability where coupled human and meteorological factors are likely at work. A time series of total MODIS Terra + Aqua fire counts for SEA derived from the data used in Reid et al. (2012) is presented in Fig. 10(g) (note that the scale for IC is 4 times that for the MC). To account

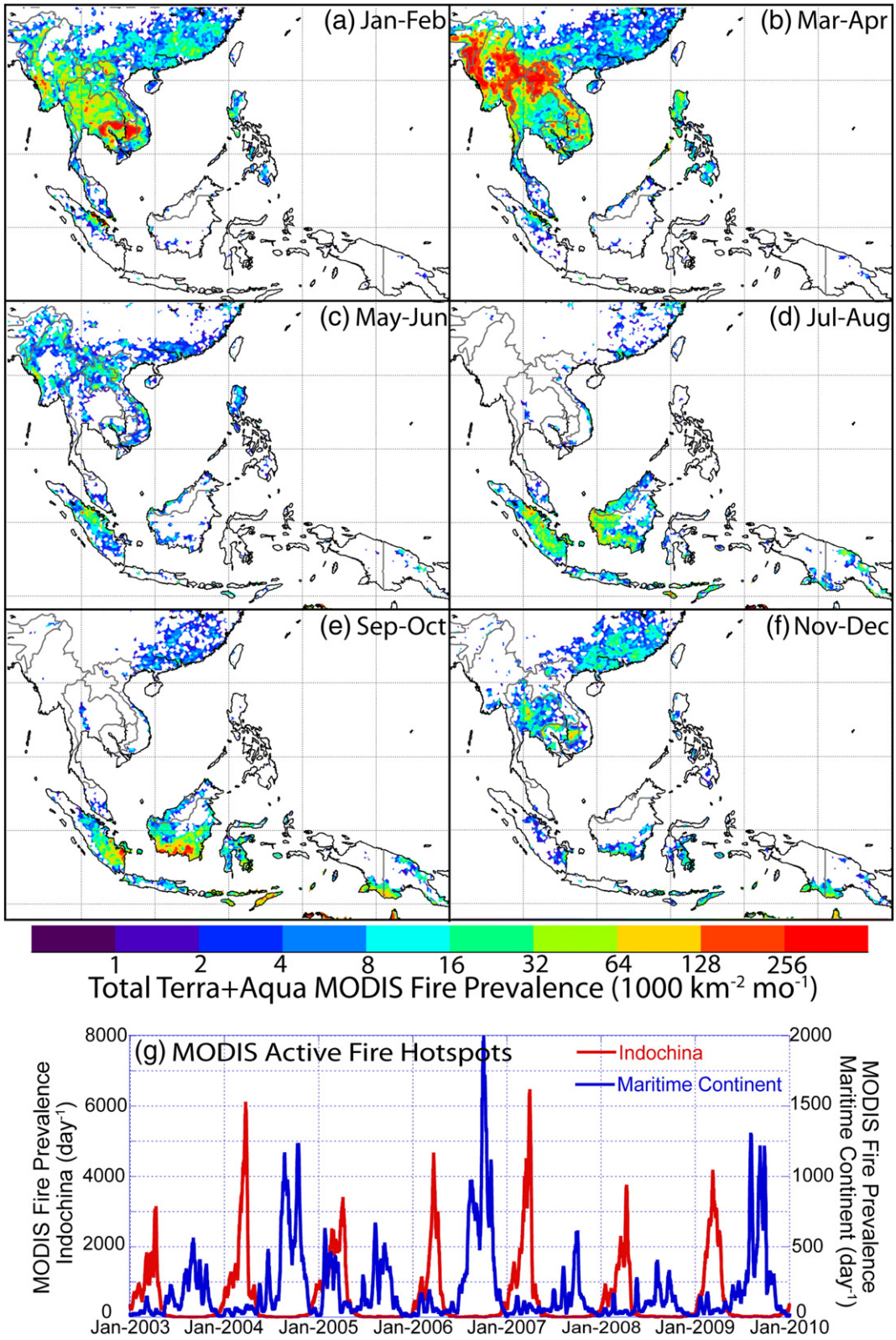

Fig. 10. (a)–(f) Bi-monthly (see corresponding inset) MODIS fire prevalence for 2003–2009 based on Giglio et al. (2006) and Reid et al. (2012). (g) Fire count time series for Indochina and the Maritime Continent for 2003–2009 derived from Reid et al. (2012).

for orbit variability and clouds, these data were smoothed with a 9 day boxcar average.

The interannual variability in observed fire activity across SEA is striking, particularly in the MC. Within IC, fire activity is a typically a ramp, starting in late December and peaking in April followed by a rapid falloff with monsoon onset. This is likely due to increased drying of fuels as the dry season progresses. At the end of the season, larger diameter fuels become combustible. Interannual IC average and peak fire prevalence for the 2003–2009 seasons was 190 k ± 50 k detected fires per year and 4.5 k ± 1.2 k per day, or roughly ±25% interannual variability. In the MC however, this is 70 k ± 35 k per year and 1 k ± 0.6 k day, or ±50–60%. As we discuss in the next sub-section, owing to the high cloud cover of the region, the MC numbers are likely a significant underestimate relative to the IC. Thick smoke from fires in dense fuels with capping cumulus clouds and widespread fair weather cumulous in the MC may also suppress fire detection (Csiszar et al., 2006; Fig. 3d), but this effect has not been quantified for SEA.

Indochina, with the exception of inventory work undertaken for Thailand (Vongmahadlek et al., 2009), to our knowledge does not have a systematic examination of interannual variation of fire in the literature. As discussed in Section 3.2 the IC burning season has considerably less cloud cover than its MC counterpart, thus allowing better remote sensing observability. Monsoonal behavior in Thailand is only weakly coupled in regard to ENSO (Cook and Buckley, 2009). As discussed in Section 5.1, fire is used for a variety of purposes in the region including deforestation, swidden, and agriculture burn off. The relationships between these burning behaviors and factors of meteorology or economics in IC are largely un-documented in the peer reviewed literature.

In the MC, extensive work has been published on interannual variability. The relationships between ENSO, negative precipitation anomalies, and overall fire activity are obvious (Nichol, 1998). Fire outbreaks were punctuated by the large events of the 1990s and more recently 2006 and 2009 fire seasons (e.g., Siegert et al., 2001; Stolle and Lambin, 2003; Parameswaran et al., 2004; Langmann and Heil, 2004; Wang et al., 2004a; Fuller and Murphy, 2006; Field and Shen, 2008; van der Werf et al., 2004, 2008; Langner and Siegert, 2009; Field et al., 2009; van der Kaars et al., 2010; Reid et al., 2012; Wang et al., 2013-this issue). The conceptual model of El Niño related fire activity is straightforward: warm phase ENSO/El Niño conditions lead to negative dry season precipitation anomalies in the MC (McBride et al., 2003). The eastward extension in the monsoonal trough and the Walker circulation introduces anomalous subsidence over the MC. El Niño also results in cooler waters around the MC, which may reduce maritime convection or latent heat flux; conversely during La Niña positive SST anomalies are located upstream of enhanced convection over the MC (McBride et al., 2003). Lasting negative precipitation anomalies result in an increase in flammability of fuels across the spectrum, as well as the draining of peatlands. Peatlands drained of moisture are, at some critical tipping point, ignited accidentally by adjacent agricultural maintenance fires, or deliberately for (frequently illegal) forest conversion fires (Stolle and Lambin, 2003; Vayda, 2006; Miettinen et al., 2011a,b). These peatland fires cannot be easily extinguished except by flooding; they last for days, weeks, or perhaps months at varying combustion rates until the rainy season starts (Miettinen et al., 2010). Because the region is under large scale subsidence and fires are in general larger, fire, smoke and burn scar observability is improved. Even Java, which does not experience significant boreal summertime precipitation, nevertheless shows an ENSO signal (Reid et al., 2012). The negative precipitation anomalies over the whole MC have the additional effect that smoke can be transported further (Reid et al., 2012; Xian et al., 2013-this issue). Thus, while warm ENSO years indisputably show extensive burning, the improved observability associated with the El Niño meteorology will exaggerate the effect in any basic statistical analysis of interannual variation in fire counts, the carbon budget or downwind aerosol optical depth.

The ENSO–precipitation–peat drainage relationship to fire activity in the MC is so strong it has been studied almost to the exclusion of all other meteorological and socio-economic scenarios. Agricultural waste burning is also a significant component of fire activity across the region, with less interannual variability and a closer proximity to human populations. Agricultural and deforestation fire activity will have different temporal patterns related to a host of meteorological sensitivities as described in Section 4.2, including the MJO and tropical waves (Reid et al., 2012). Stolle and Lambin (2003) studied both meteorology and social-economic factors driving fire in Sumatra for the period around and after the massive 1997 fire event. This study gives an excellent overview of the types of factors one should consider. For the 1997 El Niño year, they found that land use fires in Sumatra were set to take advantage of the dry weather. Most often fires were in forest areas set aside for agricultural conversions as well as old plantations which used the dry weather to burn off old trees scheduled for replacement. Fires in forested areas were shown to be heavily concentrated near roads, while in other land covers fires were relatively suppressed near roads. Conversely, small holders and swidden practitioners who often get the blame for burning activity did not appear to be as significant a contributor as large plantations. Fires were rare in areas where land use practice does not indicate burning, such as forests set aside for lumber production and newly established plantations. Conversely, in the wetter 1998 season, small holders and slash burning appeared to contribute more to the (much lower) overall amount of fire activity.

At finer time scales, fire activity is well known to have a strong diurnal cycle over the whole globe, peaking in the afternoon with a minimum early in the morning (e.g., Giglio, 2007); in SEA, this is also the case (Giglio, 2007; Reid et al., 2012; Hyer et al., 2013-this issue). However, as discussed in these papers, there is a fair amount of variability from location to location within SEA. For example, Giglio (2007) used TRMM VIRS to find that observed active hot spot fires peaked around 12:30 LST on Borneo, but 14:30 in IC. Widths and shapes of the fire peaks also varied. However at even finer resolution, Hyer et al. (2013-this issue) used geostationary MTSAT data to find more complexity, showing fire peaks in some regions as being after 15:00 — which is well outside MODIS viewing times.

5.4. Quantitative fire activity monitoring

Fire activity can be monitored using a variety of methods, including a) active fire hotspot with thermal signature fires

from polar (e.g., Advanced Very High Resolution Radiometer—AVHRR: Wooster and Strub, 2002; Flasse and Ceccato, 1996; Langner and Siegert, 2009; Along Track Scanning Radiometer-ATSR: Fuller and Murphy, 2006; van der Werf et al., 2006; MODIS: Justice et al., 2002; Giglio et al., 2003a, 2006); high inclination (e.g., TRMM Visible Infrared Scanner—VIRS: Giglio et al., 2000, 2003b; Giglio, 2007); and geostationary (e.g., Geostationary Operational Environmental Satellite-GOES: Prins et al., 1998; Prins et al., 2008; Reid et al., 2009; Multi-Functional Transport Satellite—MTSAT: Hyer et al., 2013-this issue) satellite sensors; b) burn scars from before and after images, which are compared to detect surface spectral albedo changes from both medium (e.g., ATSR: Simon et al., 2004; MODIS: Roy et al., 2005; Giglio et al., 2009; Miettinen and Liew, 2009) and high resolution (e.g., LandSat: Giri and Shrestha, 2000; Miettinen et al., 2007; SPOT: Liew et al., 1998) radiances; c) simple imagery, where individual fire plumes are observed and counted (Liew et al., 1998); and d) ground inventory (i.e., boots on the ground).

Each of the above methods has its own advantages and disadvantages depending on application. AVHRR and MODIS can yield long time series (Fuller and Murphy, 2006) and, for example, diurnal cycles can be derived from TRMM (Giglio, 2007) and MTSAT (Hyer et al., 2013-this issue). Data such as presented in Fig. 10 do a reasonable job providing semi-quantitative information on large signals. However, quantitative fire characterization and emission modeling still face significant challenges. Estimation of smoke flux from both active fire hotspot and burn scar fire products introduces large uncertainties from variations in fire behavior as well as basic observational challenges such as attribution of fuels (Reid et al., 2009; Hyer and Reid, 2009). There are many reasons that current state-of-the-science fire products can be considered only semi-quantitative in SEA in general, and of even lower precision in the MC. Beginning with the fundamental measurement of fire hotspots, cloud cover blocks the heat signature of fires and, even during "good weather", cloud cover substantially hinders fire detection (Giglio et al., 2006; Schroeder et al., 2008a,b). Fortunately, thin cirrus does not always block thermal signature of fires (Reid et al., 2009). Large fires can also produce capping cumulus clouds which block IR signals (Fig. 3(d)). Under perfect observing conditions, MODIS fire detection will exhibit variability caused by variation in pixel geometry across the scan as well as gaps between orbits near the equator (Giglio et al., 2006). Very large smoke events can produce smoke optical thickness so high that IR fire retrievals can be affected (Csiszar et al., 2006). Because of the strong diurnal cycle of burning mentioned in Section 5.2, regional variability in fire ignition behavior can lead to large biases, even over short distances (Hyer et al., 2013-this issue). Even slight changes in the orbit track and subsequent alteration to overpass times can result in vastly different fire counts (Giglio, 2007). All of these issues combine to suggest that regardless of method, satellites only observe a small and widely varying fraction of actual fires (Schroeder et al., 2008b). For example, a recent study by Yokelson et al. (2011) found that over Mexico, a much easier environment than SEA in general, of 56 fires located by an airborne search, mostly at MODIS overpass time, only 10 appeared as MODIS hotspots.

Fire verification studies in SEA have shown widely varying results depending on application. For example, a study in Thailand showed more than 90% of MODIS active fire detections over forested regions were ground verified (Tanpipat et al., 2009). However, these fires generally burned over several days and there were multiple possibilities for detection. In addition, the study did not address fires that actually burned, but were not detected as hotspots. For agricultural burning in Thailand, local scientists are more skeptical on the use of satellite data (e.g., Kanabkaew and Oanh, 2011). For Sumatra, Indonesia, Stolle et al. (2004) examined 8 active fire product (including mainstay MODIS, AVHRR, ATSR and OLS fire products), and found that two-third of the fires detected by one dataset were not detected by any other dataset, nor did any of the datasets detect fires in all of their test areas. Hyer et al. (2013-this issue) examined both geostationary and MODIS active fire products in the entire MC in detail. They showed that the correlation between different satellite fire products (MODIS MOD/MYD14 active fires from Terra and Aqua and WF_ABBA active fires from MTSAT) varies as a function of spatial and temporal scale, with all products showing similar patterns at coarse scales and highly divergent patterns at finer scales. Overall, MTSAT, with its 4 km pixel size, detected only twice the number of fires as Aqua MODIS, despite having 24 regional scans every 24 h versus Aqua's 2. This demonstrates the relative trade-offs between spatial resolution and sampling rates.

In addition to simple fire counts, other sub-pixel fire characterization products are available. For Southeast Asia, fire radiative power (FRP) is available from MODIS MOD14 and MTSAT WF_ABBA fire products. Field studies have shown that fire radiative power can be strongly related to the rate of fuel combustion (Wooster, 2002), and satellite studies have shown that differences in FRP over broad areas reflect patterns of fire behavior (Wooster and Zhang, 2004). Hyer et al. (2013-this issue) also examined retrievals of fire radiative power (FRP) from MODIS MOD14 and the very recently made available MTSAT WF_ABBA products, and found even greater divergence than simple fire count. Quantitative applications of this method are hindered by the extremely noisy behavior of the sub-pixel FRP retrieval, which like all other sub-pixel fire retrieval methods is extremely sensitive to background characterization, pixel geometry, and pixel point spread function (Giglio and Kendall, 2001; Wooster et al., 2005; Calle et al., 2009; Hyer et al., 2013-this issue).

Burn scar algorithms suffer their own drawbacks. While they are not sensitive to cloud cover during a fire, they nevertheless require multiple timely looks at the same location. The high cloud cover in SEA can similarly interfere with these products (Giglio et al., 2009). Forest regrowth/greening can occur so rapidly that burn scars may become impossible to detect if successive looks are not within two to three weeks (Eva and Lambin, 1998). Burling et al. (2011) found that for fires in North America, the MODIS active fire hotspot algorithm detected 5 of 14 fires sampled from the air at overpass time; the MODIS burn scar algorithm captured none. This should be considered an easier observing environment than SEA.

Many fires occurring in this region are too small to be detected by either fire hot spot or burn scar satellite products (e.g. Miettinen and Liew, 2009). Tansey et al. (2008), considering only fires in degraded peat swamp forest, found errors of omission in MODIS active fire data on the order of

60%. This problem can be exacerbated by smoldering fires that burn at lower temperatures (common in peat burning), as well as fires burning understory vegetation beneath closed canopies, or stacked fuel. Waste fuel burning, such as in Fig. 3(h) are ubiquitous in SEA. With a small area foot print (on the order of square meters) and low temperature, they are almost impossible to detect by common hot spot or burn scar satellite products. All current detection methods significantly undersample fire activity in all seasons and locations. To the extent that patterns of burning on broad scales are driven by the largest fires, satellite fire products can capture these patterns by extrapolation; however, the appropriate methods for this extrapolation, and the limits of the accuracy obtainable, have not been determined.

5.5. Biomass burning particle emissions

As shown in the previous section, satellite fire counts from both polar (MODIS, AVHRR, ATSR/AATSR) and the geostationary sensors (WF_ABBA from MTSAT) are semi-quantitative at best in the IC, and likely qualitative in the MC, with extremely large discrepancies found in an intercomparison of satellite products in Indonesia (Hyer et al., 2013-this issue). We can consider how broad differences in methodology impact estimates of biomass burning fluxes using these products. For active fire based algorithms, while qualitative agreement has been shown to be good at coarse temporal and spatial scales, patterns observed by different sensors and different algorithms diverge at finer scales (Reid et al., 2009; Hyer et al., 2013-this issue). Similarly, in SEA burn scar algorithms such as the MODIS product from Giglio et al. (2009) will also have large uncertainties and some systematic biases, that are currently less well-characterized relative to active fire data in this region (e.g. Miettinen et al., 2007, L. Giglio personal communication). However, very recently attempts have been made to estimate emissions from such data (e.g., Chang and Song, 2010; Giglio et al., 2010; van Der Werf et al., 2010).

The best results for fire monitoring and fluxes will likely be obtained by a multi-sensor, multi-algorithm approach, but such products are under construction. Recent attempts have been made by Giglio et al. (2010) but have not been substantively verified in SEA. Regardless of fundamental data source (active fire or burn scar), the conversion of fire detection or area to smoke flux is extremely difficult. A number of assumptions need to be made, including burned area, fuel load, burn completeness, and emission factors (Crutzen and Andreae, 1990; Streets et al., 2003a; Reid et al., 2005a, 2009; van der Werf et al., 2010; Akagi et al., 2011). These dramatically increase the overall uncertainty for an individual fire.

The magnitude of diversity in fire monitoring products can be gauged through a simple comparison of emissions products which make use of fire hot spots (such as FLAMBE, Reid et al., 2009) and burn scars (such as GFEDv3 van Der Werf et al., 2010). Fig. 11 shows a comparison between the two products for 2005–2007. Given are $PM_{2.5}$ smoke fluxes for FLAMBE and GFEDv3 (Fig. 11(a) and (c), respectively) as well as their modal months (Fig. 11(b) and (d), respectively). The ratios of the two fluxes are given (Fig. 11(e)) as well as the difference in the modal months (Fig. 11(f)). Qualitatively the two products agree in relative geography and modal month. Quantitatively, there are strong differences. Clearly there is strong regional variability in the products, with localized ratios frequently swinging ± an order of magnitude. Modal months largely agree, but differences of up to two months over large areas occur in several locations.

Comparisons such as that presented in Fig. 10 may demonstrate diversity, but do not reflect specific uncertainty in any one product. Given the complexity of the SEA environment, we have reason to believe that both or all products should have very large error bars. Fig. 3(d) illustrates some limitations of active fire detection methods; the scene shows massive smoke production, but few detected hot spot fires. Locations with ratios of FLAMBE to GFED >1, such as the interior of Borneo, suggest that fires, were captured by active fire data, but missed by burn scar detection algorithms because of their size or persistent cloud cover. For either active fire or burn scar detection, sampling bias must be considered, as the more favorable burning years may result in fires of significantly larger sizes and thus enhanced observability, compared with more typical years (Miettinen and Liew, 2009; Laris, 2005). Low ratios of FLAMBE to GFED seen in southern Sumatra and southern Borneo, most likely reflect the explicit treatment of peat fuels in GFED (van der Werf et al., 2010), whereas FLAMBE treats burning in peat areas the same as other tropical forest fires (Reid et al., 2009). Missing in both products are the small fires or stack and burn events that circumstantial evidence suggests are prevalent throughout SEA and not captured by any current satellite products (e.g., Fig. 3(h)). The significance of these sources in the region could be large, especially because of their concentration near human population centers. Understanding the role of these small, overlooked fires requires some means of estimating their emissions. Hence, while emissions from such sources are likely significant, receptor modeling will try to link observations of e.g. AOD to the more observable larger fires.

Reid et al. (2009) describe some of the complexities and difficulties of developing and evaluating fire and emission products. One point from that study must be emphasized if the community is to move forward in SEA: No fire product, and likely no combination of fire products, provides comprehensive detection of open burning in SEA. All fire products are to some degree statistically under-sampling fire activity. That is, products have different sensitivities to fire and environmental characteristics (e.g., size, intensity, canopy, cloud cover, etc.) which relate to a complex probability of detection and accurate characterization. Observing conditions in the region dictate that statistical inference, rather than direct application of products, is required to obtain an accurate estimate of fire activity in all but the most controlled conditions.

The complexity of the remote sensing-fire system, which may invite pessimism, should be taken as a challenge. Indeed, the community is already responding with new innovative ways to close “top-down” versus “bottom-up” emissions. For example, lidar has been used to study burn depth in peatlands (Ballhorn et al., 2009). Synthetic aperture radar can be used to evaluate above ground biomass before, after, and during recovery of fire, as well as be used for monitoring hydrology of the peatlands (e.g., Langner and Siegert, 2009; Hoekman, 2007). Such systems suffer less from cloud interference.

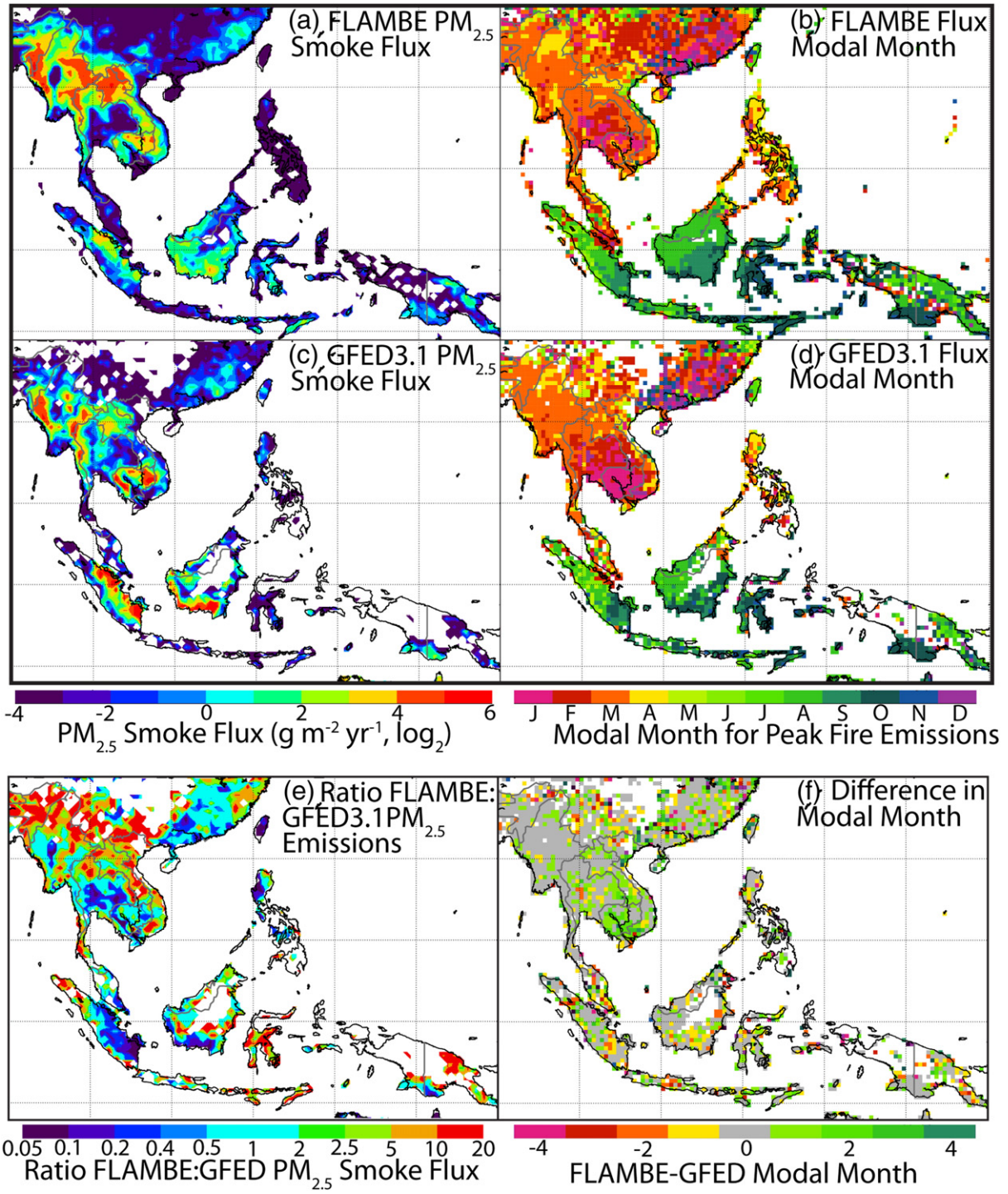

Fig. 11. Comparison of $PM_{2.5}$ emission properties (2003–2009) from the original FLAMBE and GFED3.1 products. Included are (a) and (c), emissions and (b) and (d) the modal month of emissions. (e) Ratio of FLAMBE to GFED3.1. (f) Difference in modal month, FLAMBE-GFED3.1.

6. Bulk properties of Southeast Asian aerosol particles

In this section, the bulk chemical, microphysical, and optical properties of SEA aerosol particles are reviewed, emphasizing those needed for aerosol remote sensing. Compared to other parts of the world, there are very few direct in situ measurements of aerosol microphysical properties in SEA, with none to our knowledge within Indochina itself. However, some information can be inferred from existing chemistry studies. Aged particles throughout SEA, including those from biomass burning in the MC, have high ionic fractions, which corroborate isolated reports of high hygroscopicity. Black

carbon measurements have also been made by both thermal and optical techniques. Regardless of method, aerosol particles have high but variable measured black carbon contents, ranging from 10 to 25% in most cases, with values even as high as 50% being reported for Manila in independent studies. This suggests that particles can be highly absorbing. To help bring some consistency to comparisons across SEA, climatological average AERONET data are provided and compared to other isolated retrievals in the literature. Even though AERONET data collection has been intermittent and spatially sparse, it nevertheless demonstrates high regional AODs, and considerable variability in particle absorption and size. However, there is some inconsistency between column integrated AERONET and in situ measurements, likely due to sampling bias.

6.1. Nature of aerosol particle properties and their measurement in SEA

To apply aerosol remote sensing to practical problems such as air quality, radiative forcing, or cloud impacts, we are interested in microphysical models which drive the relationship between mass, size, angular scattering, and absorption. To put it another way, we are interested in methods that link particle mass, number, speciation, thermodynamics, optical properties, or radiative flux which can be measured in situ, with what can be measured by satellite, such as spectral or angular radiance, lidar backscatter, or polarization. From a climate point of view (e.g., Penner et al., 1994; Dubovik et al., 2002; Reid et al., 2005b), this has been done through a series of bulk parameters such as the spectral mass extinction, scattering, or absorption efficiencies (α_e, α_s, α_a, respectively), single scattering albedo (ω_o), hygroscopic growth factor for light scattering (f(rh)) and asymmetry factor (g). With more interest in aerosol cloud interactions, CCN efficiencies are another bulk quantity in high demand. For satellite retrievals and some databases (such as Shettle and Fenn, 1979; Hess et al., 1998, etc.), potential representative size distributions, shapes and indices of refraction are compiled to build a forward model. Aerosol retrievals derive their products largely by comparing measured radiances to a lookup table of forward model results generated with these assumed aerosol optical properties.

Despite SEA's high population density and clear global relevance, relative to other parts of the world there are few peer reviewed papers on measurements of aerosol properties in SEA. The aforementioned bulk properties and forward retrieval models are general in nature and not tuned for the SEA environment. The March–April 2001 NASA TRACE-P mission is the one major relevant campaign, but that campaign was focused on gas chemistry and was conducted largely north of the SEA domain (Jacob et al., 2003; Verma et al., 2008). Further we show that conditions also prohibit frequent aerosol sun-sky retrievals — a mainstay of the aerosol field. Based on SEA's population and social economic status we would expect aerosol loadings to be high. Both intensive and extensive parameters likely vary dramatically with SEA geography. Such environmental diversity is a truism for frequent travelers of the region.

Given the spatial and temporal heterogeneity of aerosol properties in SE Asia, considerations for representativeness are of paramount importance. Owing to the complex nature of SEA sources, meteorology and atmospheric chemistry, no one site or even a few sites can adequately represent the current aerosol picture in any detail. Issues of representativeness are compounded by the difficulty in making even simple measurements. High SEA temperatures and humidity make thermodynamic control during sampling a challenge. For example, when measuring $PM_{2.5}$, even the temperature of the sampling box can impact RH in the sampling lines and hence the effective cut-point. The realization that aerosol particles in the MC have a substantial semi-volatile fraction (He et al., 2010) may change previous thinking about the formulation of sampling strategies. For bulk optical or microphysical properties, preference is given to making measurements "dry." This is typically achieved by heating or diluting with a dry air source. Heating in particular should be avoided if possible to minimize volatilization of organics.

The co-mingling of geographic sampling, aerosol type, active photochemistry, and thermodynamics makes reconciliation between chemical, microphysical, and optical measurements over the SEA domain a serious challenge. "Chemical evolution" can be easily invoked to explain any difference even if differences are solely artifactual. There are entirely open ended questions regarding the sources of secondary aerosol precursor gases, transformation mechanisms and the resulting impact on total particle mass, hygroscopicity, and optical properties. Ultimately, an understanding of how the climate system responds to these evolving particles will require considerable effort, including the coupling of in situ measurements to modeling and remote sensing systems.

6.2. Urban and industrial aerosol environment

Travelers in SEA will likely notice differences in emission sources between urban centers. For example, 2 stroke engine vehicles, high emitters of particles and incomplete combustion products, are common in Jakarta but have been banned in Bangkok, leading to vastly improved air quality in Thailand. Significant mobile sources still remain in Bangkok, and diesel truck and bus emissions are significant in Manila. Trash is often burned in less developed cities throughout SEA. Meat cooking is a major emitter in most SEA urban centers. Oil, gas and petrochemical industrial activity is distributed throughout the region. Singapore has a modern vehicle fleet and air quality controls, but has significant petroleum refining activity. Extensive shipping occurs across the South China Sea, to Singapore and through the Strait of Malacca; its NO_2 signal is clearly visible by satellite (e.g., Fig. 2; Eyring et al., 2005; Franke et al., 2009). Of these examples, some are well-known and documented in sources such as the CIA fact book (https://www.cia.gov/library/publications/the-world-factbook/), while others are anecdotal and the opinion of the authors (some are travelers, some are local). Portions of these sources are included in global inventories (e.g., Streets et al., 2003b,c; Yevich and Logan, 2003; Bond et al., 2004). But in the peer-reviewed scientific literature, detailed information is exceedingly scarce. For example, there is to our knowledge only one published paper on fundamental air quality parameters for Jakarta, the most populous urban area in SEA (Zou and Hooper, 1997). Most countries now have air quality monitoring networks, but data availability to the global science community is limited and to date underutilized.

Even so, we would expect some differences between countries due to varying sampling protocols, siting, and quality assurance procedures.

To our knowledge See et al. (2006) is the only peer reviewed paper that has reported comprehensive in situ measurements of key microphysical properties of "urban" pollution in a SEA city-namely Singapore. By filter sampling ions, elements, thermal organic carbon (OC) and black carbon (BC), with particle sizers, a nephelometer and an aethelometer for one year from March 2001 to 2002, this study generated the first published dataset of its kind. See et al. (2006) offers a glimpse of how particles in SEA compare to other parts of the world. For non-smoke/hazy days, they derived a green wavelength mass scattering efficiency of $3.1\,m^2g^{-1}$, which is very close to what is considered typical for a sulfate pollution environment (e.g., Waggoner and Weiss, 1980). Their absorption efficiency, of $0.6\,m^2g^{-1}$ leads to a dry ω_o value of 0.8, which is very low by global standards, but not too low in light of the 10% BC mass fraction they report (Martins et al., 1998; Bond and Bergstrom, 2006). Hygroscopicity was not measured, but they found 40% ionic composition with more than half being associated SO_4^-, suggesting that these particles have high hygroscopicity similar to other urban environments.

While See et al., 2006 is an important paper, we must be mindful that Singapore tends to be cleaner than most other SEA urban environments. To date there have been two Asian megacity aerosol chemistry intercomparisons: Oanh et al. (2006) and Hopke et al. (2008). While these studies do not provide microphysical measurements, differences in chemistry between SEA urban centers are nonetheless enlightening. These intercomparison studies included Bandung and Lembang in Indonesia, Hanoi in Vietnam, Bangkok in Thailand, and Manila in the Philippines. Data is provided by Hopke et al. (2008) for "Malaysia" implying the Malay Peninsula. In addition to these two, isolated studies have also been performed on Jakarta (Zou and Hooper, 1997), Bandung, Indonesia (Lestari and Mauliadi, 2009), and Chiang Mai, Thailand (Pengchai et al., 2009). Balasubramanian et al. (2003) provides the basic chemistry data utilized in See et al. (2006). All of these papers generate relative loadings of mass concentrations and composition. While full composition certainly helps with apportionment, from a remote sensing point of view we can infer much from these papers regarding particle absorption and hygroscopicity. A summary of key properties is included in Table 1.

In all SEA megacities particle loadings are high, with the greatest particle concentrations in Hanoi and Jakarta. But there are significant differences for individual cities even between studies. For example there is a greater than factor of 2 difference between Hopke et al. (2008) and Oanh et al. (2006) for Bandung, Hanoi, and the Thailand dry season. Values reported by these studies for Manila also differ strongly. This difference could largely be sampling location (e.g., upwind or downwind side of a city, or proximity to major streets). Sampling protocol could also be important. From a remote sensing point of view, however, these measurements indicate perhaps a problem with representativeness.

Black carbon as a surrogate for absorption also shows large differences between regions. In comparison to the Singapore measurements of Balasubramanian et al., 2003 and See et al. (2006), very high black carbon (BC) mass fractions exist in other urban environments. From different studies, Manila shows an almost unbelievable 50% black carbon mass fraction-suggestive of an exceedingly high $>3\,m^2g^{-1}$ mass absorption efficiency (Bond and Bergstrom, 2006). Anecdotal reports of the diesel exhaust in Manila's traffic are consistent with this high number. Bangkok and Hanoi also have very high black carbon mass fractions, ranging from 15 to 30%. Finally, similar to See et al. (2006) all of these papers point to high soluble fraction, notably sulfate and nitrate. From this again we expect very high hygroscopicity which may temper overall ambient ω_o.

Table 1
Southeast Asian regional reports of particulate matter and black carbon (BC) concentration.

	$PM_{2.5}$ ($\mu g\,m^{-3}$)	Coarse PM_{10}–$PM_{2.5}$ ($\mu g\,m^{-3}$)	BC ($\mu g\,m^{-3}$)=%
Bandung, Java, Indonesia[a]	13±12	18±8	3=23%
Bandung. (dry seas.)[b]	48±11	19±6	11±7=23%
Bandung (wet seas.)[b]	39±10	19±6	10±5=26%
Bandung (dry seas.)[c]	53	30	10=26%
Bandung (wet seas.)[c]	38	24	7.5=20%
Bangkok, Thailand (urban)[a]	24±10	39±22	7=30%
Bangkok (suburban)[a]	20±9	26±13	4=20%
Bangkok (dry seas.)[c]	50	26	8=16%
Bangkok (wet seas.)[c]	18	15	5=28%
Bukit Tinggi, Sumatra Ind.[d]	4.5	5	0.66=14%
Hanoi, Vietnam[a]	36±16	50±25	5=20%
Hanoi (dry seas.)[c]	124	138	na
Hanoi (wet seas.)[c]	33	46	na
Jakarta, Indonesia (dry seas.)[e]	~90	~45	na
Jakarta, Indonesia (wet seas.)[e]	~65	~35	na
Lembang, Java Ind.[a]	16±11	8±11	1.5=9%
Malaysia[a]	29±10	19±6	1=3.5%
Manila, Philippines[a]	27±8	23±14	14=52%
Manila (dry seas.)[d]	44	10	21=48%
Manila (wet seas.)[d]	43	12	23=53%
Pear River Delta[f]	74±37	na	3.5=9%
Pontianak, Kalimantan Ind.[d]	9.5	12	1.5=16%
Singapore (non-haze)[g]	19±3	na	2±1=10%
Singapore (haze w/smoke)[g]	39±8	na	3+/− =7%

[a] Hopke et al. (2008). Only total BC is reported.
[b] Lestari and Mauliadi (2009). Only fine BC is reported.
[c] Oanh et al. (2006). Std dev not given.
[d] Maenhaut et al. (2002), rural sites. Medians rather than means provided.
[e] Zou and Hooper (1997) only TSP given.
[f] Duan et al. (2007). Means of 10 sites in the Pearl River Delta.
[g] See et al., 2006/Balasubramanian et al., 2003.

6.3. Biomass burning

There are even fewer comprehensive papers with measurements of biomass burning in SEA than there are on urban pollution. This is problematic, since just as we found large differences in aerosol properties across cities, we expect similarly large differences between burning sources. We found no direct measurements of smoke optical properties reported for IC at the writing of this review. However, we do expect publication of several papers in the near future associated with BASE Asia and 7SEAS.

For the MC, what few smoke studies exist focus on the massive 1997 smoke event. Other than these, there are very few in situ measurements suitable for constraining satellite

retrievals. The most notable study was Gras et al. (1999) who flew into smoke exiting the southern MC in October 1997. Light absorption was estimated from polycarbonate filters, leading to green ω_o values of 0.88–0.92. These are typical for aged biomass burning from forested regions (Reid et al., 2005b), although Gras et al. (1999) believe these values are a lower bound with more realistic values as much as 0.04 higher. One significant revelation from this study was that they found very high hygroscopicity (e.g., f(80%) = 1.5–2). This is considered very high when compared to other burning regions (e.g., Reid et al., 2005b). It has been noted that the 1997 smoke plume had very high levels of SO_2, and SO_4^- corresponding to the high hygroscopicity (Ikegami et al., 2001). The inference of high hygroscopicity was supported by their laboratory peat burning experiments which also showed an order of magnitude increase in SO_2 emissions relative to most other fuels.

Strictly speaking, the See et al. (2006) paper discussed in the previous section is the only set of in situ absorption measurements to appear in the peer reviewed literature outside of the 1997 event. Results suggested that hazy days with suspected smoke impact were slightly less absorbing than typical urban pollution ($\omega_o = 0.82$) although thermal measurements of BC suggest high BC mass fractions (7% for haze versus 9% for non-haze days). Even here however the interpretation of the data is problematic in that it is segregated between hazy and non-hazy days occurred in a sampling year (2001) which showed lower than average burning rates (Reid et al., 2012).

The mixing of smoke with heavy industrial and domestic pollution is likely commonplace in the MC and likely leads to reactions between species and perhaps contextual or sampling bias. For example, for the largest burning events, as described in Section 3.3, peat is the likely source. The smoke dominated plumes such as described in Gras et al. (1999) certainly include a significant peat burning component. The properties of aerosol from SEA agricultural burning still have to be estimated based on studies from other regions.

While there have been few measurements of optical properties, there have been a few lab measurements and extrapolations which give very different views of the biomass burning system. Most troubling are divergent estimates of ambient ionic mass fraction and hygroscopicity. Again, this is a very important issue as this provides a critical link between observed scattering or AOD, and ambient mass concentrations needed for regional air quality and modeling. From the work of Ikegami et al. (2001), the peat smoke is high in sulfate and SO_2. This was corroborated by high ammonium and sulfate emission factors found for Indonesian peat by Iinuma et al. (2007) in laboratory burns. This increase in ionic mass fraction leads to high hygroscopicity (e.g., Kotchenruther and Hobbs, 1998; Gras et al., 1999; Roberts et al., 2002; Reid et al., 2005a,b; Carrico et al., 2010). This also makes the smoke very good CCN (Langmann and Graf, 2003), which is typically true for most biomass burning particles (e.g., Reid et al., 2005a). It is widely believed that owing to the volcanic nature of region, sulfur loads in the peat and soils are high, which results in the high SO_2 and sulfate emissions (Langmann and Graf, 2003). Chand et al. (2005), however, extensively examined the properties of Sumatran peat smoke in the laboratory as well. As expected (Reid et al., 2005a), as peat combustion is largely smoldering they derived high mass scattering efficiencies (6–8.1 $m^2 g^{-1}$), and low mass absorption efficiencies is (0.04–0.06 $m^2 g^{-1}$; $\omega_o = 0.99$). However, they found very low sulfur fractions and subsequently low smoke particle hygroscopicity (f(80%) = 1.05) and poor CCN efficiency (Dusek et al., 2005). Electron microcopy of particles showed many hollow shells unlike most smoldering particles (e.g., Martins et al., 1997; Reid et al., 1998).

The differences between field and laboratory measurements of smoke particle properties are particularly problematic for the science in general, and specifically for the application of remote sensing in models. Because of the rapid evolution of biomass burning aerosol it is hard to meaningfully compare field results to those from laboratory fires. Similarly, the location from which the peat is collected is likely important. Some peatlands may have high volcanic sulfur, others less so. Burns with low sulfate, but high co-emission of SO_2, could increase in ionic mass fraction from secondary mass production during smoke particle evolution as shown in Fig. 10a of Yokelson et al. (2009), thus increasing hygroscopicity in time, (such as suggested by Chand et al., 2005 and Dusek et al., 2005 with support from Kotchenruther and Hobbs, 1998). Indeed, we know that many facets of smoke evolution are rapid and extensive. Gas/particle phase relationships, secondary particle production, evaporation, and their consequences on key optical properties depend on the environment (e.g., Martins et al., 1998; Reid et al., 1998; Reid et al., 2005a,b; Capes et al., 2008; Grieshop et al., 2009; Akagi et al., 2011). Hygroscopicity may even decrease in some circumstances (e.g., Liousse et al., 1995; Magi and Hobbs, 2003).

A number of studies on aerosol composition for smoke in SEA have been reported, but most of these studies were focused on measuring specific aerosol components, and the specific measurements reported are not easy to apply to remote sensing problems. Commonly reported are total mass, elemental composition, organic carbon/elemental carbon (OC/EC) and water-soluble ionic and organic species over a limited period of time (Gras et al., 1999; Nakajima et al., 1999; Narukawa et al., 1999; Radojevic and Hassan, 1999; Muraleedharan et al., 2000; Okada et al., 2001; Salam et al., 2003; Radzi bin Abas et al., 2004; See et al., 2007; He et al., 2010). A comprehensive characterization of aerosols carried out in Singapore on a daily basis for a year (Balasubramanian et al., 2003) revealed that a significant fraction of the total mass can be attributed to organic constituents. However, data on detailed speciation of organic aerosols (OA) in urban aerosols especially in SEA are still limited. This is probably due to analytical difficulties and the complexity of the compounds present.

6.4. Rural

In addition to urban and biomass burning emissions we must consider rural emissions. Here we must infer much. As noted in Section 3, much of the landscape can be classified as “mosaic” which is a combination of rural villages, small holders, and various forms of agriculture and secondary forest. In some cases such as on Java, these mosaic landscapes can have very high population densities. In terms of total emissions, uncertainties are very large. Often scientists have to resort to simple population maps multiplied by some emission factor. Assumptions need to be made for domestic fuel uses, such as whether household fuel is propane, charcoal, wood, or some form of crop residue.

Yevich and Logan (2003) is an accepted baseline for our understanding of global rural emissions from biofuels. They report that both wood fuels and crop residues are extensively used in SEA for domestic use. The relative partition, however, changes dramatically from country to country. In Indonesia, which has rapid forest regrowth, residents are heavily dependent on wood fuels, leaving 73% of crop residue to burn in the field. Vietnam, however, utilizes 43% of crop residue for domestic use, and burns an equal amount in the field. Industrial biofuel usage is also prevalent in SEA, and in particular in Indonesia. All year long wood is burned for making bricks, roof tiles and charcoal (Yevich and Logan, 2003; Christian et al., 2003b; 2010).

There have been few published studies of aerosol chemistry and absorption in rural SE Asia. Maenhaut et al. (2002) looked at rural sites on Sumatra and Kalimantan (included in Table 1). Compared to the concentrations found in urban environments, $PM_{2.5}$ was quite low, ranging from 5 to 15 $\mu g\,m^{-3}$. Optically derived black carbon mass fraction was still high however, ~15%. However, during fire episodes, $PM_{2.5}$ concentrations were found to be as high as 1600 $\mu g\,m^{-3}$ (See et al., 2007).

A high black carbon fraction and hence likely particle absorption are to be expected in rural environments. Diesel and two stroke engines are commonplace and contribute significantly to pollution loadings. Even during fire events, fossil fuel sources cannot be ignored (See et al., 2007). Black carbon emissions from domestic cook stoves are also significant. Mass fractions of BC are highly variable, but average around 25% (Roden et al., 2009; Akagi et al., 2011).

6.5. Volcanic

Given the recent improvements in space-based observation of atmospheric constituents, there has been a radical advance in monitoring volcanic emissions of such species as ash and SO_2 (e.g., review papers bookended by Rose et al., 2000 to Thomas and Watson, 2010). Much of this technology however, has not been rigorously applied to SEA, and quantitative measurements that can be used to build remote sensing algorithms are generally lacking. This is troubling as SEA hosts significant volcanic activity. Mt. Pinatubo on the island of Luzon, Philippines, for example, erupted in 1991 and emitted approximately 11 km^3 of tephra (ash, rock, etc.) and 10 Mt of sulfur [Bluth et al., 1992], with effects felt worldwide. The injection of SO_2 to heights of 34 km caused global surface temperatures to drop by 0.40 °C the first year and 0.25 °C the following year [Parker et al., 1996]. The 1815 colossal eruption of Tambora on the island of Sumbawa, Indonesia is the largest eruption in recorded history (6 times that Pinatubo). The eruption plume reached a height of 43 km and emitted approximately 160 km^3 of tephra and 60 Mt of sulfur [Sigurdsson and Carey, 1989]. The Tambora SO_4 aerosol layer circulated the globe and caused anomalous cold weather throughout North America and Europe during the summer of 1816. These climatic perturbations led to the naming of 1816 as the 'Year without a Summer'. In 1883, Krakatau, an island volcano in the Sunda Straits between Java and Sumatra erupted and ejected 10 km^3 of tephra and 15 Mt S up to 40 km height [Self, 1992; Self and Rampino, 1981]. Like the Tambora eruption, the injection of SO_2 into the stratosphere by Krakatau had global climatic effects, including a reduction in the average global surface temperature by 0.3 °C in the Northern Hemisphere [Robock, 2005].

Volcanoes emit various amounts of gases (H_2O, CO_2, SO_2, H_2S, etc.), liquids (H_2O, H_2SO_4) and solids (glass, minerals from volcanic ash, volcanogenic salts); the time varying composition of volcanic aerosol plumes depends on their initial makeup and concentrations, fallout, and atmospheric interactions. The magnitude of volcanic activity affects the emission behavior of volcanic aerosols and their subsequent local, regional and global effects. Mild, effusive events often release volcanic emissions of such species as SO_2 and H_2S continuously from weeks to years into the planetary boundary layer to lower troposphere depending on the altitude of the source (e.g., Arndt et al., 1997). Violent, explosive eruptions emit large gas and ash plumes into the troposphere and sometimes the stratosphere with potential global climatic effects. The tectonic setting of SEA has produced a high density of volcanic epicenters and an extreme level of volcanic activity with a history of eruptions that are explosive and often catastrophic. These eruptions are dominated by large ash and gas plumes, pyroclastic flows, lava flows, lahars and, depending on the location and magnitude of the eruption, tsunamis.

The Tambora, Krakatau and Pinatubo eruptions often dominate the discussion of SEA volcanic emissions and aerosol properties; however, they represent only 3 of the 200 Holocene volcanoes in the region. Based on historical records, 80% of the Holocene volcanoes in Indonesia erupted between 1894 and 1994 (Simkin and Siebert, 1994; Siebert et al., 2010). SEA eruptive events are dominated by explosive activity with numerous volcanoes that also experience periods of quiescent degassing. Thus, from an aerosol point of view we need to consider ash emissions, reactive species which can oxidize to particulate matter such as SO_2 and H_2S, which are continuously outgassing, and the combination of these emissions types.

Like for all other aerosol species, the application of remote sensing requires knowledge of aerosol optical properties such as spectral single scattering albedo, spectral asymmetry parameter or phase function and, for many model applications, mass scattering and absorption efficiencies. However, because of the danger in flying near volcanic ash, there are very few direct measurements of large ascending or evolving volcanic plumes; to our knowledge none in SEA. This leaves us with little to anchor AOD-mass transfer functions.

We can infer some information on large ash eruptions, however, from flights performed around the Pacific Northwest several decades ago (e.g., Radke, et al., 1976; Hobbs et al., 1983, 1991). Similarly, recent highly controlled flights in more diluted volcanic plumes were undertaken in Central America (Carn et al., 2011) and Iceland (Mt. Hekla — Hunton et al., 2005; Eyjafjallajokull — Schumann et al., 2011). Of these only Schumann et al. (2011) report any optical property (ω_o and g). We expect the optical parameters of ash to be somewhat akin to airborne dust. Nominally, scattering cross section should go as cross sectional area; mass extinction efficiencies be linear with volume median diameter, and single scattering albedo to decrease with size (e.g., Reid et al., 2003). So, if size can be constrained, we may be able to infer some key optical properties from measurements. Here, however we are presented with a problem: reports of ash particle size in the above papers varies by an order of magnitude, ranging from VMDs of 0.8 to

10s of μm. Part of this variability is no doubt due to the extreme difficulty in measuring coarse mode aerosol particles (e.g., Reid et al., 2002, 2006). However, Hobbs et al. (1983, 1991) found considerable differences based on eruption type using identical instrumentation. Further, Hobbs et al. (1983, 1991) and Schumann et al. (2011) found large reductions in mean particle size as the plume was transported due to settling. This is optically important; for example, Schumann et al. (2011) found ω_o increase from 0.85 to 0.95 for effective diameters ranging from 3 to 0.5 μm.

In addition to ash, aerosol scientists must contend with the constant stream of SO_2 being emitted from active volcanoes. For example, Merapi volcano is the most active volcano in Indonesia and emits 100–400 t/day of SO_2 (Symonds et al., 1987; Nho et al., 1996). The reported average SEA total SO_2 emission rate from 1972 to 2000 is $2.4–3.0\times10^6$ t/year (excluding the 1991 eruption of Pinatubo) (Halmer et al., 2002). Such emissions result in nearly half of sulfur deposition in Indonesia (Arndt et al., 1997). However, because the majority of this region is not heavily monitored, quiescent emissions are underestimated.

Ultimately, all sulfur emitted will eventually be oxidized and converted to H_2SO_4 unless washed out (Hobbs et al., 1982; 1991). The timescale for this conversion depends heavily on the nature of the release. In major ash plumes, reaction rates are expected to be slow and limited by turbulent diffusion at the edge of the plume. For thinner plumes, such as measured by Schumann et al. (2011) the SO_2 half-life may be a day to several days. For venting of SO_2 into a tropical marine environment, we would expect half lives on the order of 6 h (Porter et al., 2002), although plumes aloft may have 10 times that rate (Carn et al., 2001). The difference of properties of primary ash versus secondary sulfate plumes can now be distinguished by satellite (Scollo et al., 2011).

In conclusion, we know that volcanic emissions are important to the SEA atmosphere, but the quantity and fundamental properties of these emissions are largely unconstrained. Given the complexity of the SEA meteorological system coupled with high cloud cover, volcanic emissions and impacts are difficult to monitor from space. However, a promising development is that scientists have learned to use volcanic emissions to their advantage in that they do not covary with meteorology. Sulfate from SO_2 emissions is a relatively easy non-absorbing aerosol species to retrieve from visible and infrared satellite radiances. Scientists have been able to study the impact of volcanic sulfate aerosol particles on clouds in tropical environments (e.g., Yuan et al., 2011; Eguchi et al., 2011; Kenta et al., 2011).

6.6. AERONET and other sun–sky derived properties

Inference of aerosol properties from sun–sky inversions is one of the few consistent methods practiced over the world. From a global aerosol science point of view, one of the first data sources many aerosol scientists look to is the Aerosol Robotic Network (AERONET, Holben et al., 1998) of sun photometers. The Skynet network also sees some use (Kim et al., 2004). Spectrally dependent total and fine mode optical depth, Angstrom exponents, and other optical properties can be derived from these direct observations. Sun–sky retrievals from these networks provide estimates of such intensive properties as vertically integrated size distribution, single-scattering albedo, and asymmetry parameter. Dubovik and King, 2000, and Dubovik et al. (2002) assembled a global picture of aerosol optical properties from AERONET observations, and are among the highest cited aerosol papers (as of publication date 1300+ citations). Although it can be argued that such products are not well verified to be accurate, they are nonetheless considered to be consistent for such species as pollution, smoke and dust (Haywood et al., 2003; Reid et al., 2003, 2006, 2008; Schuster et al., 2005, 2009).

Even AERONET sun photometers however, which are deployed over the globe, have only recently begun wide spread deployment in the region as part of 7SEAS. The few AERONET sites which have seen 8+ years of longevity, such as in Vietnam and Thailand, have had inconsistent operation periods to date, and are not widely exploited in publications. While AERONET data are very valuable for aerosol science in SEA, we must caution that at times, thin uniform cirrus pass though cloud screening. Cloud screening mechanisms are implemented in the AERONET level 2 products (Holben et al., 1998 and Smirnov et al., 2000). However recent papers by Chew et al. (2011) and Huang et al. (2011) who compared lidar to AERONET in SEA suggest that thin uniform cirrus may skew climatological values of total AOD by as much as 0.035. This matches the estimate of cloud optical depth for "sub-visual cirrus" of 0.03 given by Sassen and Cho (1992). The next generation of cloud screening is expected to correct these lapses. Fortunately, this error is sequestered to the coarse mode in the spectral deconvolution algorithm (O'Neill et al., 2003). Other than maritime aerosols near coastal and over ocean sites, and local sites, SEA is likely to have little coarse mode AOD that would typically be dust. Hence, for individuals interested in smoke and pollution, we recommend using the fine mode AOD.

Currently a large group of papers in preparation associated with 7SEAS attempts to fully analyze the AERONET record. While we recommend interested readers examine these papers, we provide a brief synopsis here. For brevity and consistency, data is presented along Dec–May/Jun–Nov monsoonal lines used for presenting satellite remote sensing data. Given in Table 2 are level 2 quality assured average and standard deviation aerosol optical depth (500 nm), fine mode optical depth computed from O'Neill et al., 2003 (500 nm), Angstrom exponent derived from a mean of 440–870 nm data, and column water vapor (cm). Also given are average Dubovik and King (2000) full-sky retrievals of 440 nm single scattering albedo ω_o and finally effective radius. These instruments have varying start dates, and because of high regional cloud cover, very few full-sky retrievals. Although the temporal record is insufficient to develop a climatology of aerosol properties, providing average intrinsic and extrinsic properties for approximate wet and dry seasons at this point can yield insight into variability.

Regarding total AOD, we find that average values are typically high throughout SEA, and seasonally even higher in areas impacted by biomass burning. As expected, seasonal AODs/water vapor are opposite/in phase to the monsoonal trough. Overall, AODs appear to be higher in the IC versus the MC. Absorption is quite variable, with ω_o varying between 0.85 (Hong Kong) and 0.99 (Dongsha Island in the northern South China Sea).

Table 2
Basic optical depth, absorption, and size properties from AERONET over the region. Included is the aerosol optical depth (AOD; 500 nm), fine mode optical depth (Fine-AOD), Angstrom exponent, precipitable water vapor (Water), single scattering albedo retrievals (ω_o; 440 nm for AODs > 0.4), and retrieved effective radius (r_{eff}; μm).

Site	Location	N	AOD (500 nm)	Fine-AOD (500 nm)	Angstrom	Water (cm)	N	ω_o (440 nm)	N	r_{ff} (μm)
Dec–May										
Bac Giang	North of Hanoi, Viet.	5222	0.67 ± 0.30	0.59 ± 0.33	1.4 ± 0.2	2.5 ± 1.3	495	0.90 ± 0.03	513	0.16 ± 0.03
Bac Lieu	South of Ho Chi Minh, Viet.	3735	0.26 ± 0.15	0.18 ± 0.13	1.1 ± 0.3	4.0 ± 0.7	21	0.94 ± 0.02	59	0.16 ± 0.02
Bandung	Western Java, Indonesia	1514	0.27 ± 0.19	0.21 ± 0.18	1.2 ± 0.3	3.2 ± 0.3	10	0.91 ± 0.07	16	0.19 ± 0.04
Chaing Mai	Northern Thailand	725	0.71 ± 0.40	N/A	1.7 ± 0.2	3.1 ± 0.75	40	0.90 ± 0.02	56	0.14 ± 0.01
Dongsha Island	Northern South China Sea	2054	0.31 ± 0.24	0.27 ± 0.24	1.4 ± 0.4	3.4 ± 0.7	25	0.95 ± 0.02	83	0.17 ± 0.02
Hong Kong	Pearl River Delta	6018	0.55 ± 0.30	0.47 ± 0.28	1.4 ± 0.2	2.1 ± 1.0	57	0.85 ± 0.05	65	0.18 ± 0.03
Lulin	Mountian Peak, Taiwan	2913	0.11 ± 0.14	0.10[a] ± 0.14	1.5 ± 0.5	0.5 ± 0.3	21	0.93 ± 0.03	123	0.15 ± 0.02
Manila	Luzon, Phillipines	4235	0.22 ± 0.17	0.16 ± 0.15	1.0 ± 0.3	3.5 ± 0.8	46	0.89 ± 0.05	303	0.15 ± 0.02
NCU_Taiwan	S. Suburb of Taipei, Taiwan	3017	0.45 ± 0.27	0.35 ± 0.24	1.3 ± 0.2	2.2 ± 1	89	0.93 ± 0.03	186	0.17 ± 0.03
Silpakorn	W. Suburb of Bangkok, Thai.	14,434	0.52 ± 0.26	0.44 ± 0.26	1.4 ± 0.3	3.5 ± 0.9	1104	0.89 ± 0.03	1407	0.16 ± 0.02
Singapore	Malay Peninsula	4356	0.32 ± 0.17	0.23 ± 0.16	1.2 ± 0.3	4.4 ± 0.5	32	0.94 ± 0.02	78	0.17 ± 0.02
Songkhla	C. Malay Peninsula, Thai.	4794	0.21 ± 0.11	0.14 ± 0.10	0.9 ± 0.5	3.4 ± 0.7	10	0.89 ± 0.03	124	0.17 ± 0.03
Jun–Nov										
Bac Giang	North of Hanoi, Vietnam	6608	0.70 ± 0.49	0.62 ± 0.48	1.3 ± 0.3	4.1 ± 1.2	389	0.94 ± 0.03	454	0.20 ± 0.05
Bac Lieu	South of Ho Chi Min, Viet.	2502	0.19 ± 0.19	0.12 ± 0.10	0.9 ± 0.3	4.7 ± 0.5	10	0.95 ± 0.01	26	0.16 ± 0.03
Bandung	Western Java, Indonesia	2532	0.36 ± 0.26	0.30 ± 0.25	1.3 ± 0.3	2.1 ± 0.6	49	0.95 ± 0.02	124	0.18 ± 0.03
Chiang Mai	Northern Thailand	N/A	N/A	N/A	N/A	N/A	N/A	N/A	N/A	N/A
Dongsha Island	Northern South China Sea	657	0.20 ± 0.17	0.16 ± 0.18	1.0 ± 0.5	4.5 ± 0.7	3	0.99 ± 0.01	13	0.19 ± 0.04
Hong Kong	Pearl River Delta	4939	0.51 ± 0.30	0.43 ± 0.30	1.3 ± 0.2	3.2 ± 1.2	53	0.89 ± 0.03	70	0.19 ± 0.03
Lulin	Mountain Peak, Taiwan	2696	0.04 ± 0.03	0.02 ± 0.02	1.0 ± 0.7	0.9 ± 0.3	N/A	N/A	9	0.16 ± 0.02
Manila	Luzon, Philippines	1254	0.24 ± 0.18	0.14 ± 0.14	1.0 ± 0.3	4.5 ± 0.7	21	0.90 ± 0.04	83	0.17 ± 0.03
NCU_Taiwan	S. Suburb of Taipei, Taiwan	5664	0.34 ± 0.25	0.28 ± 0.23	1.3 ± 0.3	3.7 ± 1.0	126	0.95 ± 0.02	282	0.19 ± 0.04
Silpakorn	W. Suburb of Bangkok, Thai.	3533	0.31 ± 0.22	0.23 ± 0.22	1.0 ± 0.4	4.3 ± 1.0	104	0.92 ± 0.03	75	0.18 ± 0.03
Singapore	Malay Peninsula	5835	0.32 ± 0.23	0.22 ± 0.18	1.3 ± 0.3	4.5 ± 0.4	34	0.94 ± 0.03	214	0.16 ± 0.02
Songkhla	C. Malay Peninsula, Thai.	1478	0.15 ± 0.08	0.08 ± 0.05	0.9 ± 0.4	4.7 ± 0.4	N/A	N/A	23	0.14 ± 0.02

AERONET sites at Chiang Mai and Silpakorn Universities in Thailand, and at Bac Giang and Bac Lieu in Vietnam are considered to represent IC. The average Dec to May AOD for the two Thai sites are above 0.50, being higher in the north due to the proximity and frequency of regional fires. Fine mode fractions tend to be high, again as expected in this tropical environment. In comparison to total AOD, this also shows that any cloud screening issues AERONET may have, do not impact interpretation of data at the semi-quantitative level. The corresponding 440 nm ω_o is 0.89 and effective radius is 0.16 for both sites, within the expected range for biomass burning (Reid et al., 2005b). This also agrees with the SKYNET derived value of $\omega_o = 0.9$ at 550 nm given by Kim et al. (2004) for Sri-Samprong, a site in northern Thailand. During the wet season both the SSA and effective particle radius rise (0.03 and 0.02, respectively), but the number of successful retrievals is greatly reduced. This is not only because of cloud cover, but also the requirement that $AOD_{440\,nm} > 0.4$ for an inversion to be categorized as level 2. Bac Giang in northern Vietnam has the highest AODs all year around in SEA and, as we discuss in the next subsection, often contains high aerosol concentrations in the lower and middle troposphere originating throughout Asia. Bac Giang represents a very different climate due to the persistent clouds during the non-monsoonal period and strong regional and local biomass burning in both periods. The development around Hanoi also makes the site heavily influenced by local pollution as well. Haze has been known to develop in the region, leading to large particle sizes in the Oct–Nov period (Eck et al., 2012). The Bac Lieu site to the south of Ho Chi Minh City is considerably cleaner. Because of the low AOD there are few retrievals of aerosol optical properties available.

There are three AERONET sites with multi-year data records in the MC, Songkhla, Thailand (7° N), Singapore (1° N) and Bandung, Indonesia (7° S). AODs in these locations are typically half that of the IC. Overall, these sites have significantly lower fine mode fraction than their IC counterparts. There are potentially both physical explanations and measurement artifact reasons for this for this. First, sites such as Singapore and Songkhla likely have a coarse mode sea salt component, with AODs which average 0.04–0.06 (Smirnov et al., 2003). Based on the PM10/PM2.5 ratios found in Bandung in Table 1 and the papers therein, road, agriculture and construction dust are also a factor. However, in the MC we must also be concerned with the aforementioned cirrus contamination. Given the lower overall AOD, the relative fine/coarse partition in the MC is more sensitive to cirrus contamination. Given the high humidity and hygroscopicity of particles in the region, particle ω_o varies from 0.91 to 0.95 for Singapore and Bandung. There are very few absorption retrievals for Songkhla. In comparison, broadband retrievals made by Hoyningen-Huene et al. (1999) in Malaysia during the 1997 El Niño fire events suggested visible ω_o values on the order of 0.91.

Finally, we can examine a handful of locations in other parts of SEA. Hong Kong shows high AODs (~0.85); this is not surprising given its location the middle of the highly populated Pearl River Delta. Manila shows low AODs (~0.21) and ω_o (0.89). At Dongsha Island, in the northern South China Sea, the three retrievals all have very high ω_o (0.99). Finally, there is Lulin station in Taiwan, which has the unique capability of

observing aged smoke being transported out of the IC. With particle size and ω_o slightly higher than Chiang Mai in the source region, aerosol optical properties are consistent with known evolution (Reid et al., 2005b).

Taken as a whole, the AERONET data suggests a fair degree of diversity in aerosol properties in SEA. On a site by site basis, we can qualitatively understand some of the derived values of key optical properties (e.g., Hong Kong has the highest fractional absorption due to industrial sources; Hanoi is surrounded by mountains on three sides and is prone to haze, thus having the highest AODs, etc.). Further, we can perhaps justify differences between the MC and IC, based on social geography. But, quantitative rationales for site by site differences are still somewhat elusive. For example, surface measurements in Manila suggest a 50% mass fraction, single scattering albedos higher than Hong Kong, with lower measured BC fractions. Does this suggest sampling bias at the surface? Bac Liew and Bac Giang, represent extreme differences in AOD, particle size, and Angstrom exponent, yet ω_o retrievals yield surprising similar results. These AERONET measurements can be used to derive clear hypotheses for further study.

7. Long range aerosol transport patterns

Because large aerosol events in SEA are almost always associated with biomass burning, the focus of the literature has been biomass burning transport. Smoke from fires in IC during January–April has been observed to travel in west–southwesterly winds over the mountains of Laos at an altitude of 2–4 km. Once in the free troposphere, the smoke can be transported out over the Pacific Ocean and beyond. However, strong wind shear and surface level south easterly winds bring pollution and dust from East Asia into the SCS/ES and eventually IC and the MC. This effectively decouples smoke aloft from pollution and dust in the boundary layer. For fire in the MC, smoke typically stays within boundary layer and convective boundary layer. Large scale modeling studies suggest early season fires in Sumatra and Borneo transport smoke into the southwesterly monsoonal winds to the SCS/ES, for eventual scavenging in the summer monsoonal trough. Smoke and pollution from Java and other islands are transported into the central Indian Ocean. However, in El Niño years, fires progress long past the typical end date of the summer monsoon. When surface winds in the SCS/ES reverse back to a more northeasterly pattern, smoke from Borneo is transported across to the Malay Peninsula and into the Indian Ocean. Finally, a number of studies have indicated that convection throughout the Maritime Continent can pump both gases and aerosol particles into the upper troposphere.

7.1. Introduction to transport phenomenon and aerosol vertical profiles

Research into basic aerosol transport phenomena in SEA was almost nonexistent until just a few years ago. This is particularly true for IC, though it also holds for the MC. But even for the MC, most previous studies that addressed transport treated it as a supporting role rather than a core topic. Some transport information can be found in the review paper by Lawrence and Lelieveld (2010), but much of SEA is dealt with only on the periphery. However, in association with papers in this special issue (e.g., Campbell et al., 2013-this issue; Salinas et al., 2013-this issue; Wang et al., 2013-this issue; Xian et al., 2013-this issue) as well as the recent Reid et al. (2012), knowledge of transport phenomenology in the MC is starting to solidify.

Monsoonal flow patterns and in particular their associated vertical wind shear, are the controlling features of large scale aerosol transport in SEA. The shear component manifests itself in the vertical profile of the aerosol particles. For demonstration purposes, we provide in Fig. 12 vertical profiles derived from Campbell et al. (2013-this issue) who used the NASA Cloud–Aerosol Lidar with Orthogonal Polarization—CALIOP, which has provided global datasets since the summer of 2006 (Winker et al., 2010). Average profiles are the standard CALIOP products aggregated from 5 km cloud free retrievals for 2007–2009. Provided are average vertical profiles broken down into three month biomass burning seasons: February–April and August–October to capture the peak IC and MC burning periods, respectively, as well as the transitional periods. Averages are given over 5 regions labeled in Fig. 12(a) which are not shown explicitly in Campbell et al. (2013-this issue). These are (a) the Gulf of Tonkin; (b) the Bay of Bengal; (c) Borneo; (d) the South China Sea; and (e) an ocean region south of Sumatra on the edge of the West Sumatran Low. It is known that CALIOP retrievals can have large systematic biases based on uncertainty in selecting the appropriate lidar ratio (e.g., Oo and Holz, 2011; Campbell et al., 2013-this issue). This is discussed in Section 8. But in the context of this section, these plots are referred to in subsequent subsections to ascertain relative seasonal differences in aerosol vertical distribution.

Because CALIOP was launched in late 2006, we cannot match the time periods to those of other satellites provided in Figs. 1 and 2. However, the 2007–2009 period does cover one ENSO cycle, and we have no reason to believe that this time period is substantively different in regards to relative vertical profile. Between the CALIPSO profiles, satellite data provided in Figs. 1 and 2, the meteorology fields provided in Figs. 6 and 7, and the fire data in Figs. 10 and 11, a picture of the regional aerosol transport emerges. Focus is largely on biomass burning, as it is these events which often have observable long range transport. This is not to diminish the importance of urban air quality. Indeed, in Fig. 1 the plume from Java is quite clear entering the Indian Ocean. But such features have been rarely studied in SEA.

7.2. Long-range aerosol transport in Indo-China

As shown in Section 5, IC biomass burning activity is highest in the mid to late winter monsoon period. Emissions ramp up in January–February, peak in March–April, and decay quickly in May with the onset of the summer monsoon. Overall, much of the basic transport patterns for smoke in the IC can be surmised from Figs. 1 and 6. Surface winds tend to be light during the winter monsoonal burning season (Fig. 6(a)). Precipitation is low; likely allowing long aerosol lifetime. The high mountain ridges (e.g., Fig. 3b) have a tendency to inhibit smoke transport out of the valleys of Thailand, Burma and Cambodia. Indeed, the Min–Max plots of Fig. 1(a) and (c) clearly show boundaries set by these mountain ranges (e.g., separation between west and east in Sumatra along the Barisan Range, Borneo along the Crocker Range, and Thailand

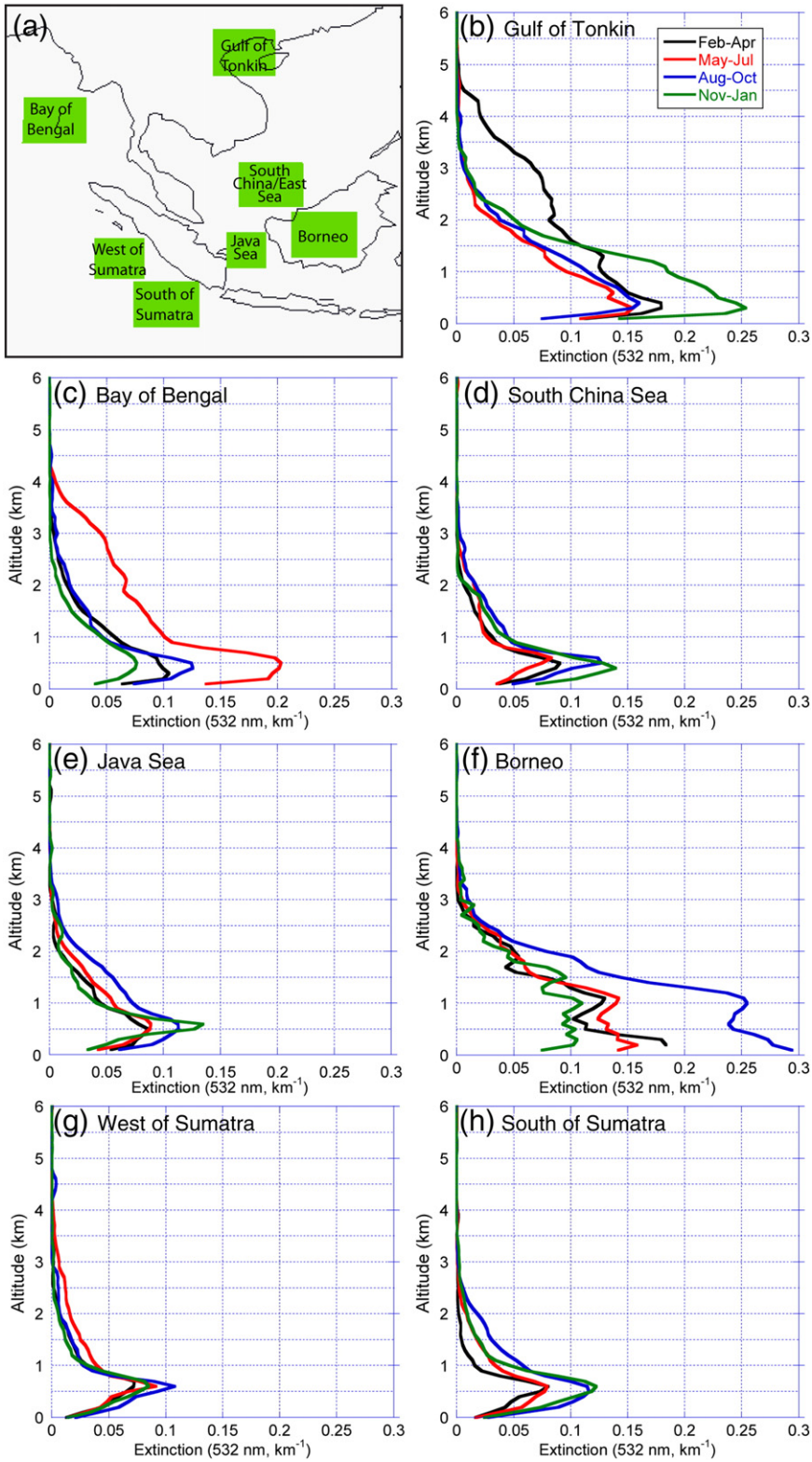

Fig. 12. Average 2007–2009 seasonal (see insets) CALIOP 532 nm extinction profiles over Southeast Asia taken from the analysis by Campbell et al. (2013-this issue). Given in (a) is a map of the domain, (b) the Gulf of Tonkin; (c) the Bay of Bengal; (d) the southern South China Sea; (e) the Java Sea; (f) the biomass burning areas of Borneo; (g) an oceanic zone west of Sumatra; and (h) a zone on the southern border of the West Sumatran Low. Similar profiles for Singapore and Thailand can be found in Campbell et al. (2013-this issue).

and Vietnam along the Annamite range in Laos). Smoke that is transported aloft and over the mountain ranges of Burma and Laos is caught in the free tropospheric westerlies, and transported over northern Vietnam into the Pacific Ocean (Tang et al., 2003a,b; Satake et al., 2004; Verma et al., 2008; Lin et al., 2009; Reid et al., 2009) or from Burma (Myanmar) into the Southeastern Tibetan Plateau (Engling et al., 2011). Plumes are frequently shown in these papers to reach as far as Taiwan, including the free troposphere receptor site on Lulin Mountain (Wang et al., 2007; Wai et al., 2008; Lin et al., 2009), southern Japan (Tang et al., 2003a,b; Satake et al., 2004) and Hawaii (Reid et al., 2009). Aircraft observations near Europe even identified one exceptionally large IC pollution and smoke event that had traversed 2/3 of the globe (Stohl et al., 2007).

The shape of this plume aloft is very well captured in the OMI aerosol index climatology (Fig. 1(g)), which is enhanced by both the smoke's absorbing nature and altitude. The height distribution of this plume is clearly visible in CALIOP profiles over the Gulf of Tonkin from Fig. 12(b) with a dominant peak from 2 to 3 km, and reaching as high as 5 km. Over Thailand itself, from in-situ lidar profiles by Iwasaki et al. (2007) and Huang et al. (2011) as well as CALIOP data from Campbell et al. (2013-this issue), smoke is typically confined to the lower 2 km with a thin convective boundary layer perhaps as high as 4 km. Hence a transport mechanism is required to elevate the plume over the Annamite Range into the westerlies.

The NASA Visible Earth true color images of Fig. 3(a) and (b) for April 7, 2002 show the importance of the complicated orography of IC. Individual smoke pockets are present in mountain valleys. In large scale or global models (e.g., the examples of Tang et al., 2003a,b; Satake et al., 2004 or Reid et al., 2009), low resolution results in simple advection over the mountains and transport out over northern Vietnam and the Pacific Ocean. Ultimately the models can replicate these relative vertical profiles, but in reality, transport is probably not so simple, and is more episodic in nature. Mesoscale simulations by Lin et al. (2009) point to the importance of mountain meteorology to lift the smoke out of the biomass burning region. They suggest lee side mountain troughs may be required to move the smoke over the mountain ranges for the largest events. An hourly diurnal cycle observed at a mountain site on the Tibetan Plateau could be attributed to complex boundary layer mixing features (as suggested by Engling et al., 2011), or perhaps, in our opinion, to anabatic/katabatic flows.

The transport of IC smoke by the westerlies aloft brings it over the Crachin stratus deck of the Gulf of Tonkin (Fig. 7(a) and (e)). This creates an interesting scenario with absorbing aerosol particles over clouds and radiative perturbations over 100 $W m^{-2}$ (Hsu et al., 2003; Section 8). At the same time, Fig. 6(a) shows that this stratus region is fed underneath with air from the northern SCS/ES. Very often this transport pattern of extreme vertical wind shear brings pollution and dust from China through the Gulf of Tonkin and into northern Vietnam (e.g., Arndt et al., 1998; Cohen et al., 2010a,b; Wang et al., 2012). With IC smoke above a stratus deck fed by polluted air from China, the Crachin may be an especially complicated example of aerosol–stratus interaction in heavily polluted environments.

The final scenario for the winter monsoon is the transport of smoke and pollution further south into the MC. As evident in the topographic maps of Fig. 5(b), the mountains between Laos and Vietnam do not extend all the way to the south. Instead there is a large open plain in southern Vietnam associated with the Mekong River and delta. We have occasionally observed boreal spring-time smoke from southern Thailand and Cambodia making its way into the South China Sea along this pathway, then being transported by the north easterlies down into the Malay Peninsula. At times, the smoke is wrapped back around into Thailand. On an even larger scale as part of the Siberian Anticyclone, Newell and Evans (2000) found that pollution emissions from major industrial centers such as the Pearl River Delta Region, Langzhou and even as far north Beijing can are often transported in the SCS/ES. Air masses flow down the SCS/ES, wrapping around the IC, into the Malay Peninsula and perhaps the Bay of Bengal. Given the frequency in which pollution and dust from east Asia has been observed at the northern SCS/ES Dongsha Island site (e.g., Cohen et al., 2010a, 2010b), such transport of some pollution to the wintertime tropics is likely commonplace.

During the summer monsoon, the winds over the water around the IC (Bay of Bengal and South China Sea) align as largely southwesterly; see Fig. 6. The land area of the IC is within the monsoonal trough and does not have a significant prevailing direction other than light westerly. Given the high precipitation rate associated with the monsoon, we expect aerosol lifetimes to be short. However, there are two important features. First and foremost, with westerly winds in the boundary layer and aloft, IC becomes a good receptor for Indian air masses (Lawrence and Lelieveld, 2010). Indeed, Fig. 1 shows that even during the monsoon, estimates of the AODs in the Bay of Bengal range from 0.2 to 0.4. Lidar data in Fig. 12(c) suggests that this transport is largely in the marine boundary layer, although in the early Indian monsoon (May–July), a land plume is visible aloft between 1 and 4 km. This supports reported lidar findings from Nair et al. (2009).

In addition to transport from the Indian subcontinent, the southwesterly winds of the summer monsoon in the SCS/ES can bring pollution and smoke from the MC into southern IC and southern Vietnam in particular. This is discussed in the next subsection.

7.3. Long-range aerosol transport in the Maritime Continent

For the MC there are few observations of aerosol vertical distribution. From what observations are available, it appears that over land, the bulk of the smoke stays within 2–3 km of the surface (Tosca et al., 2011; Campbell et al., 2013-this issue). Over water, it may be even more shallow (Campbell et al., 2013-this issue; Salinas et al., 2013-this issue); Fig. 12(e). Hence, aerosol particles released in the MC do not have a typical free troposphere transport pattern akin to other parts of the world. This makes sense as boundary layers in the tropics to subtropics are typically around 500 m, increasing to 1 to 2 km over land (Borneo). Convective boundary layers can extend another 1–3 km above these levels. In fact, the boundary layer heights can be qualitatively surmised by peaks in extinction profiles of Fig. 12 owing to hygroscopic growth. These match the boundary layer clouds at these

levels which are clearly present in the MISR climatology of Fig. 6. Smoke may reach altitudes of 3 km in a number of ways, including plume injection. However plume injection into the wet atmosphere of the MC is typically confined to the boundary layer (Tosca et al., 2011). The prevalence of clouds in the region suggests that when lofting is observed, it is due to convection in the convective boundary layer. Further, the multiple islands and high terrain suggest that high resolution mesoscale modeling may be required to capture important features at the orographic or the littoral interface such as the sea breeze (Mahmud, 2009a,b; Mahmud, in press; Wang et al., 2013-this issue).

Because smoke and pollution in the MC are largely confined within or near to the boundary layer, this simplifies interpretation of transport patterns. Boundary layer winds should be largely representative of transport, although wind shear just below and above the inversion can complicate interpretation (Atwood et al., submitted for publication). Similarly, the dominance of boundary layer aerosol makes meso-scale phenomenon important, including the sea breeze which is quite complex in the MC (e.g., Section 4). Mountain meteorology is clearly important (e.g., Sasaki et al., 2004; Wang et al., 2013-this issue; Xian et al., 2013-this issue) and even areas of recent land use change demonstrate impacts to sea breeze circulations (Tokairin et al., 2010).

Historically there have been somewhat more studies involving aerosol transport in the MC than the IC, although these studies have largely been confined to isolated biomass burning events (e.g., Koe et al., 2001; Roswintiarti and Raman, 2003; Mahmud, 2009a, 2009b, in press; Hyer and Chew, 2010; Atwood et al., submitted for publication; Wang et al., 2013-this issue). However, multi-year studies of Reid et al. (2012), Xian et al. 2013-this issue show that these case studies are fairly representative, and that large scale transport patterns are conceptually quite consistent. Smoke from the fire hotspots of central Sumatra and Borneo is largely influenced by the SCS/ES southwesterlies (Fig. 6(b)) and carried up into the Philippines for eventual scavenging into the summer monsoonal trough (Reid et al., 2012; Xian et al., 2013-this issue). There is likely bifurcation of the plume to either side of the Crocker Range in Borneo along the smoke's trajectory to the northeast (Wang et al., 2013-this issue; Xian et al., 2013-this issue). Smoke and pollution from the southern islands of Java, Bali and Timor are caught in the summertime easterlies. Once these air masses reach the southern tip of Sumatra, they can be steered northwards by the high mountain ranges and back into the SCS/ES, or pass onward into the Indian Ocean to undergo scavenging in the West Sumatran Low. The minimum and maximum AOD fields in Fig. 1(b) and (d) coupled with the surface winds in Fig. 6(b) clearly demonstrate these modes.

While the general concepts of transport in the MC are straightforward, there are numerous important complexities which must be considered. First and foremost, unlike the IC burning season which is largely dry, significant over land and ocean precipitation can fall in the MC throughout the burning season, particularly north of about 3° S latitude. Hence, much of the smoke generated on islands such as Borneo may be short lived (Reid et al., 2012; Xian et al., 2013-this issue). Similarly, sulfate models also show short lifetimes (Siniarovina, and Engardt, 2005). Longer range transport may require periods of convective suppression, such as afforded by dry phases of the Madden Julian Oscillation (Reid et al., 2012; Xian et al., 2013-this issue).

As described in Section 5, the importance of El Niño in MC fire activity is high. Transport patterns in El Niño and non-El Niño years are largely similar in the early to middle season. Precipitation deficits associated with enhanced fire activity result in less local wet deposition, thus allowing aerosol particles a somewhat longer atmospheric lifetime (Reid et al., 2012; Xian et al., 2013-this issue). However, the late fire season varies drastically between El Niño and non El Niño years. Studies of the 1997 biomass burning event found that during the month of October fire activity reached its climax and at the same time winds in the SCS/ES reverted from the more typical southwesterly to more of a wintertime northeasterly flow pattern (e.g., Koe et al., 2001). Thus, smoke being generated on Borneo was no longer transported up into the SCS/ES to the Philippines, but rather zonally across to the Malay Peninsula, Singapore and Sumatra. Reid et al. (2012) found that this was part of a recurring El Niño phenomenon in which the summer monsoon shifts back to its winter position several weeks early, thus reversing flow in the SCS/ES. However, although there is a shift in winds, large scale precipitation generally does not accompany the monsoonal shift. Forecasters at the Joint Typhoon Warning Center have suggested that this due to the Australian monsoon robbing the region of moisture (Reid et al., 2012). Hence, dry season fires continue to burn or even accelerate, but easterly winds transport the smoke zonally into the Indian Ocean under skies freer of clouds. This phenomenon has occurred for 3 of the last 4 El Niño events (1997, 2004, 2006), and a full description of the 2006 event can be found in Xian et al. 2013-this issue. In the 2009 El Niño event, this did not occur. Fire activity was indeed enhanced in the early to mid-season corresponding to enhanced peat fires, but large scale fire activity ended with the transition of the monsoon.

While the above papers clearly present MC aerosol transport in a series of concepts, the complexity of regional mesoscale phenomenon could lead to significant departures from idealized cases derived from global models. Although not discussed currently in the existing literature, the authors of this paper all note many peculiar phenomena in presented model simulations. For example in Fig. 3(d) as well as the figures of Xian et al. 2013-this issue we clearly see massive smoke loadings over southern Kalimantan, Borneo. The models have such smoke in the early and middle seasons into the SCS/ES. But as we can see from Fig. 12(e), aerosol extinction does not peak during the Aug–Oct timeframe. Smoke also appears to dissipate faster in visual imagery than what one would infer in the models. This could be due to complex boundary layer flows or convective precipitation. Regardless, transport on Borneo requires considerable future attention.

Finally a few words should be said regarding transport during the winter monsoon. While the MC largely sees heavy precipitation, at the ITCZs most southern extent in January and February, central Sumatra and parts of Borneo can at times experience prolonged dry spells (Reid et al., 2012). Central Sumatra often exhibits biomass burning activity during these periods (Field and Shen, 2008; Reid et al., 2012). In 2005 a large fire outbreak occurred there in January–February, with smoke

being transported into the Indian Ocean. However, smoke from these types of fires has been known to be transported onto the Malay Peninsula (Balasubramanian, et al., 2003). These off season dry periods appear to be exacerbated in El Niño winters, leading to large fire outbreaks on Borneo in March–April 1998 (Siegert and Hoffman, 2000; Gutman et al., 2000), and observed fire activity on Borneo and central Sumatra in 2004 and 2006 (Reid et al., 2012). Again, smoke from these fires is generally transported to the west (Gutman et al., 2000). In addition to local smoke production, Asian pollution and smoke can be advected in the MC via the northeasterly flows of the SCS/ES. While studies of the winter monsoon have focused on the northern half of the SCS/ES, there is no reason not to expect transport to the south. Indeed, the wintertime Siberian Anticyclone has been shown to bring large scale European and Asian air masses into the MC (Newell and Evans, 2000).

7.4. Convective pumping and the summer monsoonal anti-cyclone

While the vast majority of aerosol dynamics occurs in the lower troposphere, the nature of the mid and upper tropospheric aerosol environment has recently been receiving increased attention, notably through the SEAC^{4}RS campaign. As discussed in Section 4, SEA is topped by the summer monsoonal anticyclone (Fig. 5(f)). This region hosts an extensive CO maximum (Duncan et al., 2007; Jiang et al., 2007) and is believed to be largely fed from the Indian subcontinent (Livesey et al., 2008; Park et al., 2009). However, the presence of significant biomass burning in the MC coupled with summer time convection and, at times severe storms (e.g., Fig. 6(f)), suggests that smoke can be convectively pumped to the upper troposphere. Indeed, Gonzi and Palmer (2010) found several cases during the 2006 El Niño event in the MC of both CO and aerosol particles being pumped to nearly 15 km. The MLS CO product provided in Fig. 2(b) suggests this may be a common occurrence. The CO layer of the anticyclone also has an associated aerosol layer, the so called Asian Troposphere Aerosol Layer (ATAL). The ATAL is a diffuse aerosol layer between 13 and 18 km observed by Kim et al. (2003), Iwasaki et al. (2007), and Tobo et al. (2007), and only recently seen over large scales in reprocessed CALIPSO data (Vernier et al., 2011). Optically thin, Vernier et al. speculate that the origin of these particles may be primary particles pumped up through convection, as well as secondary processes. We note here that while the pumping of primary particles is quite possible, under most circumstances the associated convection scavenges most particles. The remaining low particle counts may exist with high concentrations of precursor gases in a high actinic flux environment. Under such circumstances homogeneous nucleation of particles is theoretically possible, and has been observed (e.g., Perry and Hobbs, 1994; Hegg and Baker, 2009; Weigelt et al., 2009). Stohl et al. (2007) in particular observed such behavior in SEA air transported to Europe.

8. The view of aerosol particles in Southeast Asia from space: diversity in common aerosol products

In the final section of this review, we examine the diversity among common satellite based aerosol products in SEA. Aerosol optical depth, lidar and radiative flux products are now a mainstay of aerosol research, and are frequently applied successfully throughout the world at a range of scales, from case studies to climatological trends. SEA, however, hosts one of the most hostile environments on the planet for aerosol remote sensing. Ubiquitous cloud cover, shallow/sediment loaded waters, complex land surfaces, evolving microphysics, and strong diurnal cycles conspire to create both random and systematic biases in all kinds of retrievals. These can confuse measurement artifact with the actual environment, with different instruments presenting what could be construed as conflicting information on the aerosol environment. This said, if the strengths and weaknesses of different sensors are considered, taken as a whole, a more consistent picture of SEA begins to emerge. Clearly, for aerosol problems in SEA, the selection of specific satellite products heavily depends on the application, and requires considerable forethought by investigators. Even the selection of Terra versus Aqua MODIS can have important consequences. MISR and OMI also have important roles to play.

8.1. Introduction to aerosol remote sensing in Southeast Asia

In the previous sections we have provided an overview of the nature of the SEA environment, meteorology, aerosol properties and transport. With this context covered, we turn our attention to a core component of 7SEAS: the use of remote sensing to understand the aerosol system. Given the environmental and political complexity of SEA, remote sensing is a powerful tool. However, this complexity makes SEA perhaps the most challenging region in the world for aerosol remote sensing. There are few verification studies of satellite aerosol products in SEA of any sort, and only one which has looked in detail at differences between two sensors (Xiao et al., 2009). What we do know for practical application is largely based on what can be inferred from global studies.

We will present an overview of what the standard products from remote sensing can provide to understand the aerosol system, as well as key points on the magnitude of uncertainty. This is done as a series of "face value" presentations of baseline products in a "level 3" gridded format (e.g., such as provided by Giovanni, [http://disc.sci.gsfc.nasa.gov/giovanni, Acker and Leptoukh, 2007]). In the case of aerosol and cloud products in SEA, some rudimentary comparisons are made; typically along the monsoonal lines used in Fig. 6. This is done purely to illustrate baseline differences of which scientists should be mindful. There is very limited information in the peer reviewed literature on product "intercomparison" and a baseline comparison demonstrates the relative magnitudes of uncertainty. At the same time, "face value" comparisons are potentially very misleading, as there are significant biases associated with sampling and context (e.g., Myhre et al., 2004; Li et al., 2009; Levy et al., 2009; Zhang and Reid, 2009, 2010; Kahn et al., 2011; Shi et al., 2011b). Even so, the literature is littered with articles that do in fact use these products at face value, often resulting in misleading or erroneous interpretations. Our review below is, in part, an attempt to clarify the key issues when utilizing these products at face value, pointing to examples of relevant literature for greater detail. Throughout the review, we also maintain a distinction between primary verification, where products are verified against well-known standards

over appropriate domains, versus secondary verification, where one reasonably well characterized product is used to evaluate the other, versus finally intercomparison, which highlights differences and allows reconciliation only through inference.

We will discuss dark target aerosol products (e.g., from MODIS or AVHRR), aerosol retrievals from MISR multi-angle observations and Total Ozone Mapping Spectrometer (TOMS) and OMI UV radiance observations, active methods such as CALIOP, and finally top of atmosphere fluxes obtained by CERES. For each sensor, we discuss how they compare to the sensors presented before it. Polarization and polarimetry observations (such as POLDER), are not included in this review of SE Asia at this time simply due to a lack of any published material on the region. However, it is a topic of future investigation of the 7SEAS and SEAC^{4}RS program.

The basis of this section can be found in Figs. 1 and 2, Figs. 13–17, and Tables 3 and 4. Some commonly reported retrievals are provided in Fig. 13 for the boreal winter and summer monsoonal periods composited for 2005–2007. These are: (a) and (b) the 630 nm weekly NOAA AVHRR product (Ignatov and Stowe, 2002a,b; Ignatov et al., 2004); (c) and (d) the standard Aqua MODIS collection 5 operational product (Remer et al., 2005; Levy et al., 2007); (e) and (f) the Aqua MODIS Deep Blue Product version 5.1 (Hsu et al., 2004, 2006); and (g) and (h) the SeaWiFS Deep Blue Product (Sayer et al., 2011). For later cross reference, the standard 558 nm version 22 MISR product (Kahn et al., 2007, 2010) is also included in Fig. 13(i) and (j). Similarly, the near UV derived OMI products at 483.5 nm (Torres et al., 2002, 2007) are provided in Fig. 14. Key differences and regressions of some of these products are provided in Fig. 17. Because of the framing bias such comparisons can portray, a series of pair-wise regressions of 2×2 degree boxes between satellite products (Table 3) for four over ocean and two over land locations (locations of these points are on Fig. 13(c)) for AODs<1 are given. We draw from the literature AERONET comparisons for MODIS and MISR (Table 4). For two IC and two MC locations, we also present associated time series (Fig. 16). Finally, a detailed pair-wise comparison between MODIS and MISR drawn from Shi et al. (2011b) is presented in Fig. 17. Between all of these products, the multi-dimensional nature of satellite aerosol observations begins to take shape.

8.2. Dark target aerosol products

Dark target retrievals (DTRs) are the most basic of retrievals (Fraser et al., 1984), and given their broad use and application to large swath sensors, they are the backbone of the global aerosol system. DTRs relate increases in top-of-atmosphere reflected spectral radiance relative to an estimated dark lower boundary condition such as the ocean or dark forest, to infer the atmospheric radiance. These be done at multiple wavelengths, but given the darkness of the ocean surface in the red, early methods were with the red bands of AVHRR over water (e.g., Rao et al., 1989). Based on a series of microphysical models as a constraint, AOD is retrieved. If multiple wavelengths are available over ocean, some microphysical quantities such as the relative contributions of fine and coarse mode aerosol particles can also be estimated. This whole procedure is predicated on the sensor and algorithms ability to isolate cloud-affected aerosol particle scattering radiances from those of the surface and clouds.

Conceptually, over ocean DTRs are the simplest retrievals, and hence it is easier to examine individual areas of bias for SEA. In Fig. 13 we include the NOAA AVHRR, MODIS Aqua collection 5, MODIS Aqua Deep Blue, and SeaWiFS Deep Blue algorithm. These dark target data sets represent in general different perturbations of the basic methodology. We fully acknowledge that many other algorithms exist and are applied to the region; these include for AVHRR, the Global Aerosol Climatology Project (GACP) product of Mishchenko et al. (1999), the Indian AVHRR products of Hashim et al. (2004) and Parameswaran et al. (2004), and a large collection of ocean sensor products as outlined by Myhre et al. (2004, 2005a). There has been sporadic use of geostationary data as well (e.g., Janjai and Wattan, 2011).

All of the products presented in Fig. 13, show the same basic patterns of AOD (except for Aqua Deep Blue because of albedo constraints in the MODIS Deep Blue product precluding retrieval over most of the area). High AODs exist in the Bay of Bengal and the coast of Asia. In the MC, there are high AODs in the southern South China Sea, as well as in the Indian Ocean south of Sumatra during the summer monsoon. Also in all cases, products clearly identify regions of high AOD with known fire activity. However if we intercompare using MODIS Aqua Col 5 as a baseline (Fig. 15; Table 3) significant quantitative differences are apparent (we use this product for a baseline because it is the most commonly used product available). Differences between algorithms can arise at any stage of the DTR process, including radiance calibration, lower boundary condition, microphysics, cloud screening, etc. sampling and contextual biases can also create differences (e.g., Zhang and Reid, 2009). We cannot resolve these issues here. However, a brief example and discussion is given on each of these topics.

8.2.1. Comparison of Terra and Aqua MODIS collection 5

Fig. 15(a) and (b) shows the mean monsoonal differences between MODIS Terra and Aqua. The nature of the MODIS Col 5 algorithm is the same for the Terra and Aqua spacecraft. Aside from radiance calibration, the only source of differences between Terra and Aqua retrieved AOD is sampling, i.e. diurnal variability in aerosol loadings between ~10:30 and 13:30 LST or diurnal cloud fraction. If we examine regression statistics for Terra versus Aqua for our test plots from Table 3, we see slopes significantly different from 1, with Aqua being lower than Terra over both land and water for our selected areas. Again, examining seasonal average face value products in conjunction with pair wise regressions can give different information about relative information content of different analysis methods.

Close examination of Fig. 15 and Table 3 shows a number of interesting features. First and foremost, over ocean agreement of the average product is very close over most of our study domain (within ±0.025). Globally, the mean difference between Terra and Aqua MODIS is 0.015 (Remer and Kaufman, 2006; Li et al., 2009; Zhang and Reid, 2010; Shi et al., 2011a); most of this difference can be attributable to the radiance calibration. However, over land the differences can be quite large; differences of −0.025 to −0.075 are visible over much of the land area. On average, 0.025 of this can be

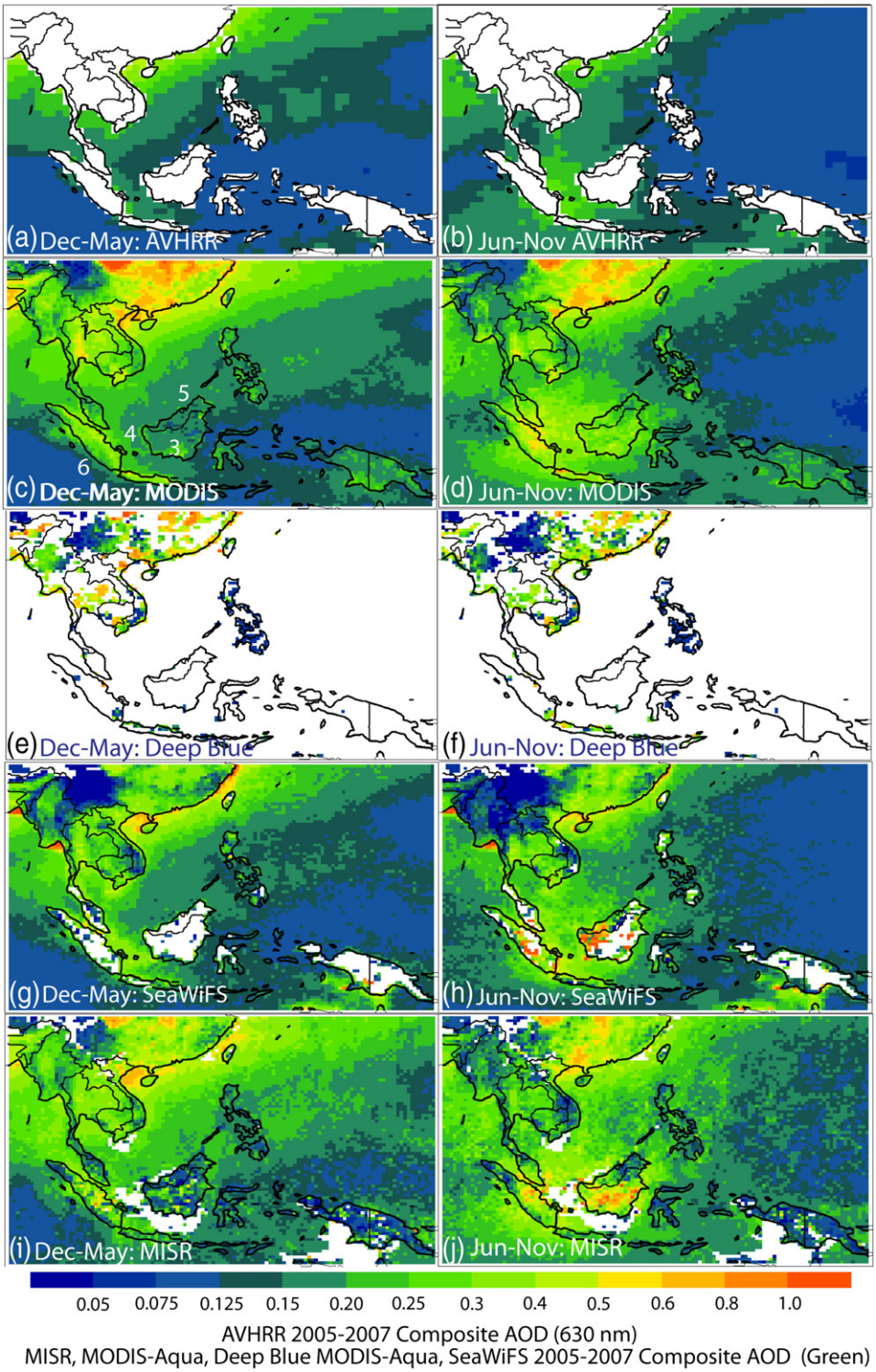

Fig. 13. Mean 2005–2007 monsoonal (December–May and June–November) AOD from (a) and (b) AVHRR PATMOS (1°×1°), (c) and (d) Terra MODIS Col 5 (0.5°×0.5°), (e) and (f) Terra MODIS Deep Blue(0.5°×0.5°), (g) and (h) SeaWiFS Deep Blue (0.5°×0.5°) and (h) and (i) Terra MISR (0.5°×0.5°). Included on (c) are the locations for the regressions in Table 1, and the time series of Fig. 15. 1. Thailand; 2) Gulf of Tonkin; 3) Southern Kalimantan; 4) Java Sea; 5) South China Sea; and 6) South of Sumatra.

attributable to known radiance calibration bias at the global level which feeds the retrieved radiances and how this is fed into the lower boundary condition parameterization (Hyer et al., 2011). The remaining half to two thirds may be reasonably a result of some biome specific aspect of the lower boundary condition, or as we discuss later, perhaps a cloud

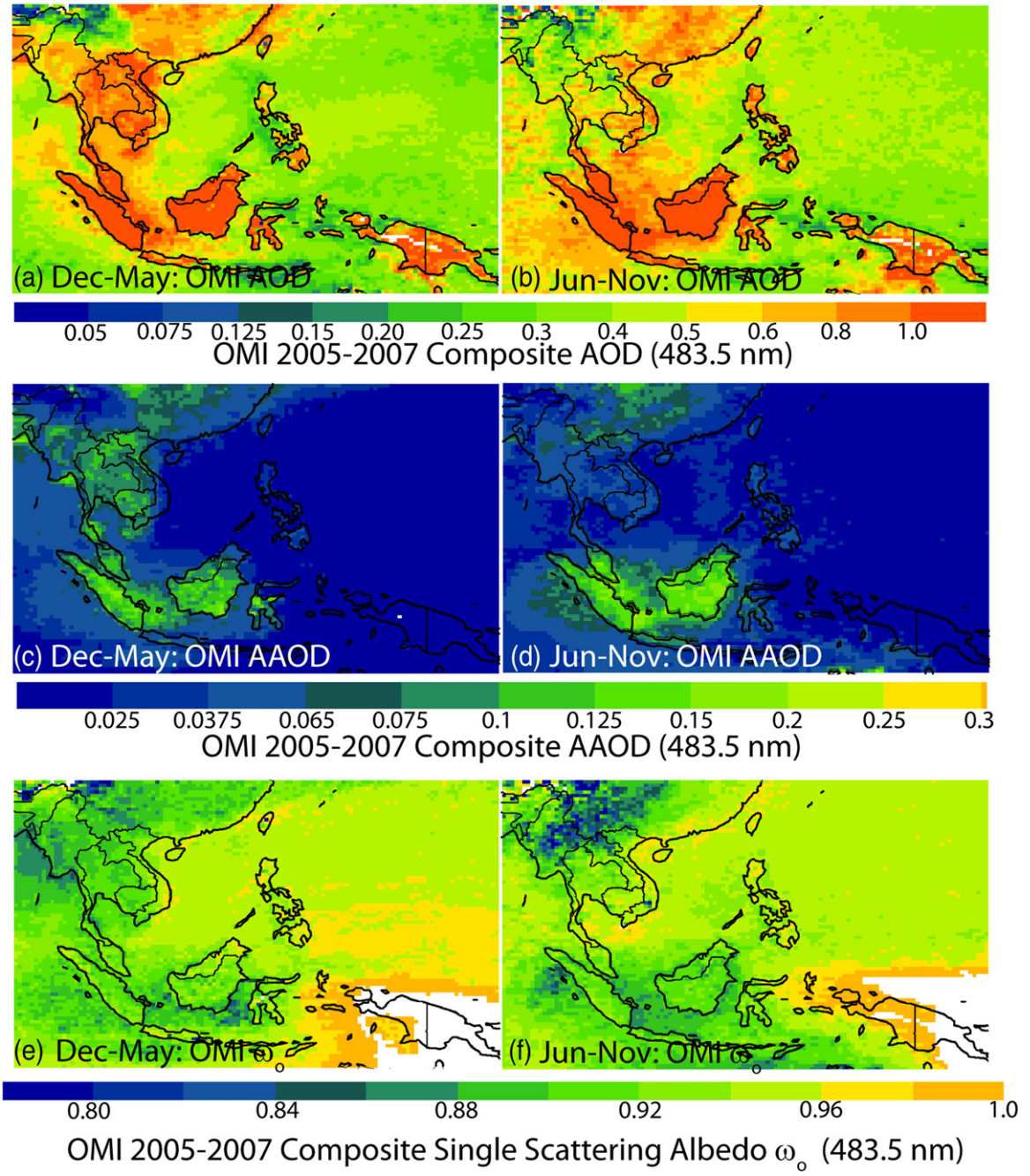

Fig. 14. Mean 2005–2007 monsoonal averages (December–May and June–November) for OMAERO v3 from (a) and (b) OMI AOD, (c) and (d) OMI AAOD, and (e) and (f) single scattering albedo (ω_o).

issue. Finally, we observe odd diurnal behavior in the island of Borneo and in central Sumatra; the afternoon Aqua MODIS AOD is substantially lower than the morning Terra AOD. Even in the Java Sea, Terra MODIS is higher than Aqua. This is in spite of the well-known fire phenomenology where fire activity in the region increases throughout the day (Giglio, 2007; Hyer et al., 2013-this issue). Here the reason for the difference can be found in Fig. 3(d). For large biomass burning events, the surface is opaque and the retrieval fails or the pixel is flagged as cloud. Thus, since morning smoke is more observable from the retrieval point of view, it appears as the higher AOD.

The above differences at the monsoonal level are enlightening and in particular highlight sampling differences. To go further, it is helpful to consider a pair-wise comparison, where both Terra and Aqua MODIS retrieved in the same location in the same day. Examination of the regressions in Table 3 shows generally good correlations over water, as well as slopes within 10%. However, the comparison is worse over land with low slopes (Southern Borneo/Kalimantan $r^2 = 0.53$

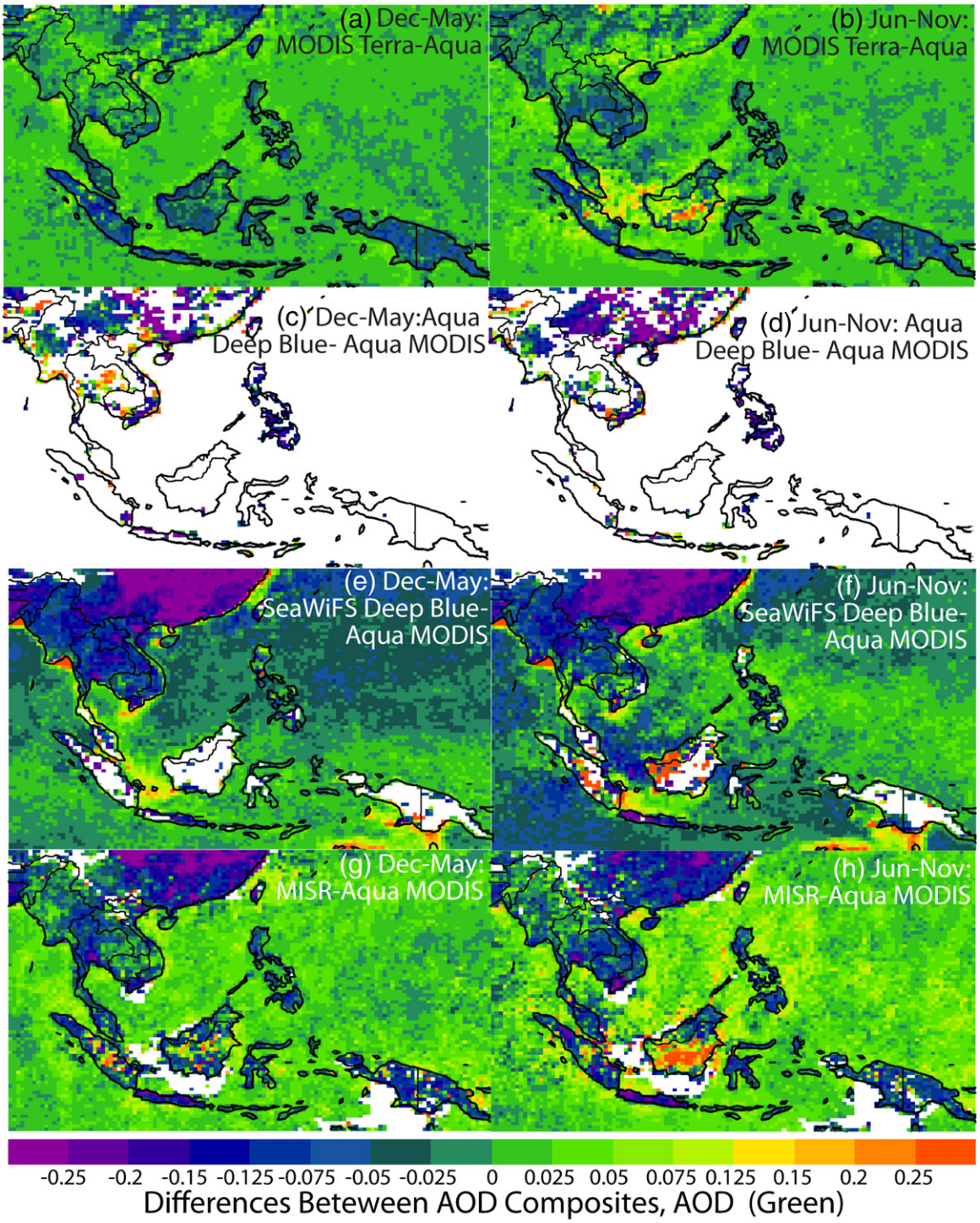

Fig. 15. Average 2005–2007 monsoonal average (December–May and June–November) AOD differences between (a) and (b) Aqua and Terra MODIS Col 5, (b) and (c) Aqua MODIS and Deep Blue, (d) and (e) Aqua MODIS and SeaWiFS Deep Blue and (g) and (h) Aqua MODIS and MISR.

and Thailand $r^2 = 0.53$). Further, Terra MODIS tend to have AODs ~20–25% lower than Aqua. This could very well be a result of radiance calibration for channels in the retrievals. All indications point to calibration differences between the two sensors having strong non-linear impacts on the retrievals. The land based difference between Terra and Aqua is commonplace throughout the globe (Hyer et al., 2011, Appendix D) and is likely due to the combination of many effects such as viewing

geometry differences, variations in meteorological conditions at the overpass times, different levels of cloud contamination, and very small radiance calibration differences can sizably affect the lower boundary condition. However, despite doing a pairwise comparison, diurnal cycle of burning could systematically lead to higher AODs in the afternoon. Diurnal differences of similar magnitude have been observed before in biomass burning regions. (e.g., Reid et al., 1999).

8.2.2. SeaWiFS Deep Blue and the lower boundary conditions

This over-land bias between Terra and Aqua leads us to the next issue; the lower boundary condition. Boundary condition effects are exemplified in comparisons of Terra MODIS Col 5 to the Deep Blue algorithms for MODIS Aqua and SeaWiFS (Fig. 15(c)–(f). Open deep water ocean radiance is generally well known and some form of reflectance model is used (e.g., Cox and Munk, 1954). In green to blue wavelengths, ocean color has variability due to constituent loads such as chlorophyll, but the ocean is nearly black at red or longer wavelengths outside of sun glint, and so most aerosol retrievals operate in the red to near IR. With the exception of perturbations due to wind speed (e.g., Zhang and Reid, 2006) the radiometric properties of open deep water are relatively constant and we do not expect significant divergence across products in this respect. In the littoral zone, however, these spectral assumptions often break down. Shallow water where the ocean bottom contributes to the water leaving radiance, sediment loads from rivers, and the surf zone/shoals all make defining the lower boundary condition a challenge in all optical and IR wavelengths. Southeast Asia has thousands of islands, large delta regions (most notably the Mekong and Sittang), and large shallows (such as the Java Sea and south of Vietnam with depth ranges 20–60 m). The social economics of SEA place major sources precisely in these challenging regions For all satellite sensors, in these "class 2" waters, observability and aerosols loadings are expected to be anti-correlated, thus making aerosol remote sensing a significant challenge.

Because Deep Blue uses blue wavelengths which have greater penetration in water, it is particularly susceptible to bias from shallow water. Since there is more variability in ocean color in the blue, a complete algorithm at these wavelengths would have to account for ocean biology and sediment loads. Conversely, the AVHRR and MODIS sensors, which operate in the red wavelengths, would be expected to have the smallest artifact in shallow waters. These expectations are confirmed in Figs. 13 and 15. In SeaWiFS Fig. 13(e) and (f), or the differences between Aqua MODIS and SeaWiFS in Fig. 14(e) and (f) we can see differences of AOD up to 0.2 in the littoral zone along the coast of Asia, the Mekong and Sittang deltas, and in the shallows of the Java Sea between Borneo and Sumatra. However, while these features exist, it is noteworthy that this is a significant improvement over previous versions of Deep Blue. We expect further improvements in the future.

Over land, the lower boundary condition problem is much more complex. Land surfaces have variable angular reflectance at all wavelengths and no set reflectance function can be used. This problem essentially eliminates all other DTR retrievals in SEA save the MODIS Col. 5 and Deep Blue Products, and the new SeaWiFS Deep Blue Product. For MODIS Col. 5, radiance at 2.12 μm is used to estimate reflectance in the visible (Levy et al., 2007). At this long wavelength, fine mode particles have very small optical cross-sections, so it is regressed onto albedo in the green, where particles are optically active. For Deep Blue algorithms, a surface climatology is used with perturbations to account for bidirectional reflectance. In the current (collection 5) MODIS operational products, a Deep Blue retrieval is included only for a limited range of high albedos.

Between MODIS Col 5 and the MODIS and SeaWiFS Deep Blue, over land differences are very striking (Fig. 15(c) and (d), (e) and (f); Table 3). Particularly noticeable are the more arid regions in the northern part of the domain. Lower boundary condition biases for brighter surfaces in Col 5 are well documented (e.g., Levy et al., 2010; Hyer et al., 2011). However, aerosol particles from these northern regions are known for transport into northern SEA during the winter monsoon (Section 7.1) and thus it is difficult at times to differentiate what are the real aerosol loadings and what is artifact. Similar issues arise for urban centers which also have higher albedos and high aerosol loadings, such as Bangkok, Hanoi, and Jakarta. In general, MODIS Col. 5 is known to have difficulty and high biases in these types of land surfaces (Levy et al., 2010; Oo et al., 2010; Hyer et al., 2011).

8.2.3. Optical properties

Optical retrievals do not constrain the variability of aerosol particle bulk optical properties. Instead, they retrieve aerosol information through the comparison of spectral radiance data to a series of a priori optical models in a look-up table based on forward radiative transfer simulations. The NOAA AVHRR performs a single-wavelength retrieval; MODIS Col 5 uses six wavelengths over water, and two wavelengths over land for microphysics (466 and 660 nm), with 2.1 μm and 1.4 μm bands used to constrain the lower boundary condition. Many of these retrievals attempt to simultaneously constrain multiple atmospheric properties, such as spectral AOD and, over ocean, fine/coarse AOD partition and effective radius (variability in the land surface currently precludes such retrievals). There are two key difficulties in this process. First, one must be sure the optical models are representative of the scene. Second, even if such a model exists, the radiances do not provide a unique solution to particle size distributions, chemistries and absorptions (i.e., solution degeneracy). Retrievals can have large uncertainties for heterogeneous air masses, and systematic biases for air masses of consistent optical properties. For higher optical depths where multiple scattering is a factor, errors in the optical model can amplify. This is exemplified in the regressions of Table 3, where we see regional differences in slope among satellite sensors, yet still strong correlations. These differences in slope are likely caused by the combination of differences in microphysical models coupled with radiometric sensitivity.

Based on the high and variable BC content of the urban atmosphere, coupled with biomass burning in a chemically active environment, we expect SEA to be one of the most challenging regions for constraining aerosol optical properties from space. Since both MODIS instruments have the same optical models, we expect them to behave similarly for major plumes in the IC, and generally this appears to be the case in Fig. 15(a) and (b). This similarity of behavior in the presence of relatively high concentrations of particles is encouraging,

but the lower boundary condition differences may overwhelm the signal for regional and seasonal averages. The differences between MODIS and SeaWiFS Deep Blue, however are much more significant and do not always covary as much with landform. Certainly the hotspot between Borneo and the Malay Peninsula is suspicious. In the absence of strong verification data, it is very difficult to ascertain microphysical bias: this is discussed at the end of this subsection.

8.2.4. Cloud screening and impacts

The use of DTRs is predicated on accurately isolating cloud-free parts of the scene, and cloud bias is an important issue. This is particularly true in SEA with its very high cloud cover and ubiquitous thin cirrus. Indeed, Tian et al. (2008) had great difficulty separating aerosol signals from cloud contamination in the MC. Sub-visual TTL cirrus contamination may even be uncorrectable or even detectable except at the broadest scales. Typically cloud masks are constructed from a variety of infrared and textural features. For most boundary layer clouds, these appear be largely adequate for MODIS. For SEA, Zhang and Reid (2010) found virtually no difference in mean AOD for all data versus means where additional cloud clearing requirements were applied. Similarly, Myhre et al., 2004, 2005a found little evidence for cloud bias in the NOAA AVHRR product (though there was bias in the AVHRR Global Aerosol Climatology Project—GACP product), suggesting stringent cloud clearing. But given the high cloud cover in the region, particularly the ubiquitous thin cirrus layers, residual cloud contamination (Zhang et al., 2005a; Zhang and Reid, 2006; Robert Holz, personal communication 2012) or failure to account for the radiative perturbations clouds have on adjacent clear retrievals (e.g., Wen et al., 2006, 2008; Marshak et al., 2008; Yang and Di Girolamo, 2008) likely biases retrievals in the region. In particular, the pedagogical study by Yang and Di Girolamo (2008) showed that the different sampling strategies commonly used in aerosol retrievals for mitigating these radiative perturbations can produce very different and potentially large biases within aerosol climatologies. They showed that such biases are a strong function of solar zenith angle, implying that some differences in aerosol climatologies derived from satellites in different orbital configurations (which determine the solar zenith angles that are sampled) may, in part, arise from this effect.

The physical nature of aerosol particles in the vicinity of clouds, and how cloud processes affect potential artifacts in aerosol retrievals, is an area of intense research. Given the high cloud fractions of SEA, it is one of the dominant scientific issues. Many intercomparison studies have attempted to ascertain why there are differences between aerosol climatologies from satellites (e.g., Myhre et al., 2004,2005a; Li et al., 2009; Kahn et al., 2009, 2010, 2011): aerosol algorithms, models, radiative transfer, and sampling are all investigated. The remaining unexplained differences between products are often assumed to be caused by cloud artifacts-although there is often only indirect evidence that this is so. How sensors classify clear air and cloud is universally acknowledged as critical information in interpreting data. There is widespread belief that regions of clouds are associated with regions of high AOD. On the physical side, higher AODs near cloud should be expected due to halos of high humidity and aerosol detrainment from clouds (Radke and Hobbs, 1991; Perry and Hobbs, 1996; Lu et al., 2003). The degree to which higher AOD occur in haloes around clouds has been studied by Koren et al. (2007), Redemann et al. (2009), Tackett and Di Girolamo (2009), and Várnai and Marshak (2011). Typically the size of halos is reported to be on the order of 2–5 km around individual clouds. However, cloud formation does covary with increased area of humidity, such as from large scale transport or large scale boundary layer deepening and hence higher boundary layer humidity. This can lead to large fields of so called "Twilight zones" around clouds of tens of kilometers (Koren et al., 2007) with complicated radiation fields (e.g., Chiu et al., 2010). Thus, cloud mask dimensions relative to cloud are clearly important. At the same time, however, Zhang et al. (2005a) and Zhang and Reid (2006) maintain that while such "twilight" features exist, the textural characteristics of the AOD retrievals themselves demonstrate patterns associated with cloud contamination — perhaps as much as 70% of the increase in over ocean AOD in the vicinity of clouds. Much of this however, is due to mid-level to high clouds associated with large cloud features. Zhang and Reid (2006) found that screening algorithms for smaller cumulus clouds appear to be adequate, including in the oceans around SEA, even though, in a location such as SEA, a large fraction of cloud contamination will be associated with the ubiquitous thin cirrus.

8.2.5. Comparison to AERONET

The combination of lower boundary condition, variable aerosol particle microphysics, and cloud issues makes interpretation of individual retrievals in SEA difficult. Despite potential sampling biases during ground truthing procedures, much value can be placed in comparison to sun photometers such as AERONET. A full AERONET comparison is outside this review. However, there is some limited direct verification data available for SEA for MODIS from Reid et al. (2009) and Hyer et al. (2011). Notably, Hyer et al. (2011) provided as supplemental material MODIS AERONET statistics for most AERONET sites around the world. A summary of MODIS Col 5 regressions is available in Table 3. Statistics in Table 4 are based on over-land retrievals, except for Singapore. Overall, the efficacy of MODIS Col 5 varies considerably by site. Sites in Thailand generally perform very well; correlations are good and slopes are within 10%. Terra performs slightly better than Aqua. However, Thailand does show a very strong y axis intercept and slope bias. This is in part because the microphysical properties vary as a function of AOD (clean background of rural and sulfate aerosols vs. polluted events dominated by biomass burning smoke). In the case of Thailand, the best fit regression line does not match the low AOD portion of the curve. This can make interpretation of such regressions difficult. While the regressions for Thailand behave reasonably well, the same cannot be said for regressions for other parts of SEA. In general, correlations are lower and, in some cases like Singapore and Bac Lieu, show poor overall skill.

Comparison of these satellite products to AERONET does not address potential differences due to sampling or other contextual biases. There are very few AERONET sampling sites relative to the diversity of aerosol and geographic features in SEA (e.g., Figs. 13 and 15). Further, any pair-wise comparison is predicated on successful retrievals both from the ground and from space. In the cloudy environment of SEA

in some locations these are rare occurrences. Verification may also have contextual biases; for example, sun photometers generally do a good job of screening for clouds, and hence pair-wise comparisons to sun photometer data will be weighed against periods of likely cloud artifact. Reid et al. (2009) found for example, that by assimilating MODIS data in SE Asia, correlations between model and observations sometimes decreased; this was attributed to residual cloud contamination in assimilated satellite AODs. Pervasive cirrus likely skews all of our interpretation of remote sensing data in the region. Not only are thin cirrus clouds difficult to detect by passive satellite sensors, they can even corrupt well screened sun photometer verification data (Chew et al., 2011; Huang et al., 2011). Similarly, from Fig. 2 we can see that in some cases, smoke optical depths are so high that satellite retrievals are impossible.

8.3. Adding the multi-angle perspective of MISR

Multi-angle viewing instruments such as MISR have the benefit of additional view angles on the same location, thus allowing the land surface and atmospheric components of the at-sensor radiance to be more effectively isolated. While we focus on MISR here, it is noteworthy that other methods do make use of multi-angle viewing, including the two angle AATSR system (e.g., Kokhanovsky et al., 2009), and the MODIS multiple look method of Multi-angle Implementation of Atmospheric Correction (MAIAC) (Lyapustin et al., 2011a,b) which has different angles and loadings on different days. These data products are less widely used, and published papers using them have so far not covered SEA.

The multi-angle nature of the MISR often results in a more robust retrieval and produces some information on microphysics over land and water (e.g., relative contribution of AOD from small, medium and large particles as well as some information on absorption and particle sphericity). MISR has been very well characterized, has stable calibration, and generally verifies better globally than any other single satellite product (Kahn et al., 2007, 2010; Zhang and Reid, 2010). For smoke, MISR has been applied to obtain additional microphysical degrees of freedom for size and absorption (e.g., Matichuk et al., 2007; Chen et al., 2008), although the MISR team is still working to improve the smoke model (Olga Kalashnakova, personal communication 2012). The angular sensitivity of MISR often makes the cloud screening more effective, particularly for thin cirrus (Di Girolamo and Davies, 1994; Pierce et al., 2010). Even the impact of potential fair weather cumulus contamination on MISR aerosol properties has been shown to be negligible (Zhao et al., 2009).

The multi-angle capability of MISR also leads to the unique capability of stereoscopic cloud and aerosol heights. For smoke and volcanic plumes, this capability has been well exercised (e.g., Kahn et al., 2007; Mazzoni et al., 2007; Fromm et al., 2008; Mims et al., 2010; Val Martin et al., 2010). Recently, work on SEA biomass burning plume heights has also been published leading to a unique dataset (Tosca et al., 2011).

The cost of the added information provided by MISR is less frequent overpasses, typically once every 8 days in the tropics. The morning overpass helps aerosol studies, as there are fewer clouds and optical depths are more manageable, but adds sampling bias against the afternoon when more fires take place. These sampling issues need to be accounted for in its usage. MISR AOD data, to our knowledge, has not been used specifically in scientific studies about SEA outside of the MODIS–MISR intercomparison of Xiao et al. (2009). We will not go into great detail on MISR efficacy as we did with the DTRs, but we can infer its utility in a number of global studies (Kahn et al., 2005, 2009, 2010; Zhang and Reid, 2010; Shi et al., 2011b), as well as regional studies in the nearby Indian Ocean and Subcontinent (e.g., Di Girolamo et al., 2004; Dey and Di Girolamo, 2010, 2011).

Because of its use of forward viewing angles, MISR reaches multiple scattering regimes at lower optical depths than nadir viewing instruments (Kokhanovsky et al., 2010). While MODIS, for example, can perform retrievals for AODs over 2, the number of successful retrievals for MISR falls off

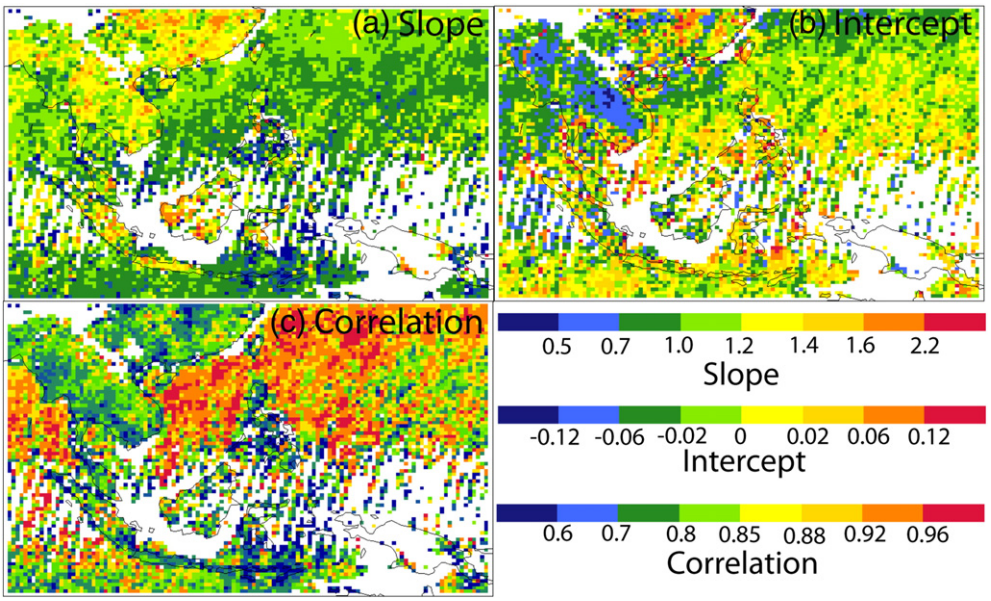

Fig. 16. Regression statistics for MISR versus MODIS, drawn from Shi et al. (2011b) (2005–2007).

precipitously for AODs>0.8. While its calibration has been stable, MISR also experiences a uniform +0.02 and 0.04 AOD bias over water relative to Terra and Aqua MODIS collection 5, respectively, likely due to radiometric calibration (Kahn et al., 2009, 2010; Zhang and Reid, 2010). A low bias, on the order of ~20% for AODs>~0.4 relative to AERONET, is also currently present in the data over polluted environments known to contain a large fraction of absorbing aerosols. This is in part to due to the unduly high single scattering albedo retrieved by MISR in such environments due inadequate microphysical models within the MISR retrieval process (Kahn et al., 2009; Dey and Di Girolamo, 2010). Further, for high AOD conditions the algorithm sometimes assigns atmospheric radiance to the lower boundary condition, further reducing retrieved AOD (Olga Kalashnakova, personal communication 2012). Both of these issues are currently being resolved by the MISR team for subsequent versions of the aerosol product. However, in both of these cases, biases tend to be more uniform than for other sensors. Finally, comparison of MISR AOD fields to known MODIS cloud artifacts over the globe suggests it is not immune from cloud artifacts. There are land features where MISR may also be uncertain, in particular rough terrain (Shi et al., 2011b); however, high elevations and rough terrain are generally excluded from the retrieval (Kahn et al., 2009).

Based on the monsoonal averages of MISR AOD from Fig. 13(i) and (j), we can see important differences between MISR and the DTRs for SEA, specifically between Aqua MODIS Col 5 in Fig. 15(g) and (h). First, the MISR retrieval has a 60 m bathymetry mask which precludes it from attempting retrievals in river deltas, the Java Sea, and Southern Papua. Over most of the oceans where retrievals are performed, the differences between MISR and Aqua are similar to the aforementioned global study of 0.03, again likely associated with a radiometric bias. However, over the SCS/ES MISR there are regions where the differences are much larger (~0.06–0.12). Aerosol retrievals are not as sensitive to bright surfaces, and show much lower AODs in the northern arid domain, indicating that DTR AODs in these areas are likely biased high. Interestingly, despite MISRs known underestimation of AOD for high AOD levels, MISR retrieves higher average AOD on Borneo than other satellite sensors. This may be because MODIS Col 5 retrievals experience a small negative bias over dark forest areas, in similar fashion to the positive bias seen over bright surfaces (Hyer et al., 2011).

Because of sampling differences, intercomparison of MISR and other instruments is limited to gross observations. Xiao et al. (2009) did a comparison of MODIS and MISR for IC and showed correlated spatial bias between the two products. Some land surface types led to large differences, such as wetlands and savannas, yet better agreement in forest and urban centers. Other factors were not statistically robust. In terms of specific verification metrics of MISR in SEA there are only two works we can draw from: A comparison of MISR products to AERONET by Kahn et al. (2010), and a relative comparison of MISR to MODIS Col 5, by Shi et al. (2011b). Regressions by Kahn et al. are given in Table 3, and data extracted by Shi et al., are given in Fig. 17. Kahn et al. (2010) examined three AERONET sites in SEA; Bac Gaing in Vietnam, and Pimai and Mukdahan in Thailand. These sites were also used by Hyer et al. (2011) to evaluate MODIS Col 5, although it should be emphasized that in Table 3 regressions for each sensor to AERONET have different populations (i.e., they are not globally pairwise). In general, MISR has higher correlations, and performs markedly better in the northern Vietnam urban environment. However, its low bias is apparent for these high AOD regions. These results should not be heavily weighted due to MISR's few verification opportunities. Bac Gaing had only 9 samples in its regression, while in Thailand Pimai had 43, and Mukdahan 54. Seasonally there are, in some cases, only a few retrieval opportunities. There is currently no primary verification in the MC for MISR published in the peer review literature.

To help control for relative sampling, Kahn et al. (2010) did perform a pair-wise comparison to MODIS Col5 over the globe (their Fig. 6). For IC, the differences between MISR and MODIS do in fact show MISR yielding lower values than MODIS. But other than that, it is difficult to infer more about MISRs behavior in SEA from this paper. Recently Shi et al. (2011b) generated global pair wise regression of MODIS against MISR with all point regression statistics provided as supplemental materials. For SEA, these are given in Fig. 16 for 2005–2007 (although seasonal data is available in the supplemental materials of Shi et al. (2011b)).

Over water, the two products generally compare very well, with high correlations, slopes within 20% of unity and intercepts within 0.02-even in regions of low AOD. In remote marine conditions MISR's 0.02 bias is evident, and in very clean conditions correlations drop simply because there is no dynamic range in the regression. Over land, correlations drop precipitously and slopes increase. Much work on intercomparison and verification remains to be done, to resolve the clear differences between products illustrated here. Fig. 16 gives an indication of the challenge of applying aerosol remote sensing data in this complex region.

In regard to our own comparisons in Table 3 of MISR to MODIS, we find patterns similar to those in Kahn et al. (2010) and Shi et al. (2011b). MISR's known underestimate of absorption is leading to a slope reduction relative to MODIS of varying degrees in SEA. The MISR–MODIS relationship is not linear, but rather curved with MISR progressively underestimating AOD at higher and higher AODs. The lowest slopes are associated with measurements over land or closer to biomass burning sources.

8.4. UV methods

A set of products completely different from dark target and multi-angle retrievals comes from UV observations from the TOMS and OMI instruments. The OMI Aerosol Index (AI) is shown in Fig. 1(e) and (f). In Fig. 14, we also include the OMI aerosol retrieval of Torres et al. (2002, 2007) for (a) and (b) 483.5 nm AOD, (c) and (d) 483.5 absorption AOD, and (e) and (f) single scattering albedo (ω_o).

Historically, TOMS has provided an AI product which is a measure of the departure of the satellite measured, near-UV radiation's angstrom exponent, from calculations for the pure molecular atmosphere at 340 and 380 nm (Hsu et al., 1996, 1999; Torres et al., 1998, 2007). For TOMS

$$\mathrm{AI} = -100\left[\log_{10}(I_{340}/I_{380})^{\mathrm{meas}} - \log_{10}(I_{340}/I_{380})^{\mathrm{calc}}\right].$$

For OMI, this was reduced to the use of a single 354 nm channel:

$$AI = -100\left[\log_{10}\left(I_{354}{}^{meas}/I_{354}{}^{calc}\right)\right].$$

If the AI is near zero, then the observed intensity (OMI) or intensity angstrom exponent (TOMS) fits the Rayleigh models. Positive values of AI are seen in the presence of UV absorbing aerosol species such as those containing black carbon from biomass burning or anthropogenic pollution, or iron in desert dust and volcanic ash. This effect is enhanced for species higher in the atmosphere, or over bright surfaces such as dust or cloud. These lead to significant contextual sensitivities. Non-absorbing aerosol particles result in a slight negative AI value, which generally cannot be discerned from the background noise. An alternative retrieval which enhances non-absorbing species has recently been proposed by Penning de Vries et al. (2009) for the Scanning Imaging Absorption Spectrometer for Atmospheric CHartographY—SCIAMACHY instrument.

Given the longevity of the TOMS and OMI aerosol index time series (which begins in 1988) coupled with its sensitivity to absorbing smoke particles and volcanic ash, even in cloud environments, the AI is a commonly used aerosol satellite product both globally and for the SEA region. Often treated as a quick qualitative indicator of large events, it has been utilized for situational awareness, broad climatologies, interannual variability, and rough comparisons to models for smoke (e.g., Herman et al., 1997; Ji and Stocker, 2002; Duncan et al., 2003b) and volcanic emissions (Seftor et al., 1997; Tupper et al., 2004; Carn et al., 2008). This is particularly true for the massive Indonesia El Niño smoke events of 1997 and 2006 (e.g., Duncan et al., 2003a; Gonzi and Palmer, 2010) and large pyro-CBs (Rosenfeld et al., 2007; Fromm et al., 2008, 2010). In some cases it is even used quantitatively (Streets et al., 2003a, b; Zhang et al., 2005d).

Because of its simultaneous sensitivities to absorption, height, and clouds, quantitative application of the AI is quite complicated. In our comparisons in Table 3, there was absolutely no correlation between AI and any AOD retrieval (even the OMI AOD retrieval discussed below). This said, the AI can at times provide a powerful and useful signal. Fig. 1(e) and (f) shows that the AI very nicely highlights the IC smoke transect and smoke on Borneo. For IC, the height of smoke transport off the continent at ~3 km clearly benefits the AI.

In Borneo, the AI is very localized over the source relative to other satellite AOD fields, (i.e., much higher and isolated relative to the AOD maps). Substantial burning also occurred on Sumatra for this time period, but it does not appear. There are a few physical possibilities to describe this dichotomy. Perhaps the plumes are higher over Borneo than the corresponding areas over water (e.g., Fig. 12). These plumes may be more embedded in clouds as well, also increasing signal. Also, the high AI over Borneo may also be indicating something missed in other products. Traditional retrievals cannot function in high AODs. The OMI AI may be indicating that smoke AODs are much higher than a climatological average of retrievals suggests, simply due to omission. Certainly imagery in Xian et al. 2013-this issue for this 2006 time period, or even the example in our Fig. 3(c) and (d), supports this suggestion. OMI AI may be a key tool in the future for determining the contribution of thick plumes or hazes to the aerosol budget.

There have also been direct TOMS AOD retrievals beginning with Torres et al. (1995) and, more recently, an algorithm which expands on the AI (Torres et al., 1998, 2007). This method retrieves both total AOD and aerosol absorption optical depth (AAOD). The AI is very nearly proportional to AAOD over many land surface types. This AAOD has appeal for some modelers for evaluating global estimates of BC, including SE Asia (e.g., Koch et al., 2009). But, the large footprint of OMI pixels (13×24 km at nadir in global mode) leads to ambiguity in regions with high cloud cover. Globally, the OMI AOD products tend to have significant high biases (e.g., Myhre et al., 2004, 2005a,b), which we can easily surmise in Fig. 14(a) and (b). For example, the direct application of OMI retrievals to SEA has met with significant difficulty (Tian et al., 2008). Average seasonal optical depths (Fig. 14, compare to Fig. 13) over much of the MC are clearly unphysical, and the AAOD also has features which correlate with deltas and shallow bathometry. These products are not without merit, however. Studies have shown that the products do have quantitative skill in some conditions (e.g. Torres et al., 2007; Curier et al., 2008; Ialongo et al., 2010). But like the other satellite products here, their application is difficult in the complex SEA environment.

We do not have sufficient AERONET retrievals to assess AAOD at this time, and even then the retrievals themselves require verification. Correlations between the OMI OMAERO V3 AOD and Terra and Aqua MODIS in our comparison, however were generally poor (Table 3). Even with the difference in wavelength (483.5 versus 550 nm), we expected some correlation. The reason for the poor apparent performance can be found in Fig. 16. OMI AOD has a significant amount of variability, but it does, in some cases, pick up seasonal trends over water. Over land, in southern the product appears not to contain the signal of aerosol particles. Conversely in Thailand there is clear positive signal. It is easy to simply dismiss the "noise" as cloud, but a serious evaluation of the product in this part of the world has never been attempted. Developers expect to AAOD to be better, and indeed simply from Fig. 14 patterns appear more realistic. Hand analyses with additional information have allowed for such parameters as ω_o to be estimated (Nakajima et al., 1999). Making the best use of the information from UV observations is an area of great interest for advancing aerosol science in the region.

8.5. Space-based lidar

Space-based lidars provide perhaps the most unique dataset for studying aerosol and cloud environments. Their ability to profile aerosol layers near the planet surface, even when attenuated by optically-thin cirrus layers in the upper troposphere such as are prevalent in SEA, adds a critical third dimension to studies. The first space-based lidar data was collected with the 1994 Lidar In-space Technology Experiment—LITE shuttle mission (Hoff and Strawbridge, 1996; Winker et al., 1996), followed by an aerosol component to the Geoscience Laser Altimeter System mission (GLAS; Spinhirne et al., 2005). For both of these instruments, aerosol analysis has been quite limited. However, the last 5 years has seen a revolution in

aerosol and cloud research with the launch and application of the NASA Cloud–Aerosol Lidar with Orthogonal Polarization (CALIOP), which has provided global datasets since the summer of 2006 (Winker et al., 2009).

CALIOP follows the A-train orbital track, collecting a curtain of elastic backscatter measurements at 532 and 1064 nm, with linear polarization sensitivity in the 532 nm band. Consecutive orbital tracks on a single day near the equator are nominally ~2800 km apart. Thus, CALIOP provides daytime and nighttime data along two-to-four total overpasses over SEA each day. CALIOP products include a vertical feature mask, an indirect retrieval of aerosol extinction, and a series of cloud products (Winker et al., 2009). The uniqueness of these data has resulted in their high demand for number of aerosol studies, which are only now starting to be published for SEA (Campbell et al., 2013-this issue), but nonetheless have broad applicability. These include: a) global transport and model validation studies (e.g., Yumimoto et al., 2008; Uno et al., 2008; Uno et al., 2009); b) surface emission estimates and injection scenario characterization (e.g., Bessagnet et al., 2008; Amiridis et al., 2010), c) pyro-cumulonimbus plume identification and dispersion (Fromm et al., 2010); d) volcanic plume monitoring (e.g., Carn et al., 2008, 2009; Campbell et al., 2011); e) variational data assimilation for global transport forecasting (e.g., Campbell et al., 2010; Zhang et al., 2011); f) four-dimensional ensemble Kalman filter data assimilation (e.g., Sekiyama et al., 2010); and (g) aerosols in the vicinity of clouds (Tackett and Di Girolamo, 2009; Várnai and Marshak, 2011).

Despite the high demand for CALIOP data, the uniqueness, sparseness, and complex error propagation of lidar data makes verification a challenge. Verification has been undertaken in the form of total AOD verification as an indicator of integrated product efficacy (e.g. Kittaka et al., 2011; Campbell et al., 2013-this issue), an assessment of parameterizations necessary to invoke aerosol property retrievals (Oo and Holz, 2011), and isolated vicarious examinations (Kacenelenbogen et al., 2011). A more comprehensive study associated with this special section is the only evaluation currently available for SEA (Campbell et al., 2013-this issue). But, we can draw parallels to the retrieval issues associated with the DTR system. CALIPSO must consider a lower boundary condition, and the strong surface return disrupts boundary layer retrievals. CALIPSO profiles over cloud must also cope with decreased signal-to-noise from cloud scatter. Microphysically, the estimate of the aerosol lidar ratio (that is the relative difference between unknown particulate extinction and backscatter terms within the single static elastic-scattering lidar equation; Fernald, 1984), is underdetermined in an elastic backscatter system. This has led some to constrain such retrievals using an independent source of AOD data (e.g., Campbell et al., 2010; Oo and Holz, 2011). Cloud bias can also be an issue, as clouds are not always properly identified and screened for subsequent aerosol analysis. In the case of lidar penetration of thin cirrus, forward scattering of laser light from ice crystals can be problematic in that they limit proper resolution of aerosol layer boundaries and internal structure (e.g., Winker and Poole, 1995).

Finally for this review, there are some factors worth noting for the profiles in Fig. 12. First, qualitatively these are largely correct, although vigilance must always be exercised in SEA. More pertinent however, is potential bias in the assumed lidar ratio. In general over water in SEA, the retrieval categorizes smoke as "polluted dust," leading to a bulk underestimate of integrated AOD of more than 30% (Campbell et al., 2013-this issue). Hence, the values given in Fig. 12 for over water should be considered lower limits. Over land the opposite is true, with CALIOP overestimating AOD. By combining CALIOP with an external source of AOD data, better estimates of extinction can be obtained (e.g., Campbell et al., 2010; Oo and Holz, 2011). However, given the difficulty of obtaining accurate AOD measurements in SEA, this may not be a complete solution. Indeed, Robert Holz (personal communication 2012) demonstrated a persistent overestimation of AOD in MODIS products due to thin cirrus.

8.6. Radiative fluxes

Sections 8.1–8.5 dealt with the monitoring of aerosol particles from space. Here, we turn our attention to remote sensing of radiative impacts by aerosol particles. Given the direct nature of aerosol particles' influence on the energy budget, a discussion of the measurement of radiative fluxes belongs here. Monitoring the radiative energy balance between the incoming and outgoing top of atmosphere (TOA) shortwave and longwave radiative fluxes is crucial for climate studies (Yu et al., 2006; Hansen et al., 2005). Changes in aerosol radiative forcing (e.g., Zhang et al., 2005c; Patadia et al., 2008a, 2011) or land forcing (e.g., Anantharaj et al., 2010) can be calculated from fluxes inferred from TOA measurements. However, before aerosol radiative forcing can be calculated, reliable values of radiative fluxes are needed. There are several approaches for estimating the reflected shortwave and the emitted longwave radiative fluxes at the top of atmosphere including radiative transfer (Davison et al., 2004; Remer and Kaufman, 2006; Wang et al., 2007; Rajeev et al., 2008) and observational approaches (Christopher et al., 2006). Radiative transfer techniques use narrow-band measurements such as MODIS to infer broadband fluxes, and require numerous assumptions about wavelength dependent surface and aerosol properties. Further, uncertainties in these methods are related directly to uncertainties in derived AOD as described earlier. On the other hand, measurement-based approaches rely on well calibrated broadband radiance measurements and convert them to fluxes, but require the use of angular models (Zhang et al., 2005c; Christopher et al., 2006). The Clouds and the Earth's Radiant Energy System (CERES) instruments on the Terra and Aqua satellites (also available from TRMM) measure radiances in the shortwave (0.3 to 5 μm), window (8–12 μm), and total (0.3–200 μm) spectral ranges (Wielicki et al., 1996). The longwave radiances are calculated as the difference between total and shortwave fluxes. However, to interpret these TOA fluxes from CERES (20 km spatial resolution at nadir), higher spatial resolution measurements and retrievals are needed, as discussed in the previous subsections. The CERES radiances are converted to fluxes using MODIS point spread function-weighted aerosol properties, and angular models (Zhang et al., 2005b). These fluxes can then be quantified, in terms of the forcing per unit optical depth for various aerosol types, as needed for climate studies.

In SEA environments, the separation of the aerosol signal from the ground and clouds is a difficult task. Fig. 17 shows the 2006–2010 winter and summer monsoonal mean (2006–2010)

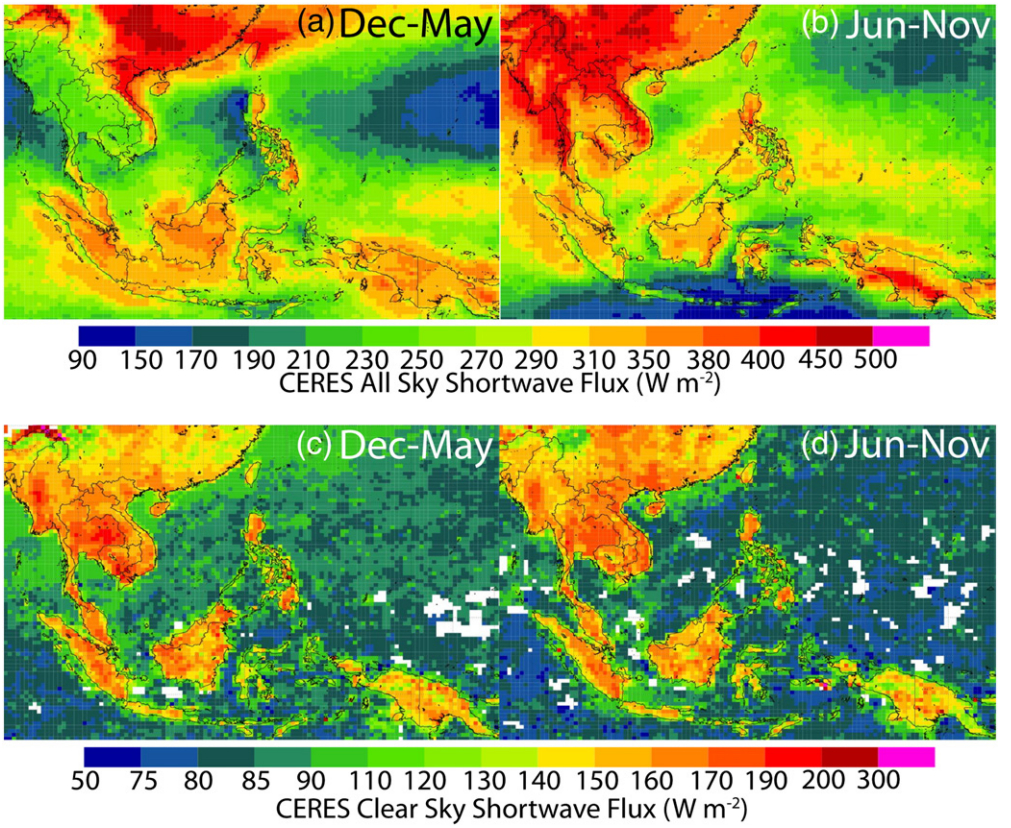

Fig. 17. Average 2006–2008 monsoonal (December–May and June–November) CERES (a) and (b) all sky and (c) and (d) clear sky fluxes.

shortwave fluxes from Terra CERES (Edition 3A) for (a) and (b) all sky and (c) and (d) cloud cleared "clear sky." These are derived from Feng and Christopher (2013-this issue). Note that the color scales are different for aerosol and clear sky fluxes since all sky fluxes have much larger shortwave values. In their processing, clouds have been removed from the CERES footprint using the MODIS and CERES scene identification. The spatial patterns of all sky fluxes over ocean are consistent with the meteorology and cloud fields of Section 4. Fluxes follow the monsoonal trough although the land–ocean boundaries cause some artifacts. When it comes to the aerosol impacts however, monsoonal differences are not easy to compare at face value. Once clear sky fluxes are estimated at overpass, values need next to be converted to diurnally averaged values (Anderson et al., 2005). Ultimately, the derivation of fluxes involves the subtraction of clear sky and aerosol sky fluxes and any uncertainties in these numbers can propagate to the final estimates. Feng and Christopher (2013-this issue) derived an instantaneous forcing efficiency of ~$-70\,W\,m^{-2}$/AOD (550 nm). Thus, instantaneously for major smoke events, forcing can be of the same magnitude as the background (clear sky) flux over ocean. However over land, since clear sky reflected fluxes are much larger in this region, the aerosol loading must be high enough to derive reliable aerosol forcing values (Feng and Christopher, 2013-this issue). For major events, total top of atmosphere forcing is on the order of $-50\,W\,m^{2}$ (Davison et al., 2004; Rajeev et al., 2008; Feng and Christopher, 2013-this issue). Further down wind in biomass burning receptor sites such as at Mt Lulin, top of atmosphere fluxes range from 0.4 to $-1.9\,W\,m^{2}$ (Wang et al., 2007). When averaged over the domain, the low clear sky fraction of SEA results in a diurnally averaged cloud-free aerosol forcing values for this region of around $-6\,W\,m^{-2}$ (Feng and Christopher, 2013-this issue).

There are several further challenges that remain when assessing aerosol radiative effects. First it is important to separate the natural from other components; this cannot be done using satellite data alone. While column measurements of MODIS and CERES provide an excellent opportunity to calculate TOA forcing (Feng and Christopher, 2013-this issue; Christopher and Zhang, 2004), in situ measurements are needed to determine aerosol type and size. Figs. 3 and 6 show the ubiquitous cloud cover in this region that necessitates a closer study of forcing estimates derived from satellite studies. Indeed, for the thin cirrus scenario, aerosol particles may still be an important contributor to the TOA radiation budget. A careful assessment of clear sky reflected fluxes is needed since forcing is calculated as the difference in shortwave fluxes between clear and aerosol skies (Bellouin et al., 2008). While it is relatively simpler over oceans to obtain clear sky fluxes (provided cloud cover is not an issue), due to the inhomogeneous background derivation, over land fluxes is a much harder problem. Thus uncertainty for AOD and fluxes increases dramatically for the over land problem. Finally, error estimates are needed for forcing calculations including CERES measurement uncertainties (calibration of CERES radiances, ~$0.4\,W\,m^{-2}$, conversion of CERES filtered

Table 3
Regressions between aerosol optical depth (AOD) products of daily data for 2005–2007. Data are from daily averaged 2×2 degree latitude longitude boxes. "TM"=Terra MODIS. "AM"=Aqua MODIS.

	Thailand	Gulf of Tonkin	Southern Kalimantan	Java Sea	South China Sea/East Sea	South of Sumatra
Type	Land	Ocean	Land	Ocean	Ocean	Ocean
Location	Lat: 14–16S Long: 100-102E	Lat: 19–21S Long: 107−109E	Lat: 1–3S Long: 113−115E	Lat: 2–4N Long: 106−108E	Lat: 7–9S Long: 113−115E	Lat: 5–7S Long: 98−101E
Terra vs Aqua MODIS	0.03+0.82*AM r^2=0.66	0.04+0.95*AM r^2=0.73	0.03+0.75*AM r^2=0.53	0.01+0.96*AM r^2=0.87	0.02+0.93*TA r^2=0.78	0.0+1.1*TA r^2=0.87
SeaWiFS vs Terra MODIS	0.07+0.62*TM r^2=0.67	0.11+0.79*TM r^2=0.75	0.04+0.86*TM r^2=0.73	0.03+0.87*TM r^2=0.73	0.01+0.91*TM r^2=0.56	0.02+0.72*TM r^2=0.77
SeaWiFS vs Aqua MODIS	0.03+0.9*TM r^2=0.78	0.10+0.87*AM r^2=0.79	0.04+0.85*TM r^2=0.75	0.04+0.85*AM r^2=0.75	0.02+0.85*AM r^2=0.75	0.01+0.86*AM r^2=0.74
Terra MISR vs Terra MODIS	0.06+0.65*TM r^2=0.81	0.21+0.71*TM r^2=0.58	0.06+0.57*TM r^2=0.42	0.06+0.81*TM r^2=0.51	0.07+0.92*TM r^2=0.57	0.04+0.81*TM r^2=0.76
Terra MISR vs Aqua MODIS	0.09+0.54*AM r^2=0.53	0.12+0.93*AM r^2=0.75	0.06+0.51*AM r^2=0.23	0.08+0.88*AM r^2=0.63	0.04+1.2*AM r^2=0.55	0.04+0.90*AM r^2=0.72
OMI vs Terra MODIS	0.27+1.28*TM r^2=0.19	0.26+0.93*TM r^2=0.32	1.3+1.7*TM r^2=0.09	0.35+1.4*TM r^2=0.13	0.29+0.57*TM r^2=0.07	0.33+1.5*TM r^2=0.23
OMI vs Aqua MODIS	0.26+1.21*AM r^2=0.18	0.27+1.0 *AM r^2=0.28	1.4+1.7*AM r^2=0.07	0.35+1.5*AM r^2=0.22	0.25+1.18*AM r^2=0.16	0.33+1.7*AM r^2=0.17

radiances to radiances, ~0.4 $W m^{-2}$), radiance to flux conversion (~0.5 $W m^{-2}$, e.g., Loeb et al., 2003), MODIS AOD (to be evaluated for the region), and sub-pixel contamination and cloud biases. Uncertainties need to be revisited for SEA, based on in situ and satellite analysis.

8.7. Gas products

Finally, in this review, a few statements on gas products are appropriate. Providing a review of gas retrievals and data products for SEA would likely take an even greater amount of space than the aerosol retrievals. Gas retrievals benefit from better constraint of the optical properties of the target species relative to aerosol retrievals. However, they must generally separate multiple absorbing species in the spectral regions where they have sensitivity, and in some cases can experience interference from aerosol particles (the sensitivity to aerosol particles used to generate the TOMS and OMI AI may be considered a noise factor in the retrieval of ozone). Trace gas retrievals do not have the benefit of such extensive validation networks as AERONET, and generally must be validated using sparse and costly in situ measurements, with their associated challenges of representativeness. But, they do have advantages which aid aerosol research. They are very sensitive to the upper troposphere and clearly aid in the understanding of emission sources and transport pathways (e.g., Fig. 2). NO_2, SO_2, CO, CO_2, and a variety of trace products are now regularly produced from multiple platforms, and are powerful tools for understanding atmospheric composition (Logan et al., 2008). The interested reader should refer to the review paper by Wagner et al. (2008). The complexity of the SEA emissions and carbon cycle will likely require reconciliation of all of these various atmospheric products.

9. Discussion and conclusions: moving forward in the Southeast Asian aerosol system

This review was conducted for the benefit of aerosol scientists wishing to begin research in the Southeast Asian (SEA) region, including the scientists in the 7 Southeast Asian Studies and Southeast Asia Composition, Cloud, Climate Coupling Regional Study (SEAC^{4}RS). The complexity of the relationships between geographic, socio-economic, meteorological, and aerosol microphysical factors, and how they relate

Table 4
Published verification metrics from MODIS from Hyer et al. (2011) and MISR verification metrics from Kahn et al. (2010). "A"=AERONET.

Site	Terra-MODIS	Aqua-MODIS	Terra-MISR
Singapore[a]	−0.15+2.1*A; r^2=0.14; N=98	0.02+1.27*A; r^2=0.14; N=197	
Thailand			
Chiang Mai	−0.19+1.07*A; r^2=0.74; N=595	−0.17+1.10*A; r^2=0.62; N=302	
Chiang Mai Met	−0.14+1.07*A; r^2=0.77; N=1712	−0.11+1.07*A; r^2=0.65; N=1145	
Mukdahan	−0.10+0.93*A; r^2=0.89; N=9672	−0.09+0.91*A; r^2=0.88; N=5183	0.04+0.74*A; r^2=0.92; N=54
Pimai	−0.09+1.07*A; r^2=0.83; N=6142	−0.08+1.06*A; r^2=0.81; N=3445	0.22+0.49*A; r^2=0.81; N=43
Silpakorn	0.07+1.03*A; r^2=0.78; N=2499	0.03+1.11*A; r^2=0.82; N=2114	
Vietnam			
Bac Giang	0.02+1.01*A; r^2=0.62; N=2694	0.07+0.96*A; r^2=0.62: N=2447	0.22+0.49*A; r^2=0.80; N=18
Bac Lieu	0.04+1.36*A; r^2=0.58; N=261	−0.07+2.2*A; r^2=0.14: N=182	

[a] In Singapore there are <10 MODIS data points that are flagged very good, and showed no correlation. These are "good retrievals."

to real world impacts, pose a daunting scientific challenge. Compounding scientific problems are great observability difficulties posed by the SEA environment for both in situ and remote sensing measurements.

Remote sensing, coupled with models and more isolated measurements, is likely our best hope for immediate growth in understanding of the SEA system. Current satellite based aerosol, cloud, and precipitation products diverge more in SEA than perhaps any other region of the globe. High variability in cloud features and surface characteristics lead to many different aerosol retrieval biases. Verification data, or even any consistent aerosol data of any sort, is rare. Great care must be taken when selecting products for a specific scientific application.

Despite remote sensing's challenges, a qualitative picture of key processes is beginning to form. This can be demonstrated in Fig. 18, where we provide time series of key aerosol optical depth products for the regression in Table 4. Also provided is the regional Aerosol Index (AI). The year 2006 was selected for this time series given its high level of biomass burning activity. With the exception of perhaps OMI AOD, the different satellite products track one another reasonable well. In some cases, such as the Java Sea, the comparison is quite good. Even with OMI, if we only look at the lower troughs in the data, it too would show qualitative agreement. Hence, from a seasonality or climatology point of view, there is consistency. However, we also see evidence quantitative failing. Consider the aerosol index for Southern Kalimantan and the Java Sea in comparison to AOD products from MIST, MODIS, and SeaWiFS. While they qualitatively track, quantitatively there are very large differences. For example, the Java Sea has higher AODs than its own Southern Kalimantan source region. However, OMI AI shows (correctly) much higher aerosol loadings in the source region, than over the Java Sea. Sampling issues of when and where a quantitative retrieval can be made dictate our view of the aerosol system. This is the crux of the SEA environmental monitoring problem and demonstrates why products cannot be taken at face value.

Scientists are beginning to couple aerosol lifecycle, meteorological and climate views of the environmental system and reconcile them to understand observability challenges. To proceed past qualitative or semi-quantitative descriptions of processes to quantitative numbers, however, will require considerable effort in the community. There are several immediate steps that can be taken by individuals as well as long term goals to be set by organizations.

First and foremost, individual scientists need to acknowledge the complexity of the SEA aerosol system and design experiments appropriately. Quantities inferred from satellite observations of SEA have generally only one or two significant figures (e.g., average AOD is 0.1, 0.2, 0.3, versus 0.155). Adding false precision undermines the validity of the hypothesis test and ultimately defeats the purpose of the investigation. For example, how do we interpret a climate model simulation showing perhaps a 10% impact in precipitation due to aerosol indirect effects in an environment where baseline uncertainties in aerosol optical depth and precipitation are both much higher? The answer to these problems is to first frame the question appropriately so that it can be reasonably addressed with the tools available. Second, the complex meteorological context of any measurement must be considered in the analysis to minimize the possibility that any derived quantity is unduly influenced by confounding and sampling bias. Finally, as SEA is heavily influenced by environmental factors at diurnal to interseasonal scales, some accounting for scale is required. Up scaling from individual measurements and test plots can now be met with downscaling from global climate modeling. Studies of such linkages should be encouraged.

At the organization or agency level, SEA presents many problems which will require effort on the decadal time scale. Perhaps most importantly, there must be the will for the creation and support of databases of field observations, satellite products and model output. All of these data streams need to be maintained and verified. The creation of such datasets can be achieved by several organizations, mining multiple international data streams. Once created, the data can be mined, cross checked and verified. Open access is imperative.

The creation of a SEA environmental database will require technological investments in uncertainty estimation and statistical inference. As we demonstrated, simple “linear” development of environmental systems using products at face value is particularly problematic for SEA. For example, using MODIS to detect fires, followed by assigning emissions, to incorporate into a model, followed by verification or even data assimilation with satellite data can still leave very large uncertainties. Recognizing that the entire environment is significantly undersampled, advanced statistical methods need to be generated to account for observing conditions. For some observations, specialization of product algorithms for SEA is likely necessary.

In conclusion, SEA presents one of aerosol science's greatest challenges, where poor air quality and high climate change vulnerability meet with limited observability and spatial complexity. Addressing SEA's environmental issues will require cooperation from all levels of research, from “boots on the ground” to hand map changes on the land surface in local areas to large international programmatic efforts. Progress in this area will be faster and more certain if scientists understand the context of their work and how it can be used by the community.

Acronyms

7SEAS	7 Southeast Asian Studies
AAOD	Absorption Aerosol Optical Depth
AERONET	Aerosol Robotic Network
AI	Aerosol Index
AIRS	Atmospheric Infrared Sounder
AMSR	Advanced Microwave Scanning Radiometer
AOD	Aerosol Optical Depth
APHRODITE	Asian Precipitation-Highly-Resolved Observational Data Integration Towards the Evaluation of Water Resources
ASTR	Advanced Spaceborne Thermal Emission and Reflection Radiometer
ATSR	Along Track Scanning Radiometer
AVHRR	Advanced Very High Resolution Radiometer
CALIOP	Cloud–Aerosol Lidar with Orthogonal Polarization
CALIPSO	Cloud–Aerosol Lidar and Infrared Pathfinder Satellite Observations

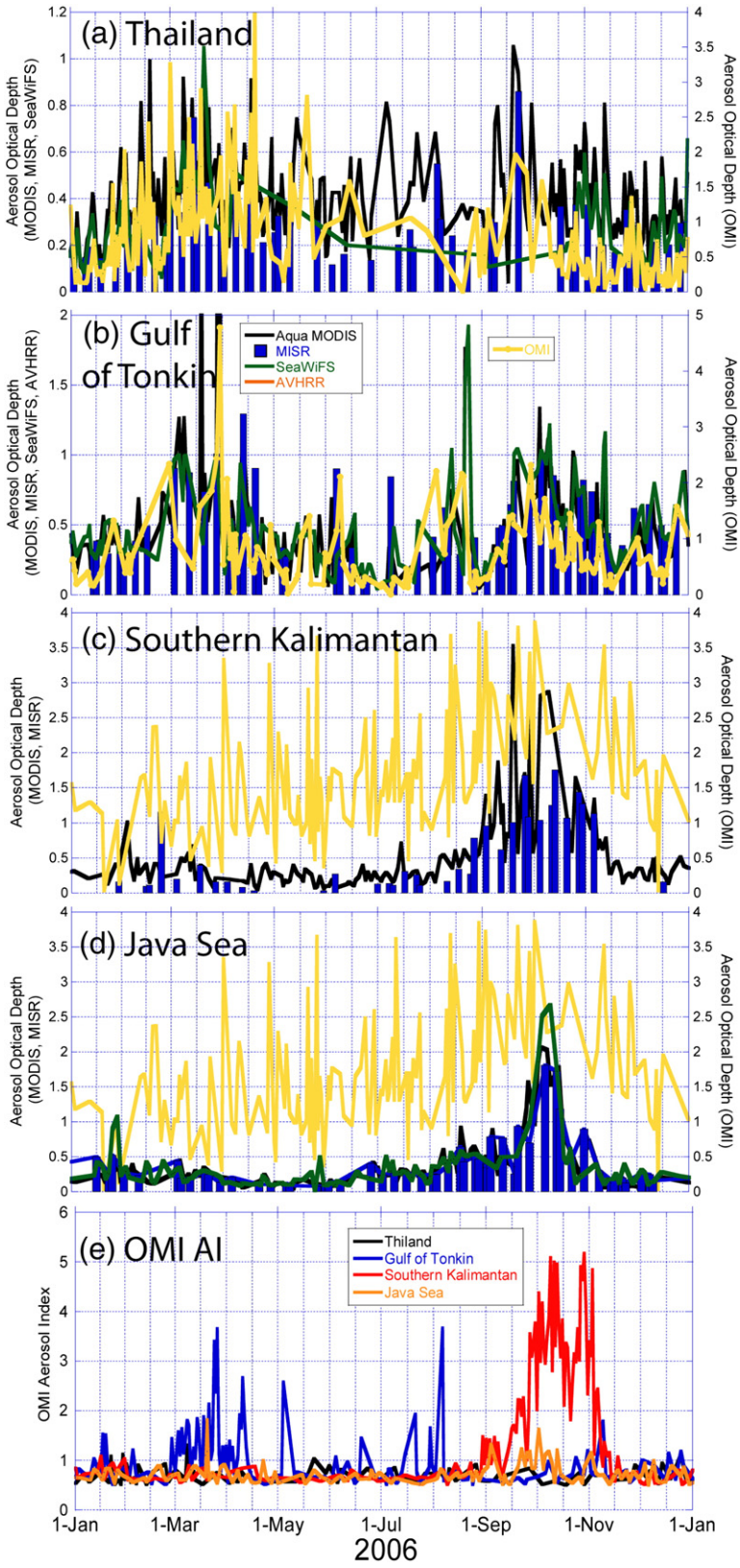

Fig. 18. Time series of AOD products for 2006: (a)Thailand (b) the Gulf of Tonkin; (c) Southern Kalimantan; (d) Java Sea. The OMI aerosol index (AI) for these four locations is given in (e). Locations correspond to the regressions in Table 2. Because of the 8 day overpass schedules for MISR, data is presented as a series of bars.

CERES Clouds and the Earth's Radiant Energy System
CMA Chinese Meteorological Agency
CMORPH Climate Prediction Center MORPHing technique
CNES Centre National d'Etudes Spatiales
COMS Communication, Ocean and Meteorological Satellite
DMSP Defense Meteorological Satellite Program
DPSS Defense Polar Orbiting Satellite System
DTR Dark Target Retrieval
ENSO El Niño/Southern Oscillation
FLAMBE Fire Locating and Modeling of Burning Emissions
GCOM Global Change Observing Mission
GFED Global Fire Emissions Database
GOES Geostationary Operational Environmental Satellite
GRAPE Global Retrieval of ATSR Cloud Parameters and Evaluation
HIRS High Resolution Infrared Sounder
IC Indochina
IPCC Intergovernmental Panel on Climate Change
IPWG International Precipitation Working Group
ISCCP International Satellite Cloud Climatology Project
ISRO Indian Space Research Organization
HRPP High Resolution Precipitation Products
JAXA Japanese Space Agency
JPSS Joint Polar Orbiting Satellite System
LandSat Land Satellite
MC Maritime Continent
MISR Multi-angle Imaging SpectroRadiometer
MLS Microwave Limb Sounder
MODIS Moderate Resolution Imaging Spectroradiometer
MOD # Product number for MODIS Terra
MSG METEOSAT Second Generation
MTSAT Multi-Functional Transport Satellite
MYD # Product number for MODIS Aqua
NASA National Aeronautical and Space Administration
NOAA National Oceanic and Atmospheric Administration
LANDSAT Land-use Satellite or Land Remote-Sensing Satellite
OMI Ozone Monitoring Instrument
OLS Operational Line Scanner
PARASOL Polarization and Anisotropy of Reflectances for Atmospheric Sciences coupled with Observations from a Lidar
PATMOS Pathfinder Atmospheric Science dataset
PMW Passive MicroWave
POLDER POLarization and Directionality of the Earth's Reflectances
SCIAMACHY Scanning Imaging Absorption Spectrometer for Atmospheric CHartographY
SCS/ES South China Sea/East Sea
SEA Southeast Asia
SEAC^{4}RS Southeast Asia Composition, Cloud, Climate Coupling Regional Study
SeaWiFS Sea-viewing Wide Field-of-view Sensor
SPOT Système Pour l'Observation de la Terre
TM Thematic Mapper, on LANDSAT
TMI TRMM Microwave Imager
TOA Top of Atmosphere
TOMS Total Ozone Mapping Spectrometer
TOVS TIROS Operational Vertical Sounder
TRMM Tropical Rainfall Measuring Mission
TTL Tropopause Transition Layer
UV Ultraviolet
VIRS Visible Infrared Scanner
WF_ABBA WildFire-Automated Biomass Burning Algorithm

Acknowledgements

This paper was compiled with the efforts of many individuals on the 7 Southeast Asian Studies team across Southeast Asia and the United States. Funding for the construction of this review was predominantly through the Naval Research Laboratory Base Program and the NASA Interdisciplinary Science Program. We are grateful to the AERONET program and its members for the use of Southeast Asian regional data. Randall Johnson and Jianglong Zhang were supported by the Office of Naval Research Code 32. James Campbell was supported by the Office of Naval Research Code 32. F. Joseph Turk's contribution was performed at the Jet Propulsion Laboratory, under a contract with the National Aeronautics and Space Administration. Larry Di Girolamo was partially supported under contract with the Jet Propulsion Laboratory. Vietnam funding provided by the program for application-oriented fundamental research projects (Ministry of Science and Technology). We would like to thank Ralph Kahn and Andrew Sayer (NASA GSFC) for helpful comments. We are very grateful to the two anonymous reviewers for taking the time to perform a thorough review of this long manuscript and making many helpful suggestions. Finally, we remember our friend and colleague, Dr. Greg Leptoukh who recently passed away. He was instrumental in creating innovative ways to visualize and analyze satellite aerosol products. He will be greatly missed.

References

Acker, J.G., Leptoukh, G., 2007. Online analysis enhances use of NASA Earth science data. EOS Trans. AGU 88, 14–17.
Adger, W.N., 2003. Social capital, collective action and adaptation to climate change. Ecol. Econ. 79, 384–404.
Aditama, T.Y., 2000. Impact of haze from forest fires to respiratory health: Indonesia experience. Respirology 5, 169–174.
Adler, R.F., Kidd, C., Petty, G., Morissey, M., Goodman, H.M., 2001. Intercomparison of global precipitation products: the third precipitation intercomparison project (PIP-3). Bull. Am. Meteorol. Soc. 82, 1377–1396.
Akagi, S.K., Yokelson, R.J., Weidinmyer, C., Alvarado, M.J., Reid, J.S., Karl, T., Crounse, J.D., Wennberg, P.O., 2011. Emission factors for open and domestic biomass burning for use in atmospheric models. Atmos. Chem. Phys. 11, 4039–4072. http://dx.doi.org/10.5194/acp-11-4039-2011.
Alauddin, M., 2004. Environmental economic development: a South Asian perspective. Ecol. Econ. 51, 251–270.
Amiridis, V., Giannakaki, E., Balis, D.S., Gerasopoulos, E., Pytharoulis, I., Zanis, P., Kazadzis, S., Melas, D., Zerefos, C., 2010. Smoke injection heights from agricultural burning in Eastern Europe as seen by CALIPSO. Atmos. Chem. Phys. 10, 11567–11576. http://dx.doi.org/10.5194/acp-10-11567-2010.
Anantharaj, V.G., Nair, U.S., Lawrence, P., Chase, T.N., Christopher, S.A., Jones, T.A., 2010. Comparison of satellite-derived TOA shortwave fluxes to estimates from GCM simulations constrained by satellite observations of land characteristics. Int. J. Climatol. 30, 2088–2104. http://dx.doi.org/10.1002/joc.2107.
Anderson, T.L., Charlson, R.J., Bellouin, N., Boucher, O., Chin, M., Christopher, S.A., Haywood, J., Kaufman, Y.J., Kinne, S., Ogren, J.A., Remer, L.A., Takemura, T., Tanré, D., Torres, O., Trepte, C.R., Wielicki, B.A., Winker, D.M., Yu, H., 2005. A-Train strategy for quantifying direct aerosol forcing of climate: step-wise development of an observational basis for aerosol optical depth, aerosol forcing efficiency, and aerosol anthropogenic fraction. Bull. Am. Meteorol. Soc. 86, 1795–1809. http://dx.doi.org/10.1175/BAMS-86-12-1795.
Arndt, R.L., Carmichael, G.R., Roorda, J.M., 1998. Seasonal source-receptor relationships in Asia. Atmos. Environ. 32, 1397–1406.
Arndt, R.L., Carmichael, G.R., Streets, D.G., Bhatti, N., 1997. Sulfur dioxide emissions and sectorial contributions to sulfur deposition in Asia. Atmos. Environ. 31 (1553–1572), 1997.

Ashok, K., Behera, S.K., Rao, S.A., Weng, H., Yamagata, T., 2007. El Niño Modoki and its possible teleconnection. J. Geophys. Res. 112, C11007. http://dx.doi.org/10.1029/2006JC003798.

Astin, I., Di Girolamo, L., Van de Poll, H.M., 2001. Baysian confidence intervals for true fractional coverage from finite transect measurements: implications for cloud studies from space. J. Geophys. Res. 106, 17303–17310.

Atwood, S. A., Reid, J. S., Kreidenweiss, S. M., Yu, L. E., Salinas, S. V., Chew, B.-N., Balasubramanian, B., submitted for publication. Examination of Singapore as a receptor site for smoke in the Maritime Continent during the 2009 El Niño fire season, Atmospheric Environment.

Bala Subrahamanyam, D., Kiran Kumar, N.V.P., Dutt, C.B.S., Anurose, T.J., Kunhikrishnan, P.K., Mohan, M., 2011. Characterization of air–sea interaction processes over the Bay of Bengal during the winter phase of ICARB field experiment. Atmos. Res. 99, 97–111.

Balasubramanian, R., Qian, W.-B., Decesari, S., Facchini, M.C., Fuzzi, S., 2003. Comprehensive characterization of $PM_{2.5}$ aerosols in Singapore. J. Geophys. Res. 108, 4523. http://dx.doi.org/10.1029/2002JD002517.

Balasubramanian, R., Victor, T., Begum, R., 1999. Impact of biomass burning on rainwater acidity and composition in Singapore. J. Geophys. Res. 104, 26,881–26,890. http://dx.doi.org/10.1029/1999JD900247.

Ballhorn, U., Siegert, F., Mason, M., Limin, S., 2009. Derivation of burn scar depths and estimation of carbon emissions with LIDAR in Indonesian peatlands. Proc. Natl. Acad. Sci. 106, 21213–21218.

Barbel, L., 2007. A model study of smoke-haze influence on clouds and warm precipitation formation in Indonesia 1997/1998. Atmos. Environ. 41, 6838–6852.

Bellouin, N., Jones, A., Haywood, J., Christopher, S.A., 2008. Updated estimate of aerosol direct radiative forcing from satellite observations and comparison against the Hadley. J. Geophys. Res. 113, D10205. http://dx.doi.org/10.1029/2007JD009385.

Betha, R., Pradani, M., Lestari, P., Jsoi, U.M., Reid, J.S., Balasubramanian, R., 2013. Chemical speciation of trace metals emitted from Indonesian peat fires for health risk assessment. Atmos. Res. 122, 571–578 (this issue).

Bessagnet, B., Menut, L., Aymoz, G., Chepfer, H., Vautard, R., 2008. Modeling dust emissions and transport within Europe: the Ukraine March 2007 event. J. Geophys. Res. 113, D15202. http://dx.doi.org/10.1029/2007JD009541.

Berg, W., L'Ecuyer, T., Kummerow, C., 2006. Rainfall climate regimes: the relationship of regional TRMM rainfall biases to the environment. J. Appl. Meteorol. Climatol. 45, 434–454.

Bluth, G.J.S., Doiron, S.D., Schnetzler, C.C., Krueger, A.J., Walter, L.S., 1992. Global tracking of the SO_2 clouds from the June, 1991 Mount Pinatubo eruptions. Geophys. Res. Lett. 19, 151–154.

Boccippio, D.J., Koshak, W., Blakeslee, R., Driscoll, K., Mach, D., Buechler, D., Boeck, W., Christian, H.J., Goodman, S.J., 2000. The Optical Transient Detector (OTD): instrument characteristics and cross-sensor validation. Journal of Atmosphere and Ocean Technology 17, 441–458.

Boccippio, D.J., Koshak, W.J., Blakeslee, R.J., 2002. Performance assessment of the optical transient detector and lightning imaging sensor. Part I: predicted diurnal variability. Journal of Atmosphere and Ocean Technology 19, 1318–1332.

Bond, T.C., Bergstrom, R.W., 2006. Light absorption by carbonaceous particles: an investigative review. Aerosol Sci. Technol. 40, 27–67. http://dx.doi.org/10.1080/02786820500421521.

Bond, T.C., Streets, D.G., Yarber, K.F., Nelson, S.M., Woo, J.-H., Klimont, Z., 2004. A technology-based global inventory of black and organic carbon emissions from combustion. J. Geophys. Res. 109, D14203. http://dx.doi.org/10.1029/2003JD003697.

Bucsela, E.J., Celarier, E.A., Wenig, M.O., Gleason, J.F., Veefkind, J.P., Boersma, K.F., Brinksma, E.J., 2006. Algorithm for NO_2 vertical column retrieval from the ozone monitoring instrument. IEEE Trans. Geosci. Remote. Sens. 44, 1245–1258.

Burling, I.R., Yokelson, R.J., Akagi, S.K., Urbanski, S.P., Wold, C.E., Griffith, D.W.T., Johnson, T.J., Reardon, J., Weise, D.R., 2011. Airborne and ground-based measurements of the trace gases and particles emitted by prescribed fires in the United States. Atmospheric Physics and Chemistry Discussions 11, 18677–18727. http://dx.doi.org/10.5194/acpd-11-18677-2011.

Burling, I.R., Yokelson, R.J., Griffith, D.W.T., Johnson, T.J., Veres, P., Roberts, J.M., Warneke, C., Urbanski, S.P., Reardon, J., Weise, D.R., Hao, W.M., de Gouw, J., 2010. Laboratory measurements of trace gas emissions from biomass burning of fuel types from the southeastern and southwestern United States. Atmos. Chem. Phys. 10, 11115–11130. http://dx.doi.org/10.5194/acp-10-11115-2010.

Campbell, J.R., Reid, J.S., Westphal, D.L., Zhang, J., Hyer, E.J., Welton, E.J., 2010. CALIOP aerosol subset processing for global aerosol transport model data assimilation. IEEE J. Sel. Topics Appl. Earth Observ. Remote Sens. 3, 203–214. http://dx.doi.org/10.1109/JSTARS.2010.2044868.

Campbell, J.R., Shiobara, M., 2008. Glaciation of a mixed-phase boundary layer cloud at a coastal Arctic site as depicted in continuous lidar measurements. Polar Sci. 2, 121. http://dx.doi.org/10.1016/j.polar.2008.04.004.

Campbell, J.R., Welton, E.J., Krotkov, N.A., Stewart, S.A., Fromm, M.D., 2011. Likely seeding of cirrus clouds by stratospheric Kasatochi volcanic aerosol particles near a mid-latitude tropopause fold. Atmospheric Environment submitted, January.

Campbell, J.R., Reid, J.S., Westphal, D.L., Zhang, J., Tackett, J.L., Chew, B.N., Welton, E.J., Shimizu, A., Sugimoto, N., Aoki, K., Winker, D.M., 2013. Characterizing the vertical profile of aerosol particle extinction and linear depolarization over Southeast Asia and the Maritime Continent: The 2007–2009 view from CALIOP. Atmos. Res. 122, 520–543 (this issue).

Calle, A., Casanova, J.L., Gonzalez-Alonso, F., 2009. Impact of point spread function of MSG-SEVIRI on active fire detection. Internaitonal Journal of Remote Sensing 30, 4567–4579.

Capes, G., Johnson, B., McFiggans, G., Williams, P.I., Haywood, J., Coe, H., 2008. Aging of biomass burning aerosols over West Africa: aircraft measurements of chemical composition, microphysical properties, and emission ratios. J. Geophys. Res. 113, D00C15. http://dx.doi.org/10.1029/2008JD009845.

Carn, S.A., Froyd, K., Anderson, B.E., Wennberg, P., Crounse, J., Spencer, K., Dibb, J., Krotkov, N.A., Browell, E.V., Hair, J.W., Diskin, G., Sachse, G., Vay, S., 2011. In situ measurements of tropospheric volcanic plumes in Ecuador and Colombia during TC^4. J. Geophys. Res. 116, D00J24. http://dx.doi.org/10.1029/2010JD014718.

Carn, S.A., Krueger, A.J., Krotkov, N.A., Yang, K., Evans, K., 2009. Tracking volcanic sulfur dioxide clouds for aviation hazard mitigation. Nat. Hazard. 51, 325–343. http://dx.doi.org/10.1007/s11069-008-9228-4.

Carn, S.A., Prata, A.J., Karlsdótti, S., 2008. Circumpolar transport of a volcanic cloud from Hekla (Iceland). J. Geophys. Res. 113, D14311. http://dx.doi.org/10.1029/2008JD009878.

Carrico, C.M., Petters, M.D., Kreidenweis, S.M., Sullivan, A.P., McMeeking, G.R., Levin, E.J.T., Engling, G., Malm, W.C., Collett Jr., J.L., 2010. Water uptake and chemical composition of fresh aerosols generated in open burning of biomass. Atmos. Chem. Phys. 10, 5165–5178. http://dx.doi.org/10.5194/acp-10-5165-2010.

Chand, D., Schmid, O., Gwaze, P., Parmar, R.S., Helas, G., Zeromskiene, K., Wiedensohler, A., Massling, A., Andreae, M.O., 2005. Laboratory measurements of smoke optical properties from the burning of Indonesian peat and other types of biomass. Geophys. Res. Lett. 32, L12819. http://dx.doi.org/10.1029/2005GL022678.

Chang, C.-P., Ding, Y., Lau, N.-C., Johnson, R.H., Wang, B., Yasunari, T. (Eds.), 2011. The Global Monsoon System: Research and Forecast, second ed. World Sci Pub, Singapore.

Chang, C.-P., Wang, Z., Mcbride, J., Liu, C.-H., 2005a. Annual cycle of Southeast Asia-Maritime Continent rainfall and asymmetric monsoon transition. J. Clim. 18, 287–301.

Chang, C.-P., Harr, P.A., Chen, H.-J., 2005b. Synoptic disturbances over the equatorial South China Sea and Western Maritime continent during boreal winter. Mon. Weather Rev. 133, 489–503.

Chang, D., Song, Y., 2010. Estimates of biomass burning emissions in tropical Asia based on satellite-derived data. Atmos. Chem. Phys. 10, 2335–2351.

Chen, W.-T., Kahn, R.A., Nelson, D., Yau, K., Seinfeld, J.H., 2008. Sensitivity of multiangle imaging to the optical and microphysical properties of biomass burning aerosols. J. Geophys. Res. 113, D10203. http://dx.doi.org/10.1029/2007JD009414.

Chew, B.N., Campbell, J.R., Reid, J.S., Giles, D.M., Welton, E.J., Salinas, S.V., Liew, S.C., 2011. Tropical cirrus cloud contamination in sun photometer data. Atmos. Environ. Atmos. Env. 45, 6724–6731. http://dx.doi.org/10.1016/j.atmosenv.2011.08.017.

Chiu, J.C., Marshak, A., Knyazikhin, Y., Wiscombe, W.J., 2010. Spectrally-invariant behavior of zenith radiance around cloud edges simulated by radiative transfer. Atmos. Chem. Phys. 10, 11295–11303 ISSN 1680–7316.

Christian, H.J., Blakeslee, R.J., Boccippio, D.J., Boeck, W.L., Buechler, D.E., Driscoll, K.T., Goodman, S.J., Hall, J.M., Koshak, W.J., Mach, D.M., Steward, M.F., 2003a. Global frequency and distribution of lightning as observed from space by the Optical Transient Detector. J. Geophys. Res. 108, 4005. http://dx.doi.org/10.1029/2002JD002347.

Christian, T.J., Kleiss, B., Yokelson, R.J., Holzinger, R., Crutzen, P.J., Hao, W.M., Saharjo, B.H., Ward, D.E., 2003b. Comprehensive laboratory measurements of biomass-burning emissions: 1. Emissions from Indonesian, African, and other fuels. J. Geophys. Res. 108, 4719. http://dx.doi.org/10.1029/2003JD003704.

Christian, T.J., Yokelson, R.J., Cárdenas, B., Molina, L.T., Engling, G., Hsu, S.-C., 2010. Trace gas and particle emissions from domestic and industrial biofuel use and garbage burning in central Mexico. Atmos. Chem. Phys. 10, 565–584.

Christopher, S.A., Zhang, J., 2004. Cloud-free shortwave aerosol radiative effect over oceans: strategies for identifying anthropogenic forcing from Terra satellite measurements. Geophys. Res. Lett. 31, L18101. http://dx.doi.org/10.1029/2004GL020510.

Christopher, S.A., Zhang, J., Kaufman, Y., Remer, L.A., 2006. Satellite-based assessment of anthropogenic aerosol radiative forcing. Geophys. Res. Lett. 33, L15816. http://dx.doi.org/10.1029/2005GL025535.
Center for International Earth Science Information Network (CIESIN), 2004. Gridded Population of the World (GPW). Version 3 Columbia University, Palisades, NY. http://beta.sedac.ciesin.columbia.edu/gpw.
Cochrane, M.A., 2003. Fire science for rainforests. Nature 421, 913–919.
Cohen, D.D., Crawford, J., Stelcer, E., Bac, V.T., 2010a. Long range transport of fine particles windblown soils and coal fired power station emissions into Hanoi between 2001–2008. Atmos. Environ. 44, 3761–3769.
Cohen, D.D., Crawford, J., Stelcer, E., Bac, V.T., 2010b. Characterization and source apportionment of fine particulate sources at Hanoi between 2001–2008. Atmos. Environ. 44, 320–328.
Cohn, S.A., Angevine, W.M., 2000. Boundary layer height and entrainment zone thickness measured by lidars and wind-profiling radars. J. Appl. Meteorol. 39, 1233–1247.
Cook, B.I., Buckley, B.M., 2009. Objective determination of monsoon season onset, withdrawal, and length. J. Geophys. Res. 114, D23109. http://dx.doi.org/10.1029/2009JD012795.
Corlett, R.T., 2009. The Ecology of Tropical East Asia. Oxford University Press, New York.
Cox, C., Munk, W., 1954. Measurement of the roughness of the sea surface from photographs of the sun glitter. J. Opt. Soc. Am. 44, 838–850.
Crutzen, P.J., Andreae, M.O., 1990. Biomass burning in the tropics: impacts on atmospheric chemistry and biogeochemical cycles. Science 250, 1669–1678.
Curier, R.L., Veefkind, J.P., Braak, R., Veihelmann, B., Torres, O., de Leeuw, G., 2008. Retrieval of aerosol optical properties from OMI radiances using a multiwavelength algorithm: application to western Europe. J. Geophys. Res. 113, D17. http://dx.doi.org/10.1029/2007JD008738.
Csiszar, I.A., Morisette, J.T., Giglio, L., 2006. Validation of active fire detection from moderate-resolution satellite sensors: the MODIS example in northern Eurasia. IEEE Trans. Geosci. Remote Sens. 44, 1757–1764.
Dai, A., 2006. Precipitation characteristics in eighteen coupled climate models. J. Clim. 19, 4605–4630.
Davison, P.S., Roberts, D.L., Arnold, R.T., Colvile, R.N., 2004. Estimating the direct radiative forcing due to haze from the 1997 forest fires in Indonesia. J. Geophys. Res. 109, D10207. http://dx.doi.org/10.1029/2003JD004264.
Dawud, Y., 1998. Smoke episodes and assessment of health impacts related to haze from forest fires: Indonesian experience. Health Guidelines for Vegetation Fire Events, Lima, Peru, Oct 6–9, 1998; WHO, 1999.
Dey, S., Di Girolamo, L., 2010. A climatology of aerosol optical and microphysical properties over the Indian Subcontinent from nine years (2000–2008) of Multiangle Imaging SpectroRadiometer (MISR) data. J. Geophys. Res. 115, D15204. http://dx.doi.org/10.1029/2009JD013395.
Dey, S., Di Girolamo, L., 2011. A decade of change in aerosol properties over the Indian subcontinent. Geophys. Res. Lett. 38, L14811. http://dx.doi.org/10.1029/2011GL048153.
Dey, S., Di Girolamo, L., Zhao, G., Jones, A.L., McFarquhar, G.M., 2011. Satellite-observed relationships between aerosol and trade-wind cumulus cloud properties over the Indian Ocean. Geophys. Res. Lett. 38, L01804. http://dx.doi.org/10.1029/2010GL045588.
Di Girolamo, L., Davies, R., 1994. A band-differenced angular signature technique for cirrus cloud detection. IEEE Trans. Geosci. Remote Sens. 32, 890–896.
Di Girolamo, L., Bond, T.C., Bramer, D., Diner, D.J., Fettinger, F., Kahn, R.A., Martonchik, J.V., Ramana, M.V., Ramanathan, V., Rasch, P.J., 2004. Analysis of Multi-angle Imaging SpectroRadiometer (MISR) aerosol optical depths over greater India during winter 2001–2004. Geophysical Review Letters 31, L23115. http://dx.doi.org/10.1029/2004GL021273.
Di Girolamo, L., Menzies, A., Zhao, G., Mueller, K., Moroney, C., Diner, D.J., 2010b. MISR Level 3 Cloud Fraction by Altitude Theoretical Basis. JPL D-62358 Jet Propulsion Laboratory, Pasadena, CA.
Di Girolamo, L., Liang, L., Platnick, S., 2010a. A global view of one-dimensional solar radiative transfer through oceanic water clouds. Geophys. Res. Lett. 37, L18809. http://dx.doi.org/10.1029/2010GL044094.
Ding, Y.H., 2002. Summer monsoonal rainfall in China. J. Meteorol. Soc. Jpn. 70, 373–396.
Ding, Y.H., Chan, J.C.L., 2005. The East Asian summer monsoon: an overview. Meteorol. Atmos. Phys. 89, 117–142.
Dinku, T., Chidzambwa, S., Ceccato, P., Connor, S.J., Rpoelewski, C.F., 2008. Validation of high resolution satellite rainfall products over complex terrain. Int. J. Remote. Sens. 29, 4049–4110.
Duan, J.C., Tan, J.H., Cheng, D.X., Bi, X.H., Deng, W.J., Sheng, G.Y., Fu, J.M., Wong, M.H., 2007. Sources and characteristics of carbonaceous aerosol in two large cities in the Pearl River Delta region, China. Atmos. Environ. 41, 2895–2903.
Dubovik, O., Holben, B.N., Eck, T.F., Smirnov, A., Kaufman, Y.J., King, M.D., Tanre, D., Slutsker, I., 2002. Variability of absorption and optical properties of key aerosol types observed in worldwide locations. J. Atmos. Sci. 59, 590–608.
Dubovik, O., King, M.D., 2000. A flexible inversion algorithm for retrieval of aerosol optical properties from Sun and sky radiance measurements. J. Geophys. Res. 105, 20,673–20,696.
Duncan, B.N., Bey, I., Chin, M., Mickley, L.J., Fairlie, T.D., Martin, R.V., Matsueda, H., 2003a. Indonesian wildfires of 1997: impact on tropospheric chemistry. J. Geophys. Res. 108, 4458. http://dx.doi.org/10.1029/2002JD003195.
Duncan, B.N., Martin, R.V., Staudt, A.C., Yevich, R., Logan, J.A., 2003b. Interannual and seasonal variability of biomass burning emissions constrained by satellite observations. J. Geophys. Res. 108, 4100. http://dx.doi.org/10.1029/2002JD002378.
Duncan, B.N., Strahan, S.E., Yoshida, Y., Steenrod, S.D., Livesey, N., 2007. Model study of the cross-tropopause transport of biomass burning pollution. Atmos. Chem. Phys. 7, 3713–3736. http://dx.doi.org/10.5194/acp-7-3713-2007.
Dusek, U., Frank, G.P., Helas, G., Iinuma, Y., Zeromskiene, K., Gwaze, P., Henning, T., Massling, A., Schmid, O., Herrmann, H., Wiedensohler, A., Andreae, M.O., 2005. "Missing" cloud condensation nuclei in peat smoke. Geophys. Res. Lett. 32, L11802. http://dx.doi.org/10.1029/2005GL022473.
Ebert, E.E., Janowiak, J.E., Kidd, C., 2007. Comparison of near-real-time precipitation estimates from satellite observations and numerical models. Bull. Am. Meteorol. Soc. 88, 47–64.
Eck, T.F., et al., 2012. Fog- and cloud-induced aerosol modification observed by the Aerosol Robotic Network (AERONET). J. Geophys. Res. 117, D07206. http://dx.doi.org/10.1029/2011JD016839.
Eguchi, K., Uno, Itsushi, Yumimoto, Keiya, Takemura, Toshihiko, Nakajima, Takashi Y., Uematsu, Mitsuo, Liu, Zhaoyan, 2011. Modulation of cloud droplets and radiation over the North Pacific by sulfate aerosol erupted from Mount Kilauea. SOLA, vol. 7, pp. 77–80. http://dx.doi.org/10.2151/sola.2011-020, JOI JST.JSTAGE/sola/2011-020.
Emmanuel, S.C., 2005. Impact to lung health of haze from forest fires: the Singapore experience. Respirology 5, 175–182.
Engling, G., Zhang, Y.-N., Chan, C.-Y., Sang, X.-F., Lin, M., Ho, K.-F., Li, Y.-S., Lin, C.-Y., Lee, J.J., 2011. Characterization and sources of aerosol particles over the southeastern Tibetan Plateau during the Southeast Asia biomass-burning season. Tellus-B 63, 117–128.
Eva, H., Lambin, E.F., 1998. Remote sensing of biomass burning in tropical regions: sampling issues and multisensor approach. Remote Sens. Environ. 64, 292–315.
Eyring, V., Kohler, H.W., van Aardenne, J., Lauer, A., 2005. Emissions from international shipping: 1, the last 50 years. J. Geophys. Res. 110, D17305. http://dx.doi.org/10.1029/2004JD005619.
Feng, N., Christopher, S.A., 2013. Satellite and surface-based remote sensing of Southeast Asian aerosols and their radiative effects. Atmos. Res. 122, 544–554 (this issue).
Fernald, F.G., 1984. Analysis of atmospheric lidar observations: some comments. Appl. Optics 23, 652–653.
Field, R.D., Shen, S.S.P., 2008. Predictability of carbon emissions from biomass burning in Indonesia. J. Geophys. Res. 113, G04024. http://dx.doi.org/10.1029/2008JG000694.
Field, R.D., van der Werf, G.R., Shen, S.S.P., 2009. Human amplification of drought-induced biomass burning in Indonesia since 1960. Nat. Geosci. 2, 185–188.
Flasse, S.P., Ceccato, P., 1996. A contextual algorithm for AVHRR fire detection. Int. J. Remote. Sens. 17, 419–424.
Fox, J., Fujita, Y., Ngidang, D., Peluso, N., Potter, L., Sakuntaladewi, N., Sturgen, J., Thomas, D., 2009. Policies, political economy, and swidden in Southeast Asia. Hum. Ecol. 37, 305–322. http://dx.doi.org/10.1007/s10745-009-9240-7.
Franke, K., Richter, A., Bovensmann, H., Eyring, V., Jöckel, P., Hoor, P., Burrows, J.P., 2009. Ship emitted NO_2 in the Indian Ocean: comparison of model results with satellite data. Atmos. Chem. Phys. 9, 7289–7301. http://dx.doi.org/10.5194/acp-9-7289-2009.
Fraser, R.S., Kaufman, Y.J., Mahoney, R.L., 1984. Satellite measurements of aerosol mass and transport. Atmos. Environ. 18, 2577–2584.
Friedl, M.A., McIver, D.K., Hodges, J.C.F., Zhang, X.Y., Muchoney, D., Strahler, A.H., Woodcock, C.E., Gopal, S., Schneider, A., Cooper, A., Baccini, A., Gao, F., Schaaf, C., 2002. Global land cover mapping from MODIS: algorithms and early results. Remote Sens. Environ. 83, 287–302.
Fromm, M., Lindsey, D.T., Servranckx, R., Yue, G., Trickl, T., Sica, R., Doucet, P., Godin-Beekmann, S., 2010. The untold story of pyrocumulonimbus. Bull. Am. Meteorol. Soc. 91, 1193–1209.
Fromm, M., Shettle, E.P., Fricke, K.H., Ritter, C., Trickl, T., Giehl, H., Gerding, M., Barnes, J.E., Neill, M., Massie, S.T., Blum, U., McDermid, I.S., Leblanc, T., Deshler, T., 2008. Stratospheric impact of the Chisholm pyrocumulonimbus eruption: 2. Vertical profile perspective. J. Geophys. Res. 113, D08203. http://dx.doi.org/10.1029/2007JD009147.
Fu, J.S., Hsu, N.C., Gao, Y., Huang, K., Li, C., Lin, N.-H., Tsay, S.-C., 2012. A regional chemical transport modeling to identify the influences of biomass burning during 2006 BASE-ASIA. Atmos. Chem. Phys. 12, 3837–3855. http://dx.doi.org/10.5194/acp-12-3037-2012.

Fueglistaler, S., Dessler, A.E., Dunkerton, T.J., Folkins, I., Fu, Q., Mote, P.W., 2009. Tropical tropopause layer. Rev. Geophys. 47, RG1004. http://dx.doi.org/10.1029/2008RG000267.

Fukushima, M., Kanzaki, M., Hara, M., Ohkubo, T., Preechapanya, P., Choocharoen, C., 2008. Secondary forest succession after the cessation of swidden cultivation in the montane forest area in Northern Thailand. Forest Ecol. Manage. 255, 1994–2006.

Fuller, D.O., Murphy, K., 2006. The enso-fire dynamic in insular Southeast Asia. Clim. Change 74, 435–455. http://dx.doi.org/10.1007/s10584-006-0432-5.

Gadde, B., Bonnet, S., Menke, C., Garivait, S., 2009. Air pollutant emissions from rice straw open field burning in India, Thailand and the Philippines. Environ. Pollut. 157, 1554–1558.

Gettelman, A., Kinnison, D.E., Dunkerton, T.J., Brasseur, G.P., 2004. Impact of monsoon circulations on the upper troposphere and lower stratosphere. J. Geophys. Res. 109, D22101. http://dx.doi.org/10.1029/2004JD004878.

Giglio, L., 2007. Characterization of the tropical diurnal fire cycle using VIRS and MODIS observations. Remote Sens. Environ. 108, 407–421.

Giglio, L., Csiszar, I., Justice, C.O., 2006. Global distribution and seasonality of active fires as observed with the Terra and Aqua MODIS sensors. J. Geophys. Res. 111, G02016. http://dx.doi.org/10.1029/2005JG000142.

Giglio, L., Descloitres, J., Justice, C.O., Kaufman, Y.J., 2003a. An enhanced contextual fire detection algorithm for MODIS. Remote Sens. Environ. 87, 273–282.

Giglio, L., Kendall, J.D., 2001. Application of the Dozier retrieval to wildfire characterization — A sensitivity analysis. Remote Sensing of the Environment 77, 34–49. http://dx.doi.org/10.1016/S0034-4257(01)00192-4.

Giglio, L., Kendall, J.D., Mack, R., 2003b. A multi-year active fire dataset for the tropics derived from the TRMM VIRS. Int. J. Remote. Sens. 24, 4505–4525.

Giglio, L., Kendall, J.D., Tucker, C.J., 2000. Remote sensing of fires with the TRMM VIRS. Int. J. Remote. Sens. 21, 203–207.

Giglio, L., Loboda, T., Roy, D.P., Quayle, B., Justice, C.O., 2009. An active-fire based burned area mapping algorithm for the MODIS sensor. Remote Sens. Environ. 36, 408–420.

Giglio, L., Randerson, J.T., van der Werf, G.R., Kasibhatla, P.S., Collatz, G.J., Morton, D.C., DeFries, R.S., 2010. Assessing variability and long-term trends in burned area by merging multiple satellite fire products. Biogeosciences 7, 1171–1186. http://dx.doi.org/10.5194/bg-7-1171-2010.

Giri, C., Shrestha, S., 2000. Forest fire mapping in Huay Kha Khaeng Wildlife Sanctuary, Thailand. Int. J. Remote. Sens. 21, 2023–2030.

Goh, A.Z.-C., Chan, J.C.L., 2010. Internannual and interdecadal variation of tropical cyclone activity in the South China Sea. Int. J. Clim. 30, 827–843.

Goldammer, J.G., 2006. History of equatorial vegetation fires and fire research in Southeast Asia before the 1997–98 episode: a reconstruction of creeping environmental changes. Mitig. Adapt. Strateg. Glob. Chang. 12, 13–32.

Gonzi, S., Palmer, P.I., 2010. Vertical transport of surface fire emissions observed from space. J. Geophys. Res. 115, D02306. http://dx.doi.org/10.1029/2009JD012053.

Gras, J.L., Jensen, J.B., Okada, K., Ikegami, M., Zaizen, Y., Makino, Y., 1999. Some optical properties of smoke aerosol in Indonesia and tropical Australia. Geophys. Res. Lett. 26, 1393–1396.

Grieshop, A.P., Logue, J.M., Donahue, N.M., Robinson, A.L., 2009. Laboratory investigation of photochemical oxidation of organic aerosol from wood fires 1: measurement and simulation of organic aerosol evolution. Atmos. Chem. Phys. 9, 1263–1277. http://dx.doi.org/10.5194/acp-9-1263-2009.

Gutman, G., Csiszar, I., Romanov, P., 2000. Using NOAA/AVHRR products to monitor El Niño impacts: focus on Indonesia in 1997–98. Bull. Am. Meteorol. Soc. 81, 1189–1205.

Halmer, M.M., Schmincke, D.J., Graf, H.-F., 2002. The annual volcanic gas input into the atmosphere, in particular into the stratosphere: a global data set for the past 100 years. J. Volcanol. Geotherm. Res. 115, 511–528.

Hamid, E.Y., Kawasakim, Z.-I., Mardiana, T., 2001. Impact of the 1998–1998 El Niño event on lighting activity over Indonesia. Geophys. Res. Lett. 28, 147–150.

Hansen, J., Sato, M., Ruedy, R., Nazarenko, L., Lacis, A., Schmidt, G.A., Russell, G., Aleinov, I., Bauer, M., Bauer, S., Bell, N., Cairns, B., Canuto, V., Chandler, M., Cheng, Y., Del Genio, A., Faluvngi, G., Fleming, E., Friend, A., Hall, T., Jackman, C., Kelley, M., kiang, N., Kock, D., Lean, J., Lerner, J., Lo, K., Menon, S., Miller, R., Minnis, P., Novakov, T., Oinas, V., Perlwitz, Ja, Perlwitz, Ju, Rind, D., Romanou, A., Shindell, D., Stone, P., Sun, S., Tausnev, N., Thresher, D., Wielicki, B., Wong, T., Yao, M., Zhang, S., 2005. Efficacy of climate forcings. J. Geophys. Res. 110, D18104. http://dx.doi.org/10.1029/2005JD005776.

Hansen, M.C., Stehman, S.V., Potapov, P.V., Arunarwati, B., Stolle, F., Pittman, K., 2009. Quantifying changes in the rates of forest clearing in Indonesia from 1990 to 2005 using remotely sensed data sets. Environ. Res. Lett. 4, 034001–034012.

Hansen, T.S., Mertz, O., 2006. Extinction or adaptation? Three decades of change in shifting cultivation in Sarawak, Malaysia. Land Degrad. Dev. 17, 135–148.

Hashim, M., Kanniah, K.D., Ahmad, A., Rasib, A.W., Ibrahim, A.L., 2004. The use of AVHRR data to determine the concentration of visible an invisible tropospheric pollutants from a 1997 forest fire in Southeast Asia. Int. J. Remote. Sens. 25, 4781–4794.

Haywood, J.M., Francis, P., Dubovik, O., Glew, M., Holben, B.N., 2003. Comparison of aerosol size distributions, radiative properties and optical depths determined by aircraft observations and sunphotometers during SAFARI-2000. J. Geophys. Res. 108, 8471. http://dx.doi.org/10.1029/2002JD002250.

He, J., Balasubramanian, R., 2009a. Rain-aerosol coupling in the tropical atmosphere of Southeast Asia: distribution and scavenging ratios of major ionic species. J. Atmos. Chem. 60, 205–220.

He, J., Balasubramanian, R., 2009b. A study of gas/particle partitioning of SVOCs in the tropical atmosphere of Southeast Asia. Atmos. Environ. 43, 4375–4383.

He, J., Balasubramanian, R., Burger, D.F., Hicks, K., Kuylenstierna, J.C.I., Palani, S., 2011. Dry and wet atmospheric deposition of nitrogen and phosphorus in Singapore. Atmos. Environ. 45, 2760–2768.

He, J., Zielinska, B., Balasubramanian, R., 2010. Composition of semi-volatile organic compounds in the urban atmosphere of Singapore: influence of biomass burning. Atmos. Chem. Phys. 10, 11401–11413.

Hegg, D.A., Baker, M.B., 2009. Nucleation in the atmosphere. Rep. Prog. Phys. P72, 056801. http://dx.doi.org/10.1088/0034-4885/72/5/056801.

Hergoualch, K., Verchot, L.V., 2011. Stocks and fluxes of carbon associated with land use change in Southeast Asian tropical peatlands: a review. Global Biogeochem. Cycles 25, GB2001. http://dx.doi.org/10.1029/2009GB003718.

Hess, M., Koepke, P., Schult, I., 1998. Optical properties of aerosols and clouds: the software package OPAC. Bull. Am. Meteorol. Soc. 79, 831–844.

Herman, J.R., Bhartia, P.K., Torres, O., Hsu, N.C., Seftor, C.J., Celarier, E., 1997. Global distribution of UV-absorbing aerosols from Nimbus 7/TOMS data. J. Geophys. Res. 102, 16,911–16,922. http://dx.doi.org/10.1029/96JD03680.

Hobbs, P.V., Tuell, J.P., Hegg, D.A., Radke, L.F., Eltgroth, M.W., 1982. Particles and gases in the emissions from the 1980–1981 volcanic eruptions of Mt. St. Helens. J. Geophys. Res. 87, 11,062–11,086. http://dx.doi.org/10.1029/JC087iC13p11062.

Hobbs, P.V., Hegg, D.A., Radke, L.F., 1983. Resuspension of volcanic ash from Mount St. Helens. J. Geophys. Res. 88, 3919–3921.

Hobbs, P.V., Radke, L.F., Lyons, J.H., Ferek, R.H., Coffman, D.J., Casadevall, T.J., 1991. Airborne measurements of particle and gas emissions from the 1990 volcanic eruptions of Mt Redoubt. J. Geophys. Res. 96 (D10), 18,735–18,752. http://dx.doi.org/10.1029/91JD01635.

Hoekman, D.H., 2007. Satellite radar observations of tropical peat swamp forest as a tool for hydrological modeling and environmental protection. Aquat. Conserv. Mar. Freshwat. Ecosyst. 17, 265–275.

Hoff, R.M., Strawbridge, K.B., 1996. LITE observations of anthropogenically produced aerosols. In: Ansmann, A., Neuber, R., Rairoux, P., Wandinger, U. (Eds.), Advances in Atmospheric Remote Sensing with Lidar. Springer, Berlin, pp. 145–148.

Hogan, T.F., Rosmond, T.E., 1991. The description of the Navy Operational Global Atmospheric Prediction Systems spectral forecast model. Mon. Weather Rev. 119, 1786–1815.

Holben, B.N., Eck, T.F., Slutsker, I., Tanre, D., Buis, J.P., Setzer, A., Vermote, E., Reagan, J.A., Kaufman, Y., Nakajima, T., Lavenu, F., Jankowiak, I., Smirnov, A., 1998. AERONET — a federated instrument network and data archive for aerosol characterization. Remote Sens. Environ. 66, 1–16.

Hooijer, A., Page, S., Jauhiainen, J., Lee, W.A., Lu, X.X., Idris, A., Anshari, G., 2011. Subsidence and carbon loss in drained tropical peatlands: reducing uncertainty and implications for CO_2 emission reduction options. Biogeosci. Discuss. 8, 9311–9356. http://dx.doi.org/10.5194/bgd-8-9311-2011.

Hopke, P.K., Cohen, D.D., Begum, B.A., Biswas, S.K., Ni, B., Pandit, G.G., Santoso, M., Chung, Y.-S., Davy, P., Markwitz, A., Waheed, S., Siddique, N., Santos, F.L., Pabroa, P.C.B., Seneviratne, M.C.S., Wimolwattanapun, W., Bunprapob, S., Vuong, T.B., Hien, P.D., Markowicz, A., 2008. Urban air quality in the Asian region. Sci. Total Environ. 404, 103–112. http://dx.doi.org/10.1016/j.scitotenv.2008.05.039 ISSN 0048–9697.

Hou, A., Jackson, G.S., Kummerow, C., Shepherd, J.M., 2008. Global precipitation measurement. In: Michaelides, S. (Ed.), Precipitation: Advances in Measurement, Estimation, and Prediction. Springer. 131–170.

Hoyningen-Huene, W., Schmidt, T., Schienbein, S., Kee, C.A., Tick, L.J., 1999. Climate-relevant aerosol parameters of South-East-Asian forest fire haze. Atmos. Environ. 33, 3183–3190.

Hsu, N.C., Herman, J.R., Bhartia, P.K., Seftor, C.J., Torres, O., Thompson, A.M., Gleason, J.F., Eck, T.F., Holben, B.N., 1996. Detection of biomass burning smoke from TOMS measurements. Geophys. Res. Lett. 23, 745–748.

Hsu, N.C., Herman, J.R., Torres, O., Holben, B.N., Tanre, D., Eck, T.F., Smirnov, A., Chatenet, B., Lavenu, F., 1999. Comparisons of the TOMS aerosol index with sun-photometer aerosol optical thickness: results and applications. J. Geophys. Res. 104, 6269–6279. http://dx.doi.org/10.1029/1998JD200086.

Hsu, N.C., Herman, J.R., Tsay, S.-C., 2003. Radiative impacts from biomass burning in the presence of clouds during boreal spring in Southeast Asia. Geophys. Res. Lett. 30, 1224. http://dx.doi.org/10.1029/2002GL016485.
Hsu, N.C., Tsay, S.-C., King, M.D., Herman, J.R., 2004. Aerosol properties over bright-reflecting source regions. IEEE Trans. Geosci. Remote Sens. 42, 557–569. http://dx.doi.org/10.1109/TGRS.2004.824067.
Hsu, N.C., Tsay, S.-C., King, M.D., Herman, J.R., 2006. Deep Blue retrievals of Asian aerosol properties during ACE Asia. IEEE Trans. Geosci. Remote Sens. 44, 3180–3195. http://dx.doi.org/10.1109/TGRS.2006.879540.
Huang, J., Hsu, N.C., Tsay, S.-C., Jeong, M.-J., Holben, B.N., Berkoff, T.A., Welton, E.J., 2011. Susceptibility of aerosol optical thickness retrievals to thin cirrus contamination during the BASE-ASIA campaign. J. Geophys. Res. 116, D08214. http://dx.doi.org/10.1029/2010JD014910.
Huffman, G.J., Adler, R.F., Bolvin, D.T., Gu, G., Nelkin, E.J., Bowma, K.P., Hong, Y., Stocker, E.F., Wolff, D.B., 2007. The TRMM Multi-satellite precipitation analysis: quasi-global, multi combined-sensor precipitation estimates at fine scale. J. Hydrometeorol. 8, 38–55.
Hunton, D.E., Viggiano, A.A., Miller, T.M., Ballenthin, J.O., Reeves, J.M., Wilson, J.C., Lee, S.-H., Anderson, B.E., Brune, W.H., Harder, H., Simpas, J.B., Oskarsson, N., 2005. In-situ aircraft observations of the 2000 Mt. Hekla volcanic cloud: composition and chemical evolution in the Arctic lower stratosphere. J. Volcanol. Geotherm. Res. 145, 23–34.
Hyer, E.J., Chew, B.N., 2010. Aerosol transport model evaluation of an extreme smoke episode in Southeast Asia. Atmos. Environ. 44, 1422–1427.
Hyer, E.J., Reid, J.S., 2009. Baseline uncertainties in biomass burning emission models resulting from spatial error in satellite active fire location data. Geophys. Res. Lett. 36, L05802. http://dx.doi.org/10.1029/2008GL036767.
Hyer, E.J., Reid, J.S., Zhang, J., 2011. An over-land aerosol optical depth data set for data assimilation by filtering, correction, and aggregation of MODIS Collection 5 optical depth retrievals. Atmos. Meas. Technol. 4, 379–408. http://dx.doi.org/10.5194/amt-4-379-2011.
Hyer, E.J., Reid, J.S., Prins, E.M., Hoffman, J.P., Schmidt, C.C., Miettinen, J.I., Giglio, L., 2013. Patterns of fire activity over Indonesia and Malaysia from polar and geostationary satellite observations. Atmos. Res. 122, 504–519 (this issue).
Ialongo, I., Buchard, V., Brogniez, C., Casale, G.R., Siani, A.M., 2010. Aerosol single scattering albedo retrieval in the UV range: an application to OMI satellite validation. Atmos. Chem. Phys. 10, 331–340. http://dx.doi.org/10.5194/acp-10-331-2010.
Ignatov, A., Stowe, L., 2002a. Aerosol retrievals from individual AVHRR channels. Part I: retrieval algorithm and transition from Dave to 6S radiative transfer model. J. Atmos. Sci. 59, 313–334.
Ignatov, A., Stowe, L., 2002b. Aerosol retrievals from individual AVHRR channels. Part II: quality control, probability distribution functions, information content, and consistency checks of retrievals. J. Atmos. Sci. 59, 335–362.
Ignatov, A., Sapper, J., Cox, S., Laszlo, I., Nalli, N.R., Kidwell, K.B., 2004. Operational Aerosol Observations (AEROBS) from AVHRR/3 on board NOAA-KLM satellites. J. Atmos. Ocean. Technol. 21, 3–26.
Iinuma, Y., Brüggemann, E., Gnauk, T., Müller, K., Andreae, M.O., Helas, G., Parmar, R., Herrmann, J.H., 2007. Source characterization of biomass burning particles: the combustion of selected European conifers, African hardwood, savanna grass, and German and Indonesian peat. J. Geophys. Res. 112, D08209. http://dx.doi.org/10.1029/2006JD007120.
Ikegami, M., Okada, K., Zaizen, Y., Makino, Y., Jensen, J.B., Gras, J.L., Harjanto, H., 2001. Very high weight ratios of S/K in individual haze particles over Kalimantan during the 1997 Indonesian forest fires. Atmos. Environ. 35, 4237–4242. http://dx.doi.org/10.1016/S1352-2310(01)00247-3.
IPCC, 2007a. Impacts, adaptation, and vulnerability. In: Parry, M.L., Canziani, O.F., Palutikof, J.P., van der Linden, P.J., Hanson, C.E. (Eds.), Climate Change 2007. Cambridge University Press, United Kingdom.
IPCC, 2007b. The physical science basis. In: Solomon, S., Qin, D., Manning, M., Chen, Z., Marquis, M., Averyt, K.B., Tingor, M., Miller, H.L. (Eds.), Climate Change 2007. Cambridge University Press, United Kingdom.
Iwasaki, S., Maruyama, K., Hayashi, M., Ogino, S.-Y., Ishimoto, H., Tachibana, Y., Shimizu, A., Matsui, I., Sugimoto, N., Yamashita, K., Saga, K., Iwamoto, K., Kamiakito, Y., Chabangborn, A., Thana, B., Hashizume, M., Koike, T., Oki, T., 2007. Characteristics of aerosol and cloud particle size distributions in the tropical tropopause layer measured with optical particle counter and lidar. Atmos. Chem. Phys. 7, 3507–3518. http://dx.doi.org/10.5194/acp-7-3507-2007.
Jacob, D.J., Crawford, J.H., Kleb, M.M., Connors, V.S., Bendura, R.J., Raper, J.L., Sachse, G.W., Gille, J.C., Emmons, L., Heald, C.L., 2003. Transport and Chemical Evolution over the Pacific (TRACE-P) aircraft mission: design, execution, and first results. J. Geophys. Res. 108, 9000. http://dx.doi.org/10.1029/2002JD003276.
Jamandre, C.A., Narisma, G.T., 2013. Spatio-temporal validation of satellite-based rainfall estimates in the Philippines. Atmos. Res. 122, 599–608 (this issue).
Janjai, S., Wattan, R., 2011. Development of a model for the estimation of photosynthetically active radiation from geostationary satellite data in a tropical environment. Remote Sens. Environ. 115, 1680–1693.
Janowiak, J.E., Kousky, V.E., Joyce, R.J., 2005. Diurnal cycle of precipitation determined from the CMORPH high spatial and temporal resolution global precipitation analyses. J. Geophys. Res. 110, D23105. http://dx.doi.org/10.1029/2005JD006156.
Jensen, E.J., Toon, E.B., Selkirk, H.B., Spinhirne, J.D., Schoeberl, M.R., 1996. On the formation and persistence of subvisible cirrus clouds near the tropical tropopause. J. Geophys. Res. 101, 21,361–21,375. http://dx.doi.org/10.1029/95JD03575.
Ji, Y., Stocker, E., 2002. Seasonal, intraseasonal, and interannual variability of global land fires and their effects on atmospheric aerosol distribution. J. Geophys. Res. 107, 4697. http://dx.doi.org/10.1029/2002JD002331.
Jiang, J.H., Livesey, N.J., Su, H., Neary, L., McConnell, J.C., Richards, N.A.D., 2007. Connecting surface emissions, convective uplifting, and long-range transport of carbon monoxide in the upper troposphere: new observations from the Aura Microwave Limb Sounder. Geophys. Res. Lett. 34, L18812. http://dx.doi.org/10.1029/2007GL030638.
Jiang, J.H., Su, H., Schoeberl, M.R., Massie, S.T., Colarco, P., Platnick, S., Livesey, N.J., 2008. Clean and polluted clouds: relationships among pollution, ice clouds, and precipitation in South America. Geophys. Res. Lett. 35, L14804. http://dx.doi.org/10.1029/2008GL034631.
Johnson, R.H., Ciesielski, P.E., Hart, K.A., 1996. Tropical inversions near 0°C. J. Atmos. Sci. 53, 1838–1855.
Johnson, R.H., Rickenbach, T.M., Rutledge, S.A., Ciesielski, P.E., Schubert, W.H., 1999. Trimodal characteristics of tropical convection. J. Clim. 12, 2397–2418.
Joyce, R.J., Janowiak, J.E., Arkin, P.A., Xie, P., 2004. CMORPH: a method that produces global precipitation estimates from passive microwave and infrared data at high spatial and temporal resolution. J. Hydrometeorol. 5, 487–503.
Justice, C.O., Giglio, L., Korontzi, S., Owens, J., Morisette, J.T., Roy, D., Descloitres, J., Alleaume, S., Petitcolin, F., Kaufman, Y.J., 2002. The MODIS fire products. Remote Sens. Environ. 83, 244–262.
Kacenelenbogen, M., Vaughan, M.A., Redemann, J., Hoff, R.M., Rogers, R.R., Ferrare, R.A., Russell, P.B., Hostetler, C.A., Hair, J.W., Holben, B.N., 2011. An accuracy assessment of the CALIOP/CALIPSO version 2/version 3 daytime aerosol extinction product based on a detailed multi-sensor, multi-platform case study. Atmos. Chem. Phys. 11, 3981–4000. http://dx.doi.org/10.5194/acp-11-3981-2011.
Kahn, R.A., Gaitley, B.J., Garay, M.J., Diner, D.J., Eck, T.F., Smirnov, A., Holben, B.N., 2010. Multiangle Imaging SpectroRadiometer global aerosol product assessment by comparison with Aerosol Robotic Network. J. Geophys. Res. 115, D23209. http://dx.doi.org/10.1029/2010JD014601.
Kahn, R.A., Li, W.-H., Moroney, C., Diner, D.J., Martonchik, J.V., Fishbein, E., 2007. Aerosol source plume physical characteristics from space-based multi-angle imaging. J. Geophys. Res. 112, D11205. http://dx.doi.org/10.1029/2006JD007647.
Kahn, R.A., Nelson, D.L., Garay, M., Levy, R.C., Bull, M.A., Martonchik, J.V., Diner, D.J., Paradise, S.R., Wu, D.L., Hansen, E.G., Remer, L.A., 2009. MISR aerosol product attributes, and statistical comparisons with MODIS. IEEE Trans. Geosci. Remote Sens. 47, 4095–4114.
Kahn, R.A., Gaitley, A.B., Martonchik, J.V., Diner, D.J., Crean, K., Holben, B.N., 2005. MISR global aerosol optical depth validation based on two years of coincident AERONET observations. J. Geophys. Res. 110, D10S04. http://dx.doi.org/10.1029/2004JD004706.
Kahn, R.A., Garay, M.J., Nelson, D.L., Levy, R.C., Bull, M.A., Diner, D.J., Martonchik, J.V., Hansen, E.G., Remer, L.A., Tanre, D., 2011. Response to "Toward unified satellite climatology of aerosol properties. 3. MODIS versus MISR versus AERONET. J. Quant. Spectrosc. Radiat. Transfer 112, 901–909. http://dx.doi.org/10.1016/j.jqsrt.2010.11.001.
Kanabkaew, T., Oanh, N.T.K., 2011. Development of spatial and temporal emissions inventories for crop residue field burning. Environ. Model Assess. 16, 453–464. http://dx.doi.org/10.1007/s10666-010-9244-0.
Kauppi, P.E., Ausubel, J.H., Fang, J., Mather, A.S., Sedjo, R.A., Waggoner, P.E., 2006. Returning forests analyzed with the forest identity. Proc. Natl. Acad. Sci. U. S. A. 103, 17574–17579.
Kenta, E., Uno, I., Yumimoto, K., Takemura, T., Nakajima, T.Y., Uematsu, M., Liu, L., 2011. Modulation of cloud droplets and radiation over the North Pacific by sulfate aerosol erupted from Mount Kilauea. SOLA 7, 77–80.
Kiladis, G.N., Wheeler, M.C., Haertel, P.T., Straub, K.H., Roundy, P.E., 2009. Convectively coupled equatorial waves. Rev. Geophys. 47. http://dx.doi.org/10.1029/2008RG000266.
Kim, D.-H., Sohn, B.-J., Nakajima, T., Takamura, T., Takemura, T., Choi, B.-C., Yoon, S.C., 2004. Aerosol optical properties over east Asia determined from ground-based sky radiation measurements. J. Geophys. Res. 109, D02209.
Kim, Y.-S., Shibata, T., Iwasaka, Y., Shi, G., Zhou, X., Tamura, K., Ohashi, T., 2003. Enhancements of aerosols near the cold tropopause in summer over Tibetan Plateau: lidar and balloon borne measurements in 1999 at Lhasa, Tibet, China. Proc. SPIE 4893, 496–503. http://dx.doi.org/10.1117/12.466090.

Kittaka, C., Winker, D.M., Vaughan, M.A., Omar, A., Remer, L.A., 2011. Intercomparison of column aerosol optical depths from CALIPSO and MODIS-Aqua. Atmos. Meas. Technol. 4, 131–141.
Kobayashi, H., Matsunaga, T., Hoyano, A., Aoki, M., Komori, D., Boonyawat, S., 2004. Satellite estimation of photosynthetically active radiation in Southeast Asia: impacts of smoke and cloud cover. J. Geophys. Res. 109, D04102. http://dx.doi.org/10.1029/2003JD003807.
Koch, D., Schulz, M., Kinne, S., McNaughton, C., Spackman, J.R., Balkanski, Y., Bauer, S., Berntsen, T., Bond, T.C., Boucher, O., Chin, M., Clarke, A., De Luca, N., Dentener, F., Diehl, T., Dubovik, O., Easter, R., Fahey, D.W., Feichter, J., Fillmore, D., Freitag, S., Ghan, S., Ginoux, P., Gong, S., Horowitz, L., Iversen, T., Kirkevåg, A., Klimont, Z., Kondo, Y., Krol, M., Liu, X., Miller, R., Montanaro, V., Moteki, N., Myhre, G., Penner, J.E., Perlwitz, J., Pitari, G., Reddy, S., Sahu, L., Sakamoto, H., Schuster, G., Schwarz, J.P., Seland, Ø., Stier, P., Takegawa, N., Takemura, T., Textor, C., van Aardenne, J.A., Zhao, Y., 2009. Evaluation of black carbon estimations in global aerosol models. Atmos. Chem. Phys. 9, 9001–9026. http://dx.doi.org/10.5194/acp-9-9001-2009.
Koe, L.C.C., Arellano, A.F., McGregor, J.L., 2001. Investigating the haze transport from the 1997 biomass burning in Southeast Asia: its impacts on Singapore. Atmos. Environ. 35, 2723–2734.
Koh, L., 2007. Impending disaster or sliver of hope for Southeast Asian forests? The devil may lie in the details. Biodivers. Conserv. 16, 3935–3938. http://dx.doi.org/10.1007/s10531-007-9177-3.
Kokhanovsky, A.A., Curier, R.L., De Leeuw, D., Grey, W.M.F., Lee, K.H., Bennouna, Y., Schoemaker, R., North, P.R.J., 2009. The inter-comparison of AATSR dual-view aerosol optical thickness retrievals with results from various algorithms and instruments. Int. J. Remote. Sens. 30, 4525–4537.
Kokhanovsky, A.A., Deuze, J.L., Diner, D.J., Dubovik, O., Ducos, F., Emde, C., Garay, M.J., Grainger, R.G., Heckel, A., Herman, M., Katsev, I.L., Keller, J., Levy, R., North, P.R.J., Prikhach, A.S., Rozanov, V.V., Sayer, A.M., Ota, Y., Tanre, D., Thomas, G.E., Zege, E.P., 2010. The inter-comparison of major satellite aerosol retrieval algorithms using simulated intensity and polarization characteristics of reflected light. Atmos. Meas. Technol. 3, 909–932. http://dx.doi.org/10.5194/amt-3-909-2010.
Koren, I., Remer, L.A., Kaufman, Y.J., Rudich, Y., Martins, J.V., 2007. On the twilight zone between clouds and aerosols. Geophys. Res. Lett. 34 (L08), 805. http://dx.doi.org/10.1029/2007GL029253.
Kotchenruther, R., Hobbs, P.V., 1998. Humidification factors of aerosols from biomass burning in Brazil. J. Geophys. Res. 103, 32,081–32,090.
Kunii, O., Kanagawa, S., Yajima, I., Hisamatsu, Y., Yamamura, S., Amagai, T., Ismail, I.T.S., 2002. The 1997 haze disaster in Indonesia: its air quality and health effects. Arch. Environ. Heal. 57, 16–22.
Langmann, B., Graf, H.F., 2003. Indonesian smoke aerosols from peat fires and the contribution from volcanic sulfur emissions. Geophys. Res. Lett. 30, 1547. http://dx.doi.org/10.1029/2002GL016646.
Langmann, B., Heil, A., 2004. Release and dispersion of vegetation and peat fire emissions in the atmosphere over Indonesia 1997/1998. Atmos. Chem. Phys. 4, 2145–2160.
Langner, A., Miettinen, J., Siegert, F., 2007. Land cover change 2002–2005 in Borneo and the role of fire derived from MODIS imagery. Glob. Chang. Biol. 23, 2329–2340.
Langner, A., Siegert, F., 2009. Spatiotemporal fire occurrence in Borneo over a period of 10 years. Glob. Chang. Biol. 15, 48–62.
Laris, P.S., 2005. Spatiotemporal problems with detecting and mapping mosaic for regimes with coarse-resolution satellite data in savanna environments. Remote Sens. Environ. 99, 412–424.
Lau, K.-M., Kim, M.K., 2006a. Observational relationships between aerosol and Asian monsoon rainfall, and circulation. Geophys. Res. Lett. 33, L21810. http://dx.doi.org/10.1029/2006GL027546.
Lau, K.-M., Kim, M.K., 2006b. Aerosol induced anomalies in the Asian summer monsoon- the role of the Tibetan Plateau. Clim. Dyn. 26, 855–864.
Lau, K.M., Kim, K.M., 2011. Comment on "'Elevated heat pump' hypothesis for the aerosol–monsoon hydroclimate link: 'grounded' in observations?" by S. Nigam and M. Bollasina. J. Geophys. Res. 116, D07203. http://dx.doi.org/10.1029/2010JD014800.
Lau, N.-C., Ploshay, J.J., 2009. Simulation of synoptic- and subsynoptic-scale phenomena associated with the East Asian summer monsoon using a high-resolution GCM. Mon. Weather Rev. 137, 137–160.
Lawrence, M.G., Lelieveld, J., 2010. Atmospheric pollutant outflow from southern Asia: a review. Atmos. Chem. Phys. 10, 11017–11096. http://dx.doi.org/10.5194/acp-10-11017-2010.
Le, H.A., Oanh, N.T.K., 2010. Integrated assessment of brick kiln emission impacts on air quality. Environ. Monit. Assess. 171, 381–394.
Leifled, J., Muller, M., Fuhrer, J., 2011. Peatland subsidence and carbon loss from drained temporal fens. Soil Use Manag. 27, 170–176.
Lestari, P., Mauliadi, Y.D., 2009. Source apportionment of particulate matter at urban mixed site in Indonesia using PMF. Atmos. Environ. 43, 1760–1770.
Levy, R., Leptoukh, G., Kahn, R., Zubko, V., Gopalan, A., Remer, L., 2009. A critical look at deriving monthly aerosol optical depth from satellite data. IEEE Trans. Geosci. Remote Sens. 47, 2942–2956.
Levy, R.C., Remer, L.A., Kleidman, R.G., Mattoo, S., Ichoku, C., Kahn, R., Eck, T.F., 2010. Global evaluation of the Collection 5 MODIS dark-target aerosol products over land. Atmos. Chem. Phys. 10, 10399–10420. http://dx.doi.org/10.5194/acp-10-10399-2010.
Levy, R.C., Remer, L.A., Mattoo, S., Vermote, E.F., Kaufman, Y.J., 2007. Second-generation operational algorithm: retrieval of aerosol properties over land from inversion of Moderate Resolution Imaging Spectroradiometer spectral reflectance. J. Geophys. Res. 112, D13211.
Li, W., Luo, C., Wang, D., Lei, T., 2010. Diurnal variations of precipitation over the South China Sea. Meteorol. Atmos. Phys. 109, 33–46.
Li, Z., Zhao, X., Kahn, R., Mishchenko, M., Remer, L., Lee, K.-H., Wang, M., Laszlo, I., Nakajima, T., Maring, H., 2009. Uncertainties in satellite remote sensing of aerosols and impact on monitoring its long-term trend: a review and perspective. Ann. Geophys. 27, 2755–2770.
Liew, S.C., Lim, O.K., Kwoh, L.K., Lim, H., 1998. A study of the 1997 forest fires in Southeast Asia using SPOT quicklook mosaics. IGARSS '98–1998 International Geoscience and Remote Sensing Symposium Proceedings, vol. 1–5, pp. 879–881.
Lin, C.-Y., Hsu, H.-M., Lee, Y.H., Kuo, C.H., Sheng, Y.-F., Chu, D.A., 2009. A new transport mechanism of biomass burning from Indochina as identified by modeling studies. Atmos. Chem. Phys. 9, 7901–7911. http://dx.doi.org/10.5194/acp-9-7901-2009.
Lin, I.-I., Chen, J.P., Wong, G.T.F., Huang, C.-W., Lien, C.-C., 2007. Aerosol input to the South China Sea: results from the moderate resolution imaging spectroradiometer, the quick scatterometer, and the measurements of pollution in the troposphere sensor. Deep-Sea Res. II 54, 1589–1601.
Liousse, C., Devaux, C., Dulac, F., Cachier, H., 1995. Aging of savannah biomass burning aerosols: consequences on their optical properties. J. Atmos. Chem. 22, 1–17.
Livesey, N.J., Filipiak, M.J., Froidevaux, L., Read, W.G., Lambert, A., Santee, M.L., Jiang, J.H., Pumphrey, H.C., Waters, J.W., Cofield, R.E., Cuddy, D.T., Daffer, W.H., Drouin, B.J., Fuller, R.A., Jarnot, R.F., Jiang, Y.B., Knosp, B.W., Li, Q.B., Perun, V.S., Schwartz, M.J., Snyder, W.V., Stek, P.C., Thurstans, R.P., Wagner, P.A., Avery, M., Browell, E.V., Cammas, J.-P., Christensen, L.E., Diskin, G.S., Gao, R.-S., Jost, H.-J., Loewenstein, M., Lopez, J.D., Nedelec, P., Osterman, G.B., Sachse, G.W., Webster, C.R., 2008. Validation of Aura Microwave Limb Sounder O3 and CO observations in the upper troposphere and lower stratosphere. J. Geophys. Res. 113, D15S02. http://dx.doi.org/10.1029/2007JD008805.
Loeb, N.G., Manalo-Smith, N., Kato, S., Miller, W.F., Gupta, S.K., Minnis, P., Wielicki, B.A., 2003. Angular distribution models for top-of-atmosphere radiative flux estimation from the clouds and the Earth's radiant energy system instrument on the tropical rainfall measuring mission satellite. Part I: methodology. J. Appl. Meteorol. 42, 240–265.
Lohmann, U., Feicher, J., 2005. Global indirect aerosol effects: a review. Atmos. Chem. Phys. 5, 715–735.
Logan, J.A., Megretskaia, I., Nassar, R., Murray, L.T., Zhang, L., Bowman, K.W., Worden, H.M., Luo, M., 2008. Effects of the 2006 El Niño on tropospheric composition as revealed by data from the Tropospheric Emission Spectrometer (TES). Geophys. Res. Lett. 35, L03816. http://dx.doi.org/10.1029/2007GL031698.
Lu, M.-L., Wang, J., Flagan, R.C., Seinfeld, J.H., Freedman, A., McClatchey, R.A., Jonsson, H.H., 2003. Analysis of humidity halos around trade wind cumulus clouds. J. Atmos. Sci. 60, 1041–1059.
Lyapustin, A., Martonchick, J., Wang, Y., Laszla, I., Korkin, S., 2011a. Multi-angle implementation of atmospheric correction (MAIAC): part 1 radiative transfer basis and lookup tables. J. Geophys. Res. 116, D03211. http://dx.doi.org/10.1029/2010JD014986.
Lyapustin, A., Wang, Y., Laszlo, I., Kahn, R., Korkin, S., Remer, L., Levy, R., Reid, J.S., 2011b. Multi-angle implementation of atmospheric correction (MAIAC): part 2 aerosol algorithm. J. Geophys. Res. 116, D03210. http://dx.doi.org/10.1029/2010JD014985.
Madden, R.A., Julian, P.R., 1971. Detection of a 40–50 day oscillation in the zonal wind in the tropical Pacific. J. Atmos. Sci. 28, 702–708.
Maddux, B.C., Ackerman, S.A., Platnick, S., 2010. Viewing geometry dependencies in MODIS cloud products. J. Atmos. Ocean. Technol. 27, 1519–1528.
Maenhaut, W., De Ridder, D.J.A., Fernandez-Jimenez, M.T., Hooper, M.A., Hooper, B., Nurhayati, M., 2002. Long-term observations of regional aerosol composition at two sites in Indonesia. Nucl. Inst. Methods Phys. Res. B 189, 259–265.
Magi, B.I., Hobbs, P.V., 2003. Effects of humidity on aerosols in southern Africa during the biomass burning season. J. Geophys. Res. 108, 8495. http://dx.doi.org/10.1029/2002JD002144.
Mahmud, M., 2009a. Mesoscale model simulation of low level equatorial winds over Borneo during the haze episode of September 1997. J. Earth Syst. Sci. 118, 295–307.
Mahmud, M., 2009b. Mesoscale equatorial wind prediction in Southeast Asia during a haze episode of 2005. Geofizika 26, 67–84.
Mahmud, M., in press. Assessment of atmospheric impacts of open burning in Kalimantan, Borneo during 2004. Atmopsheric Environment.

Mahmud, M., Ross, R.S., 2005. Precipitation assessment of a superensemble forecast over South-East Asia. Meteorol. Appl. 12, 177–186.
Marchand, R., Ackerman, T., Smyth, M., Rossow, W.B., 2010. A review of cloud top height and optical depth histograms from MISR, ISCCP, and MODIS. J. Geophys. Res. 115, D16206. http://dx.doi.org/10.1029/2009JD013422.
Marshak, A., Wen, G., Coakley Jr., J.A., Remer, L.A., Loeb, N.G., Cahalan, R.F., 2008. A simple model for the cloud adjacency effect and the apparent bluing of aerosols near clouds. J. Geophys. Res. 113, D14S17. http://dx.doi.org/10.1029/2007JD009196.
Martins, J.V., Artaxo, P., Liousse, C., Reid, J.S., Hobbs, P.V., Kaufman, Y., 1998. Effects of black carbon content, particle size, and mixing on light absorption by aerosol particles from biomass burning in Brazil. J. Geophys. Res. 103, 32,041–32,050.
Martins, J.V., Artaxo, P., Hobbs, P.V., Liousse, C., Cachier, H., Kaufman, Y.J., Plana-Fattori, A., 1997. Particle size distributions, elemental compositions, carbon measurements, and optical properties of smoke from biomass burning in the Pacific Northwest of the United States. In: Levine (Ed.), Global Biomass Burning and Global Change. MIT press, Cambridge, Mass., pp. 716–732.
Masunaga, H., L'Ecuyer, T.S., 2010. The Southeast Pacific warm band and double ITCZ. J. Clim. 23 (1189–1208), 2010.
Matichuk, R.I., Colarco, P.R., Smith, J.A., Toon, O.B., 2007. Modeling the transport and optical properties of smoke aerosols from African savanna fires during the Southern African Regional Science Initiative campaign (SAFARI 2000). J. Geophys. Res. 112, D08203. http://dx.doi.org/10.1029/2006JD007528.
Maxwell, A.L., 2004. Fire regimes in north-eastern Cambodian monsoonal forests, with a 9300-years sediment charcoal record. J. Biogeogr. 31, 225–239.
Mazzoni, D., Logan, J.A., Diner, D., Kahn, R., Tong, L., Li, Q., 2007. A data-mining approach to associating MISR smoke plume height with MODIS fire measurements. Remote Sens. Environ. 107, 138–148.
McBride, J.L., Malcolm, R., Haylock, N.N., 2003. Relationships between the Maritime Continent heat source and the El Niño–Southern Oscillation phenomenon. J. Clim. 16, 2905–2914.
Mcfarquahar, G.M., Wang, H., 2006. Effects of aerosols on trade wind cumuli over the Indian Ocean: model simulations. Q. J. R. Meteorol. Soc. 132, 821–843.
Mertz, O., et al., 2009. Who counts? Demography of swidden cultivators in Southeast Asia. Hum. Ecol. 37, 281–289.
Miettinen, J., Langner, A., Siegert, F., 2007. Burnt area estimation for the year 2005 in Borneo using multi-resolution satellite imagery. Int. J. Wildland Fire 16, 45–53.
Miettinen, J., Liew, S.C., 2009. Burn-scar patterns and their effect on regional burnt-area mapping in insular South-east Asia. Int. J. Wildland Fire 18, 837–847. http://dx.doi.org/10.1071/wf08102.
Miettinen, J., Liew, S.C., 2010. Degradation and development of peatlands in Peninsular Malaysia and in the islands of Sumatra and Borneo since 1990. Land Degrad. Dev. 21, 285–296. http://dx.doi.org/10.1002/ldr.976.
Miettinen, J., Shi, C., Liew, S.C., 2010. Influence of peatland and land cover distribution on fire regimes in insular Southeast Asia. Reg. Environ. Chang. 11, 191–201. http://dx.doi.org/10.1007/s10113-010-0131-7.
Miettinen, J., Shi, C.H., Liew, S.C., 2011a. Deforestation rates in insular Southeast Asia between 2000 and 2010. Glob. Chang. Biol. 17, 2261–2270. http://dx.doi.org/10.1111/j.1365-2486.2011.02398.x.
Miettinen, J., Shi, C.H., Liew, S.C., 2011b. Influence of peatland and land cover distribution on fire regimes in insular Southeast Asia. Reg. Environ. Chang. 11, 191–201. http://dx.doi.org/10.1007/s10113-010-0131-7.
Miettinen, J., Wong, C.M., Liew, S.C., 2008. New 500 m spatial resolution land cover map of the western insular Southeast Asia region. Int. J. Remote. Sens. 29, 6075–6081.
Mims, S.R., Kahn, R.A., Moroney, C.M., Gaitley, B.J., Nelson, D.L., Garay, M.J., 2010. MISR stereo heights of grassland fire smoke plumes in Australia. IEEE Trans. Geosci. Remote Sens. 48, 25–35. http://dx.doi.org/10.1109/TGRS.2009.2027114.
Mishchenko, M.I., Geogdzhayev, I.V., Cairns, B., Rossow, W.B., Lacis, A.A., 1999. Aerosol retrievals over the ocean by use of channels 1 and 2 AVHRR data: sensitivity analysis and preliminary results. Appl. Optics 38, 7325–7341.
Mohd Noor, M., 2003. Zero burning techniques in oil palm cultivation: an economic perspectiveAvailable at http://www.chgs.com.my/download/OilPalmIndustryEconomicJournal/vol3no1/ZeroBurningTechniquesinOilPalmCultivation-anEconomicPerspective.pdf2003.
Montagnini, F., Jordan, C.F., 2005. Tropical Forest Ecology: The Basis for Conservation and Management. Springer Science, New York.
Moron, V., Robertson, A.W., Beer, R., 2009. Spatial coherence and seasonal predictability of monsoon onset over Indonesia. J. Clim. 22, 840–850.
Moroney, C., Davies, R., Muller, J.-P., 2002. Operational retrieval of cloud-top heights using MISR data. IEEE Trans. Geosci. Remote. Sens. 40, 1532–1540.
Muraleedharan, T.R., Radojevic, M., Waugh, A., Caruna, A., 2000. Chemical characterization of the haze in Brunei Darussalam during the 1998 episode. Atmos. Environ. 34, 2725–2731.
Myhre, G., Govaerts, Y., Haywood, J.M., Berntsen, T.K., Lattanzio, A., 2005a. Radiative effect of surface albedo change from biomass burning. Geophys. Res. Lett. 32, L20812. http://dx.doi.org/10.1029/2005GL022897.
Myhre, G., Stordal, F., Johnsrud, M., Diner, D.J., Geogdzhayev, I.V., Haywood, J.M., Holben, B.N., Holzer-Popp, T., Ignatov, A., Kahn, R.A., Kaufman, Y.J., Loeb, N., Martonchik, J.V., Mishchenko, M.I., Nalli, N.R., Remer, L.A., Schroedter-Homscheidt, M., Tanré, D., Torres, O., Wang, M., 2005b. Intercomparison of satellite retrieved aerosol optical depth over ocean during the period September 1997 to December 2000. Atmos. Chem. Phys. 5, 1697–1719. http://dx.doi.org/10.5194/acp-5-1697-2005.
Myhre, G., Stordal, F., Johnsrud, M., Ignatov, A., Mishchenko, M.I., Geogdzhayev, I.V., Tanré, D., Deuzé, J.-L., Goloub, P., Nakajima, T., Higurashi, A., Torres, O., Holben, B.N., 2004. Intercomparison of satellite retrieved aerosol optical depth over the ocean. J. Atmos. Sci. 61, 499–513.
Nair, V.S., Moorthy, K.K., Babu, S.S., Satheesh, S.K., 2009. Optical and physical properties of atmospheric aerosols over the Bay of Bengal during ICARB. J. Atmos. Sci. 66, 2640–2658.
Nakajima, T., Higurashi, A., Takeuchi, N., Herman, J.R., 1999. Satellite and ground-based study of optical properties of 1997 Indonesian forest fire aerosols. Geophys. Res. Lett. 26, 2421–2424. http://dx.doi.org/10.1029/1999GL900208.
Narukawa, M., Kawamura, K., Takeuchi, N., Nakajima, T., 1999. Distribution of dicarboxylic acids and carbon isotopic compositions in aerosols from 1997 Indonesian forest fires. Geophys. Res. Lett. 26, 3101–3104.
Newell, R.E., Evans, M.J., 2000. Seasonal changes in pollutant transport to the North Pacific: the relative importance of Asian and European sources. Geophys. Res. Lett. 27, 2509–2512. http://dx.doi.org/10.1029/2000GL011501.
Nichol, J., 1998. Smoke haze in Southeast Asia: a predictable recurrence. Atmos. Environ. 32, 2715–2716.
Nigam, S., Bollasina, M., 2010. "Elevated heat pump" hypothesis for the aerosol–monsoon hydroclimate link: "grounded" in observations? J. Geophys. Res. 115, D16201. http://dx.doi.org/10.1029/2009JD013800.
Nigam, S., Bollasina, M., 2011. Reply to comment by K.M. Lau and K.M. Kim on "'Elevated heat pump' hypothesis for the aerosol–monsoon hydroclimate link: 'grounded' in observations?". J. Geophys. Res. 116, D07204. http://dx.doi.org/10.1029/2010JD015246.
Nho, E.Y., Le Cloarec, M.-F., Ardouin, B., Tjetjep, W.S., 1996. Source strength assessment of volcanic trace elements emitted from the Indonesian arc. J. Volcanol. Geotherm. Res. 74, 121–129.
Oanh, N.T.K., Upadhyay, N., Zhuang, Y.-H., Hao, Z.-P., Murthy, D.V.S., Lestari, P., Villarin, J.T., Chengchua, K., Co, H.X., Dung, N.T., Lindgren, E.S., 2006. Particulate air pollution in six Asian cities: spatial and temporal distributions, and associated sources. Atmos. Environ. 40 (18), 3367–3380. http://dx.doi.org/10.1016/j.atmosenv.2006.01.050 ISSN 1352–2310.
Oanh, N.T.K., Bich, T.L., Tipayarom, D., Manadhar, B.R., Prapat, P., Simpson, C.D., Liu, L.-J.S., 2011. Characterization of particulate matter emission from open burning of rice straw. Atmos. Environ. 45, 493–502.
Okada, K., Ikegami, M., Zaizen, Y., Makino, Y., Jensen, J.B., Gras, J.L., 2001. The mixture of individual aerosol particles in the 1997 Indonesian haze episode. J. Aerosol Sci. 32, 1269–1279.
O'Neill, N.T., Eck, T.F., Smirnov, A., Holben, B.N., Thulasiraman, S., 2003. Spectral discrimination of coarse and fine mode optical depth. J. Geophys. Res. 108, 4559. http://dx.doi.org/10.1029/2002JD002975.
Oo, M.M., Jerg, M., Hernandez, E., Picon, A., Gross, B.M., Moshary, F., Ahmed, S.A., 2010. Improved MODIS aerosol retrieval using modified VIS/SWIR surface albedo ratio over urban scenes. IEEE Trans. Geosci. Remote Sens. 48, 983–1000.
Oo, M., Holz, R., 2011. Improving the CALIOP aerosol optical depth using combined MODIS-CALIOP observations and CALIOP integrated attenuated total color ratio. J. Geophys. Res. D14201. http://dx.doi.org/10.1029/2010JD014894.
Ooi, L.-H., Heriansyah, 2005. Palm pulverization in sustainable oil palm replanting. Platn Production Science 8, 345–348.
Padoch, C., Coffey, K., Mertz, O., Leisz, S.J., Fox, J., Wadley, R.L., 2007. The demise of swidden in Southeast Asia? Local realities and regional ambiguities. Dan. J. Geogr. 107, 29–41.
Page, S.E., Siegert, F., Rieley, J.O., Boehm, H.-D.V., Jaya, A., Limin, S., 2002. The amount of carbon released from peat and forest fires in Indonesia during 1997. Nature 420, 61–65.
Page, S.E., Rieley, J.O., Banks, C.J., 2011. Global and regional importance of the tropical peatland carbon pool. Glob. Chang. Biol. 17, 798–818.
Page, S.E., Rieley, J.O., Wust, R., 2006. Chapter 7 Lowland tropical peatlands of Southeast Asia. In: Martini, I.P., Martinez Cortizas, A., Chesworth, W. (Eds.), Developments in Earth Surface Processes, Elsevier, 2006, Vol, 9, Peatlands — Evolution and Records of Environmental and Climate Changes, pp. 145–172.
Palm, C.A., 1999. Carbon sequestration and trace gas emissions in slash and burning and alternative land-uses in the humid tropics. ASB Climate Change Working Group, Final Report Phase II.

Parameswaran, K., Nair, S.K., Rajeec, K., 2004. Impact of Indonesian forest fires during the 1997 El Niño on the aerosol distribution over the Indian Ocean. Adv. Space Phys. 33, 1098–1103.
Park, M., Randel, W.J., Emmons, K.L., Livesey, N.J., 2009. Transport pathways of carbon monoxide in the Asian summer monsoon diagnosed from Model of Ozone and Related Tracers (MOZART). J. Geophys. Res. 114, D08303. http://dx.doi.org/10.1029/2008JD010621.
Patadia, F., Gupta, P., Christopher, S.A., 2008a. First observational estimates of global clear sky shortwave aerosol direct radiative effect over land. Geophys. Res. Lett. 35, L04810. http://dx.doi.org/10.1029/2007GL032314.
Patadia, F., Christopher, S.A., Zhang, J., 2011. Development of empirical angular distribution models for smoke aerosols: methods. J. Geophys. Res. 116, D14203. http://dx.doi.org/10.1029/2010JD015033.
Parker, D.E., Wilson, H., Jones, P.D., Christy, J.R., Folland, C.K., 1996. The impact of Mt. Pinatubo on world-wide temperatures. Int. J. Climatol. 16, 487–497.
Pengchai, P., Chantara, S., Sopajaree, K., Wangkarn, S., Tencharoenkul, U., Rayanakorn, M., 2009. Seasonal variation, risk assessment and source estimation of PM 10 and PM10-bound PAHs in the ambient air of Chiang Mai and Lamphun, Thailand. Environ. Monit. Assess. 154, 197–218. http://dx.doi.org/10.1007/s10661-008-0389-0.
Penner, J.E., Charlson, R., Hales, J., Laulainen, N., Leifer, R., Novakov, T., Ogren, J.A., Radke, L., Schwartz, S., Travis, L., 1994. Quantifying and minimizing uncertainty of climate forcing by anthropogenic aerosols. Bull. Am. Meteorol. Soc. 75, 375–400. http://dx.doi.org/10.1175/1520-0477((1994) 075 < 0375:QAMUOC > 2.0.CO;2).
Penning de Vries, M.J.M., Beirle, S., Wagner, T., 2009. UV Aerosol Indices from SCIAMACHY: introducing the SCattering Index (SCI). Atmos. Chem. Phys. 9, 9555–9567. http://dx.doi.org/10.5194/acp-9-9555-2009.
Perry, K.D., Hobbs, P.V., 1994. Further evidence for particle nucleation in clear air adjacent to marine cumulus clouds. J. Geophys. Res. 99, 22,803–22,818. http://dx.doi.org/10.1029/94JD01926.
Perry, K.D., Hobbs, P.V., 1996. Influences of isolated cumulus clouds on the humidity of their surroundings. J. Atmos. Sci. 53, 159–174.
Pierce, J.R., Kahn, R.A., Davis, M.R., Comstock, J.M., 2010. Detecting thin cirrus in Multiangle Imaging Spectroradiometer aerosol retrievals. J. Geophys. Res. 115, D08201. http://dx.doi.org/10.1029/2009JD013019.
Porter, J.N., Horton, K.A., Mouginis-Mark, P.J., Lienert, B., Sharma, S.K., Lau, E., Sutton, A.J., Elias, T., Oppenheimer, C., 2002. Sun photometer and lidar measurements of the plume from the Hawaii Kilauea Volcano Pu'u O'o vent: aerosol flux and SO_2 lifetime. Geophys. Res. Lett. 29, 1783. http://dx.doi.org/10.1029/2002GL014744.
Posselt, D.J., van den Heever, S.C., Stephens, G.L., 2008. Trimodal cloudiness and tropical stable layers in simulation sof radiative convective equilibrium. Geophys. Res. Lett. 35, L08802. http://dx.doi.org/10.1029/2007GL033029.
Prins, E.M., Feltz, J.M., Menzel, W.P., Ward, D.E., 1998. An overview of GOES-8 diurnal fire and smoke results for SCAR-B and the 1995 fire season in South America. J. Geophys. Res. 103, 31,821–31,836.
Prins, E.M., Csiszar, I., Shroeder, W., Schmidt, C., Giglio, L., Hoffman, J., Wooster, M., Reid, J., Hyer, E., Govaerts, Y., 2008. Global Geostationary Fire Monitoring: Sensor and Data Issues and Recommendations 2008. CGMS-36, NOAA-WP-21 . (E. M.).
Pu, R., Yu, Q., Gong, P., Biging, G.S., 2005. EO-1 Hyperion, ALI and Landsat 7 ETM+data comparison for estimating forest crown closure and leaf area index. Int. J. Remote. Sens. 26, 457–474.
Qadri, S.T. (Ed.), 2001. Fire, Smoke, and Haze: The ASEAN Response Strategy. Manila, Asian Development Bank and Association of Southeast Asia Nations.
Radke, L.F., Hobbs, P.V., 1991. Humidity and particle fields around some small cumulus clouds. J. Atmos. Sci. 48, 1190–1193.
Radke, L.F., Hobbs, P.V., Stith, J.L., 1976. Airborne measurements of gases and aerosols from volcanic vents on Mt. Baker. Geophys. Res. Lett. 3, 93–96.
Radojevic, M., Hassan, H., 1999. Air quality in Brunei Darussalam during the 1998 haze episode. Atmos. Environ. 33, 3651–3658.
Radzi bin Abas, M., Oros, D.R., Simoneit, B.R., 2004. Biomass burning as the main source of organic aerosol particulate matter in Malaysia during haze episodes. Chemosphere 55, 1089–1095.
Rajeev, K., Parameswaran, K., Nair, S.K., Meenu, S., 2008. Observational evidence for the radiative impact of Indonesian smoke in modulating the sea surface temperature of the equatorial Indian Ocean. J. Geophys. Res. 113, D17201. http://dx.doi.org/10.1029/2007JD009611.
Ramage, C.S., 1968. Role of a tropical "maritime continent" in the atmospheric circulation. Mon. Weather Rev. 96, 365–370.
Randel, W.J., Park, M., Emmons, L., Kinnison, D., Bernath, P., Walker, K.A., Boone, C., Pumphrey, H., 2010. Asian monsoon transport of pollution to the stratosphere. Science 328, 611–613. http://dx.doi.org/10.1126/science.1182274.
Rao, C.R.N., Stowe, L.L., McClain, E.P., 1989. Remote sensing of aerosols over the oceans using AVHRR data theory, practice and applications. Int. J. Remote. Sens. 10, 743–749.
Rasmusson, E.M., Wallace, J.M., 1983. Meteorological aspects of the El Niño/Southern Oscillation. Science 16, 1195–1202. http://dx.doi.org/10.1126/science.222.4629.1195.
Redemann, J., Zhang, Q., Russell, P.B., Livingston, J.M., Remer, L.A., 2009. Case studies of aerosol remote sensing in the vicinity of clouds. J. Geophys. Res. 114 (D06), 209. http://dx.doi.org/10.1029/2008JD010774.
Reid, J.S., Brooks, B., Crahan, K.K., Hegg, D.A., Eck, T.F., O'Neill, N., de Leeuw, G., Reid, E.A., Anderson, K.D., 2006. Reconciliation of coarse mode sea-salt aerosol particle size measurements and parameterizations at a subtropical ocean receptor site. J. Geophys. Res. 111, D02202. http://dx.doi.org/10.1029/2005JD006200.
Reid, J.S., Eck, T.F., Christopher, S.A., Hobbs, P.V., Holben, B.R., 1999. Use of the Angstrom exponent to estimate the variability of optical and physical properties of aging smoke particles in Brazil. J. Geophys. Res. 104, 27473–27489. http://dx.doi.org/10.1029/1999JD900833.
Reid, J.S., Hobbs, P.V., Ferek, R.J., Blake, D.R., Martins, J.V., Dunlap, M.R., Liousse, C., 1998. Physical, chemical, and optical properties of regional hazes dominated by smoke in Brazil. J. Geophys. Res. 103, 32059–32080.
Reid, J.S., Hyer, E.J., Prins, E.M., Westphal, D.L., Zhang, J.L., Wang, J., Christopher, S.A., Curtis, C.A., Schmidt, C.C., Eleuterio, D.P., Richardson, K.A., Hoffman, J.P., 2009. Global monitoring and forecasting of biomass-burning smoke: description and lessons from the Fire Locating and Modeling of Burning Emissions (FLAMBE) program. IEEE J. Sel. Top. Appl. Remote Sens. 2, 144–162.
Reid, J.S., Reid, E.A., Walker, A., Piketh, S.J., Cliff, S.S., Mandoos, A., Tsay, S.-C., Eck, T.F., 2008. Dynamics of Southwest Asian dust particle size characteristics with implications for global dust research. J. Geophys. Res. 113, D14212. http://dx.doi.org/10.1029/2007JD009752.
Reid, J.S., Westphal, D.L., Livingston, J.M., Savoie, D.L., Maring, H.B., Jonsson, H.H., Eleuterio, D.P., Kinney, J.E., Reid, E.A., 2002. Dust vertical distribution in the Caribbean during the Puerto Rico Dust Experiment. Geophys. Res. Lett. 29 (7), 1151. http://dx.doi.org/10.1029/2001GL014092.
Reid, J.S., Jonsson, H.H., Maring, H.B., Smirnov, A., Savoie, D.L., Cliff, S.S., Reid, E.A., Livingston, J.M., Meier, M.M., Dubovik, O., Tsay, S.-C., 2003. Comparison of size and morphological measurements of coarse mode dust particles from Africa. J. Geophys. Res. 108, 8593. http://dx.doi.org/10.1029/2002JD002485.
Reid, J.S., Koppmann, R., Eck, T., Eleuterio, D., 2005a. A review of biomass burning emissions part II: intensive physical properties of biomass burning particles. Atmos. Chem. Phys. 5, 799–825 (SRef-ID: 1680-7324/acp/2005-5-799. http://www.atmos-chem-phys.org/acp/5/799/).
Reid, J.S., Eck, T., Christopher, S., Dubovik, O., Koppmann, R., Eleuterio, D., Holben, B., Reid, E.A., Zhang, J., 2005b. A review of biomass burning emissions part III: intensive optical properties of biomass burning particles. Atmos. Chem. Phys. 5, 827–849 SRef-ID: 1680-7324/acp/2005-5-827. http://www.atmos-chem-phys.org/acp/5/827/.
Reid, J.S., Xian, P., Hyer, E.J., Flatau, M.K., Ramirez, E.M., Turk, F.J., Sampson, C.R., Zhang, C., Fukada, E.M., Maloney, E.D., 2012. Multi-scale meteorological conceptual analysis of observed active fire hotspot activity and smoke optical depth in the Maritime Continent. Atmos. Chem. Phys. 12, 2117–2147. http://dx.doi.org/10.5194/acp-12-2117-2012.
Remer, L.A., Kaufman, Y.J., Tanré, D., Mattoo, S., Chu, D.A., Martins, J.V., Li, R.-R., Ichoku, C., Levy, R.C., Kleidman, R.G., Eck, T.F., Vermote, E., Holben, B.N., 2005. The MODIS aerosol algorithm, products and validation. J. Atmos. Sci. 62, 947–973.
Remer, L.A., Kaufman, Y.J., 2006. Aerosol direct radiative effect at the top of the atmosphere over cloud free ocean derived from four years of MODIS data. Atmos. Chem. Phys. 6, 237–253.
Ridout, 2002. Sensitivity of tropical pacific convection to dry layers at mid- to upper levels: simulation and parameterization tools. J. Atmos. Sci. 59, 3362–3381.
Rieley, J.O., Page, S.E., 2005. Wise Use of Tropical Peatlands: Focus on Southeast Asia. ALTERRA — Wageningen University and Research Centre and the EU INCO — STRAPEAT and RESTORPEAT Partnerships, Wageningen, The Netherlands.
Rigg, J., 2003. Southeast Asia: The Human Landscape of Modernization and Development. Routledge, London.
Risk, M.J., Sherwood, O.A., Keikoop, J.M., Llewellyn, G., 2003. Smoke signals from corals: isotopic signature of the 1997 Indonesian 'haze' event. Mar. Geol. 202, 71–78.
Robock, A., 2005. Cooling following large volcanic eruptions corrected for the effect of diffuse radiation on tree rings. Geophys. Res. Lett. 32, L06702. http://dx.doi.org/10.1029/2004GL022116.
Roberts, G.C., Artaxo, P., Zhou, J., Sweitlicki, E., Andreae, M.O., 2002. Sensitivity of CCN spectra on chemical and physical properties of aerosol: a case study from the Amazon basin. J. Geophys. Res. 107, 8070. http://dx.doi.org/10.1029/2001JD000583.
Roden, C.A., Bond, T.C., Conway, S., Pinel, A.B.S., Maccarty, N., Still, D., 2009. Laboratory and field investigations of particulate and carbon monoxide emissions from traditional and improved cook stoves. Atmos. Environ. 43, 1170–1181. http://dx.doi.org/10.1016/j.atmosenv.2008.05.041.

Rose, W.I., Bluth, G.J.S., Ernst, G.G.J., 2000. Integrating retrievals of volcanic cloud characteristics from satellite remote sensors: a summary. Philos. Transact. Math. Phys. Eng. Sci. 358, 1585–1606.
Rosenfeld, D., 1999. TRMM observed first direct evidence of smoke from forest fires inhibiting rainfall. Geophys. Res. Lett. 26, 3105–3108. http://dx.doi.org/10.1029/1999GL006066.
Rosenfeld, D., Fromm, M., Trentmann, J., Luderer, G., Andreae, M.O., Servranckx, R., 2007. The Chisholm firestorm: observed microstructure, precipitation and lightning activity of a pyro-cumulonimbus. Atmos. Chem. Phys. 7, 645–659. http://dx.doi.org/10.5194/acp-7-645-2007.
Rosenfeld, D., Woodley, W.L., 2000. Deep convective clouds with sustained supercooled liquid water down to −37.5 °C. Nature 405, 440–442.
Roswintiarti, O., Raman, S., 2003. Three-dimensional simulations of the mean air transport during the 1997 forest fires in Kalimantan, Indonesia using a mesoscale numerical model. Pure Appl. Geophys. 160, 429–438.
Roy, D.P., Jin, Y., Lewis, P.E., Justice, C.O., 2005. Prototyping a global algorithm for systematic fire-affected area mapping using MODIS time series data. Remote Sens. Environ. 97, 137–162.
Saji, N.H., Goswami, B.N., Vinayachandran, P.N., Yamagata, T., 1999. A dipole mode in the tropical Indian Ocean. Nature 401, 360–363.
Saji, N.H., Yamagata, T., 2003. Structure of SST and surface wind variability during Indian Ocean Dipole Mode years: COADS observations. J. Clim. 16, 2735–2751.
Salam, A., Bauer, H., Kassin, K., Ullah, S.M., Puxbaum, H., 2003. Aerosol chemical characteristics of a mega-city in Southeast Asia (Dhaka-Bangladesh). Atmos. Environ. 37, 2517–2528.
Salinas, S.V., Chew, B.N., Miettinen, J., Campbell, J.R., Welton, E.J., Reid, J.S., Yu, L.Y., Liew, S.C., 2013. Physical and optical characteristics of the October 2010 haze event over Singapore: A photometric and lidar analysis. Atmos. Res. 122, 555–570 (this issue).
Sapiano, M.R.P., Arkin, P.A., 2009. An intercomparison and validation of high resolution precipitation estimates with 3-hourly gauge data. J. Hydrometeorol. 10, 149–166.
Sasaki, T., Wu, P., Mori, S., Hamada, J.-I., Tauhid, Y.I., Yamanaka, M.D., Sribimawati, T., Yoshikane, T., Kimura, F., 2004. Vertical moisture transport above the mixed layer around the mountains in western Sumatra. Geophys. Res. Lett. 31, L08106. http://dx.doi.org/10.1029/2004GL019730.
Sassen, K., Cho, B.S., 1992. Subvisual-thin cirrus lidar datasets for satellite verification and climatological research. J. Appl. Meteorol. 31, 1275–1285.
Sassen, K., Liou, K.N., Kinne, S., Griffin, M., 1985. Highly supercooled cirrus cloud water: confirmation and climate implications. Science 227, 411–413.
Satake, S., Uno, I., Takemura, T., Carmichael, G.R., Tang, Y., Streets, D., Sugimoto, N., Shimizu, A., Uematsu, M., Han, J.-S., Ohta, S., 2004. Characteristics of Asian aerosol transport simulated with a regional-scale chemical transport model during the ACE-Asia observation. J. Geophys. Res. 109, D19S22. http://dx.doi.org/10.1029/2003JD003997.
Satori, G., Williams, E., Lemperger, I., 2009. Variability of global lightning activity on the ENSO time scale. Atmospheric Research 91, 500–507.
Sayer, A.M., Hsu, N.C., Bettenhausen, C., Smirnov, A., Thomas, G.E., Zhang, J., 2011. SeaWiFS Ocean Aerosol Retrieval (SOAR): algorithm, validation, and comparison with other datasets. Journal of Geophysical Research submitted.
Schafer, R., May, P.T., Keenan, T.D., McGuffie, K., Ecklund, W.L., Johnson, P.E., Gage, K.S., 2001. Boundary layer development over a tropical island during the Maritime Continent thunderstorm experiment. J. Atmos. Sci. 58, 2163–2179.
Schmidt-Vogt, D., Leisz, S.J., Mertz, O., Heinimann, A., Thiha, T., Messerli, P., Epprecht, M., Cu, P.V., Chi, V.K., Hardiono, M., Dao, T.M., 2009. An assessment of trends in the extent of swidden in Southeast Asia. Hum. Ecol. 37, 269–280.
Schott, F.A., Xie, S.-P., McCreary Jr., J.P., 2009. Indian Ocean circulation and climate variability. Rev. Geophys. 47, RG1002. http://dx.doi.org/10.1029/2007RG000245.
Schroeder, W., Csiszar, I., Morisette, J., 2008a. Quantifying the impact of cloud obscuration on remote sensing of active fires in the Brazilian Amazon. Remote Sens. Environ. 112, 456–470.
Schroeder, W., Prins, E., Giblio, L., Csiszar, I., Schmidt, C., Morisette, J., Morton, D., 2008b. Validation of GOES and MODIS active fire detection products using ASTER and ETM plus data. Remote Sens. Environ. 112, 2711–2726.
Schumann, U., Weinzierl, B., Reitebuch, O., Schlager, H., Minikin, A., Forster, C., Baumann, R., Sailer, T., Graf, K., Mannstein, H., Voigt, C., Rahm, S., Simmet, R., Scheibe, M., Lichtenstern, M., Stock, P., Rüba, H., Schäuble, D., Tafferner, A., Rautenhaus, M., Gerz, T., Ziereis, H., Krautstrunk, M., Mallaun, C., Gayet, J.-F., Lieke, K., Kandler, K., Ebert, M., Weinbruch, S., Stohl, A., Gasteiger, J., Groß, S., Freudenthaler, V., Wiegner, M., Ansmann, A., Tesche, M., Olafsson, H., Sturm, K., 2011. Airborne observations of the Eyjafjalla volcano ash cloud over Europe during air space closure in April and May 2010. Atmos. Chem. Phys. 11, 2245–2279. http://dx.doi.org/10.5194/acp-11-2245-2011.
Schuster, G.L., Dubovik, O., Holben, B.N., Clothiaux, E.E., 2005. Inferring black carbon content and specific absorption from Aerosol Robotic Network (AERONET) aerosol retrievals. J. Geophys. Res. 110, D10S17. http://dx.doi.org/10.1029/2004JD004548.
Schuster, G.L., Lin, B., Dubovik, O., 2009. Remote sensing of aerosol water uptake. Geophys. Res. Lett. 36, L03814. http://dx.doi.org/10.1029/2008GL036576.
Scollo, S., Kahn, R.A., Nelson, D.L., Coltelli, M., Diner, D.J., Garay, M.J., Realmuto, V.J., 2011. MISR observations of Etna volcanic plumes. Journal of Geophysical Research submitted.
Seavoy, R., 1975. The origin of tropical grasslands in Kalimantan, Indonesia. J. Trop. Geogr. 40, 48–52.
See, S.W., Balasubramanian, R., Wang, W., 2006. A study of the physical, chemical, and optical properties of ambient aerosol particles in Southeast Asia during hazy and nonhazy days. J. Geophys. Res. 111, D10S08. http://dx.doi.org/10.1029/2005JD006180.
See, S.-W., Balasubramanian, R., Rinawati, E., Karthikeyan, S., Streets, D.G., 2007. Characterization and source apportionment of PM2.5 in Sumatra, Indonesia during a recent peat fire episode. Environ. Sci. Technol. 41, 3488–3494.
Seftor, C.J., Hsu, N.C., Herman, J.R., Bhartia, P.K., Torres, O., Rose, W.I., Schneider, D.J., Krotkov, N., 1997. Detection of volcanic ash clouds from Nimbus 7/total ozone mapping spectrometer. J. Geophys. Res. 102, 16,749–16,759. http://dx.doi.org/10.1029/97JD00925.
Segah, H., Tani, H., Hirano, T., 2010. Detection of fire impact and vegetation recovery over tropical peat swamp forest by satellite data and ground based NDVI instrument. Int. J. Remote. Sens. 31, 5297–5314.
Sekiyama, T.T., Tanaka, Y.T., Shimizu, A., Miyoshi, T., 2010. Data assimilation of CALIPSO aerosol observations. Atmos. Chem. Phys. 10, 39–49.
Self, S., 1992. Krakatau revisited: the course of events and interpretations of the 1883 eruption. GeoJournal 8, 109–121.
Self, S., Rampino, M.R., 1981. The 1883 eruption of Krakatau. Nature 294, 699–704.
Shen, Y., Xiong, A., Wang, Y., Xie, P., 2010. Performance of high-resolution satellite precipitation products over China. J. Geophys. Res. 115, D02114. http://dx.doi.org/10.1029/2009JD012097.
Shettle, E.P., Fenn, R.W., 1979. Models for the aerosols of the lower atmosphere and the effects of humidity variations on their optical properties. AFGL-TR-79-0214, 94 pp. Air Force Res. Lab., Wright-Patt Air Force Base, Ohio.
Shi, Y., Zhang, J., Reid, J.S., Holben, B.N., Hyer, E.J., Curtis, C., 2011a. An analysis of the collection 5 MODIS over-ocean aerosol optical depth product for its implication in aerosol assimilation. Atmos. Chem. Phys. 11, 557–565.
Shi, Y., Zhang, J., Reid, J.S., Hyer, E.J., Eck, T.F., Holben, B.N., Kahn, R.A., 2011b. Where do we need additional in situ aerosol and sun photometer data?: a critical analysis of spatial biases between MODIS and MISR aerosol products. Atmospheric Measurement Technology submitted.
Siebert, L., Simkin, T., Kimberly, P., 2010. Volcanoes of the World, 3rd edition. University of California Press and Smithsonian Institution. 568 pp.
Siegert, F., Hoffman, A.A., 2000. The 1998 forest fires in east Kalimantan (Indonesia): a quantitative evaluation using high resolution, multi-temporal ERS-2 SAR images and NOAA AVHRR hotspot data. Remote Sens. Environ. 72, 64–77.
Siegert, F., Ruecker, G., Hinrichs, A., Hoffmann, A.A., 2001. Increased damage from fires in logged forests during droughts caused by El Niño. Nature 414, 437–440.
Sigurdsson, H., Carey, S., 1989. Plinian and co-ignimbrite tephra fall from the 1815 eruption of Tambora volcano. Bull. Volcanol. 51, 243–270.
Silva, F.S., Cristale, J., Andre, P.A., Saldiva, P.H.N., Marcho, M.R.R., 2010. PM2.5 and PM10: the influence of sugarcane burning on potential cancer risk. Atmos. Environ. 44, 5133–5138.
Simkin, T., Siebert, L., 1994. Volcanoes of the World, 2nd edition. Geoscience Press, Tucson. 349 pp.
Simon, M., Plummer, S., Fierens, F., Hoelzemann, J.J., Arino, O., 2004. Burnt area detection at global scale using ATSR-2: the GLOBSCAR products and their qualification. J. Geophys. Res. 109, D14S02. http://dx.doi.org/10.1029/2003JD003622.
Siniarovina, U., Engardt, M., 2005. High-resolution model simulations of anthropogenic sulphate and sulphur dioxide in Southeast Asia. Atmos. Environ. 39, 2021–2034.
Smirnov, A., Holben, B.N., Dubovik, O., Frouin, R., Eck, T.F., Slutsker, I., 2003. Maritime component in aerosol optical models derived from Aerosol Robotic Network data. J. Geophys. Res. 108, 4033. http://dx.doi.org/10.1029/2002JD002701.
Smirnov, A., Holben, B.N., Eck, T.F., Dubovik, O., Slutsker, I., 2000. Cloud screening and quality control algorithms for the AERONET database. Remote Sens. Environ. 73, 337–349.
Smirnov, A., et al., 2011. Maritime aerosol network as a component of AERONET- first results and comparison with global aerosol models and satellite retrievals. Atmospheric Measurement Technology 4, 583–597.

Srinivas, N., Rao, S.R., Kumar, K.S., 2009. Trace metal accumulation in vegetables grown in industrial and semi-urban areas-a case study. Appl. Ecol. Environ. Res. 7, 131–139.
Sow, S.K., Juneng, L., Tangang, F.T., Hussin, A.G., Mahmud, M., 2011. Numerical simulation of a severe late afternoon thunderstorm over Peninsular Malaysia. Atmospheric Research 99, 248–262.
Spinhirne, J.D., Palm, S.P., Hart, W.D., Hlavka, D.L., Welton, E.J., 2005. Cloud and aerosol measurements from GLAS: overview and initial results. Geophys. Res. Lett. 32, L22S03. http://dx.doi.org/10.1029/2005GL023507.
Stohl, A., Forster, C., Huntrieser, H., Mannstein, H., Mcmillan, W.W., Petzold, A., Schlager, H., Weinzierl, B., 2007. Aircraft measurements over Europe of an air pollution plume from Southeast Asia? Aerosol and chemical characterization. Atmos. Chem. Phys. 7 (3), 913–937.
Stolle, F., Chomitz, K.M., Lambin, E.F., Tomich, T.P., 2003. Land use and vegetation fires in Jambi Province, Sumatra, Indonesia. Forest Ecol. Manage. 179, 277–292.
Stolle, F., Dennis, R.A., Kurniwan, I., Lambin, E.F., 2004. Evaluation of remote sensing-based active fire datasets in Indonesia. Int. J. Remote. Sens. 25, 471–479.
Stolle, F., Lambin, E.F., 2003. Interprovincial and interannual differences in the causes of land-use fires in Sumatra, Indonesia. Environ. Conserv. 30, 375–387.
Streets, D.G., Yarber, K.F., Woo, J.H., Carmichael, G.R., 2003a. Biomass burning in Asia: annual and seasonal estimates and atmospheric emissions. Global Biogeochem. Cycles 17, 1099. http://dx.doi.org/10.1029/2003 GB002040.
Streets, D.G., Bond, T.C., Carmichael, G.R., Fernandes, S.D., Fu, Q., He, D., Klimont, Z., Nelson, S.M., Tsai, N.Y., Wang, M.Q., Woo, J.-H., Yarber, K.F., 2003b. An inventory of gaseous and primary aerosol emissions in Asia in the year 2000. J. Geophys. Res. 108, 8809. http://dx.doi.org/10.1029/2002JD003093.
Streets, D.G., Yarber, K.F., Woo, J.-H., Carmichael, G.R., 2003c. Biomass burning in Asia: annual and seasonal estimates and atmospheric emissions. Global Biogeochem. Cycles 17. http://dx.doi.org/10.1029/2003 GB002040.
Stubenrauch, C., et al., 2011. Assessment of Global Cloud Data Sets from Satellites. World Climate Research, Program Report (manuscript in preparation).
Sun, Y., Solomon, S., Dai, A., Portmann, R.W., 2007. How often will it rain? J. Clim. 20, 4801–4818. http://dx.doi.org/10.1175/JCLI4263.1 http://dx.doi.org/.
Sundarambal, P., Balasubramanian, R., Tkalich, P., He, J., 2010. Impact of biomass burning on ocean water quality in Southeast Asia through atmospheric deposition: field observations. Atmos. Chem. Phys. 10, 11323–11336. http://dx.doi.org/10.5194/acp-10-11323-2010.
Suyanto, S., Applegate, G., Permana, R.P., Khusuiyah, N., Kurniawan, I., 2004. The role of fire in changing land use and livelihoods in Riau-Sumatra. Ecol. Soc. 9, 15.
Symonds, R.B., Rose, W.I., Reed, M.H., Lichte, F.E., Finnegan, D.L., 1987. Volatilization, transport and sublimation of metallic and nonmetallic elements in high temperature gases at Merapi Volcano, Indonesia. Geochim. Cosmochim. Acta 51, 2083–2101.
Tackett, J.L., Di Girolamo, L., 2009. Enhanced aerosol backscatter adjacent to tropical trade wind clouds revealed by satellite-based lidar. Geophys. Res. Lett. 36, L14804. http://dx.doi.org/10.1029/2009GL039264.
Tang, Y., et al., 2003a. Influences of biomass burning during the Transport and Chemical Evolution Over the Pacific (TRACE-P) experiment identified by the regional chemical transport model. J. Geophys. Res. 108, 8824. http://dx.doi.org/10.1029/2002JD003110.
Tang, Y., et al., 2003b. Impacts of aerosols and clouds on photolysis frequencies and photochemistry during TRACE-P: 2. Three-dimensional study using a regional chemical transport model. J. Geophys. Res. 108, 8822. http://dx.doi.org/10.1029/2002JD003100.
Tanpipat, V., Honda, K., Nuchaiya, P., 2009. MODIS hotspot validation over Thailand. Remote Sens. 1, 1043–1054. http://dx.doi.org/10.3390/rs1041043.
Tansey, K., Beston, J., Hoscilo, A., Page, S.E., Paredes Hernández, C.U., 2008. Relationship between MODIS fire hot spot count and burned area in a degraded tropical peat swamp forest in Central Kalimantan, Indonesia. J. Geophys. Res. 113, D23112. http://dx.doi.org/10.1029/2008JD010717.
Thomas, H., Watson, I., 2010. Observations of volcanic emissions from space: current and future perspectives. Nat. Hazard. 54, 323–354. http://dx.doi.org/10.1007/s11069-009-9471-3.
Tian, B., Waliser, D.E., Kahn, R.A., Li, Q., Yung, Y.L., Tyranowski, T., Geogdzhayev, I.V., Mishchenko, M.I., Torres, O., Smirnov, A., 2008. Does the Madden – Julian Oscillation influence aerosol variability? J. Geophys. Res. 113, D12215. http://dx.doi.org/10.1029/2007JD009372.
Tipayarom, D., Kim Oanh, N.T., 2007. Effects from open rice straw burning emission on air quality in the Bangkok Metropolitan Region. J. Sci. Asia 33, 339–345.
Tobo, Y., et al., 2007. Balloon-borne observations of high aerosol concentrations near the summertime tropopause over the Tibetan Plateau. Atmospheric Research 84, 233–241.
Tokairin, T., Sofyan, A., Kitada, T., 2010. Effect of land use changes on local meteorological conditions in Jakarta, Indonesia: towards the evaluation of the thermal environment of megacities in Asia. Int. J. Climatol. 30, 1931–1941.
Toratani, M., Fukushima, H., Murakamim, H., 2005. Atmospheric correction for satellite ocean color data in Upper Gulf of Thailand. IEEE International Geoscience and Remote Sensing Symposium v1-8 proceedings, 1916–1919.
Torres, O., Herman, J.R., Bhartia, P.K., Ahmad, Z., 1995. Properties of Mount Pinatubo aerosols as derived from Nimbus 7 total ozone mapping spectrometer measurements. J. Geophys. Res. 100, 14,043–14,055. http://dx.doi.org/10.1029/95JD01224.
Torres, O., Bhartia, P.K., Herman, J.R., Ahmad, Z., Gleason, J., 1998. Derivation of aerosol properties from satellite measurements of backscattered ultraviolet radiation: theoretical basis. J. Geophys. Res. 103, 17,099–17,110. http://dx.doi.org/10.1029/98JD00900.
Torres, O., Decae, R., Veefkind, J.P., de Leeuw, G., 2002. In: Stammes, P., Noordhoek, R. (Eds.), OMI Aerosol Retrieval Algorithm, in OMI Algorithm Theoritical Basis Document. : Clouds, Aerosols and Surface UV Irradiance, ATBD-OMI-03, vol. III. KNMI, De Bilt, Netherlands, pp. 46–71 (Available at http://www.knmi.nl/omi/research/documents).
Torres, O., Tanskanen, A., Veihelmann, B., Ahn, C., Braak, R., Bhartia, P.K., Veefkind, P., Levelt, P., 2007. Aerosols and surface UV products from Ozone Monitoring Instrument observations: an overview. J. Geophys. Res. 112, D24S47. http://dx.doi.org/10.1029/2007JD008809.
Tosca, M.G., Randerson, J.T., Zender, C.S., Flanner, M.G., Rasch, P.J., 2010. Do biomass burning aerosols intensify drought in equatorial Asia during El Niño? Atmos. Chem. Phys. 10, 3515–3528. http://dx.doi.org/10.5194/acp-10-3515-2010.
Tosca, M.G., Randerson, J.T., Zender, C.S., Nelson, D.L., Diner, D.J., Logan, J.A., 2011. Dynamics of fire plumes and smoke clouds associated with peat and deforestation fires in Indonesia. J. Geophys. Res. 116, D08207. http://dx.doi.org/10.1029/2010JD015148.
Tupper, A., Carn, S., Davey, J., Kamada, Y., Potts, R., Prata, F., Tokuno, M., 2004. An evaluation of volcanic cloud detection techniques during recent significant eruptions in the western 'Ring of Fire'. Remote Sens. Environ. 91, 27–46.
Turk, F.J., Xian, P., 2013. An assessment of satellite-based high resolution precipitation datasets for atmospheric composition studies in the maritime continent. Atmospheric Research 122, 579–598 (this issue).
Uno, I., Yumimoto, K., Shimizu, A., Hara, Y., Sugimoto, N., Wang, Z., Liu, Z., Winker, D.M., 2008. 3D structure of Asian dust transport revealed by CALIPSO lidar and a 4DVAR dust model. Geophys. Res. Lett. 35, L06803. http://dx.doi.org/10.1029/2007GL032329.
Uno, I., Eguchi, K., Yumimoto, K., Takemura, T., Shimizu, A., Uematsu, M., Liu, Z., Wang, Z., Hara, Y., Sugimoto, N., 2009. Asian dust transported one full circuit around the globe. Nat. Geosci. 2, 557–560.
Ushio, T., et al., 2009. A Kalman Filter approach to the global mapping of precipitation (GSMap) from combined microwave and infrared radiometric data. J. Meteorol. Soc. Jpn. 87, 137–151. http://dx.doi.org/10.2151/jmsj.87A.137.
Val Martin, M., Logan, J.A., Kahn, R.A., Leung, F.-Y., Nelson, D.L., Diner, D.J., 2010. Smoke injection heights from fires in North America: analysis of 5 years of satellite observations. Atmos. Chem. Phys. 10, 1491–1510. http://dx.doi.org/10.5194/acp-10-1491-2010.
van der Kaars, S., Tapper, N., cook, E.J., 2010. Observed relationships between El-Nino Southern Oscillation, rainfall variaiblity and vegetation and fire history on Halmahera, Maluku, Indonesia. Glob. Chang. Biol. 16, 1705–1714. http://dx.doi.org/10.1111/j.1365-2486.2009.02025.x.
van der Werf, G.R., et al., 2004. Continental-scale partitioning of fire emissions during the 1997 to 2001 El Niño/La Nina period. Science 303, 73–76.
van der Werf, G.R., Randerson, J.T., Giglio, L., Collatz, G.J., Kasibhatla, P.S., Arellano Jr., A.F., 2006. Interannual variability in global biomass burning emissions from 1997 to 2004. Atmos. Chem. Phys. 6, 3423–3441. http://dx.doi.org/10.5194/acp-6-3423-2006.
van der Werf, G.R., et al., 2008. Climate regulation of fire emissions and deforestation in equatorial Asia. Proc. Natl. Acad. Sci. 104, 20350–20355.
van der Werf, G.R., Randerson, J.T., Giglio, L., Collatz, G.J., Mu, M., Kasibhatla, P.S., Morton, D.C., DeFries, R.S., Jin, Y., van Leeuwen, T.T., 2010. Global fire emissions and the contribution of deforestation, savanna, forest, agricultural, and peat fires (1997–2009). Atmos. Chem. Phys. 10, 11707–11735. http://dx.doi.org/10.5194/acp-10-11707-2010.
Várnai, T., Marshak, A., 2011. Global CALIPSO observations of aerosol changes near clouds. Geosci. Remote Sens. Lett. 8, 19–23. http://dx.doi.org/10.1109/LGRS.2010.2049982.
Vayda, A.P., 2006. Causal explanation of Indonesian forest fires: concepts, applications, and research priorities. Hum. Ecol. 34, 615–635.
Verhoeven, J.T.A., Setter, T.L., 2010. Agricultural use of wetlands: opportunities and limitations. Ann. Bot. 105, 155–163.
Verma, S., Worden, J., Payra, S., Jourdain, L., Shim, C., 2008. Characterizing the long range transport of black carbon aerosols during the Transport and Chemical Evolution over the Pacific (TRACE-P) experiment.
Vernier, J.-P., Thomason, L.W., Kar, J., 2011. CALIPSO detection of an Asian tropopause aerosol layer. Geophys. Res. Lett. 38, L07804. http://dx.doi.org/10.1029/2010GL046614.

Virts, K.S., Wallace, J.M., 2010. Annual, interannual, and intraseasonal variability of tropical tropopause transition layer cirrus. J. Atmos. Sci. 67, 3097–3112.
Vongmahadlek, C., Thao, P.T.B., Satayopas, B., Thongboonchoo, N., 2009. A compilation and development of spatial and temporal profiles of high-resolution emissions inventory over Thailand. J. Air Waste Manage. Assoc. 59845–59856.
Waggoner, A.P., Weiss, R.E., 1980. Comparison of fine particle mass concentration and light scattering extinction in ambient aerosol. Atmos. Environ. 14, 623–626.
Wai, K.M., Lin, N.H., Wang, S.-H., Dokiya, Y., 2008. Rainwater chemistry at a high-altitude station, Mt. Lulin, Taiwan: comparison with a background station, Mt. Fuji. J. Geophys. Res. 113, D06305. http://dx.doi.org/10.1029/2006JD008248.
Wang, B., Webster, P., Kikuchi, K., Yasunari, T., Qi, Y., 2006. Boreal summer quasi-monthly oscillation in the global tropics. Clim. Dyn. 27, 661–675. http://dx.doi.org/10.1007/s00382-006-0163-3.
Wang, B., Huang, F., Wu, Z., Yang, J., Fu, X., Kikuchi, K., 2009. Multi-scale climate variability of the South China Sea monsoon: a review. Dyn. Atmos. Ocean 47, 15–37.
Wang, J., Gei, C., Yang, Z., Hyer, E.J., Reid, J.S., Chew, B.-N., Mahmud, M., Zhang, Y., Zhang, M., 2013. Mesoscale modeling of smoke transport over the Southeast Asian Maritime Continent: Interplay of sea breeze, trade wind, typhoon, and topography. Atmos. Res. 122, 486–503 (this issue).
Wang, P.-H., Minnis, P., McCormick, M., Kent, G., Skeens, K., 1996. A 6-year climatology of cloud occurrence frequency from Stratospheric Aerosol and Gas Experiment II observations (1985–1990). J. Geophys. Res. 101, 29407–29429.
Wang, S.-H., et al., 2012. First detailed observations of long-range transported dust over the northern South China Sea. Atmos. Environ. 45, 4804–4808.
Wang, S.-H., Lin, N.-H., Chou, M.-D., Woo, J.-H., 2007. Estimate of radiative forcing of Asian biomass-burning aerosols during the period of TRACE-P. J. Geophys. Res. 112, D10222. http://dx.doi.org/10.1029/2006JD007564.
Wang, Y., Field, R.D., Roswintiarti, O., 2004a. Trends in atmospheric haze induced by peat fires in Sumatra Island, Indonesia and El Niño phenomenon from 1973 to 2003. Geophys. Res. Lett. 31, L04103. http://dx.doi.org/10.1029/2003GL018853.
Wang, Z., Sassen, K., Whiteman, D.N., Demoz, B.B., 2004b. Studying altocumulus with ice virga using ground-based active and passive remote sensors. J. Appl. Meteorol. 43, 449–460.
Wagner, T., Beirle, S., Deutschmann, T., Eigemeier, E., Frankenberg, C., Grzegorski, M., Liu, C., Marbach, T., Platt, U., Penning de Vries, M., 2008. Monitoring of atmospheric trace gases, clouds, aerosols and surface properties from UV/vis/NIR satellite instruments. J. Opt. A Pure Appl. Opt. 10, 104019. http://dx.doi.org/10.1088/1464-4258/10/10/104019.
Weigelt, A., Hermann, M., van Velthoven, P.F.J., Brenninkmeijer, C.A.M., Schlaf, G., Zahn, A., Wiedensohler, A., 2009. Influence of clouds on aerosol particle number concentrations in the upper troposphere. J. Geophys. Res. 114, D01204. http://dx.doi.org/10.1029/2008JD009805.
Wen, G., Marshak, A., Cahalan, R.F., 2006. Impact of 3D clouds on clear sky reflectance and aerosol retrieval in a biomass burning region of Brazil. IEEE Geosci. Remote Sens. Lett. 3, 169–172.
Wen, G., Marshak, A., Cahalan, R.F., 2008. Importance of molecular Rayleigh scattering in the enhancement of clear sky reflectance in the vicinity of boundary layer cumulus clouds. J. Geophys. Res. 113, D24207. http://dx.doi.org/10.1029/2008JD010592.
Wheeler, M., Kiladis, G.N., 1999. Convectively-coupled equatorial waves: analysis of clouds and temperature in the wavenumber-frequency domain. J. Atmos. Sci. 56, 374–399.
Whitmore, T.C., 1984. Tropical Rain Forests of the Far East, 2nd edition. Oxford University Press, Oxford0-19-854136-8. Pp 352.
Wielicki, B.A., Barkstrom, B.R., Harrison, E.F., Lee III, R.B., Smith, G.L., Cooper, J.E., 1996. Clouds and the Earth's Radiant Energy System (CERES): an Earth observing system experiment. Bull. Am. Meteorol. Soc. 77, 853–868.
Winker, D.M., Poole, L.R., 1995. Monte-Carlo calculations of cloud returns for ground-based and space-based LIDARS. Appl. Phys. B 60, 341–344.
Winker, D.M., Couch, R.H., McCormick, M.P., 1996. An overview of LITE: NASA's lidar in space technology experiment. Proc. IEEE 84, 164–180.
Winker, D.M., Vaughan, M.A., Omar, A., Hu, Y., Powell, K.A., Liu, Z., Hunt, W.H., Young, S.A., 2009. Overview of the CALIPSO mission and CALIOP data processing algorithms. J. Oceanogr. Atmos. Meas. 26, 2310–2323.
Winker, D.M., Pelon, J., Coakley Jr., J.A., Ackerman, S.A., Charlson, R.J., Colarco, P.R., Flamant, P., Fu, Q., Hoff, R., Kittaka, C., Kubar, T.L., LeTreut, H., McCormick, M.P., Megie, G., Poole, L., Powell, K., Trepte, C., Vaughan, M.A., Wielicki, B.A., 2010. The CALIPSO mission: a global 3D view of aerosols and clouds. Bull. Am. Meteorol. Soc. 91, 1211–1229.
Wiwanitkit, W., 2008. PM10 in the atmosphere and incidence of respiratory illness in Chiangmai during the smoggy pollution. Stoch. Env. Res. Risk Assess. 22, 437–440.
Wooster, M.J., 2002. Small-scale experimental testing of fire radiative energy for quantifying mass combusted in natural vegetation fires. Geophys. Res. Lett. 29, 2027. http://dx.doi.org/10.1029/2002GL015487.
Wooster, M.J., Roberts, G., Perry, G.L.W., Kaufman, Y.J., 2005. Retrieval of biomass combustion rates and totals from fire radiative power observations: FRP derivation and calibration relationships between biomass consumption and fire radiative energy release. J. Geophys. Res. 110, D24311. http://dx.doi.org/10.1029/2005JD006318.
Wooster, M.J., Strub, N., 2002. Study of the 1997 Borneo fires: quantitative analysis using global area coverage (GAC) satellite data. Global Biogeochem. Cycles 16, L1009. http://dx.doi.org/10.1029/2000 GB001357.
Wooster, M.J., Zhang, Y.H., 2004. Boreal forest fires burn less intensely in Russia than in North America. Geophys. Res. Lett. 31, L20505. http://dx.doi.org/10.1029/2004GL020805.
Wu, C.H., Hsu, H.H., 2009. Topographic influence on the MJO in the Maritime Continent. J. Clim. 22, 5433–5448.
Wu, D.L., et al., 2009a. Vertical distributions and relationships of cloud occurrence frequency as observed by MISR, AIRS, MODIS, OMI, CALIPSO, and CloudSat. Geophys. Res. Lett. 36, L09821. http://dx.doi.org/10.1029/2009GL037464.
Wu, P., Hara, M., Hamada, J.-I., Yamanaka, M.D., Kimura, F., 2009b. Why a large amount of rain falls over the sea in the vicinity 0f western Sumatra island during nighttime. Appl. Meteorol. 48, 1345–1361. http://dx.doi.org/10.1175/2009JAMC2052.1.
Wolff, D.B., Fisher, B.L., 2009. Assessing the relative performance of microwave-based rainrate retrievals using TRMM ground validation data. J. Appl. Meteorol. Climatol. 48, 1069–1099.
Wolter, K., Timlin, M.S., 1998. Measuring the strength of ENSO events — how does 1997/98 rank? Weather 53, 315–324.
Xian, P., Reid, J.S., Turk, J.F., Hyer, E.J., Westphal, D.L., 2009. Impact of modeled versus satellite measured tropical precipitation on regional smoke optical thickness in an aerosol transport model. Geophys. Res. Lett. 36, L16805. http://dx.doi.org/10.1029/2009GL038823.
Xian, P., Reid, J.S., Atwood, S.A., Johnson, R.S., Hyer, E.J., Westphal, D.L., Sessions, W., 2013. Smoke aerosol transport patterns over the Maritime Continent. Atmos. Res. 122, 469–485 (this issue).
Xiao, N., Shi, T., Calder, C.A., Munroe, D.K., Berrett, C., Wolfinbarger, S., Li, D., 2009. Spatial characteristics of the difference between MISR and MODIS aerosol optical depth retrievals over mainland Southeast Asia. Remote Sens. Environ. 113, 1–9.
Yang, S., Kuo, K.-S., Smith, E.A., 2008. Persistent nature of secondary diurnal modes of precipitation over oceanic and continental regimes. J. Clim. 21, 4115–4131.
Yang, S., Smith, E.M., 2006. Mechanisms for diurnal variability of global tropical rainfall observed from TRMM. J. Clim. 19, 5190–5226.
Yang, Y., Di Girolamo, L., 2008. Impacts of 3-D radiative transfer effects on satellite cloud detection and their consequences on cloud fraction and aerosol optical depth retrievals. J. Geophys. Res. 113, D04213. http://dx.doi.org/10.1029/2007JD009095.
Yasunaga, K., Kida, H., Satomura, T., 2003. The 600–750 hPa relative humidity minimum observed during PEM-Tropics B. Geophys. Res. Lett. 30, 2282. http://dx.doi.org/10.1029/2003GL018739.
Yasunaga, K., Yoneyama, K., Kubota, H., Okamoto, H., Shimizu, A., Kumagai, H., Katsumata, M., Sugimoto, N., Matsui, I., 2006. Melting layer cloud observed during the R/V Mirai Cruise MR01-K05. J. Atmos. Sci. 63, 3020–3032.
Yatagai, A., Arakawa, O., Kamiguchi, K., Kawamoto, H., Nodzu, M.I., Hamada, 2009. A 44 year daily gridded precipitation dataset for Asia base on a dense network of rain gauges. SOLA 5, 137–140.
Yevich, R., Logan, J.A., 2003. An assessment of biofuel use and burning of agricultural waste in the developing world. Global Biogeochem. Cycles 17, 1095. http://dx.doi.org/10.1029/2002 GB001952.
Yokelson, R.J., Christian, T.J., Karl, T.G., Guenther, A., 2008. The tropical forest and fire emissions experiment: laboratory fire measurements and synthesis of campaign data. Atmos. Chem. Phys. 8, 3509–3527.
Yokelson, R.J., Crounse, J.D., DeCarlo, P.F., Karl, T., Urbanski, S., Atlas, E., Campos, T., Shinozuka, Y., Kapustin, V., Clarke, A.D., Weinheimer, A., Knapp, D.J., Montzka, D.D., Holloway, J., Weibring, P., Flocke, F., Zheng, W., Toohey, D., Wennberg, P.O., Wiedinmyer, C., Mauldin, L., Fried, A., Richter, D., Walega, J., Jimenez, J.L., Adachi, K., Buseck, P.R., Hall, S.R., Shetter, R., 2009. Emissions from biomass burning in the Yucatan. Atmospheric Chemistry and Physics 9, 5785–5812. http://dx.doi.org/10.5194/acp-9-5785-2009.
Yokelson, R.J., Burling, I.R., Urbanski, S.P., Atlas, E.L., Adachi, K., Buseck, P.R., Wiedinmyer, C., Akagi, S.K., Toohey, D.W., Wold, C.E., 2011. Trace gas and particle emissions from open biomass burning in Mexico. Atmos. Chem. Phys. 11, 6787–6808. http://dx.doi.org/10.5194/acp-11-6787-2011.
Yu, H., et al., 2006. A review of measurement-based assessment of aerosol direct radiative effect and forcing. Atmos. Chem. Phys. 6, 613–666. http://dx.doi.org/10.5194/acp-6-313-2006.

Yuan, T., Remer, L.A., Pickering, K.E., Yu, H., 2011. Observational evidence of aerosol enhancement of lightning activity and convective invigoration. Geophys. Res. Lett. 38, L04701. http://dx.doi.org/10.1029/2010GL046052.
Yumimoto, K., Uno, I., Sugimoto, N., Shimizu, A., Liu, Z., Winker, D.M., 2008. Adjoint inversion modeling of Asian dust emission using lidar observations. Atmos. Chem. Phys. 8, 2869–2884.
Yule, C., 2010. Loss of biodiversity and ecosystem functioning in Indo-Malayan peat swamp forests. Biodivers. Conserv. 19, 393–409.
Yusef, A.A., Francisco, H., 2009. Climate change vulnerability mapping for Southeast Asia, Economy and Environment Program for Southeast Asia (EEPSEA) report, June 2009 (32 pp., available at http://www.eepsea.org).
Zhan, X., Sohlberg, R.A., Townshen, R.A., DiMiceli, C., Carroll, M.L., Eastman, J.C., Hansen, M.C., DeFries, R.S., 2002. Detection of land cover changes using MODIS 250 m data. Remote Sens. Environ. 83, 336–350.
Zhang, B.-N., Oanh, N.T.K., 2002. Photochemical smog pollution in the Bangkok Metropolitan Region of Thailand in relation to O3 precursor concentrations and meteorological conditions. Atmos. Environ. 36, 4211–4222.
Zhang, C., 2005. Madden–Julian Oscillation. Rev. Geophys. 43, RG2003. http://dx.doi.org/10.1029/2004RG000158.
Zuidema, P., Li, Z., Hill, R.J., Bariteau, L., Rilling, B., Fairall, C., Brewer, W.A., Albrecht, B., Hare, J., 2012. On trade wind cumulus cold pools. J. Atmos. Sci. 69, 258–280.
Zhang, C., Dong, M., 2004. Seasonality of the Madden–Julian Oscillation. J. Clim. 17, 3169–3180.
Zhang, C., Gottschalck, J., 2002. SST anomalies of ENSO and the Madden–Julian Oscillation in the equatorial Pacific. J. Clim. 15, 2429–2445.
Zhang, C., Mapes, B.E., Soden, B.J., 2003. Bimodality in tropical water vapor. Q. J. R. Meteorol. Soc. 129, 2847–2866.
Zhang, J., Campbell, J.R., reid, J.S., Westphal, D.L., Baker, N.L., Hyer, E.J., 2011. Evaluating the impact of assimilating CALIOP-derived aerosol extinction profiles on a global mass transport model. Geophys. Res. Lett. 38, L14801.
Zhang, J., Christopher, S.A., Remer, L., Kaufman, Y., 2005d. Satellite aerosol direct radiative forcing studies over cloud free oceans from Terra: (I) aerosol angular distribution models. J. Geophys. Res. Atmos. 110, D10S23. http://dx.doi.org/10.1029/2004JD005008.
Zhang, J., Christopher, S.A., Remer, L.A., Kaufman, Y.J., 2005a. Shortwave aerosol cloud-free radiative forcing from Terra, II: global and seasonal distributions. J. Geophys. Res. D10, S24. http://dx.doi.org/10.1029/2004JD005009.
Zhang, J., Reid, J.S., 2006. MODIS aerosol product analysis for data assimilation: assessment of Level 2 aerosol optical thickness retrievals. J. Geophys. Res.-Atmos. 111, D22207. http://dx.doi.org/10.1029/2005JD006898.
Zhang, J., Reid, J.S., Westphal, D.L., Baker, N., Hyer, E.J., 2008. A system for operational aerosol optical depth data assimilation over global oceans. J. Geophys. Res. 113, D10208. http://dx.doi.org/10.1029/2007JD009065.
Zhang, J., Reid, J.S., 2009. An analysis of clear sky and contextual biases using an operational over ocean MODIS aerosol product. Geophys. Res. Lett. 36, L15824. http://dx.doi.org/10.1029/2009GL038723.
Zhang, J., Reid, J.S., 2010. A decadal regional and global trend analysis of the aerosol optical depth using over water MODIS and MISR aerosol products. Atmos. Chem. Phys. 10, 10949–10963.
Zhang, J., Reid, J.S., Holben, B.N., 2005b. An analysis of potential cloud artifacts in MODIS over ocean aerosol optical thickness products. Geophys. Res. Lett. 32, L15803.
Zhang, S., Penner, J.E., Torres, O., 2005c. Inverse modeling of biomass burning emissions using Total Ozone Mapping Spectrometer aerosol index for 1997. J. Geophys. Res. 110, D21306. http://dx.doi.org/10.1029/2004JD005738.
Zipser, E.J., Cecil, D.J., Liu, C., Nesbitt, S.W., Yorty, D.P., 2006. Where are the most intense thunderstorms on earth? Bull. Am. Meteorol. Soc. 87, 1057–1071.
Zhao, G., Di Girolamo, L., Dey, S., Jones, A.L., Bull, M., 2009. Examination of direct cumulus contamination on MISR retrieved aerosol optical depth and angstrom coefficient over ocean. Geophys. Res. Lett. 36, L13811. http://dx.doi.org/10.1029/2009GL038549.
Zou, L.Y., Hooper, M.A., 1997. Size resolved airborne particles and their morphology in central Jakarta. Atmos. Environ. 31, 1167–1172.